

**Please cite the Published Version**

Brown, Andrew David (2018) The influence of site, bulk metal composition and individual particle structure on bioaccessibility of road dust. Doctoral thesis (PhD), Manchester Metropolitan University.

**Downloaded from:** <https://e-space.mmu.ac.uk/620800/>

**Usage rights:**  [Creative Commons: Attribution-Noncommercial-No Derivative Works 4.0](https://creativecommons.org/licenses/by-nc-nd/4.0/)

**Enquiries:**

If you have questions about this document, contact [openresearch@mmu.ac.uk](mailto:openresearch@mmu.ac.uk). Please include the URL of the record in e-space. If you believe that your, or a third party's rights have been compromised through this document please see our Take Down policy (available from <https://www.mmu.ac.uk/library/using-the-library/policies-and-guidelines>)

THE INFLUENCE OF SITE, BULK  
METAL COMPOSITION AND  
INDIVIDUAL PARTICLE STRUCTURE  
ON BIOACCESSIBILITY OF ROAD  
DUST

A D Brown

PhD 2018

THE INFLUENCE OF SITE, BULK  
METAL COMPOSITION AND  
INDIVIDUAL PARTICLE STRUCTURE  
ON BIOACCESSIBILITY OF ROAD  
DUST

ANDREW DAVID BROWN

A thesis submitted in partial fulfilment  
of the requirements of the Manchester  
Metropolitan University for the degree  
of Doctor of Philosophy

School of Science and the  
Environment

Manchester Metropolitan University

2018



# Abstract

The impact of urban air quality on human health is of worldwide concern and responsible for 40,000 early deaths in the U.K. alone. Industry's relocation to suburban areas, caused vehicle tailpipe emissions to become the largest air pollution contributor. Although new fuels, engine modifications, legislation and improved urban planning, resulted in pollutant reductions, air quality remains a concern. To that end, resuspended road dust (RD) has been identified as one of the largest contributors to urban airborne particulate matter (PM).

This study focused on potentially harmful elements (PHEs) in RD (specifically Cr, Cu, Fe and Pb) to investigate their health hazards associated with chronic exposure to urban RD. The study required seasonal collections of RD from an urban site in Manchester, U.K. over a two-year period. Total Cr, Cu, Fe and Pb concentrations in the fine fractions ( $<125\ \mu\text{m}$ ) were determined for each sample and indicated enrichment of PHEs in the smaller particles. In addition, this study reports for the first time on the seasonal and size fraction variations of the structural and chemical nature of individual RD particles, as determined by sequential analysis using computer controlled scanning electron microscopy with energy dispersive x-ray detection (CC-SEM-EDX) and micro Raman spectroscopy. Furthermore, investigation of the similarities of the  $<38\ \mu\text{m}$  fraction with the  $<10\ \mu\text{m}$  fraction, indicated that it could be used as a proxy, thereby contributing to new knowledge. To assess human risk on exposure, *in vitro* data were used to inform the seasonal and particle size variance of the

bioaccessibility via the respiratory and gastrointestinal routes. Finally, the study featured a risk assessment of the metal exposure using a version of the EPA risk assessment protocol adapted in this for use with RD, which features as a timely contribution to the field.

The study highlighted the enrichment of PHEs in finer fractions of RD, seasonal speciation of metals in different size fractions and individual particles, and behaviour of RD in simulated biological fluids. However, the hypothesis and overarching theme concerning the effect particle chemical structure has on potential human health effects proved harder to elucidate, illustrating the incredibly complex nature of this field of study. Accordingly, a final chapter featuring a comparative case study of Hg enrichment and bioaccessibility in RD from three international sites showed the relevance of this hypothesis.

# Contents

Abstract .....	i
Contents .....	iii
Acknowledgments .....	v
Introduction, Aims and Objectives .....	1
1.1 Introduction.....	2
1.2 Aims and Objectives .....	5
Literature Review .....	8
2.1 Literature Review Introduction .....	9
2.2 Particulate Matter .....	9
2.3 Road Dust as a Contributor to Airborne Particles .....	12
2.4 Sampling and Handling Techniques .....	14
2.5 Bulk Geochemical and Individual Particle Approaches to Analysis of RD.....	15
2.6 In vitro Techniques – Inhalation Route .....	19
2.7 In vitro Techniques – Ingestion Route .....	24
2.8 Risk Assessment.....	26
2.9 Literature Review – Closing Remarks.....	31
Experimental Methodology.....	32
3.1 Site and Sample Handling .....	33
3.2 Bulk Geochemistry .....	35
3.3 Individual Particle Analysis.....	36
3.3.1 CC-SEM-EDX.....	37
3.3.2 Raman Spectroscopy.....	38
3.4 Chromium (VI) Quantification.....	39
3.5 PM <sub>10</sub> Separation.....	41
3.6 In Vitro Analysis.....	43
3.6.1 Respiratory Route .....	43
3.6.2 Gastrointestinal Route.....	44
3.7 Risk Assessment.....	48
Results and Discussion.....	51
4.1 Physical Sample Characteristics.....	52
4.2 Bulk Chemical Analysis .....	56
4.3 Key Findings From Sections 4.1 and 4.2: A Short Conclusive Summary.....	65
4.4 Individual Particle Analysis.....	66
4.4.1 CC-SEM-EDX.....	67
4.4.1.1 Primary Constituents .....	68
4.4.1.2 Secondary Constituents .....	73
4.4.2 Raman Spectroscopy.....	87
4.4.2.1 Calcium Rich Particles .....	92

4.4.2.2	Iron Rich Particles .....	95
4.4.2.3	Silica Rich Particles.....	97
4.4.2.4	Titanium Rich .....	101
4.4.2.5	Other Trace Metal Rich Particles .....	102
4.4.2.6	Carbon Inclusions .....	104
4.4.2.7	Raman Observations of RD Samples .....	105
4.5	Chromium (VI) Quantification.....	111
4.6	Key Findings From Sections 4.4 and 4.5: A Short Conclusive Summary.....	118
4.7	<38 µm RD Fraction as a Proxy for Inhalable Particulates .....	120
4.7.1	Particle Size Analysis.....	121
4.7.2	Elemental Composition .....	124
4.7.3	Mobility in Simulated Biological Fluid .....	126
4.8	In Vitro Analysis.....	128
4.8.1	Respiratory Route .....	128
4.8.2	Gastrointestinal Route.....	131
4.9	Risk Assessment.....	134
4.10	Key Findings from Sections 4.7, 4.8 and 4.9: A Short Conclusive Summary .....	138
	Case study: Component-Specific Toxicity of Hg in Various Urban Road Dusts .....	140
5.1	Introduction .....	142
5.2	Experimental Methodology.....	144
5.2.1	Sampling Protocol .....	144
5.2.2	Acid Digestion Technique .....	146
5.2.3	Bioaccessibility Testing .....	147
5.2.4	Cold Vapour Atomic Absorption Spectroscopy .....	147
5.3	Results .....	148
5.3.1	Bulk Hg Concentrations .....	148
5.3.2	Artificial Lysosomal Fluid Leaching Concentrations of Hg.....	150
5.4	Conclusions.....	154
	Conclusions.....	157
	References.....	163
	Appendices .....	182
	Appendix A: Supplementary Data.....	182
	Appendix B: Conference Contributions .....	185
	Appendix C: Publications .....	191

# Acknowledgments

Many thanks to my supervisory team, Sanja Potgieter-Vermaak, Judi Barrett and Mike Bennett for all your expertise and support over the past few years. Sanja, thank you for your resilience and not allowing me to do less when more is so tempting. You go above and beyond for me, and all of your students, you're a credit to your profession. Judi, thank you for making time for me in your incredibly busy schedule, travelling in to Manchester as often as you do. Thank you for your geochemical perspectives and unremitting attention to detail. Mike, your insight and breadth of knowledge on all topics has inspired me, but I'm sure you'll be grateful for a quieter retirement now.

Among the many others who have supported my research at MMU, a big thanks to the 2<sup>nd</sup>, 6<sup>th</sup> and 7<sup>th</sup> floor technical staff, the fantastic post-grad students from all departments and the many academic staff I've met and worked with. Thank-you also, to Dr Michael Flynn for the meteorological data. Some special thanks are in order for all fellow employees of the students' union, for the comic relief if nothing else. Not forgetting the staff and students at UFPR and Wits, and a big thanks to the Potgieters, the Vermaaks and the Godois for welcoming me into your homes in your respective countries.

Lastly, my friends and family, to those whom got me to the point in my life where I could start a PhD and to the support you've shown me since, long phone calls, constant text messages and fleeting visits. For Amelia, looks like I proved you right.

## Chapter 1.

# Introduction, Aims and Objectives

*This chapter serves as an introduction to this project, providing a succinct overview of the current advancements in the topic of air quality, with a particular focus on the input from urban road dust. The chapter concludes by outlining the aims and objectives of this project.*

## 1.1 Introduction

Environmental particles of airborne size are of importance due to their impact on human health. There is a wealth of evidence to suggest that particles of respirable and inhalable size are linked to adverse health effects on humans. The World Health Organisation (WHO) suggests that particulate matter (PM) is responsible for 8% of lung cancer deaths, 5% of cardiopulmonary deaths and 3% of respiratory infection deaths (WHO 2009). This is underpinned by cohort and epidemiology studies published in scientific journals, linking mortality to PM (Dockery *et al.* 1993; Villarubia *et al.* 2012; Stockfelt *et al.* 2017)

During the latter part of the 20<sup>th</sup> century, tailpipe emissions from road vehicles were acknowledged as the biggest contributor to urban pollution (Riccio *et al.* 2016). Accordingly, scientific research and policy geared itself toward reducing tailpipe emissions for private and commercial vehicles, to the point where cars with zero tailpipe emissions are prevalent (Sperling and Gordon 2009; Ozilgen 2017), leading to a sharp decline in the contribution of tailpipe emissions to PM (Thorpe and Harrison 2008; Mathissen *et al.* 2011). This trend is expected to increase further with new diesel cars and vans being banned from sale in the U.K as of 2040 (DEFRA 2017). The diminishing influence tailpipe emissions have on air pollution has led to more emphasis being placed on other major contributors to airborne particulates, possibly the most significant being road dust (RD) (Rexeis and Hausberger 2009; Kumar *et al.* 2013a).

It is well documented that RD makes up a considerable portion of total suspended particles, believed to be in some cases up to 74% (Hien *et al.* 1999;

Harrison *et al.* 1997). Further research indicates that RD is the largest and second largest contributor to particulate matter with an aerodynamic diameter  $<10\mu\text{m}$  ( $\text{PM}_{10}$ ) and particulate matter with an aerodynamic diameter  $<2.5\mu\text{m}$  ( $\text{PM}_{2.5}$ ), respectively (Landis *et al.* 2017).

Early research on the topic of atmospheric particles correlated PM mass concentrations and numbers of particles with diseases of a cardiovascular, pulmonary and upper respiratory nature (Spengler *et al.* 1980; Quackenboss and Leibowitz. 1989). During the last decade, focus has shifted direction towards the chemical composition of these particles (soot, black carbon, organic carbon, polycyclic aromatic hydrocarbons (PAHs), inorganic elemental) (Kendal *et al.* 2001). Of late, however, the importance of the chemical structure of these particles has been recognised as it is ultimately the microchemical surface reactions between particles and body cells that determine the toxic, carcinogenic and mutagenic risks (Chen *et al.* 2010; Rohr *et al.* 2011), with metal components being heavily implicated in this process (Duong and Lee 2009). While it is well acknowledged that RD is a large contributor of metals to PM, it certainly appears that the lack of any research on the chemical microstructure of RD particles amounts to a large gap in the knowledge of this field. Current research on RD frequently uses a risk assessment equation to characterise risk of exposure to bulk concentrations of metals present (Tang *et al.* 2017; Masto *et al.* 2017), however this simply assumes all metals are 100% bioaccessible and risk assessment equations are inadequately applied to RD. *In vitro* studies are increasingly utilised to overcome this problem of bioaccessible concentrations of metals (Li *et al.* 2017). Little consideration,

however, is given to ensure the appropriate size particles are analysed or that the simulated bodily fluids are properly analogous to those present in the human body.

The primary focus of this project is to gain a comprehensive understanding of harmful metal contamination in respirable and ingestible particles present in urban road dust (Manchester, UK). Furthermore, the risk that ingestion and / or inhalation of these particle could pose to human health will be investigated by developing a fine-tuned risk assessment model utilising *in vitro* data. The bulk analysis and bioaccessibility studies focus on Cr, Cu, Fe and Pb. These four metals are of particular interest because of their abundance as environmental pollutants and their acknowledged impact on health. Cr and Pb are commonly found in a wide range of studies addressing the impact of metal pollutants on health (Gondal *et al.* 2015; Fu *et al.* 2015; Liu *et al.* 2014). Cu and Fe are both heavily implicated in the Fenton reaction (Godoi *et al.* 2016) as well as having significant input to RD from the earth's crust and anthropogenic sources (Potgieter-Vermaak *et al.* 2012a).

The study will feature seasonal collections of road dust (RD) over a period of two years. The analytical techniques used over the course of this research will determine the bulk elemental concentrations of Cr, Cu, Fe and Pb, analysis of individual particles, the bioaccessibility of these metals and a comprehensive risk assessment. In addition, a case study reporting the abundance and bioaccessibility of mercury from three different international sites, Manchester U.K., Johannesburg, South Africa and Curitiba, Brazil, is presented. The case study intends to substantiate one of the fundamental concepts of this study,

documenting that the bioaccessibility of metals is source dependent and thus the health effects vary significantly from site to site and are dependent on the chemical structure of the pollutant rather than the bulk elemental concentration. Using this approach, a comprehensive understanding of how the chemical composition of RD influences the potential health effects to humans.

To achieve this, a number of novel methods of RD analysis will be undertaken: Firstly, a dual approach to individual particle analysis using Raman Spectroscopy and computer controlled scanning electron microscopy. Quantification of hexavalent chromium in RD will also be a novel feature. Additionally, this study will expand on a method published by Boisa *et al.* (2014) to investigate the possibility of using <38 µm RD fractions as a proxy for the documented inhalable <10 µm fraction in a novel fashion. Finally, an adaptation of the USEPA inhalation risk assessment calculation will be reported and justified for use on metal contaminants in RD. Completion of these goals will contribute a valuable portion of knowledge to the field.

## **1.2 Aims and Objectives**

It is hypothesised that the chemical form in which metals are present in environmental particles is the main factor determining its fate in the environment and humans. To test this hypothesis, the aims of this study are:

- I. To gain a comprehensive understanding of the metal composition of individual inhalable and ingestible RD particles.
- II. To elucidate the bioaccessibility of inhalable and ingestible particles.

- III. Develop an appropriate risk assessment methodology for RD by modifying existing approaches.
- IV. To apply such methodologies to a case study of the human inhalation exposure to Hg in RD in three cities around the world.

These aims will be carried out objectively as described below, where numeric bullet points correspond to the respective numeric bullet points of aims above:

- I. Assessing bulk metal concentrations and the individual particle assemblage of metals in RD using ICP-OES, SEM-EDX and Raman Spectroscopy, contributing to new knowledge by describing inhalable and ingestible individual particle structure and chemical composition. Justifying the use of RD particles for inhalation estimates by showing that small size fractions of RD can be used as a proxy for inhalable sized fractions in a novel fashion.
- II. Bioaccessibility will be determined for size segregated particles, collected seasonally, by modelling the ingestion using the BARGE method and inhalation route using artificial lysosomal fluid (ALF).
- III. A risk assessment protocol will be developed by modifying the USEPA model so that it is more applicable to RD, thereby providing a new approach to risk assessment.
- IV. Finally, a case study reporting the abundance and bioaccessibility of mercury from three different international sites, Manchester, U.K., Johannesburg, South Africa and Curitiba, Brazil, is presented. The

case study intends to substantiate one of the fundamental concepts of this document, reporting that the bioaccessibility of metals is source dependent and thus the health effects vary significantly from site to site.

Together with a critical appraisal of other published studies, this study will show that the intricacies of particle structure have a profound effect on the potential harm to humans upon exposure to these particles via the inhalation and ingestion routes. The addition of this case study will further exemplify the need to perform comprehensive analysis of particles on a site-by-site basis to understand the potential risk to human health.

The next chapter is a critical review of literature on the topics covered in this chapter. The intention of completing a literature review is to provide a more comprehensive analysis of the gaps in research and to further necessitate the rationale of this study.

## Chapter 2.

# Literature Review

*This chapter provides a critical review on the topic of air pollution and the sizeable influence which road dust has on this field. This chapter will guide the reader to gaps in the knowledge on this topic and support the aims of this study outlined in chapter 1*

## 2.1 Literature Review Introduction

Air quality is of significant importance to the majority of the world's population for a variety of reasons (health implications, visibility, climate change, etc.). For example, the World Health Organisation (WHO) estimates that in 2012, 7 million premature deaths were caused by ambient air pollution worldwide (WHO 2014). Forty thousand premature deaths are believed to occur in the U.K. as a result of outdoor air pollution (Royal College of Physicians 2016). Furthermore, it is estimated that over 80% of the world's population is exposed to pollution exceeding WHO recommended concentration levels (Brauer *et al.* 2012). To understand the impact that air quality has on human and environmental health, the nature and type of pollutants need to be defined. The scientific consensus dictates that historically there are four main outdoor pollutants, ozone, nitrogen oxides, particulate matter (PM) and, less significantly in the modern era, sulfur dioxide (Brunekreef and Holgate 2002). Sources of these pollutants are numerous, but typically comprise of industrial, domestic and vehicular emissions (Mauderly 1994; Deacon *et al.* 1997; Ghio *et al.* 2012; Bernal *et al.* 2016).

## 2.2 Particulate Matter

PM can be described as airborne particles composed of resuspended road dust, resuspended minerals, trace metals, elemental carbon, organic carbon, sulfate salts, nitrate salts, ammonium, water, pollen etc. in a solid and/or liquid phase (Cheung *et al.* 2011; Srimuruganandam *et al.* 2012). The complex nature and ability to penetrate the body, implicates PM as one of the most concerning pollutants from a public health standpoint. Ordinarily, PM is

separated further into two distinct size fractions, coarse (larger than 10  $\mu\text{m}$  aerodynamic diameter) and fine (smaller than 10  $\mu\text{m}$ ) particles. The fine fraction is further classified as particulate matter smaller than 10  $\mu\text{m}$  ( $\text{PM}_{10}$ ) and particulate matter smaller than 2.5  $\mu\text{m}$  ( $\text{PM}_{2.5}$ ).  $\text{PM}_{10}$  represents the thoracic fraction of particles, capable of reaching the lower respiratory system;  $\text{PM}_{2.5}$  represents the respirable fraction, capable of reaching the portion of the lungs where gas exchange occurs (Brunekreef and Holgate 2002). Results from cohort studies support this, indicating that long-term exposure to PM can shorten life expectancy (Pope *et al.* 2002). Perez *et al.* (2015) indicate that mortality for any medical cause increased by 0.2% (confidence interval 95%) with every 10  $\mu\text{g m}^{-3}$  incremental increase in  $\text{PM}_{10}$  over a study period of 10 years in France. Moreover, cohort studies have concluded that a significant risk persists even in areas of relatively low background PM pollution (Stockfelt *et al.* 2017). Treating these two different size fractions of PM separately is justified by findings from Lopez-Villarubia *et al.* (2012) where epidemiological evidence suggested that  $\text{PM}_{10}$  had a higher impact on respiratory mortality relative to  $\text{PM}_{2.5}$ , which had a higher impact of cardiovascular mortality. Accordingly, several public health organisations have produced guidance for concentrations at which PM can pose health risks. The aforementioned research, however, shows that these guidance mass concentrations are well above that at which measurable effects on mortality have been observed. Table 2-1 summarises guidelines from WHO, European Commission and the United States Environmental Protection Agency.

Table 2-1: Airborne particulate matter guidance according to WHO, European Commission and USEPA.

		PM <sub>2.5</sub>	PM <sub>10</sub>
WHO	24 hour mean	25 µg m <sup>-3</sup>	50 µg m <sup>-3</sup>
	Annual mean	10 µg m <sup>-3</sup>	20 µg m <sup>-3</sup>
European Commission	24 hour mean	N/A	50 µg m <sup>-3</sup> *
	Annual mean	25 µg m <sup>-3</sup>	40 µg m <sup>-3</sup>
USEPA	24 hour mean	35 µg m <sup>-3</sup>	150 µg m <sup>-3</sup>
	Annual mean	12 µg m <sup>-3</sup>	N/A

\*This figure should not be exceeded more than 35 times per year

PM<sub>10</sub> and PM<sub>2.5</sub> mass concentrations have been observed to average 154.9 µg m<sup>-3</sup> and 30.0 µg m<sup>-3</sup> respectively in Cyprus based on a daily sampling period of one year between January 2012 and January 2013 (Achilleos *et al.* 2016). Studies in northern China have indicated average PM<sub>10</sub> concentrations across four monitoring sites of 144.3 µg m<sup>-3</sup> between the years 1998 and 2009 (Chen *et al.* 2016). PM<sub>10</sub> concentrations at three different sampling sites in Lebanon averaged 54.7 µg m<sup>-3</sup>, 60.7 µg m<sup>-3</sup> and 74.7 µg m<sup>-3</sup> between May 2009 and April 2010 (Massoud *et al.* 2011). Studies in Europe indicate PM<sub>10</sub> concentrations averaged 40 µg m<sup>-3</sup> over a period of one month between October and November 2008 in Holland (Boogaard *et al.* 2010). Data is available courtesy of air quality England (AQE) which shows that in 2016 PM<sub>10</sub> concentrations on Oxford Road, Manchester averaged 27 µg m<sup>-3</sup> with a maximum daily mean of 95 µg m<sup>-3</sup> from 1<sup>st</sup> of January to 31<sup>st</sup> of July 2017 (AQE 2017).

In an attempt to adhere to guidance set out, both increasingly stringent laws and public scrutiny have led to significant advancements in approaches to reduce concentration of PM (Dahl *et al.* 2006; van Vuuren *et al.* 2011). The U.K Department of Environment, Food and Rural Affairs (DEFRA) reported that emissions of PM<sub>10</sub> in the U.K fell by 42% between 1990 and 2001 (DEFRA 2005). In the same study, however, it was reported that the contribution of resuspended matter to PM<sub>10</sub> increased, while the contribution from road transport remained steady. This has led to increased attention from the scientific community on other major contributors to airborne particulates, particularly road dust (RD) (Rexeis and Hausberger 2009; Kumar *et al.* 2013a). The next section of this review chapter exclusively focuses on the toxic nature of RD and its contribution to air pollution.

### **2.3 Road Dust as a Contributor to Airborne Particles**

As iterated in the last section of this chapter, it is well documented that a significant proportion of airborne particles are derived from RD, which has been resuspended by the action of meteorological conditions or turbulence caused by traffic (Almeida *et al.* 2006; Tanner *et al.* 2008; Thorpe and Harrison 2008). A number of studies, globally have investigated the portion of RD which makes up various size fractions of PM. This has been calculated using factor analysis of radionuclides and acid soluble elements, as demonstrated by Hien *et al.* (1999) whom indicated findings from Ho Chi Minh City, Vietnam, where resuspended road dust accounted for 74% of the total suspended particulate matter. This study cited the work of Harrison *et al.* (1997), whom calculated the proportion to be  $62 \pm 3$  % in Lahore, Pakistan. In this same study, Harrison

*et al.* (1997) found that RD made up  $32 \pm 5$  % of  $PM_{2.1}$   $\mu m$  at an urban site in Birmingham, U.K. Amato *et al.* (2009) indicated that resuspension made up 32 % of  $PM_{10}$ , 15 % of  $PM_{2.5}$  and 3 % of  $PM_1$ . This was carried out using positive matrix factorization (PMF), a factor analysis technique which uses metal concentrations as determined by ICP-AES and (assumed, but not explicitly clarified) water soluble ions as indicators. In addition to these studies, Landis *et al.* (2017) concluded that RD is respectively the largest and second largest contributor to  $PM_{10}$  and  $PM_{2.5}$ , based on a study in Alberta, Canada. This study similarly used metals to inform the PMF technique of source identification.

The results of these studies outline the necessity to consider RD an important contributor to air pollution, because of its documented toxicity. In addition, the varying degrees to which it contributes to PM outline the need to study it on a site by site basis. This supposition motivates the aims of this study, to extensively characterise RD at a specific site, and add support for the hypothesis (that RD varies site to site) by means of a case study which looks at a particular metal, mercury.

This section provides a succinct justification for RD to be considered an important contributor to air pollution. The next step is to consider the practical process of collecting RD for experimental procedures. The following section considers the approaches which have been documented in literature in a critical style, to consider the best approach for the scope of this study.

## 2.4 Sampling and Handling Techniques

RD studies generally necessitate an appropriate collection technique; important considerations for a suitable technique include gaining a representative sample and one which is free from contaminants. The majority of studies opt for collection with a plastic dustpan and brush (De Miguel *et al.* 1997; Yang *et al.* 2010; Zhang *et al.* 2012; Ma and Singhirunnusorn 2012; Acosta *et al.* 2015; Li *et al.* 2015; Wei *et al.* 2015) or by simply sweeping directly into a bag (Liu *et al.* 2014). However, use of stainless steel pans have been published (Christoforidis and Stamatis 2009). The most prominent alternative technique of sample collection is by use of vacuum cleaner (Duong and Lee 2011; Watanabe *et al.* 2013; Khanal *et al.* 2014). While the use of dustpan and brush has been criticised as potentially showing a bias against smaller particles (Robertson *et al.* 2003), the evidence to support this appears to be misquoted. Additionally, there is evidence to suggest that vacuum collection of particles can cause resuspension of particles (Woodfolk *et al.* 1993), and even when allergen trapping vacuum bags are used, particles between 0.5  $\mu\text{m}$  and 1  $\mu\text{m}$  (maximum diameter tested for) still pass through the vacuum cleaner (Vaughan *et al.* 1999). Additionally, the authors indicate that there was some concern as to the nature of these particles and that they potentially originate from the components within the vacuum cleaner. In the context of the RD studies aforementioned, which used vacuum cleaners to collect RD, only Duong and Lee (2011) mention any modification to the vacuum cleaner, which interestingly happens to be use of allergen trapping vacuum bags.

Minimising the effect of meteorological conditions is a consideration for appropriate collection, a handful of studies refrain from sampling after precipitation for a week (Ma and Singhirunnusorn 2012) or two weeks (Liu *et al.* 2014). There is evidence to suggest that this may not be the best method for capturing a representative sample of all particle sizes. Bris *et al.* (1999) show that a greater efficiency of smaller particles are collected under wet conditions using vacuum collection methods, relative to dry dust. This seems like a reasonable assertion when one considers that it has already been documented that finer particles are more easily resuspended in dry conditions (Hien *et al.* 1999).

To conclude this section, the best way to collect RD is open to discussion, however, the simple approach of using a plastic dustpan and brush appears to be the best. Chiefly as it seems to bypass as many potential contaminants as possible, particularly from metal components, whether they are from a vacuum cleaner or a metal pan. There is a significant emphasis on avoiding metal contamination of RD, particularly as the majority of studies focus on the metal components within RD, this is the topic which is addressed in the following section.

## **2.5 Bulk Geochemical and Individual Particle Approaches to Analysis of RD**

RD often consists of numerous components from a range of sources particular to any given area; crustal soil and particles from abrasive action on vehicles and road surfaces are typically the main constituents (Pant and Harrison 2013; Tanner *et al.* 2008). The anthropogenic contributors to RD result in its high

enrichment with potentially harmful metals such as As, Cr, Hg, Mn, Ni, Pb V, Zn (Schauer *et al.* 2006; Lueng *et al.* 2008; Zhao *et al.* 2012; Luo *et al.* 2012).

Elucidating the elemental profile of a substance is a key step in approaches to understanding health concerns associated with RD. Generally, metals are considered one of the key causes of chronic health effects and inhalation of resuspended RD or dust ingestion are two major routes of exposure to RD (Du *et al.* 2013). Health complications due to exposure include asthma, various cancers, brain haemorrhage etc. (Charlesworth *et al.* 2011). Table 2-2 summarises common metals associated with specific chronic health conditions.

Table 2-2: Metals found in RD and associated health effects.

Metal	Health concerns	Reference
Al	Neuropathological, neurophysical and neurochemical changes	(Miu <i>et al.</i> 2003)
Cd	Carcinogenic	(Zhang <i>et al.</i> 2009)
Cr	Carcinogenic in +6 state	(Goldbohm <i>et al.</i> , 2006)
Cu	DNA damage via Fenton reaction	(Wiseman 2015)
Fe	DNA damage via Fenton reaction	(Wiseman 2015)
Mn	Heart conditions	(Cavallari <i>et al.</i> 2008)
Ni	Carcinogenic	(Kasprzak <i>et al.</i> 2003)
Pb	Affects brain and nervous system	(Zhang <i>et al.</i> 2013)
V	Affects nervous system	(Li <i>et al.</i> 2013)
Zn	Pulmonary effects	(Mueller and Seger 1985)

Typically, the analytical process of quantitative analysis of metals requires them to be in solution, unless X-ray fluorescence spectroscopy is used (XRF) (Yang *et al.* 2010). Accordingly, dissolution in concentrated acid is necessary

prior to analysis. The majority of studies opt for a microwave assisted aqua regia digestive solution (mixed HNO<sub>3</sub> and HCl 1:3 (v/v)) (Duong and Lee 2011; Jordanova *et al.* 2014; Khanal *et al.* 2014; Padoan *et al.* 2017). However, the use of HF is common in combination with other concentrated acids such as HNO<sub>3</sub> and HClO<sub>4</sub> (De Miguel *et al.* 1997; Liu *et al.* 2014) or HNO<sub>3</sub> and H<sub>2</sub>O<sub>2</sub> (Wei *et al.* 2015) to enable the complete dissolution of silicates. However, use of a suitable certified reference material (CRM) can justify the use of any of these digestion techniques. Padoan *et al.* (2017) demonstrate this, implementing a CRM to prove appropriate extraction efficiency of target elements using aqua regia.

The majority of RD studies opting to use Inductively Coupled Plasma – Mass Spectroscopy (ICP-MS) for analysis, benefitting from the low detection limit and multi-elemental nature of the instrument (De Miguel *et al.* 1997; Zhang *et al.* 2012; Watanabe *et al.* 2013; Khanal *et al.* 2014; Wei *et al.* 2015). However, Inductively Coupled Plasma – Optical Emission Spectroscopy (ICP-OES) (Sysaolva and Szakova 2006; Liu *et al.* 2014; Zannoni *et al.*, 2016) and various types of absorption spectroscopy (Duong and Lee 2011; Ma and Singhirunnusorn 2012; Acosta *et al.* 2015) techniques have also been put to effect. While the potential for a lower limit of detection associated with ICP-MS make it seem like a more attractive technique, the reality is that the metal concentrations in RD, particularly those commonly analysed, are abundant enough for this not to be a concern. ICP-MS can also be a problematic analysis technique for samples of this nature where a high percentage of total dissolved solids (%TDS) exist. In RD digests, this would result in the necessity to dilute

solutions down so that %TDS are approximately 0.2 - 1 % w/w, depending on instrument (Hein *et al.* 2017). This would open up the potential to lose accuracy due to experimenter error, though the subject of serial dilutions has not been raised in any of the papers which use ICP-MS to analyse metals in RD.

While metal concentrations in RD have been shown to be linked with subchronic health conditions, it is certain that the relationship is complex. *In vivo* studies show that the composition of particles is instrumental in alterations of cardiac function. Chen *et al.* (2010) demonstrated that over a period of six months, exposure of mice to suspended particles of various origins (oil combustion, long-range transport, traffic derived, incineration etc.) led to adverse cardiovascular events, namely alterations in both heart rate and heart variability. Rohr *et al.* (2011) further support this hypothesis, carrying out a similar experimental protocol, implicating the role of metals from local industrial sources in the cardiovascular events. Accordingly, there has been some research geared towards elucidating metal composition of individual particles by using scanning electron microscopy with energy dispersive X-ray analysis (SEM-EDX) (Ault *et al.* 2012; Weinbruch *et al.* 2014; Niu *et al.* 2016), the former authors postulating that over the three-year study period, seasonal changes in iron rich coarse particles from anthropogenic sources could correlate with the health effects that are associated with exposure. This study therefore probes the link between properties of individual particles and health effects. While this conclusion from Ault *et al.* (2012) is interesting and aligns

with the hypothesis outlined in chapter 1 of this document, the proof of this concept is not shown within the paper, nor has it been published since.

Other approaches use Raman Spectroscopy for gaining a comprehensive assessment of individual particles (Taylor and Robertson 2009; Potgieter-Vermaak *et al.* 2012a). All these studies concerned with characterising individual particles show that there is scope for analysing particles within the interest of health. None of the studies adequately link health-orientated experimentation to this approach though. Potgieter-Vermaak *et al.* (2012a) combine the single particle approach with *in vitro* experimentation. This is an interesting and novel approach, but the dataset lacks depth and there are assumptions on inhalable particle size which may not be properly substantiated. Therefore, it seems necessary to further investigate the potential use of *in vitro* techniques to complement single particle analysis. This represents a significant gap in the literature which this study aims to fill with use of both SEM-EDX and Raman Spectroscopy. Once a firmer grasp on the nature of individual particles is achieved, the challenge is then to appropriately determine the effects on human health. This will be done using *in vitro* approaches, these are outlined in the subsequent two sections, firstly regarding the inhalation route, then the ingestion route of entry.

## **2.6 *In vitro* Techniques – Inhalation Route**

*In vitro* techniques using artificially produced solutions analogous to bodily fluids have been presented as a suitable method for modelling the effects of pollutants from both PM and RD on the human body via both the inhalation and ingestion routes (Twining *et al.* 2005; Wragg and Klinck 2007; Colombo

*et al.* 2008). Often metals leached into simulated biological fluids are quantified using spectroscopic techniques and compared directly to total metals present to give bioaccessibility of metals using equation 2-1. (Boisa *et al.* 2014a). Bioaccessibility expresses the concentration of a pollutant, which is able to leach into a biological fluid and therefore assumed to be accessible to the body, as a percentage of the total concentration of that pollutant which is present (Bower *et al.* 2017). This approach essentially normalises bulk concentrations to allow deductions to be made on the form in which a pollutant is present.

Equation 2-1: Equation for bioaccessibility of any given metal.

$$\text{Bioaccessibility (\%)} = \frac{[\text{Leachates}](\text{mg kg}^{-1})}{[\text{Acid Digestion}](\text{mg kg}^{-1})} \times 100$$

Despite this, there is a lack of any standardised technique in the literature, especially for the inhalation route. Many studies disagree on the correct type of lung fluid to use and, in particular, the correct size of particle to include and the length of appropriate exposure time.

There are several different lung fluids commonly used in the literature which are designed to mimic two distinct sections of the lungs. Firstly, the extracellular environment, deep within the lungs where lung fluid exists at a fairly neutral pH of 7.4, and secondly the more acidic fluid (pH 4.5) which inhaled particles contact during phagocytosis (Zoitos *et al.* 1997; Marques *et al.* 2011). The most commonly used variant of the more neutral lung fluid is Gamble's solution (Wragg and Klinck 2007; Colombo *et al.* 2008; Cabouche *et al.* 2011; Zereni *et al.* 2012; Potgieter-Vermaak *et al.* 2012; Lima *et al.*

2013). However, there are studies detailing modified versions of Gamble's solution which include citric acid and phosphoric acid among several other reagents (Gray *et al.* 2010). Other studies modelling the extracellular environment use modified versions of phosphate-buffered saline (PBS), adjusted to pH 7.4 (Charrier *et al.* 2011, while others opt for a simulated epithelial lung fluid (SELF), which is a more complex solution with organic, inorganic and enzyme constituents (Boisa *et al.* 2014a). Comparisons between these different lung fluids in order to disseminate the differences in these approaches are challenging. This is highlighted by the fact that metal leaching varies significantly between studies even when comparable approaches were taken. For example, bioaccessibility of Pb using Gamble's solution has been reported as high as 15-41% (Wragg and Klinck 2007) and as low as 0.3% (Potgieter-Vermaak *et al.* 2012a). One could argue that the range of sources of lead and their variation between sites is responsible for this; elements with fewer sources could provide results that are more consistent. This is illustrated in studies from Zereni *et al.* (2012) and Colombo *et al.* (2008) where platinum group elements from catalytic converters were exposed to Gamble's solution; bioaccessibility of 0.11-0.43% and 0.45% respectively were reported. One exception, however, is reported in studies by Cabouche *et al.* (2011) and Boisa *et al.* (2014a), where the same certified reference material (BCR 038) was exposed to Gamble's solution and SELF, respectively. Bioaccessibility was reported to be 3.3%  $\pm$ 0.2 and 0.3% by Cabouche *et al.* (2011) and Boisa *et al.* (2014a), respectively. Ultimately, the purpose of these fluids is to serve as an appropriate proxy for human lung fluid. Unfortunately, there is very little in the way of literature to compare these

fluids with human lung fluid. One study by Leclercq *et al.* (2017) compared water, PBS and Gamble's solution to human respiratory mucus, and concluded that Gamble's solution provides comparable results.

Studies modelling the more acidic solution tend to opt for the artificial lysosomal fluid (ALF), though there are variances in the pH used, pH 4.3 (Wiseman and Zereni 2014) pH4.4 (Zereni *et al.* 2012), pH4.5 (Colombo *et al.* 2012; Potgieter-Vermaak 2012a; Witt *et al.* 2014). Table 2-3 details the composition of the four extracellular lung fluids and the ALF.

Table 2-3: Compositions of lung fluids.

	Gamble's solution (Marques <i>et al.</i> 2011) (g/L)	Modified Gamble's solution (Gray <i>et al.</i> 2010) (g/L)	Modified PBS (Charrier <i>et al.</i> 2011) (mM)	SELF (Boisa <i>et al.</i> 2014a) (g/L)	ALF (Marques <i>et al.</i> 2011) (g/L)
pH	7.4	7.4	7.2-7.4	7.4 ±0.2	4.5
Sodium chloride	6.019	6.8	114	12.04	3.21
Potassium Chloride	0.298	-	-	-	-
Magnesium chloride	0.095	-	-	0.4	0.05
Disodium hydrogen phosphate	0.126	-	7.8	0.3	0.071
sodium sulfate	0.063	-	-	0.144	0.039
calcium chloride dihydrate	0.368	-	-	0.512	0.128
sodium acetate	0.574	0.58	-	-	-
sodium hydrogen carbonate	2.604	2.3	-	5.4	
sodium citrate dihydrate	0.097	-	-	-	0.077
ammonium chloride	-	5.3	-	-	-
Phosphoric acid	-	1.2	-	-	-
Monosodium phosphate	-	1.7	-	-	-
sodium carbonate	-	0.63	-	-	-

Potassium hydrogen phthalate	-	0.2	-	-	-
Glycine	-	0.45	-	0.752	0.059
Sulfuric acid	-	0.51	-	-	-
Citric acid	-	0.42	0.3	-	20.8
Potassium phosphate	-	-	2.2	-	-
Ascorbic acid	-	-	0.2	0.036	-
L-glutathione	-	-	0.1	0.06	-
Uric acid	-	-	0.1	0.032	-
Potassium chloride	-	-	-	0.596	-
Albumin	-	-	-	0.52	-
Cysteine	-	-	-	0.244	-
DPPC	-	-	-	0.2	-
Mucin	-	-	-	1	-
Sodium hydroxide	-	-	-	-	6
Sodium tartrate	-	-	-	-	0.09
Sodium lactate	-	-	-	-	0.085
Sodium pyruvate	-	-	-	-	0.086

Another consideration for appropriate modelling of the inhalation route is the length of time particles should be exposed to lung fluids. General uncertainty amongst the scientific community, as well as documented variability of particle residence time within the lungs (depending on the individual's health Sturm 2013) usually results in a range of exposure times being modelled. For example, 4 - 24 h (Charrier *et al.* 2014), 2 - 630 h (Wragg and Klinck 2007) 1 h – 30 days (Colombo *et al.* 2008) 15 min – 72 h (Cabouche *et al.* 2011) 1 h – 28 days (Potgieter-Vermaak *et al.* 2012a). *In vivo* studies on rats indicate that 65-90% of particles are cleared within 24 h (Hoffman and Asgharian 2003).

A final consideration concerning appropriate modelling of the inhalation route is the correct size of particles to be used. Many studies opt for particles in the range of PM<sub>10</sub> and PM<sub>2.5</sub> for assessing the bioaccessibility of metals in lung

fluid, as it is believed that particles of this size are more likely to be inhaled (Dias da Silva *et al.* 2015; Zereni *et al.*, 2012). One distinct limitation, however, is the liquid to solid ratio ( $\text{mL g}^{-1}$ ), which is far higher than recommended elsewhere (Hamel *et al.* 1998; Twining *et al.* 2005; Wragg and Klinck 2007), all of whom based their estimates on comparability to the *in vivo* exposure. To overcome this, the use of larger RD particles for assessing bioaccessibility of metals via the inhalation route is common, with RD  $<20 \mu\text{m}$ ,  $<63 \mu\text{m}$  and  $<37 \mu\text{m}$  being used (Schaidler *et al.* 2007; Potgieter-Vermaak *et al.* 2012a; Guney *et al.* 2017). Despite the inability of large particles to enter the deep lungs where the more acidic lung fluid environment exists (Davies and Feddah 2003), RD aggregates can be broken down by meteorological conditions or vehicular turbulence (Thorpe *et al.* 2007). Furthermore, particle numbers increase with decreasing size (Kong *et al.* 2012), accordingly one could argue that RD fractions  $<20 \mu\text{m}$ ,  $<63 \mu\text{m}$  and  $<37 \mu\text{m}$  etc. are representative of inhalable particles. The uncertainty regarding the presence of RD as aggregates, and the representation of inhalable particles in larger fractions is something which will be addressed in this study by exhibiting how fractions of RD which can be swept from the road represent those which become airborne and are of inhalable size.

## **2.7 *In vitro* Techniques – Ingestion Route**

Similarly to the inhalation route of exposure, there are several different documented techniques for modelling human exposure to pollutants via the ingestion route. Several studies opt for a simple method, exposing either PM or RD to hydrochloric acid (Bavec *et al.* 2018) or  $0.4 \text{ mol dm}^{-3}$  glycine adjusted

to pH 1.5 with hydrochloric acid (Wang *et al.* 2016) to model the leachability of metals in the stomach. Other studies also include fluids designed to simulate the intestinal phase following the stomach phase (Wang *et al.* 2013; Huang *et al.* 2014; Li *et al.* 2017). There is also growing support for the universal BARGE method (UBM) outlined by Wragg *et al.* (2011) in which particles are exposed to artificial saliva, artificial gastric fluid, artificial duodenal fluid and artificial bile sequentially to simulate the mouth, stomach and intestines. This procedure has been implemented for use with soils and road dusts in the literature (Okorie *et al.* 2012; Reis *et al.* 2014; Goix *et al.* 2016; Bourliva *et al.* 2017). *In vivo* support for the BARGE method has also been published (Denys *et al.* 2012), whom compared the BARGE method of bioaccessibility of Sb, Ca and Pb from soils with the juvenile swine physiological model, assessing bioaccessibility of the same metals. The juvenile swine physiological model has been deemed an accurate representation of human gastrointestinal bioaccessibility (Weis and LaVelle 1991; Rees *et al.* 2009), however is not preferred in this study because of the surrounding ethical issues and financial costs.

There is also disagreement in the literature as to the size of particles which can appropriately be used for modelling the ingestion route of exposure. Ingestion of particles, especially by children, is usually assumed to happen via the hand to mouth process described by Duggan *et al.* (1985), where particles of up to 250  $\mu\text{m}$  adhere to the hands when in direct contact with soil. Other studies quote particle sizes appropriate for the hand to mouth process at up to 125  $\mu\text{m}$  (Hamel *et al.* 1998; Casteel *et al.* 1997). This seems unlikely to be

appropriate when considering ingestion of RD, but has been used in the literature to justify characterisation of metals within particles <250 µm (Okorie *et al.* 2012; Rodrigues *et al.* 2014). Other studies on gastrointestinal bioaccessibility of RD restrict themselves to smaller particles, assuming that exposure takes place through direct ingestion or via mucociliary cleansing (Gradon *et al.* 1996). Accordingly, RD particles <63 µm are commonly used although <22 µm ± 13.25 µm, <10 µm and <2.5 µm have also been published (Li *et al.* 2017; Wang *et al.* 2016; Zereni *et al.* 2017; Kong *et al.* 2011). Many of these studies cite the fact that particles up to and over 100 µm can be transported by suspension (Kennedy and Hines 2002; Yeung *et al.* 2003; Tanner *et al.* 2008). Accordingly, this study will test a number of size fractions of particles as a means to provide a valuable contribution to this area of research. This process could facilitate comparisons between studies where different size particles have been used.

This section and the one preceding outline the approaches to determining bioaccessibility of potentially harmful metals and the *in vitro* techniques used to determine this. To contextualise these quantities of bioaccessible metals in terms of human health, an approach whereby one can estimate the subsequent effects is essential. The next section critically appraises the available literature on risk assessment to find the best approach for the results of this study.

## **2.8 Risk Assessment**

Risk assessment is widely used to contextualise pollutant contamination within PM, RD and soils, with a view to assessing their impact on human health (Shi

*et al.* 2011; Wang *et al.* 2013; Singh and Gupta 2016; Mastro *et al.* 2017; Ma *et al.* 2017). Risk assessment can be defined as the process of identifying hazards and calculating their probable adverse effects with respect to exposure (Posthuma *et al.* 2008).

The most commonly used model for PM, RD and soil is based on the Risk Assessment Guidance for Superfund (RAGS): part A (USEPA 1989), which published a series of equations to calculate exposure and subsequent health risks associated with volatile chemicals and suspended soils from contaminated sites. The original documentation details a seven-step process beginning with a preliminary site inspection and ending with a five-year review in an attempt to standardise the process. This seven-step process was later adapted in the EPA Soils Screening Guidance Superfund (USEPA 1996) including a conceptual site model (CSM) as step 1. The model proposed by the USEPA is believed to be the most advanced (Cachada *et al.* 2016), and is certainly the most cited in literature, however various other countries including the UK, Canada and perhaps most notable the Netherlands have developed their own models (Canlon 2007). Despite the different approaches, the goal of each is ultimately the same, namely to assess the impact of pollutants on human health.

In literature, the process of displaying a conceptual site model (CSM) is frequently forgone; the majority of studies simply allude to pollutants, exposure sources, exposure mediums, exposure routes and exposed population in introduction and methodology sections within the text. There are, however, some more explicit examples (Tielemans *et al.* 2008; Ma *et al.* 2017), which

provide evidence of a more considered approach by conducting a CSM. Once the pollutants and the route(s) of exposure have been determined, an average daily dose (ADD) can then be calculated for a specific pollutant via either the inhalation, ingestion or dermal absorption exposure routes. Equations 2-2, 2-3 and 2-4 outline the calculations for ADD via each of these exposure routes. Table 2-4 summarises the parameters of each of the three equations (Shi *et al.* 2011; Chen *et al.* 2014; Liu *et al.* 2014; Lu *et al.* 2014; Ma *et al.* 2017).

Equation 2-2: Average daily dose of pollutant via the ingestion route.

$$ADD_{ing} = \frac{C \times R_{ing} \times CF \times EF \times ED}{BW \times AT}$$

Equation 2-3: Average daily dose of a pollutant via the inhalation route.

$$ADD_{inh} = \frac{C \times R_{inh} \times EF \times ED}{PEF \times BW \times AT}$$

Equation 2-4: Average daily dose of a pollutant via the dermal absorption route.

$$ADD_{derm} = \frac{C \times SA \times CF \times SL \times ABS \times EF \times ED}{BW \times AT}$$

Equation 2-5: Lifetime average daily dose for carcinogens via the inhalation route.

$$LADD_{inh} = \frac{C \times EF}{AT \times PEF} \times \left( \frac{R_{inh\ child} \times ED_{child}}{BW_{child}} + \frac{R_{inh\ adult} \times ED_{adult}}{BW_{adult}} \right)$$

Table 2-4: Parameters used in equations 2, 3 and 4.

Component	Definition (units)
ABS	Dermal absorption factor
AT	Averaging Time (days)
BW	Body Weight (kg)
C	Concentration of contaminant (mg kg <sup>-1</sup> )
CF	Conversion factor (kg mg <sup>-1</sup> )
ED	Exposure duration (years)
EF	Exposure frequency (days year <sup>-1</sup> )
PEF	Particle emission factor (m <sup>3</sup> kg <sup>-1</sup> )
R <sub>ing</sub>	Ingestion rate (mg day <sup>-1</sup> )

R <sub>inh</sub>	Inhalation rate (m <sup>3</sup> day <sup>-1</sup> )
SA	Surface area (cm <sup>2</sup> )
SL	Skin adherence factor (mg cm <sup>-2</sup> )

A non-carcinogenic hazard quotient (HQ) can then be calculated by dividing the ADD by a reference dose (RfD) specific to a chemical. The concept of RfD is adapted from the no-observed-adverse-effect-level (NOAEL) evaluations used to characterise drug safety (Dorato and Englehardt 2005). NOAELs are derived from either epidemiology studies on humans, or *in vivo* studies, RfDs are then calculated by dividing an NOAEL value by an uncertainty factor, which is assigned with reference of the quality of research which went towards the NOAEL value (Barnes and Dourson 1988). In the context of risk assessment of metal exposure, the reference dose acts as an exposure to metals below which the health concerns of the chemical are not a concern. Therefore, a HQ<1 is not considered a health concern. HQs from each of the three exposure routes can then be summed to give a hazard index value (HI), again, a value below 1 is not considered a concern. Carcinogenic risks are calculated by multiplying the lifetime average daily dose (LADD) from a given exposure route by an appropriate slope factor, whereby a resulting value of >1x10<sup>-6</sup> is deemed significant (Ferreira-Baptiste and De Miguel 2005; Chen *et al.* 2014; Singh and Gupta 2016; Samiksha *et al.* 2017; Masto *et al.* 2017). The slope factor represents a 95% confidence limit on the increased likelihood of cancer risk over a lifetime exposure and serves as an extrapolation of the RfD calculated from an appropriate epidemiology or *in vivo* study (Kar *et al.* 2012).

One assumption of the  $ADD_{inh}$  and  $LADD_{inh}$  calculations use here is the particle emission factor (PEF) parameter. The PEF value ( $1.32 \times 10^9 \text{ m}^3 \text{ kg}^{-1}$ ) was derived for the purpose of representing airborne quantities of soil contaminants from sites where vegetation makes up 50% of the surface coverage (USEPA 2000). The applicability of this PEF value to urban RD samples therefore questionable, as the sites, certainly in this study, have no vegetation. Despite this, it has been used in literature to assess the risks associated with metals in urban RD (Du *et al.* 2013; Ma and Singhirunnusorn 2012; Ferreira-Baptiste and De Miguel 2005). This therefore presents a problem with the risk assessment calculation which will be addressed in this document in a novel fashion.

Risk assessment in this manner is frequently applied to metals in RD, based on total concentrations of metals (Chen *et al.* 2014; Liu *et al.* 2014; Tang *et al.* 2017; Mastro *et al.* 2017) with various cases of significant carcinogenic and non-carcinogenic risks reported. One drawback to this approach is that *in vitro* studies have shown that only a portion of the total metals present is bioaccessible and thus using the total acid-soluble or total overall concentration inevitably results in an overestimate of the actual risk. Taking the bioaccessible portion into account is an approach which has been attempted before; in each case only the ingestion route of bioaccessibility was modelled, using the simplified techniques, unsupported by *in vivo* experimentation (Hu *et al.* 2011; Li *et al.* 2015; Li *et al.* 2017). This is another example of a gap in available scientific literature, again this study will address this in latter sections of this document, by using ALF to simulate lung fluid and

the UBM method to simulate the gastrointestinal route. Another modification to the usual protocol of including  $ADD_{ing}$ ,  $ADD_{inh}$  and  $ADD_{derm}$  to produce a HI featured in this study will be the dispensation of the  $ADD_{derm}$ . While this study is able to use *in vitro* techniques to develop risk assessment protocol concerning the  $ADD_{ing}$  and  $ADD_{inh}$ , the  $ADD_{derm}$  route is complex and difficult to modify. Additionally, studies have shown that  $ADD_{derm}$  makes no significant contribution to HI of Cr, Cu, Fe and Pb (Ferreira-Baptiste and De Miguel 2005; Chen *et al.* 2014; Mastro *et al.* 2017).

## **2.9 Literature Review – Closing Remarks**

This chapter has provided a detailed overview of the input RD has on air pollution in urban areas, in which gaps in the research on this topic have been pointed out explicitly. These gaps coincide with the aims as pointed out in chapter one of this document. Moving forward, the next chapter will cover the experimental approaches designed to achieve the aims of this study.

### Chapter 3.

# Experimental Methodology

*This chapter covers the experimental approaches undertaken in this study as a means to complete the aims as outlined in chapter 1 of this document.*

### 3.1 Site and Sample Handling

Road dust was collected from Oxford Road, Manchester, UK, one of the main routes into the city, passing along two of the largest universities in the UK supporting over 70,000 students. Oxford Road is heavily laden with cars, buses, motorbikes, HGVs and taxis with an average motor vehicle traffic density of 11,900 vehicles day<sup>-1</sup> between 2012 and 2016 (U.K. Department for Transport 2017). In addition to this, the road is intersected by the Manchester Oxford road railway station and the M60 raised motorway, which has an average motor vehicle traffic density of 85,500 vehicles day<sup>-1</sup> between 2012 and 2016 (U.K. Department for Transport 2017). The highly trafficked nature of Oxford road gives it the potential to be a highly anthropogenically polluted area. This is a cause for concern for those working and commuting via Oxford road, particularly the many pedestrians and cyclists (average cycle density of 510 bicycles day<sup>-1</sup> between 2012 and 2016 (U.K. Department for Transport 2017)). Figure 3-1 shows the location of the study site within Manchester and the U.K., red points on the middle diagram show train stations in Manchester.

Sampling was carried out on the road below the curb of a traffic island, Oxford Road, Manchester, UK using a plastic dustpan and brush, a similar process to that carried out by Charlesworth and Lees (1999). One sampling site was deemed to be representative of the 550 m stretch of road by rigorous analysis and statistical testing carried out previously on Oxford Road (Barrett 2010). Sampling took place seasonally over two years, starting in spring 2013 and ending in winter 2014/15, giving a total of 8 sampling campaigns. These sampling campaigns will be designated as Sp for spring (March to May), Sum

for summer (June to August), Aut for autumn (September to November), and Win for winter (December to February). Approximately 10 kg of RD was collected from the sampling site in each campaign and air dried at room temperature ( $21^{\circ}\text{C} \pm 3^{\circ}\text{C}$ ). Samples were placed in clean brown paper bags on a clean bench, topped with Benchkote<sup>®</sup> polyethylene laminated Whatman<sup>®</sup> paper and left to dry. An aliquot of each RD sample, representative of the rest of the RD sample, was sorted into a smaller brown paper bag. This was weighed daily until the mass stabilised, indicating that the aliquot, and hence the rest of the sample, was dry. Typically, this process took up to three weeks depending on relative moisture of RD samples.

The resulting dry sediment was separated into different grain size fractions using standard sieve methods. Stainless steel woven wire mesh sieves (200 mm diameter; 50 mm depth: to ISO 3310-1:2000; BS 410-1:2000) were used. The three grain-size fractions analysed in this study,  $<38\ \mu\text{m}$ ,  $63\text{-}38\ \mu\text{m}$  and  $125\text{-}63\ \mu\text{m}$  were attained using sieves of mesh sizes 0.125 mm (US std 120), 0.063 mm (US std 240) and 0.038 mm (US std 400). All equipment used was thoroughly washed to ensure that no metal contamination occurs between samples. A solution of 2% nitric acid was used to clean all non-metal equipment.

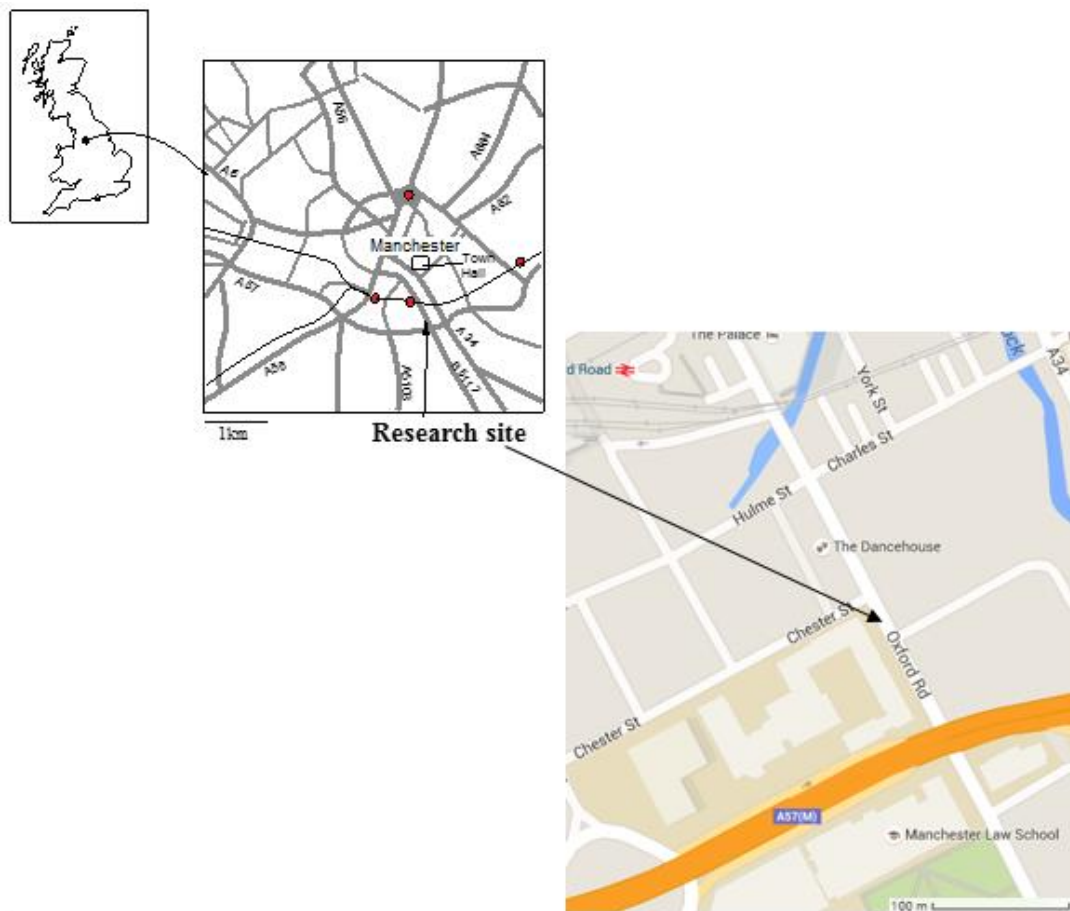


Figure 3-1: Road dust sampling site, Oxford road, Manchester, U.K.

### 3.2 Bulk Geochemistry

As discussed in chapter 1, Cr, Cu, Fe and Pb were identified as elements of specific interest regarding deleterious effects of inhalation and ingestion of RD. Prior to *in vitro* analysis carried out in the context of this study, it is necessary to analyse the pseudo-total amount of each of these elements present in RD. To quantify Cr, Cu, Fe and Pb, 500 mg  $\pm$  10 mg of each sample was accurately weighed in triplicate and digested with aqua regia (7.5 ml HCl, 2.5 ml HNO<sub>3</sub>). This process was facilitated with a 1600W CEM Mars 5 Microwave equipped with Teflon digestion tubes, this procedure is similar to many RD studies

published in literature (Duong and Lee 2011; Kumar *et al.* 2013b; Jordanova *et al.* 2014; Khanal *et al.* 2014; Padoan *et al.* 2017). Analysis was carried out using a Varian Vista MPX ICP-OES with SeaSpray nebulizer. Initial system stability checks were carried out with a 5 mg dm<sup>-3</sup> solution of manganese during the torch alignment whereby the upper values must be in excess of 300,000 counts per second, sample analysis exclusively used the axial position. A four-point linear calibration was achieved for each element, using matrix-matched standard solutions, whereby a calibration coefficient of >0.99 for all elements was determined. Five replicates were carried out per sample.

Method verification was carried out using a certified reference material (CRM), river clay sediment LGC6139. 500 mg ± 10 mg of CRM was weighed out in triplicate, digested using aqua regia and analysed using ICP-OES, this is the same technique used for the samples. Matrix matched blanks were also analysed with the samples to ensure origin of metals was from RD and not reagents/materials used in digestion process. The results of this method verification are presented in results section 4.2.

### **3.3 Individual Particle Analysis**

To determine the mineral composition of the RD samples, single particle analysis (SPA) was performed using micro-Raman Spectroscopy and computer-controlled SEM-EDX. SPA can enable a more comprehensive insight into the composition of RD relative to simple bulk analysis. It allows observations to be made regarding the incidence of different minerals and hence oxidation states of metals in a grain fraction, it allows for observations

on which elements are found with which within a particle ergo, one can cluster particles.

### **3.3.1 CC-SEM-EDX**

A Zeiss Supra 40VP field emission computer controlled scanning electron microscope with energy dispersive X-ray microanalysis (CC-SEM-EDX) was used to determine metal composition of single particles from each sample. Samples were mounted on silver foil (Alfa Aesar U.K, 0.127 mm thick, 99.9 % metal purity) using a process of tipping a small number of particles onto a laminated piece of paper, shaken gently to distribute them over a small area so that particles are adequately separated, then pressing a stub coated with silver foil onto the particles. A backscattered electron detector was used at 1000x magnification, 25 kV and working distance of 15 mm to acquire an image of the stub surface. The heavy elemental background from the silver foil enables a high contrast black and white image to be obtained. EDAX Genesis software is used to control the instrument, generating a series of images spiralling out from the centre of the stub, essentially mapping it. The program recognises particles based on their dark colour relative to the background, after a greyscale sensitivity was programmed by the operator beforehand. Each particle is exposed to an acquisition of 15 seconds, giving metal concentrations as percentage of each particle based on signal peaks at discreet KeV values indicative of either  $K\alpha$  emissions of  $L\alpha$  emissions. This procedure also uses the precise magnification value to measure particle ferret diameters in the x and y planes based on number of pixels. Particle size can be represented by average diameter, calculated from the two-dimensional

projection of a given particle. Equation 3-1, as used by Potgieter-Vermaak *et al.* (2012b), shows how average particle diameter is calculated for each particle. Where,  $D_p$  is average particle diameter,  $D_{max}$  is maximum feret diameter,  $D_{min}$  is minimum feret diameter.

Equation 3-1: Average particle diameter.

$$D_p = \sqrt[3]{(D_{max} \times D_{min}^2)}$$

### 3.3.2 Raman Spectroscopy

A Thermo Scientific DXR Raman microscope equipped with a 532 nm diode pumped solid-state laser and 50x objective were used. The instrument features a Thermo Scientific calibration tool which, when placed on the microscope stage, allows the user to perform a simultaneous alignment and calibration by placing the cross hairs within the eyepieces on a pinhole. The surface beneath the pinhole is able to move, switching between copper and polystyrene, to align then calibrate the laser, respectively. The alignment and calibration feature of the instrument is user initiated, then controlled by the instrument to ensure correct execution. Samples for Raman Spectroscopy analysis were prepared on 12.5 mm plastic sticky tabs (Agar Scientific, U.K) adhered to a glass slide. A small number of particles were tipped onto a laminated piece of paper, shaken gently to distribute them over a small area so that particles are adequately separated, then mounted on a sticky tab on a glass slide. The user then manually analyses particles in a serpentine pattern,

starting in the top left corner, rastering along to the right, then moving down and rastering along to the left. The benefit of carrying out this process on a glass slide is that it enables the user to observe coordinates on the slide, allowing the user to carry out analysis over several sessions if necessary. Two hundred particles per sample were analysed, this quantity is deemed adequate to be representative of a sample. In the literature, analysis of 50 particles is generally deemed representative (Potgieter-Vermaak *et al.* 2012b; Jentsch *et al.* 2013).

Analysis of resulting spectra was carried out using the in-built Thermo Scientific Spectral Database as a first estimate. Further verification of spectra was carried out using CrystalSleuth computer program, which uses the RRUFF database (RRUFF.info). CrystalSleuth has been well used as a method for elucidating the composition of minerals (Lammers *et al.* 2012; Wang *et al.* 2017; Kereszturi *et al.* 2017). As outlined in section 2.6, RD usually exists as aggregates, as a result of this spectra of particles often included bands from more than one distinct mineral. Incidents where this occurred and the bands overlap can present a challenge, however using the WiREcomputer program, it is possible to deconvolute the bands and gain values for each band under what appears to be a curve.

### **3.4 Chromium (VI) Quantification**

To gauge a further understanding of the toxic nature of RD, it is important to consider the toxicity of each given metal. While the role of Cu, Fe and Pb on human health is well documented and the mechanisms well known, Cr presents a different problem. Two of the most commonly occurring oxidation

states of Cr are Cr (III) and Cr (VI). Chromium (III) is a dietary requirement, playing a role in metabolism of lipids and proteins (Florence *et al.* 1980), whereas Cr (VI) is known to be carcinogenic, causing DNA strand breaks and producing 8-hydroxyguanosine, indicative of oxidative stress (O'Brien and Kortenkamp 1995; Elci *et al.* 2010). While quantification of Cr (VI) in PM has been demonstrated (Borai *et al.* 2002; Swietlik *et al.* 2011), there are currently no studies investigating Cr (VI) within road dust.

As we identified sporadic occurrences of various forms of chromate ions with the micro Raman analysis, it was decided to investigate the Cr (VI) content of the RD samples. Isolation of chromium (VI) in RD requires a method which solubilizes chromium (VI) while precipitating out chromium (III), all the while avoiding any conversion of either native species. The method used was based on EPA method 3060A (USEPA 1996). 25 ml of digestion solution (0.5 M NaOH, 0.3M Na<sub>2</sub>CO<sub>3</sub>) was mixed with 250 µl of phosphate buffer and 400 mg of MgCl<sub>2</sub>. The addition of Mg<sup>2+</sup> in phosphate buffer inhibits the oxidation during the digestion procedure. One gram of road dust was then added to the solution, mixed unheated for 5 minutes and mixed at 92.5°C ± 2.5°C for one hour. The solution was filtered and made up to 50 ml with deionised water. A Graphite Furnace Atomic Absorption Spectroscopy (GFAAS) was used to quantify Cr (VI). The protocol used a Varian AA2047 GFAAS, complete with autosampler which accurately aspirates 15 µl of sample into a graphite tube, the instrument's temperature control program ensures accurate ashing and atomising temperatures at 800°C and 2100°C, respectively. Once the sample was atomised, light from a hollow cathode lamp at a wavelength of 429 nm

was sent through the tube to the detector where background absorption was subtracted from atomic and background signal (Compton 2006).

Method development was carried out to ensure the accuracy of this method, in particular to assure the conversion between oxidation states does not occur. This was done by adding a combination of aqueous and solid Cr (VI) and (III) to the digestion solution with acid washed sand. Results of this quality assurance are presented in results section 4.5.

### **3.5 PM<sub>10</sub> Separation**

As indicated in the literature review section 2.1.6, there is a degree of uncertainty in the scientific community as to the particle sizes, which are appropriate for use with *in vitro* studies. Accordingly, the aim of this particular experiment was to see if <10 µm fraction of RD is analogous to the <38 µm fraction, and thus assess the possibility of using the larger, more abundant size fraction of RD as a proxy for PM<sub>10</sub>. This was done by first separating particles <10 µm from the <38 µm fraction, then comparing the two samples in terms of size (to verify efficiency of the separation technique), metal content and mobility of metals in simulated biological fluid.

The water deposition technique was carried out using a sedimentation-in-water process based on the principles of Stokes' law, which gives the velocity of a sphere in a viscous fluid under the force of gravity. Equation 3-2 is Stokes' law, where  $V$  is velocity of a particle;  $g$  is acceleration due to gravity;  $a$  is the diameter of a particle (cm);  $d_1$  is the density of a particle;  $d_2$  is the density of water;  $\mu$  is the viscosity of water (Haynes 2016). Density of particles was

measured to be  $3.2 \text{ g cm}^{-3}$ , as determined by a water displacement technique similar to Blake and Hartage (1986).

Equation 3-2: Stokes' law.

$$V = \frac{2ga^2(d_1 - d_2)}{9\mu}$$

The separation technique is presented in figure 3-2. The process uses a bunged  $100 \text{ cm}^3$  measuring cylinder. The distance between the  $100 \text{ cm}^3$  mark on the cylinder and the  $80 \text{ cm}^3$  mark was measured to be 3.1 cm. The time taken for particles of  $10 \text{ }\mu\text{m}$  to travel that distance is 259 s, as determined by equation 3-2.

A 2 g sample of RD was weighed into the measuring cylinder then made up to the  $100 \text{ cm}^3$  mark with deionised water. The cylinder and contents were then thoroughly agitated by hand then placed on a bench, this is shown as step a. in figure 3-2. A stopwatch was then used to time 259 s, the amount of time taken for particles larger than  $10 \text{ }\mu\text{m}$  to travel 3.1 cm, shown as step b. in figure 3-2. A  $20 \text{ cm}^3$  pipette was then inserted into the cylinder to siphon off the top 20ml of water. This process removes suspended particles  $<10 \text{ }\mu\text{m}$  from the cylinder, shown as step c. in figure 3-2. The water in the pipette, containing the  $<10 \text{ }\mu\text{m}$  particles, is then aspirated into a clean centrifuge vial, step d. in figure 3-2. The centrifuge vial and contents were then centrifuged at 2000 rpm for 15 minutes, the supernatant was then discarded, step e. in figure 3-2. The particles remaining in the centrifuge tube were then transferred to a clean weighing boat and left to dry at room temperature in a clean brown paper bag.

This process is repeated 20 times for each sample with another 20 cm<sup>3</sup> of deionised water added to the measuring cylinder before step a. to replace the 20 cm<sup>3</sup> removed at step c. on the previous iteration. The method described here is based on one described by Boisa *et al.* (2014b).

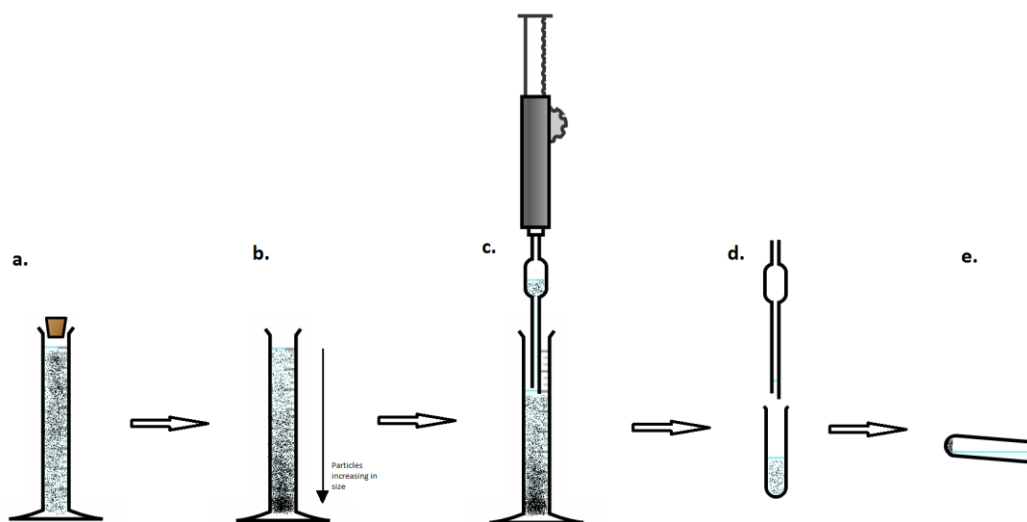


Figure 3-2: Schematic for the separation of RD by sedimentation.

Once separation was achieved, particle size distribution was carried out using SEM-EDX in the technique described here in section 3.3.2; total metal content was measured using the acid digestion protocol as described in section 3.2 and mobility of metals in ALF as described in section 4.6.1.

### 3.6 *In Vitro* Analysis

#### 3.6.1 Respiratory Route

Analyses of the leachates were carried out using the same instrumentation and parameters as the bulk metal analysis method described above,

calibration standards were matrix matched using ALF. ALF was prepared according to Colombo *et al.* (2008), where reagents listed in table 2-3 were added sequentially to deionised water, each reagent was dissolved before the next was added. The experimental protocol started with  $0.15 \text{ g} \pm 0.0015 \text{ g}$  of each RD sample being weighed out into a centrifuge vial (in triplicate), 15 ml of ALF was added to each vial, sealed and shaken by hand for 10 seconds each vial was then placed in a shaking incubator for 24 hours. On removal from the shaking incubator, samples were allowed to cool to room temperature for 10 minutes before being filtered using  $0.2 \text{ }\mu\text{m}$  Whatman® PVDF syringe filters into clean universal vials. The samples were then acidified using spectral grade  $\text{HNO}_3$  ( $310 \text{ }\mu\text{l}$ ), to achieve a 2% w/v acid solution and stored at  $4 \text{ }^\circ\text{C}$  until analysis could be performed. Analysis of the leachates was carried out using the same instrumentation and parameters as the bulk metal analysis method described in section 4.2, calibration standards were matrix matched using ALF

### **3.6.2 Gastrointestinal Route**

Gastrointestinal dissolution of metals was quantified using the universal BARGE method (UBM) (BARGE/INERIS 2010) and has been shown to be comparable to *in vivo* studies (Denys *et al.* 2012). The process involves simulation of the gastric route (GC) and the gastrointestinal route (GI). The GC route exposes RD to simulated fluids in just the mouth and stomach compartments, simulated saliva and simulated gastric fluid respectively. The GI route has the additional exposure to the intestinal compartment, modelled with simulated duodenal fluid and bile. Production of each simulated fluid required initial production of an aqueous solution of the inorganic and organic

components of each fluid separately before being combined along with enzymes. The components of the inorganic and organic solutions are outlined in table 3-1, where each number represents a mass in grams (unless stated otherwise) added to deionised water to a final volume of 250 mL. The inorganic and organic constituents of each of the four solutions were produced the day before exposure. The next day, the solutions are combined and heated to 37 °C before addition of RD. A calibrated pH meter was used to ensure the pH of each solution stayed within the strict range as described by BARGE/INERIS (2010). The entire process was scaled down, using 0.3 g of RD, rather than 0.6 g as described by BARGE/INERIS (2010), the quantity of each solution used was also halved to keep the stated liquid to solid ratio. The process of reducing the quantities in this manner has been shown not to affect the quantity of metals leached (Xia *et al.*, 2016). A schematic of how the method proceeds is displayed in figure 3-3, where the methodology that branches to the left represents the GI route and the methodology that branches to the right represents the GC route, each RD was treated in the same manner in triplicates. Analysis of the leachates was carried out using the same instrumentation and parameters as the bulk metal analysis method described above and calibration standards were matrix matched.

Table 3-1: Composition of fluids used for the UBM, each number represents a mass (g) unless stated otherwise used to make up 250 mL of the inorganic and organic solutions for each fluid.

		Simulated Saliva	Simulated Gastric Fluid	Simulated Duodenal Fluid	Simulated Bile
Inorganic	Potassium chloride	448	412	282	188
	Monosodium phosphate	444	133		

	Potassium thiocyanide	100			
	Sodium sulfate	285			
	Sodium Chloride	149	1376	3506	2630
	Calcium chloride		200		
	Ammonium chloride		153		
	Sodium hydrogen carbonate			2803.5	2893
	Potassium phosphate			40	
	Magnesium chloride			25	
	Sodium hydroxide	0.9 mL			
	Hydrochloric acid		4.15 mL	90 $\mu$ L	90 $\mu$ L
Organic	Urea	0.1	42.5	50	125
	Glucose		325		
	Glucuronic acid		10		
	Glucosamine hydrochloride		165		
Enzymes	Alpha amylase	0.0725			
	Mucin	0.025	1500		
	Uric acid	0.0075			
	Bovine serum albumin		500	500	900
	Pepsin		500		
	Calcium chloride			100	111
	Pancreatin			1500	
	Lipase			250	
	Bile				3000
Final pH		6.5 $\pm$ 0.5	1.1 $\pm$ 0.1	7.4 $\pm$ 0.2	8 $\pm$ 0.2

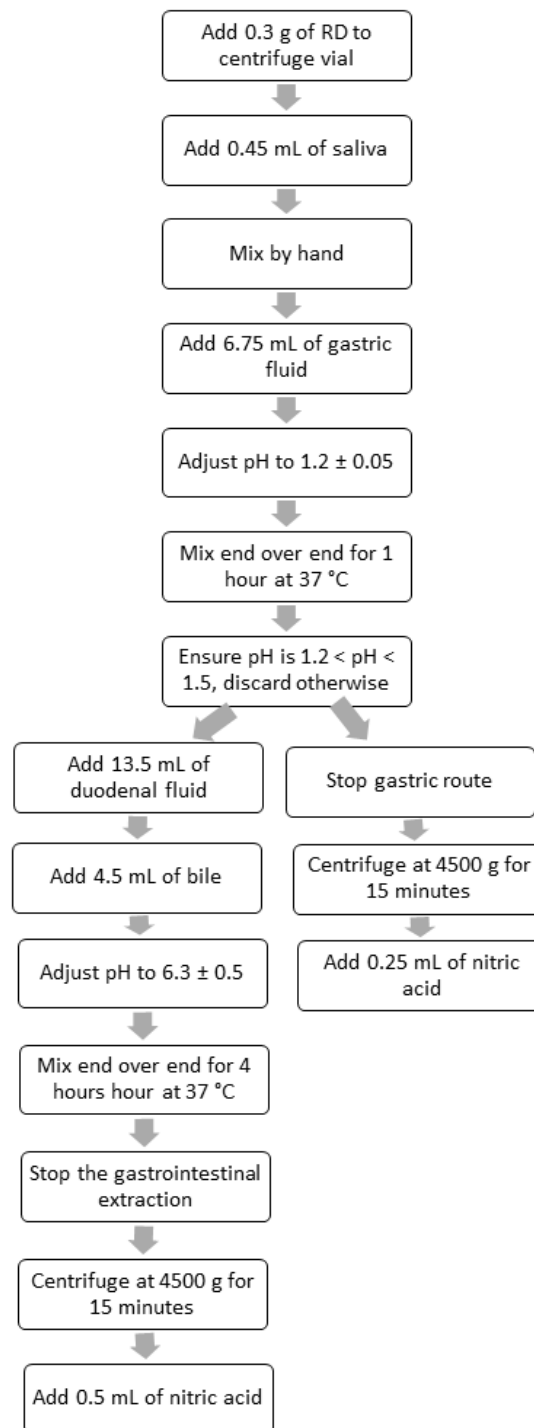


Figure 3-3: Experimental schematic for the UBM, left hand branch represents the GI route, right hand branch represents the GC route

### 3.7 Risk Assessment

The risk assessment method used for the leachate results obtained from the *in vitro* studies is based on the USEPA model (USEPA 1997), whereby the risk of detrimental health effects caused by a pollutant on an individual was calculated based on severity of exposure. Equations 3-3 and 3-4 show calculations for Average Daily Dose (ADD) of a non-carcinogenic pollutant via the ingestion and inhalation routes. Equation 3-5 shows the Lifetime Average Daily Dose (LADD) for carcinogens via the inhalation route. The parameters and values for each equation are displayed in table 3-2, several of the sources for these parameters have been cited as “this study” this indicates that either the parameter relies on experimentally determined values obtained in this research or consideration was given to derive a value appropriate for this site based on a worst-case scenario approach. It should be noted that equations 3-4 and 3-5 presented here have been adapted from equations 2-3 and 2-5 in section 2.8. The equations in section 2.8 featured a particle emission factor (PEF), which despite being used for RD in literature (Buranatrevedh 2014; Liu *et al.* 2015; Cao *et al.* 2015) is deemed to be non-representative of RD resuspension, as motivated in section 2.8. The PEF component of the equation has therefore been removed and replaced with the concentration of total suspended particles (TSP) reasoned to be derived from road dust on Oxford Road, Manchester. This was calculated with use of an Osiris monitor which collected TSP for the entirety of the study returning an average concentration of  $92.9 \mu\text{g m}^{-3}$ , this value is then multiplied the portion of TSP which RD is believed to contribute, 62% as determined by Harrison *et al.*

(1997). This term of the equation is placed as a numerator to ensure the units of  $ADD_{inh}$  and  $LADD_{inh}$  are retained. The alteration of this equation presents itself as a novelty for this research. Another novel feature of this analysis is that the risk assessment was performed on the bioaccessible portion of RD as determined by the leaching studies. Once values are inserted into Equations 3-3 and 3-4,  $ADD_{ing}$  and  $ADD_{ing}$  can be calculated. Hazard quotients (HQ) for each route of exposure can then be derived by dividing each ADD of each metal by a reference dose (RfD). The RfD value represents the threshold for which the health effects of any given pollutant can be observed (Buranatrevedh 2014; Liu *et al.* 2015; Cao *et al.* 2015). HQ values for each exposure route are then combined to obtain a hazard index value (HI). A HI greater than 1 are indicative that significant risks of non-carcinogenic health effects due to a pollutant may be observed (USEPA 2001). Regarding equation 3-5, the  $LADD_{inh}$  is multiplied by a slope factor to produce a cancer risk whereby a resulting value of  $>1 \times 10^{-6}$  is deemed significant (Ferreira-Baptiste and De Miguel 2005; Chen *et al.* 2014; Singh and Gupta 2016; Samiksha *et al.* 2017; Masto *et al.* 2017), as iterated in the literature review sections of this document. The slope factor has units of  $kg \text{ day } mg^{-1}$  and represents an upper bound approximation of the increased cancer risk based on a lifetime exposure to a carcinogen.

Equation 3-3: Average daily dose of a pollutant via ingestion route.

$$ADD_{ing} = \frac{C \times R_{ing} \times CF \times EF \times ED}{BW \times AT}$$

Equation 3-4: Average daily dose of a pollutant via inhalation route.

$$ADD_{inh} = \frac{C \times R_{inh} \times EF \times ED \times ([TSP] \times 0.62)}{BW \times AT}$$

Equation 3-5: Lifetime average daily dose for carcinogens via the inhalation route.

$$LADD_{inh} = \frac{C \times EF \times ([TSP] \times 0.62)}{AT} \times \left( \frac{R_{inh\ child} \times ED_{child}}{BW_{child}} + \frac{R_{inh\ adult} \times ED_{adult}}{BW_{adult}} \right)$$

Table 3-2: Parameters for average daily dose and lifetime average daily dose calculations

Component	Definition (units)	Adult value used	Child value used	Reference
AT	Average Time (days)	365 x ED	365 x ED	This study
BW	Body Weight (kg)	84	21	Potgieter-Vermaak <i>et al.</i> 2012
C	Concentration of contaminant (mg/kg)	Leached metal concentrations	Leached metal concentrations	This study
CF	Conversion factor (kg/mg)	1 x 10 <sup>-6</sup>	1 x 10 <sup>-6</sup>	
ED	Exposure duration (years)	24	6	This study
EF	Exposure frequency (days/year)	350	350	This study
R <sub>ing</sub>	Ingestion rate (mg/day)	200	100	USEPA 1989
R <sub>inh</sub>	Inhalation rate (m <sup>3</sup> /day)	20	5	Du <i>et al.</i> 2014
TSP	RD derived Total suspended particles (kg/m <sup>3</sup> )	5.76 x 10 <sup>-8</sup>	5.76 x 10 <sup>-8</sup>	Brown <i>et al.</i> 2015

## Chapter 4.

# Results and Discussion

*This chapter comprises the results and discussion for the Oxford Road, Manchester, UK dust samples, collected over a two-year period (2013 – 2015).*

#### 4.1 Physical Sample Characteristics

The road dust samples were handled as described in the experimental methods section of this document in section 3.1. As a recap, ~ 10 kg RD samples were collected from a traffic island on Oxford Road during a two-year period and weighed. Samples were left in brown paper bags in the laboratory until a constant mass was reached, weighed and then sieved in different size fractions, i.e. <38 µm, 63-38 µm and 125-63 µm. The masses per fraction (wet and dry) of each sample have been summarised in table 4-1. The results show that the moisture content of RD is dependent on season, with the two winter sampling campaigns containing the largest moisture content (38.45% and 28.03%). To examine how the moisture content of each RD campaign affected the distribution of mass amongst the particle size fractions, product-moment correlation coefficient was calculated using equation 4-1. Inputting continuous  $x$  and  $y$  variables, in this case moisture and mass of RD respectively, derives an  $r$  value, which falls between the range of  $-1 \leq r \leq 1$  where -1 indicates perfect negative correlation, 0 indicates no correlation and 1 indicates perfect positive correlation.

Equation 4-1: Product-moment correlation coefficient where  $-1 \leq r \leq 1$  indicating negative to positive correlation.

$$r = \frac{\sum_i \{(x_i - \bar{x})(y_i - \bar{y})\}}{\sqrt{\{[\sum_i (x - \bar{x})^2][\sum_i (y_i - \bar{y})^2]\}}}$$

Interestingly, there appeared to be a positive correlation between moisture content (%) and mass of the >125 µm fraction (as % of the total dry weight). A correlation coefficient of 0.575 was achieved, in contrast to -0.609, -0.624 and -0.326 in the 125-63 µm, 63-38 µm and <38 µm fractions, respectively. The

data suggest that if the RD is wetter, the larger size fraction (>125) represents a larger mass fraction than the rest of the size fractions. Taking into account that size fractionation took place after drying, one can possibly explain the correlation by irreversible particle aggregation under wet conditions. This supports the work of Gunawardana *et al.* (2012), who found that RD from a site in Australia existed as a large number of aggregated particles, as determined by SEM-EDX. In addition, these correlation statistics show that the mass as percentage of total dry mass in the <38  $\mu\text{m}$  fraction is less affected by moisture content than the 125-63  $\mu\text{m}$  and 63-38  $\mu\text{m}$  fractions. The explanation for this could be that the particles are aggregated in the <38  $\mu\text{m}$  fraction but the force needed to segregate is greater than that acted upon the particles in the fractioning process here, or that they simply do not exist as aggregates in the <38  $\mu\text{m}$  fraction.

Table 4-1: Wet weight, dry weight, moisture and masses of the three fractions of RD, the three sized fractions show % of the total dry mass in brackets.

Sampling campaign	Bulk Sample			Dry size-segregated sample mass (g) (% of total dry weight)			
	Wet weight (g)	Dry weight (g)	Moisture (%)	>125µm	125-63µm	63-38µm	<38µm
Spring 2013	No data	No data	No data	No data	No data	No data	No data
Summer 2013	8,060	6,830	15.3	6,370 (93.3)	365 (5.34)	72.3 (1.06)	23.7 (0.35)
Autumn 2013	9,510	7,300	19.8	7070 (91.9)	451 (6.61)	79.8 (1.17)	24.2 (0.35)
Winter 2013-14	10,200	6,270	38.5	5840. (93.7)	323 (4.72)	83.7 (1.23)	26.8 (0.39)
Spring 2014	6,700	6,400	4.26	5700 (89.2)	563 (8.25)	135 (1.97)	40.3 (0.59)
Summer 2014	No data	9,600	No data	8470 (82.9)	859 (12.6)	173 (2.54)	135.0 (1.98)
Autumn 2014	12,800	11,400	11.4	10100 (80.8)	952 (13.9)	172 (2.51)	187 (2.73)
Winter 2014-15	7,900	5700	28.03	5300 (94.1)	302 (4.41)	44.8 (0.66)	54.3 (0.79)

Figure 4-1 shows the rainfall and temperature data during the two-year sampling campaign, provided courtesy of Whitworth Meteorological Station, Manchester. Indicating the total monthly rainfall (mm), with RD moisture (secondary y-axis for top chart), as specified in table 4-1 and temperature (°C) in the bottom chart. It can be observed that rainfall fluctuates over the sampling campaign and there is no obvious seasonal pattern. For example, in January 2013 there was 51.0 mm of rain recorded, in January 2014 there was 93.4 mm. An even larger difference is observed for May 2013 and May 2014, with 48.0 mm and 113.1 mm, respectively. Considering the graphical representation of RD moisture, there appears to be a set of peaks and troughs at winter and summer respectively, with the winter campaigns showing the highest moisture content. This shape of peaks and troughs is represented in

an even more ordered fashion in the temperature chart at the bottom of the figure, only this time the peaks occur during the summer, the inverse of the RD moisture chart. Accordingly, figure 4-1 seems to show that the moisture content of RD is more dependent on the temperature than the amount of rainfall and that there is an inverse relationship, where low temperatures yield high moisture content. This is most likely due to water not being able to evaporate off in the lower winter temperatures, thus the RD stays wet for, perhaps, months. This supports the work of Omstedt *et al.* (2005) whom postulated that the speed at which road moisture evaporated correlated with RD resuspension.

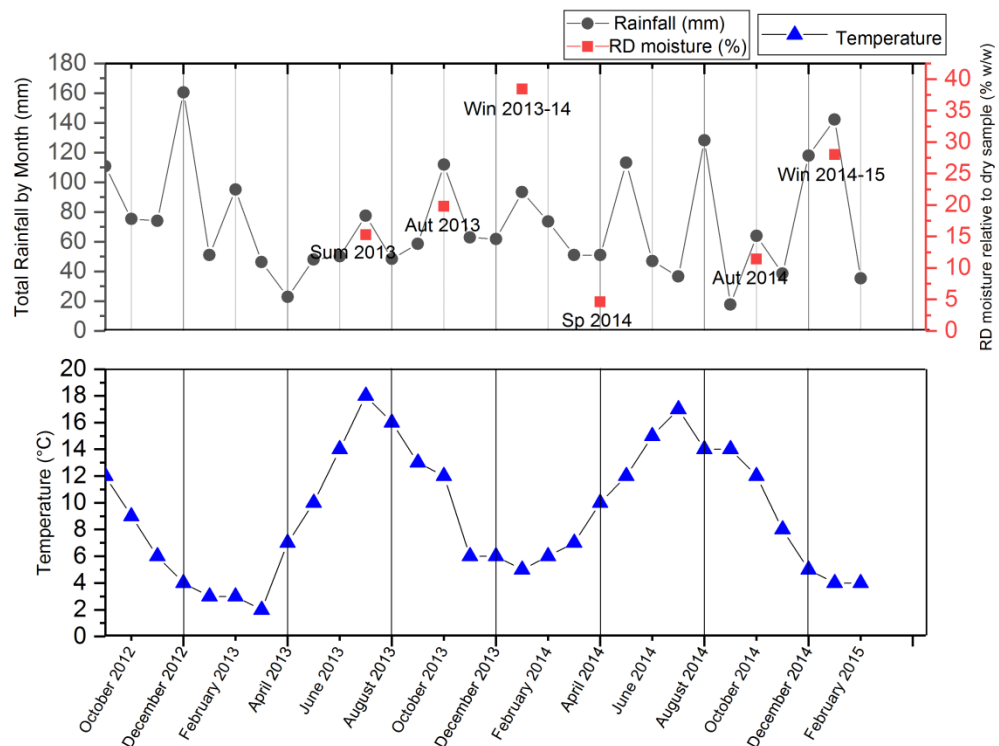


Figure 4-1: Total rainfall, black dots (top chart, primary y-axis), RD moisture, red squares (top chart secondary y-axis) and temperature, blue triangles (bottom chart) plotted in each case against the two-year sampling campaign as a time spanning x-axis.

## 4.2 Bulk Chemical Analysis

Bulk chemical analysis of RD was carried out with use of ICP-OES analysis, after acid digestion of RD, as described in section 3.2 of this document. Method verification was carried out using a certified reference material (CRM), river clay sediment LGC6139. 500 mg  $\pm$  10 mg of CRM was weighed out in triplicate, digested using aqua regia and analysed using ICP-OES, this is the same technique used for the samples. Median recoverable concentrations of Cr, Cu and Pb according to the CRM certificate along with experimentally determined median values for these metals are displayed in table 4-2. It can be observed that the recovery is within the certified values for both Cr and Pb, Cu is 0.6 mgkg<sup>-1</sup> above the certified value. With regards to Fe, there is not recoverable value detailed on the certificate for the LGC6139 reference material.

Table 4-2: Certified and experimentally determined values for certified reference material LGC6139.

	Cr (mgkg <sup>-1</sup> )	Cu (mgkg <sup>-1</sup> )	Pb (mgkg <sup>-1</sup> )
LGC6139 certified value	80 $\pm$ 3	92 $\pm$ 2	160 $\pm$ 3
LGC6139 as determined in this study	81.7 $\pm$ 1.0	94.6 $\pm$ 3.7	157.7 $\pm$ 1.8

Bulk concentrations are presented here as mg of element per kg dry soil. The four metals of interest (Cr, Cu, Fe and Pb), are displayed in Figures 4-2, 4-3 and 4-4 within the <38  $\mu$ m, 63-38  $\mu$ m and 125-63  $\mu$ m fractions, respectively. A tabulated version of the data is also presented in tables 4-3, 4-4 and 4-5, where concentrations are presented in mg kg<sup>-1</sup>. A more comprehensive metal

profile was also obtained in this experimentation, the results of this are available in appendix A, tables A-1 to A-3.

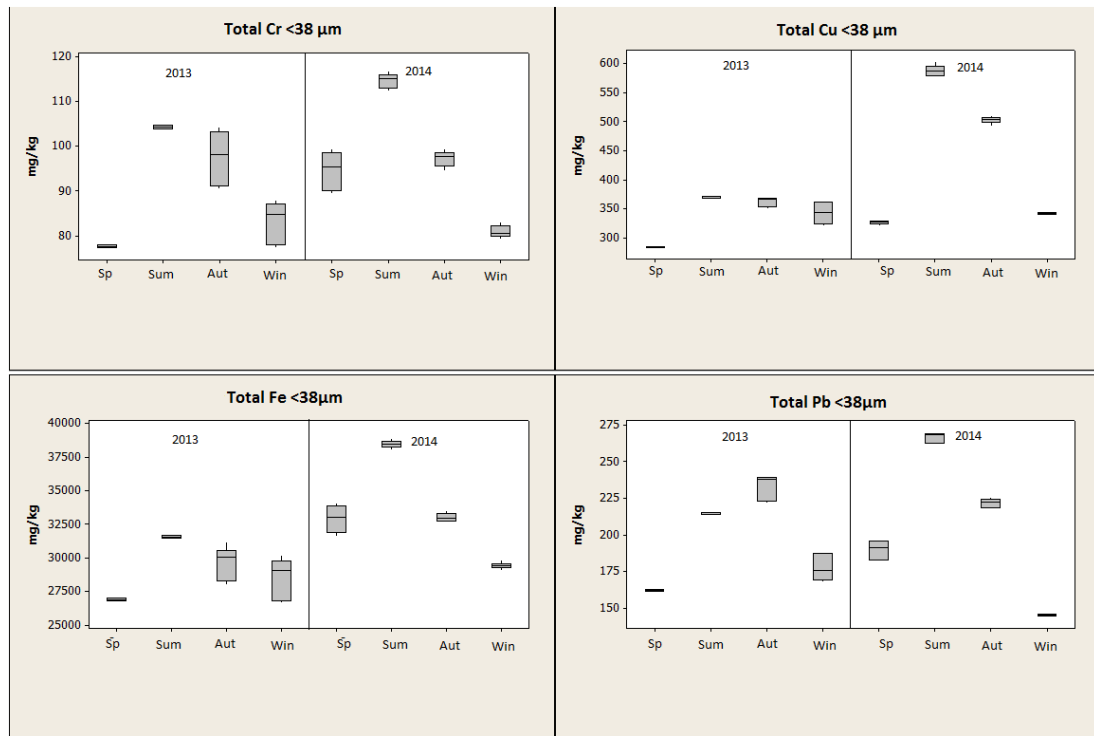


Figure 4-2: Box plots denoting the acid soluble concentrations of Cr, Cu, Fe and Pb in <38 μm fraction as determined by ICP-OES for the two-year sampling campaign (where Sp = spring, Sum = summer, Aut = autumn, Win = winter).

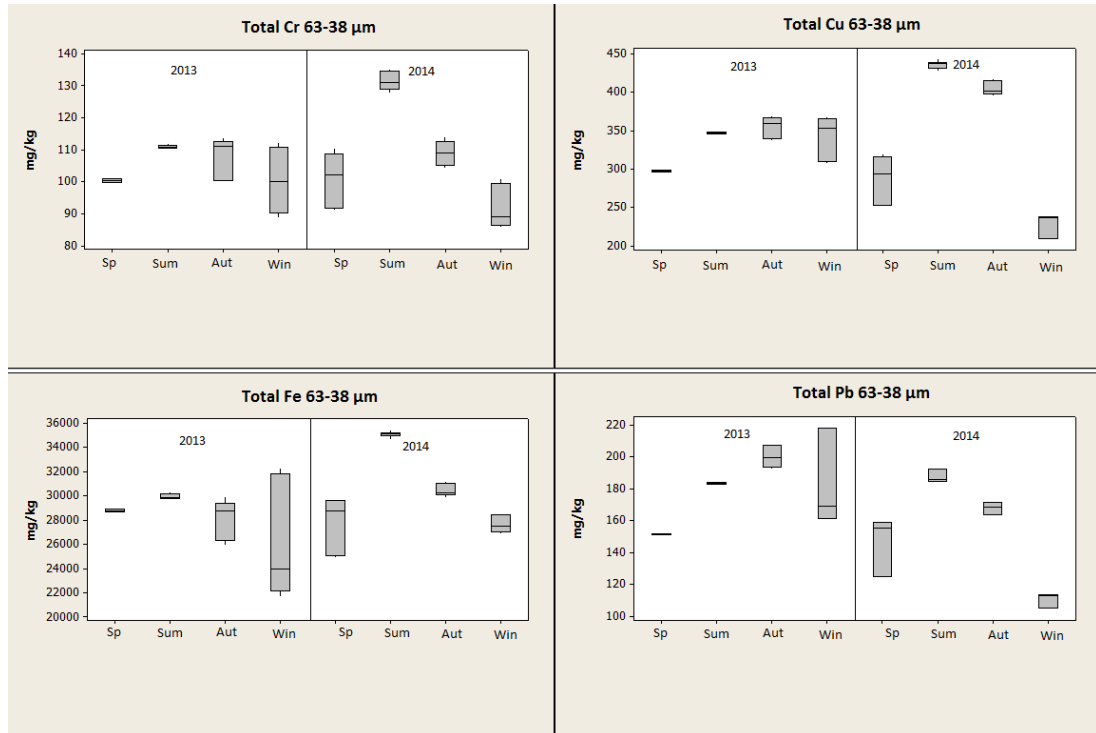


Figure 4-3: Box plots denoting the acid soluble concentrations of Cr, Cu, Fe and Pb in 63-38  $\mu\text{m}$  fraction as determined by ICP-OES for the two-year sampling campaign (where Sp = spring, Sum = summer, Aut = autumn, Win = winter).

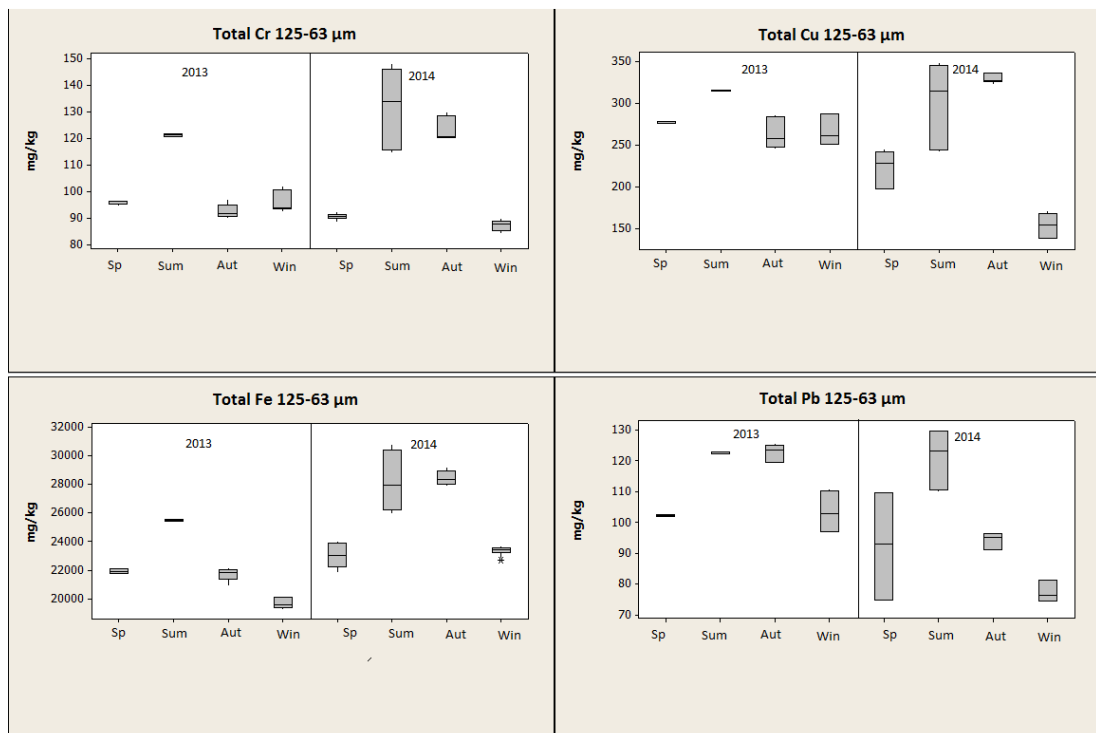


Figure 4-4: Box plots denoting the acid soluble concentrations of Cr, Cu, Fe and Pb in 125-63  $\mu\text{m}$  fraction as determined by ICP-OES for the two-year sampling campaign (where Sp = spring, Sum = summer, Aut = autumn, Win = winter).

	Cr concentrations (mg kg <sup>-1</sup> )	Cu concentrations (mg kg <sup>-1</sup> )	Fe concentrations (mg kg <sup>-1</sup> )	Pb concentrations (mg kg <sup>-1</sup> )
Sp 2013	77.6 ±0.52	284 ±0.35	26900 ±0.53	162 ±0.39
Sum 2013	104 ±0.38	369 ±0.48	31600 ±0.31	215 ±0.29
Aut 2013	97.6 ±5.42	362 ±2.0	29600 ±3.77	233 ±3.42
Win 2013/2014	83.2 ±5.1	343 ±4.76	28600 ±4.77	177 ±4.6
Sp 2014	94.7 ±3.95	327 ±1.0	32900 ±2.64	190 ±2.91
Sum 2014	115 ±1.22	589 ±1.40	38500 ±0.70	267 ±1.19
Aut 2014	97.3 ±1.57	503 ±1.18	33000 ±0.88	222 ±1.30
Win 2014/2015	80.8 ±1.60	342 ±0.40	29500 ±0.74	145 ±0.47

Table 4-3: Mean bulk metal concentrations (mg kg<sup>-1</sup>) in <38µm fraction as determined by ICP-OES with %RSD displayed as ±.

	Cr concentrations (mg kg <sup>-1</sup> )	Cu concentrations (mg kg <sup>-1</sup> )	Fe concentrations (mg kg <sup>-1</sup> )	Pb concentrations (mg kg <sup>-1</sup> )
Sp 2013	101 ±0.62	297 ±0.33	28800 ±0.46	151 ±0.38
Sum 2013	111 ±0.56	347 ±0.34	30000 ±0.77	183 ±0.4
Aut 2013	108 ±5.30	355 ±3.61	28200 ±5.24	200 ±3.06
Win 2013/2014	100 ±8.94	343 ±7.32	26000±17.19	182 ±14.32
Sp 2014	101 ±7.68	287 ±9.81	27800 ±7.39	146.0 ±10.89
Sum 2014	132 ±1.92	435 ±1.07	35100 ±0.63	187 ±1.88
Aut 2014	109 ± 3.16	405 ±2.0	30500 ±1.61	168 ±2.0
Win 2014/2015	91.8 ±6.80	228 ±5.93	27700 ±2.23	110 ±3.58

Table 4-4: Mean bulk metal concentrations (mg kg<sup>-1</sup>) in 63-38µm fraction as determined by ICP-OES with %RSD displayed as ±.

	Cr concentrations (mg kg <sup>-1</sup> )	Cu concentrations (mg kg <sup>-1</sup> )	Fe concentrations (mg kg <sup>-1</sup> )	Pb concentrations (mg kg <sup>-1</sup> )
Sp 2013	95.9 ± 0.75	278 ±0.60	21900 ±0.84	102 ±0.40
Sum 2013	121 ±0.37	315 ±0.36	25500 ±0.30	123 ±0.25
Aut 2013	92.5 ±2.63	263 ±6.22	21700 ±1.87	123 ±2.14
Win 2013/2014	96.0 ±3.9	266 ±5.9	19700 ±1.7	103 ±5.64
Sp 2014	90.4 ±1.19	223 ±9.07	23000 ±3.39	92.4 ±15.95
Sum 2014	132 ±10.20	302 ±14.78	28200 ±6.74	121 ± 6.84
Aut 2014	123 ±3.28	330 ±1.57	28400 ±1.63	94.1 ±2.59
Win 2014/2015	87.3 ±2.36	154 ±8.59	23300 ±1.23	77.4 ±3.94

Table 4-5: Mean bulk metal concentrations (mg kg<sup>-1</sup>) in 125-63µm fraction as determined by ICP-OES with %RSD displayed as ±.

In terms of absolute concentrations, chromium concentrations in this study ranged from 77.6 – 115 mg kg<sup>-1</sup> in the <38 µm fractions, 91.8 - 132 mg kg<sup>-1</sup> in the 63–38 µm fractions and 87.3 – 132 mg kg<sup>-1</sup> in the 125-63 µm fractions, indicating slight enrichment of Cr in 63-38 µm fraction compared to the other two. These results are comparable with those quoted in literature, although generally towards the higher end of ranges quoted. Concentrations have been observed in China ranging from 71-139 mg kg<sup>-1</sup> on RD <100 µm (Liu *et al.* 2014), 72.1 mg kg<sup>-1</sup> on RD <75 µm (Tang and Han 2017). Studies from Angola have observed concentrations of 17-34 mg kg<sup>-1</sup> in RD <100 µm (Ferreira-Baptiste and De Miguel 2005).

Copper concentrations in this study were found to range from 284 – 588 mg kg<sup>-1</sup> in the <38 µm fractions, 228 – 435 mg kg<sup>-1</sup> in the 63 – 38 µm fractions and 154 – 315 mg kg<sup>-1</sup> in the 125-63 µm fractions. These results showed that the <38 µm fraction of RD was more enriched with copper relative to the other two. Copper concentrations in the <38 µm fraction are 26% larger than the 63-38 µm fraction and 46% larger than the 125-63 µm fraction, based on the upper limit values for each. Copper in RD has been studied extensively in the UK. The results obtained in this study are relatively low in comparison to Birmingham and Coventry, where concentrations of 16.4 - 6,688.4 mg kg<sup>-1</sup> and 49.3 - 815 mg kg<sup>-1</sup>, respectively were reported (Charlesworth *et al.* 2003) in RD samples <1 mm. Other studies show concentrations ranging from 169 – 666 mg kg<sup>-1</sup> in particles <100 µm (Liu *et al.* 2014) and 98.0 mg kg<sup>-1</sup> in <75 µm, both of which were conducted in China. In Angola Ferreira-Baptiste and De

Miguel (2005) have been published copper concentrations of  $42 \pm 15 \text{ mg kg}^{-1}$  on RD particles  $<100 \mu\text{m}$ .

Iron concentrations in this study ranged from 26,900– 38,500  $\text{mg kg}^{-1}$  in the  $<38 \mu\text{m}$  fractions, 25,000 – 35,100  $\text{mg kg}^{-1}$  in the 63 – 38  $\mu\text{m}$  fractions and 19,700 – 28,400  $\text{mg kg}^{-1}$  in the 125-63  $\mu\text{m}$  fractions. These results showed that the  $<38 \mu\text{m}$  fraction of RD was more enriched with iron relative to the other two. Iron concentrations in the  $<38 \mu\text{m}$  fraction are 8% larger than the 63-38  $\mu\text{m}$  fraction and 26% larger than the 125-63  $\mu\text{m}$  fraction, based on the upper limit values for each. This has been shown to be quite typical in the scope of global concentrations. Concentrations in the order of 8,381-35,400  $\text{mg kg}^{-1}$  were reported in China on RD particles  $<63 \mu\text{m}$  and  $<75 \mu\text{m}$  (Luo *et al.* 2012; Tang and Han 2017), and 8,000-20,100  $\text{mg kg}^{-1}$  in Angola (Ferreira-Baptiste and De Miguel 2005). The observed concentrations in this study are significantly higher than those reported by Robertson *et al.* (2003) on RD particles  $<1\text{mm}$ , at a site less than a kilometre away (7,664-17,214  $\text{mg kg}^{-1}$ ).

Lead concentrations in this study ranged from 145 – 267  $\text{mg kg}^{-1}$  in the  $<38 \mu\text{m}$  fractions, 110– 200  $\text{mg kg}^{-1}$  in the 63–38  $\mu\text{m}$  fractions and 92 – 123  $\text{mg kg}^{-1}$  in the 125-63  $\mu\text{m}$  fractions. These results showed that the  $<38 \mu\text{m}$  fraction of RD was more enriched with lead relative to the other two. Lead concentrations in the  $<38 \mu\text{m}$  fraction are 25% larger than the 63-38  $\mu\text{m}$  fraction and 54% larger than the 125-63  $\mu\text{m}$  fraction, based on the upper limit values for each. These values are generally in line with those reported in literature, ranging from 10 - 270  $\text{mg kg}^{-1}$  in China in RD particles  $<100 \mu\text{m}$  and  $<75 \mu\text{m}$  (Liu *et al.* 2014; Tang and Han 2017), 74 - 1,856  $\text{mg kg}^{-1}$  in Angola in RD particles  $<100$

$\mu\text{m}$  (Ferreira-Baptiste and De Miguel 2005). Contrary to concentrations of Cu, lead concentrations in Manchester are higher relative to those reported in Birmingham and Coventry by Charlesworth *et al.* (2003) (0 - 146.3 mg kg<sup>-1</sup> and 0 - 199.4 mg kg<sup>-1</sup> respectively). Despite this, concentrations in this study are observed to be slightly lower than those reported at a nearby site in Manchester by Robertson *et al.* (2003) (120 - 645 mg kg<sup>-1</sup>). This is likely to be due to the phasing out of leaded fuel. The large variability in absolute concentrations of metals in RD across both the globe and even within a relatively small city such as Manchester are intriguing from a health standpoint. It is most likely that the variances can be attributed to the different anthropogenic sources in any given site. Comparison between these results and those gathered by Robertson *et al.* (2003) show how quickly a pollutant, such as lead can diminish, and a new one, iron, can present itself. This study ultimately highlights the importance to examine metal contamination at a local level. Another interesting observation is that metals are generally more enriched in the finer fractions of RD, the only exception here being Cr which is more enriched in the 63-38  $\mu\text{m}$  fraction, followed by the <38  $\mu\text{m}$  fraction. These findings support results of Potgieter *et al.* (2012a) and Barrett (2010) where metals were also found to be more enriched in the finer fractions of RD, again with the exception of Cr where the middle fraction was most enriched. This pattern of enrichment in the finer fractions is particularly interesting from a health point of view, because it highlights the need to quantify metal concentrations in the particles which can actually gain entry to the body.

Generally, the median concentrations of metals followed the order Fe>Cu>Pb>Cr. This occurs across all size fractions and sampling campaigns with the exception of summer 2014, autumn 2014 and winter 2014/2015 in the 125-63  $\mu\text{m}$  fraction, where Cr is more abundant than Pb. Published studies investigating RD concentrations worldwide have consistently shown that RD is significantly more enriched with Fe than Cr, Cu and Pb. This is believed to be because the crustal abundance of Fe is considerably greater relative to Cr, Cu and Pb (Alomary and Belhadj 2007). However, the order of abundances for Cr, Cu and Pb in RD has been shown to be readily different between sites. Assuming that Fe is always the most abundant, the order of abundance for the other three elements has been exhibited in many different orders. The order of Cr>Cu>Pb has been found in RD by Padoan *et al.* (2017) and Sutherland and Tolosa (2000) in Turin, Italy and Honolulu, Hawaii respectively. Liu *et al.* (2014) and Rasmussen *et al.* (2001) have observed the order of abundance as Cu>Cr>Pb in RD from Nanjing, China and Ottawa, Canada respectively. The order of abundance has been shown to be Pb>Cu>Cr by Soltani *et al.* (2015) in Isfahan, Iran, De Miguel *et al.* (1997) in Oslo, Norway, Shi *et al.* (2008) in Shanghai, China and Fergusson and Ryan (1984) London, U.K. Chatterjee and Banerjee (1999) have found the order Pb>Cr>Cu occurred in RD from Calcutta, India. All of which are slightly different to the order found in this study, which was generally Cu>Pb>Cr. These comparisons demonstrate the distinct nature of RD on a site-by-site basis. It also underlines the influence of anthropogenic input on the concentrations of metals found; this is a conclusion that is well supported in literature (Hopke *et al.* 1980; Crosby *et al.* 2014).

Regarding the box plots (Figures 4.2 – 4.4), it appears that the median concentrations showed an increasing trend towards summer and a decreasing trend towards winter. This is consistent across all three fractions of RD studied. Similar studies into temporal variation of metal concentrations in RD are limited; however, Robertson and Taylor (2007) found that Fe and Pb concentrations both peaked during the summer months in a one year study on metals in RD. In addition to this, both Norouzi *et al.* (2017) and Liu *et al.* (2011) indicated strong seasonal variance in metal concentrations throughout the year. Contrary to the results obtained here, both studies observed increased metal concentrations towards winter followed by a decrease towards summer. This was rationalised in both studies by the influence of precipitation, Norouzi *et al.* (2017) and Liu *et al.* (2011) note increased wet summers and dry winters. Despite the fact that there is no observable pattern in seasonal rainfall in Manchester, it is observable that the RD samples are wetter in the winter and, as iterated in section 4.1 with reference to figure 4-1, stay wet, thus water-soluble metals leach into drained water. These findings are also of importance as it was found here that the moisture content varied inversely with temperature, not rainfall. Therefore, in the summer months the particles are drier and more easily resuspended. The fact that the PHEs are more concentrated in these months presents itself as a concern for health. Referring to the data presented here, a degree of variance is observed temporally within a fraction as well as between fractions. It is observed from the box plots that a larger interquartile range is observed for most metals, particularly in the <38  $\mu\text{m}$  and 63-38  $\mu\text{m}$  fraction for the aut 2013, win 2013-14 and the sp 2014 sampling campaigns. This presents an interesting unexplained trend, all

samples were handled in the same manner and the instrumental analysis was all carried out on the same day.

### **4.3 Key Findings From Sections 4.1 and 4.2: A Short Conclusive**

#### **Summary**

Sections 4.1 and 4.2 have covered the physical characteristics and bulk metal profile of the RD samples collected over the two-year sampling campaign. This section covers the key findings from these two phases of study in a manner to keep the reader apprised with reference to the original aims of the study, but also to inform the subsequent sections. Up to this point, from the results so far discussed, we can conclude:

- Moisture content of RD is more affected by temperature than rainfall, however there is a relationship between both moisture and temperature. This washout could possibly contribute to the observed lower metal concentrations in winter months. The enrichment observed in the summer months, however, along with the drier and more easily resuspended particle indicates a potentially high risk to human health.
- Bulk metal concentrations of metals are enriched in the finer fractions of RD. The exception here being Cr, where the concentrations vary little between fraction sizes, but the middle fraction is slightly more concentrated

- Bulk metal content of RD is site dependant. Based on the comparison of this study with other published literature, it is implied that there is a large influence from anthropogenic sources.

Both of these conclusions have been discussed in a publication of this work, see Brown *et al.* (2015). Based on these findings, an understanding of the fundamental physical and bulk metal composition has been achieved. The next step of this study, in line with one of the key aims (to gain a comprehensive understanding of the metal composition of individual inhalable and ingestible RD particles), is to carry out instrumental analysis of each sample on an individual particle basis (sections 4.4 and 4.5) then qualify the term inhalable in the context of RD (section 4.6).

#### **4.4 Individual Particle Analysis**

This section summarises the results obtained from individual particle analysis, firstly by means of CC-SEM-EDX, then by Raman spectroscopy. The experimental methodologies for these techniques have been discussed in sections 3.3.1 and 3.3.2, respectively. A large portion of the individual particle analysis section encompasses metals other than Cr, Cu, Fe and Pb. The motivation behind this is part of the hypothesis of this thesis. We hypothesize that bioaccessibility of environmental particles are not only dependent on the bulk concentration of the element in question, but is also influenced by the chemical structural composition of the particle. To therefore investigate the speciation and molecular composition of these elements, their association with other elements where investigated.

#### 4.4.1 CC-SEM-EDX

Computer controlled scanning electron microscopy (CC-SEM-EDX) was carried out using a Zeiss Supra 40VP along with EDAX genius particles software, as discussed in section 3.3.1 of methodology section. The elemental composition of each individual particle was determined by X-ray analysis and the abundance of the elemental composition is provided in figure 4-5. It is observed that carbon and oxygen are the two biggest contributors to elemental abundances, making up over 50% of the total elemental content of all samples except Aut '14 <38  $\mu\text{m}$  where carbon and oxygen made up 40.6% of the total elemental content. It can be observed in these samples that carbon is more abundant in the larger fractions of RD, this is contrary to Aryal *et al.* (2015) who determined organic matter to be more abundant in the <75  $\mu\text{m}$  fraction of RD relative to the 180-75  $\mu\text{m}$  fraction, as determined by fluorescence excitation-emission spectroscopy. Wang *et al.* (2015), however, published results from nine separate RD samples which showed that concentrations of organic carbon, as determined by micro-kjedahl, in <75  $\mu\text{m}$ , 150-75  $\mu\text{m}$  and 300-150  $\mu\text{m}$  fractions varied sample to sample, with no particular pattern.

It is also observed from the total elemental composition as determined here by CC-SEM-EDX that Si is less abundant in the finer fraction. Silicon abundance was lowest in the <38  $\mu\text{m}$  fraction for seven of the eight sampling campaigns. The enrichment of Si in larger fractions of RD has been published (Cesari *et al.* 2012) where Si concentrations were found to be 4.1% - 4.5%, 3.0% – 3.2% and 2.9% - 3.2% for the 125-63  $\mu\text{m}$ , 63-38  $\mu\text{m}$  and <38  $\mu\text{m}$  size fractions respectively as determined by ICP-OES analysis of HF digestions.

Figure 4-5 also shows that metal abundances are generally higher in the finer fractions of RD, this supports the work conducted in section 4.2 of this chapter, and the studies cited within that section. The elevated abundance of these metals in finer fractions of RD in conjunction with the documented chronic health effects listed in section 2.5 of the literature review (in brief and not exhaustive, Cd, Cr, Ni – carcinogenic; Cu, Fe- DNA damaging; Pb, V-damaging to the nervous system).

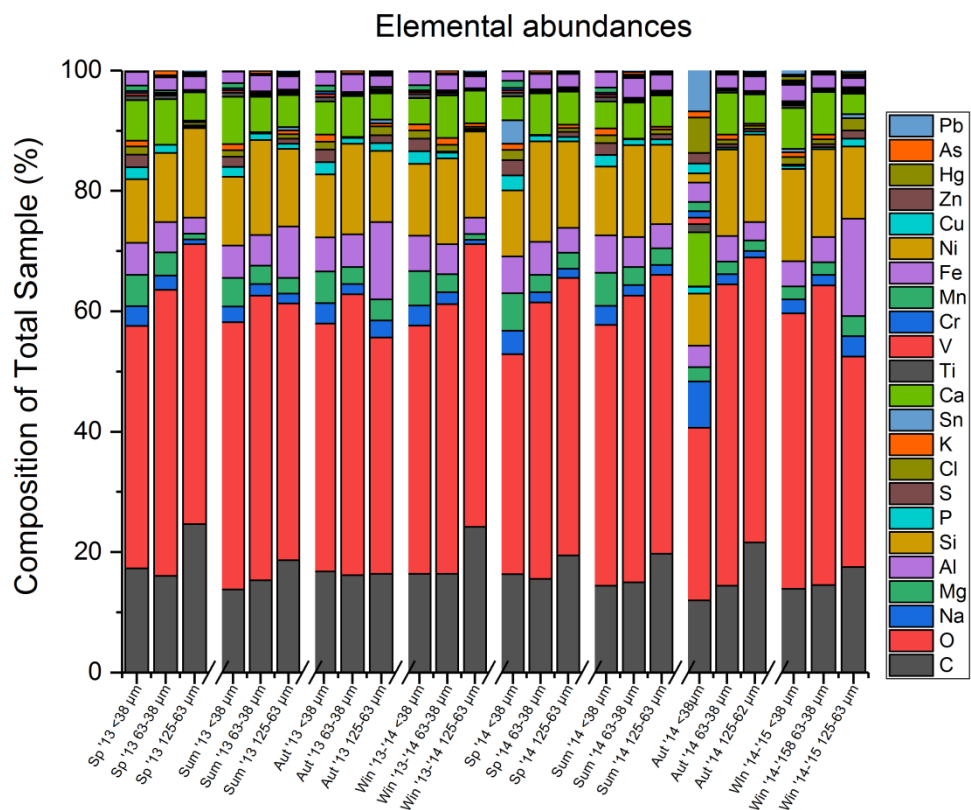


Figure 4-5: Elemental abundances given as the average fraction of each element present in the 1000 particles analysed for each sample as determined by CC-SEM-EDX.

#### 4.4.1.1 Primary Constituents

While the elemental data produced in the above figure generally supports the findings of the elemental work carried out using ICP-OES after acid digestion,

the main function of this CC-SEM-EDX work is to clarify the structure of individual particles. This can be done by calculating atomic ratios of each element in an individual particle, then grouping particles into clusters based on these ratios within a compound. This has been exhibited in published literature to characterise aerosols by clusters (Kandler *et al.* 2011; Anaf *et al.* 2012). The process of clustering in this study is based on these citations. The criteria for each classification is listed in table 4-6, AE refers to the sum of Si+P+S+Cl+K+Ca+Ti+Cr+Mn+Fe+Mg+Al+Na. The clusters selected here are not as numerous as those defined by either Kandler *et al.* (2011) or Anaf *et al.* (2012) whom both cluster silicates and calcites extensively in an attempt to elucidate different mineral classes such as quartz, feldspars, gypsum, magnesite *etc.* These mineral classes are not of chief concern in the context of this study. It was therefore decided to carry out a simpler clustering process on these classes. The criteria in table 4-6 are designed to ensure that the defining class represents the main constituent of a particle and rules out any elementally similar classes of particle. For example, if we consider the Fe rich criteria, the criterion  $Fe/AE > 0.3$  ensures that a particle is largely constituted of Fe. The next criterion in the Fe rich criteria is  $Si/Fe < 1.05$ , which is present to rule out the possibility of the particle in question being a silicate particle, the next is  $Ti/Fe < 1.3$ , which is present to ensure that the iron rich particle is iron oxide, not iron titanate. The process of characterising each particle was carried out for each sample using a purpose-built Microsoft Excel Macro spreadsheet, which used the COUNTIFS function. Additionally, some manual inspection of clusters was carried out, this is discussed further in latter parts of this section.

Table 4-6: Criteria for each particle class, where AE refers to the sum of all other elements quantified except for C and O.

Class	Criteria
Fe rich	Fe/AE >0.3, Si/Fe <1.05, Ti/Fe <1.3
Si Rich (low Al)	Si/AE >0.2, Mg/Si <0.2, Al/Si <0.2, Fe/Si <0.5, Ti/Si <0.15, Na/Si <0.7
Si Rich (high Al)	Si/AE >0.2, Al/AE >0.15, Si/Al >0.2, Ti/Al <1.3
Ca Rich	Ca/AE >0.5, Mg/Ca <0.33, Si/Ca <0.5, S/Ca <0.25, P/Ca <0.15
Titanium Rich	Ti/AE >0.3, Mg/Ti <1, Al/Ti <1, Fe/Ti <1, Si/Ti <1, S/Ti <1, Na/Ti <1
Trace Rich	(Cu+Cr+Mn+Ni+Pb+Sn+V+Zn)/AE >0.05

Figure 4-6 shows the particle classes observed in each sampling campaign. The figure indicates on the y axis the fraction of particles (from a total of 1000 particles analysed per sample) that fulfilled the criteria for a specific cluster as described in Table 4-6. The campaigns are split up by breaks on the x-axis to aid comparison. There were several incidences where particles would fit the criteria for more than one class, where this is the case, the particle is defined as both classes. This type of classification is contradictory to the work of Kandler *et al.* (2011) and Anaf *et al.* (2012) where only one cluster was allocated to a particle. The reason behind this decision to allocate more than one class to a particle in some cases is based on the conclusions of section 1 of this chapter, that particles frequently exist as aggregates, which was substantiated in work by Gunawardana *et al.* (2012). The CC-SEM-EDX individual particle analysis reveals that the clusters followed the order Si > trace elemental > Ca > Fe > Ti-rich.

The Si rich particles make up the majority of particles in all campaigns and fractions. The combined input of both the high-Al and low-Al Si-rich particles make up 70.7% to 86.0% of the total particles, this is an observation supported by Gunawardana *et al.* (2012) whom characterised RD <425 µm using SEM-EDX. It is further corroborated in published work on RD from this site using

both X-ray Fluorescence and ICP-OES from a hydrofluoric acid digestion (Potgieter-Vermaak *et al.* 2012a). This agrees with the CC-SEM-EDX instrumentation results presented here which show that Si rich particles are more abundant in the 125-63  $\mu\text{m}$  fraction. This was the case for each campaign, as would be expected, with the exception of Sp '14, where the 63-38  $\mu\text{m}$  contained more Si rich particles. This was expected as the larger fractions of RD are dominated by crustal components.

The data in figure 4-6 indicates that the portion of Ca rich particles was generally larger in the 125-63  $\mu\text{m}$  fractions, relative to the other two finer fractions. This is a similar observation to that of Zannoni *et al.* (2016) whom also found that Ca enrichment in larger fractions of RD relative to finer fractions when considering metals in RD fractions of <37  $\mu\text{m}$ , 53-37  $\mu\text{m}$  and 88-53  $\mu\text{m}$ .

Fe rich particles were identified in all but one sample (winter '14 -'15 63-38  $\mu\text{m}$ ) with abundance up to 2.1%. Iron rich particles were not found to be more abundant in the finer fraction, this is contrary to findings by Valotto *et al.* (2015), whom found that Fe rich particles are more commonly small (<5  $\mu\text{m}$ ). Manual inspection of the Fe rich CC-SEM-EDX reveals that Cr is commonly found in these particles when present in the finer fraction. 54 % of the Fe rich particles in the <38  $\mu\text{m}$  fraction contained some Cr, compared to only 12.7 % and 23.5 % of the 63-38  $\mu\text{m}$  and 125-63  $\mu\text{m}$  fractions, respectively. Taylor and Robertson (2009) found high concentrations of Cr present in iron oxide particles (up to 7.5%), as determined using electron microprobe analysis on RD. The paper by Taylor and Robertson (2009) concludes with the assertion that the origin of these iron rich particles is vehicular wear. The presence of Cr

in iron oxide particles is concerning in the context of health, because of the potential carcinogenic nature of Cr as outlined in the literature review section 2.5. The results obtained in this study potentially indicate that the finer fraction of RD contains more anthropogenically sourced Fe rich particles, because of the association with Cr observed in the SEM-EDX results, while the larger fractions simply contain crustal Fe rich particles. This is an observation which has not been reported in published literature, as far as could be establish. This is potentially a significant discovery because it would show that distribution of anthropogenically sourced metals varies throughout size fractions within RD, thus monitoring metals in appropriate size fractions is essential for understanding the health effects associated with contaminated RD.

The results also show that trace metal rich particles (Cu, Cr, Mn, Ni, Pb, Sn, V, Zn) are more abundant in the finer fraction, this is an observation which has been mentioned several times already in this chapter. Across all eight of the sampling campaigns, the <38  $\mu\text{m}$  fraction contained the most trace metal rich particles, 16.1% to 22.4% was observed in <38  $\mu\text{m}$  fraction, 7.8% to 14.0% in the 63-38  $\mu\text{m}$  fraction, 5.7% to 14.8% in the 125-63  $\mu\text{m}$  fraction, again this observation is consistent with that of Zannoni *et al.* (2016). Particles rich in these particular metals have been shown to derive from anthropogenic sources (Gunawardana *et al.* 2012).

The primary clusters covered in this section have been used to good effect for classifying clusters within the major components of aerosol particles, as exhibited by Kandler *et al.* (2011) and Anaf *et al.* (2012), the use of these clusters in the context of this study is limited. The clustering in this section

provides us with little extra detail than is obtained from the bulk analysis data in section 4.2, while it is the trace elemental structure, particularly those including Cr, Cu, Fe and Pb which we are particularly interested in. The next section describes methodology to better classify the particles which contain Cr, Cu, Fe and Pb.

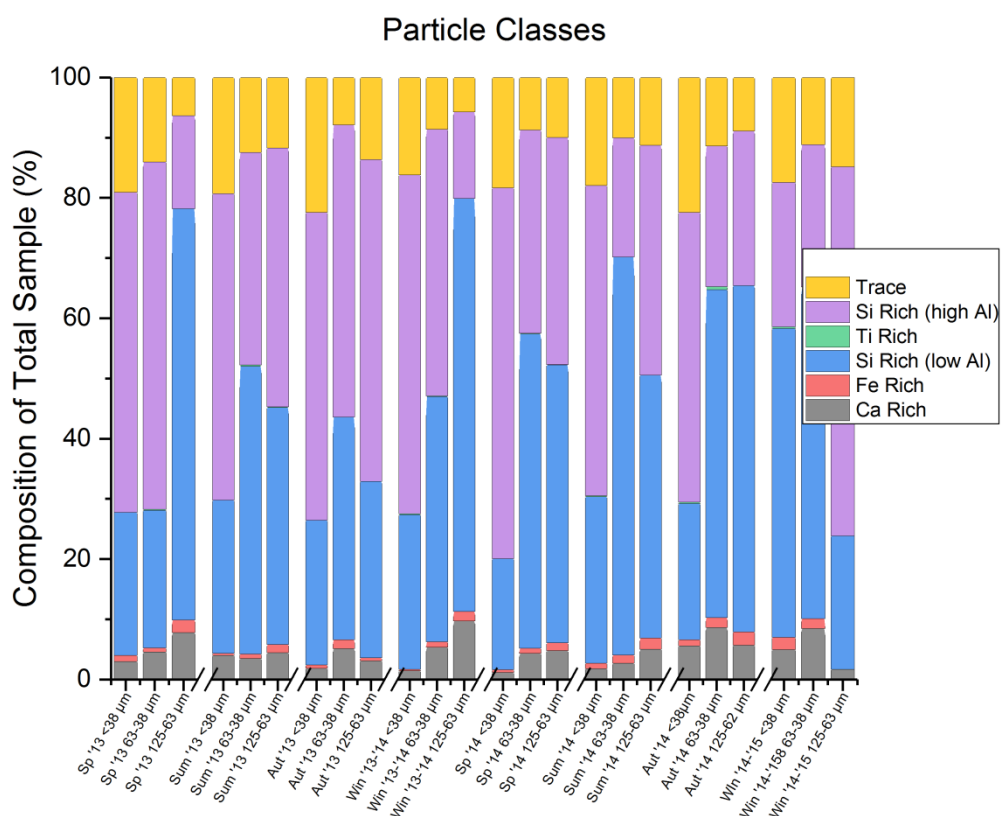


Figure 4-6: Abundance (given as the fraction of particles belonging to this cluster per total particles, expressed as a percentage) of individual particle classes / cluster, as determined by following the chemical clustering model of Kandler *et al.* (2011).

#### 4.4.1.2 Secondary Constituents

The primary clustering analysis, in the section above, indicates that the second largest particle class is trace elemental particles. However, the analysis fails

to inform us how these elements are present, thus justifying the need to better explore the trace elemental nature of these RD particles. While the clustering criteria described in the previous section is designed to characterise the main components of particles, the process fails to consider the inclusions on particles, which can often be composed of PHEs, including Cr, Cu, Fe and Pb. This section builds on the clustering technique described in section 4.4.1.1 to better characterise particles containing these four metals. Anaf *et al.* 2012 showed that clustering can be done based on atomic ratios. For example considering the chemical formula for dolomite,  $\text{CaMg}(\text{CO}_3)_2$ , atomic ratio of Ca : Mg is 1 : 1. This then informs one of the criterion within the clustering criteria for dolomite cited by Anaf *et al.* (2012), which is  $0.33 < \text{Mg}/\text{Ca} < 3$ . This represents a large margin of error for the atomic ratio, however the other criterion used to define a dolomite particle is  $\text{Mg}+\text{Ca}/\text{AE} > 0.45$ . This criterion is used to ensure that the main constituents of the particle are Mg and Ca, therefore with the albeit relaxed atomic ratio there is a large degree of certainty that this particle is dolomite. As the aim of this study is to better understand the microchemical structure of individual particles, it is necessary to investigate the form in which potentially harmful metals are present. Based on the primary clustering carried out in the previous section, it seems that a large amount of these metals are present as inclusions on particles. Therefore, to properly elucidate the nature of these metal inclusions, it may be necessary to dispense of clustering criterion which characterise a compound as the main constituent of a particle and place more emphasis on the stoichiometric ratios between elements but in a stricter manner.

To do this, literature containing speciation of Cr, Cu and Pb compounds in RD were sought and clustering criteria were then produced based on the stoichiometry of the compound. Table 4-7 details compounds containing these metals which have been observed in literature, along with relevant citations including their method of analysis and the criteria used in this study to confirm presence of these compounds. The criteria listed here attempt to contain as many criterion as possible, for example the Pb and Cr goethite particles use the iron rich criteria from section 4.4.1.1, with the addition of an appropriate atomic ratio for Pb : Fe and Cr : Fe, respectively. The criteria for some compounds, however, only consists of one criterion, which is not done by Kandler *et al.* (2011) or Anaf *et al.* (2012) whom both used multiple criteria to ensure the correct class of particle is identified. For the compounds in this section, however, the authors felt that the use of relatively strict atomic ratio boundaries alone allowed for inclusions within particles to be identified. While there is, admittedly, possibility that the atomic ratios appropriate for a particular compound could occur by chance, the rarity of these elements relative to those used by Kandler *et al.* (2011) and Anaf *et al.* (2012) would surely make this fairly unlikely. Clustering CC-SEM-EDX data in this manner, taking into account inclusions on particles, represents an approach to speciation of trace metals, which has not been attempted, on samples of this nature.

Table 4-7: Criteria for selected compound observed in RD and PM by relevant cited authors using relevant qualitative method. In appropriate criteria, AE refers to the sum of all other elements quantified except for C and O.

Compound	Observed by	Qualitative method	Criteria for clustering in this study
Cr Compounds			
PbCrO <sub>4</sub>	Potgieter-Vermaak <i>et al.</i> (2012a)	Raman Spectroscopy	1.3>Pb/Cr>0.7

PbCrO <sub>4</sub> .PbO	Potgieter-Vermaak <i>et al.</i> (2012a)	Raman Spectroscopy	2.3>Pb/Cr>1.7
K <sub>2</sub> Cr <sub>2</sub> O <sub>7</sub>	Byrne <i>et al.</i> (2017)	XANES	1.3>K/Cr>0.7
Cr goethite	Byrne <i>et al.</i> (2017)	XANES	1.3>Cr/Fe>0.7, Fe/AE >0.3, Si/Fe <1.05, Ti/Fe <1.3
MgCr <sub>2</sub> O <sub>4</sub>	Potgieter-Vermaak <i>et al.</i> (2012a)	Raman Spectroscopy	2.3>Cr/Mg>1.7
Cu Compounds			
Cu <sub>3</sub> (AsO <sub>4</sub> ) <sub>2</sub> .4H <sub>2</sub> O	This study	Raman Spectroscopy	1.8>Cu/As>1.2
CuS	Swietlik <i>et al.</i> (2015)	Sequential extraction	1.3>Cu/S>3.7
Pb Compounds			
PbCrO <sub>4</sub>	Potgieter-Vermaak <i>et al.</i> (2012)	Raman Spectroscopy	1.3>Pb/Cr>0.7
PbCrO <sub>4</sub> .PbO	Potgieter-Vermaak <i>et al.</i> (2012a)	Raman Spectroscopy	2.3>Pb/Cr>1.7
Pb <sub>2</sub> SO <sub>4</sub> O	Entwistle <i>et al.</i> (2017)	XRD	2.3>Pb/S>1.7
PbFe <sub>3</sub> (OH) <sub>6</sub> SO <sub>4</sub> AsO <sub>4</sub>	Entwistle <i>et al.</i> (2017)	XRD	3.3>Fe/Pb>2.7, 3.3>Fe/As>2.7, 1.3>As/Pb>0.7, 1.3>S/Pb>0.7,
PbMn <sub>8</sub> O <sub>16</sub>	Entwistle <i>et al.</i> (2017)	XRD	8.3>Mn/Pb>7.7
PbCO <sub>3</sub>	Barrett <i>et al.</i> (2010)	XANES	1.3>Pb/C>0.7
Pb goethite	Barrett <i>et al.</i> (2010)	XANES	1.3>Pb/Fe>0.7, Fe/AE >0.3, Si/Fe <1.05, Ti/Fe <1.3
PbMnVO <sub>4</sub> (OH)	Potgieter-Vermaak <i>et al.</i> (2012a)	Raman Spectroscopy	1.3>Pb/Mn>0.7, 1.3>Pb/V>0.7, 1.3>V/Mn>0.7

Using the criteria detailed in table 4-7, another purpose-built Microsoft Excel Macro spreadsheet again using the COUNTIFS function, similarly to that which is described in section 4.4.1.1, was produced. The number of particles containing any amount of Cr was also noted for each sample, this is so that the number of particles which contain Cr but were not identified as any of the compounds in table 4-7 can be identified as undefined. The same process was carried out for Cu and Pb. The results of this clustering process are displayed in figures 4-7, 4-8 and 4-9 for Cr, Cu and Pb respectively. The compounds PbCrO<sub>4</sub> and PbCrO<sub>4</sub>.PbO are present in the table under the definitions of both

Cr compounds and Pb compounds, obviously because they contain both of these elements.

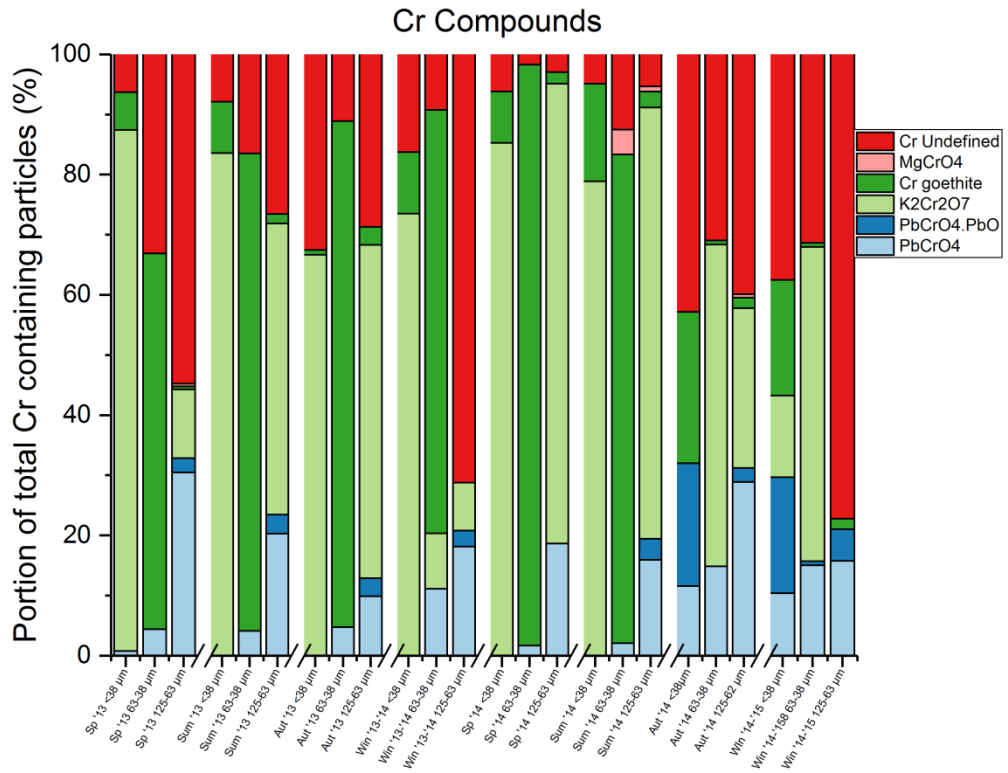


Figure 4-7: Chromium compounds in particles that contained any amount of Cr, as determined by clustering analysis of CC-SEM-EDX data.

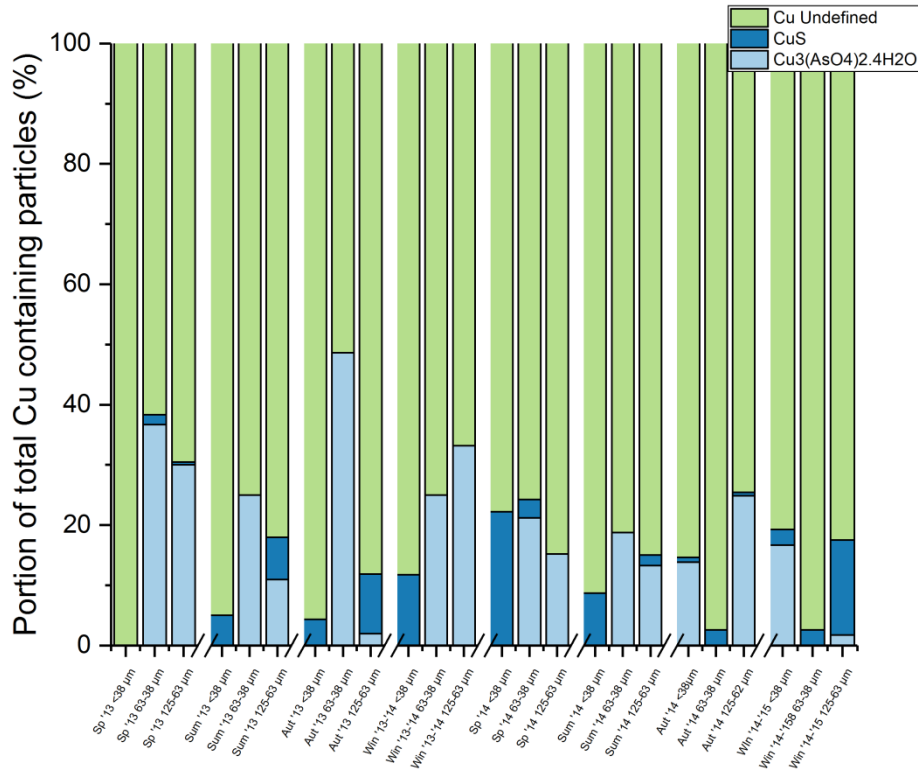


Figure 4-8: Copper compounds in particles that contained any amount of Cu, as determined by clustering analysis of CC-SEM-EDX data.

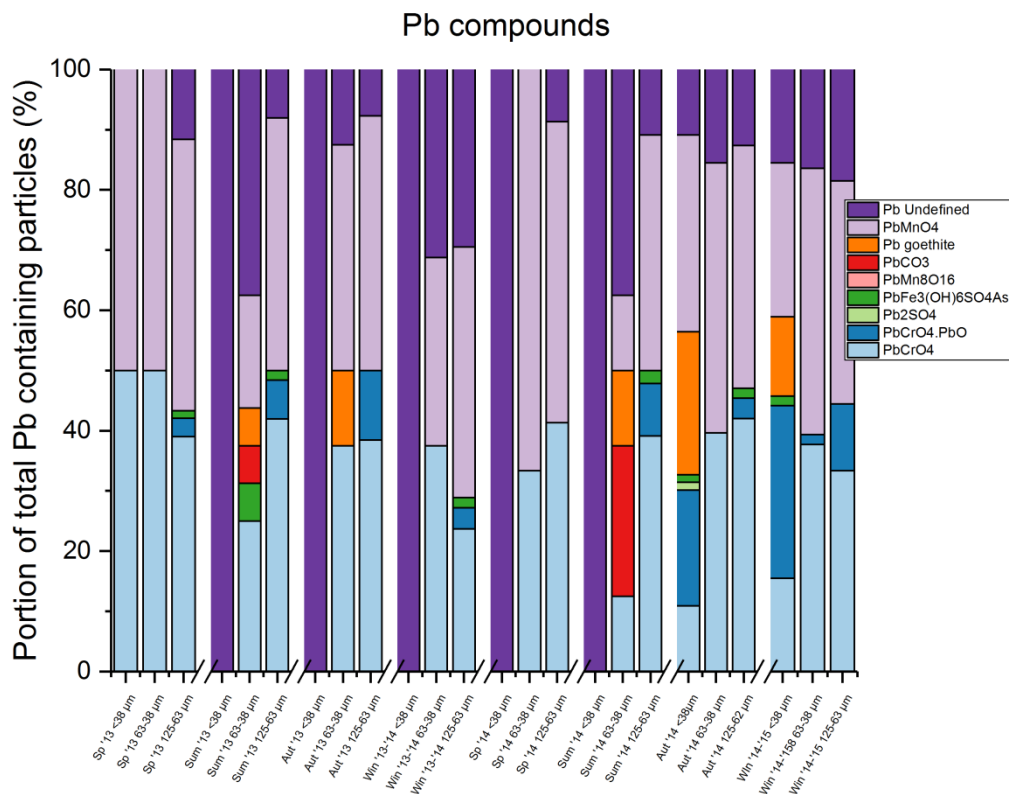


Figure 4-9: Lead compounds in particles that contained any amount of Pb, as determined by clustering analysis of CC-SEM-EDX data.

Considering the Cr compounds which are presented in figure 4-7 it was observed that the portion of particles which contain  $\text{PbCrO}_4$  is larger in the coarser fraction sizes, in each case the 125-63  $\mu\text{m}$  fraction contained the most, followed by 63-38  $\mu\text{m}$  then <38  $\mu\text{m}$ . This is contrary to the results indicated by Barrett *et al.* (2010), where  $\text{PbCrO}_4$  was shown to be more abundant in the <38  $\mu\text{m}$  fraction of RD, relative to the 63-38  $\mu\text{m}$  fraction, no results were reported for a 125-63  $\mu\text{m}$  fraction in this study, but interestingly the largest portion of  $\text{PbCrO}_4$  occurred in the 1000-500  $\mu\text{m}$  fraction.

It is also apparent from figure 4-7 that in the contribution of  $\text{PbCrO}_4\cdot\text{PbO}$  was most significant in the <38  $\mu\text{m}$  fraction of the two most recent sampling campaigns. Aside from this, it is only present in the 125-63  $\mu\text{m}$  fraction, this supports the conclusions of Potgieter-Vermaak *et al.* (2012a) who report an increased incidence of  $\text{PbCrO}_4\cdot\text{PbO}$  in the 125-63  $\mu\text{m}$  fraction of RD. The most likely source of  $\text{PbCrO}_4$  and  $\text{PbCrO}_4\cdot\text{PbO}$  in RD is from yellow road markings, Raman Spectroscopic instrumentation was carried out on broken yellow road markings picked up from several sites around Greater Manchester corroborate this, collection and analysis was carried out by the author. Appropriate spectrum is presented in appendix A, figure A-1.

Figure 4-7 shows the portion of particles containing  $\text{K}_2\text{Cr}_2\text{O}_7$ . The figure shows that  $\text{K}_2\text{Cr}_2\text{O}_7$  has a strange distribution. The first six sampling campaigns showed that a large portion of the Cr containing particles in the <38  $\mu\text{m}$  fraction are  $\text{K}_2\text{Cr}_2\text{O}_7$  (67% - 87%), with very little in the 63-38  $\mu\text{m}$  fraction (0%-9%), but a large portion of  $\text{K}_2\text{Cr}_2\text{O}_7$  particles in the 125-63  $\mu\text{m}$  fraction (8%-76%). The two most recent sampling campaigns, however, showed a larger number of

$K_2Cr_2O_7$  containing particles in the 63-38  $\mu m$  fraction relative to the other two. The distribution of  $K_2Cr_2O_7$  among the grain sizes in RD observed here is difficult to rationalise, as literature on the topic appears to be sparse. One possible explanation is that there was two distinct sources and each has more of an affinity to particles of a particular grain size based on either chemical or morphological structure. This could explain the patterns observed here where  $K_2Cr_2O_7$  makes up a larger portion of the <38  $\mu m$  and 125-63  $\mu m$  for the majority of sampling campaigns. The most likely source of  $K_2Cr_2O_7$  in RD is from cement, where it is used as an additive (De Raeve *et al.* 1998), though there appears to be a paucity in literature discussing the presence of sources of  $K_2Cr_2O_7$  in RD. The only exception to this is a brief mention of  $K_2Cr_2O_7$  in RD by Byrne *et al.* (2017) whom characterize it using X-ray absorption near edge structure (XANES), but fail to motivate the reason for its presence in RD.

The compounds discussed in this section so far,  $PbCrO_4$ ,  $PbCrO_4.PbO$  and  $K_2Cr_2O_7$  contain Cr as Cr (VI). The large incidence of Cr in this oxidation state (>50% of Cr containing particles for 21 of the 24 total samples) is of particular interest to this study in the scope of public health. As stated in both the literature review and experimental methodology chapters of this document, Cr (VI) is carcinogenic (O'Brien and Kortenkamp 1995; Elci *et al.* 2010), and has been quantified in airborne PM because of this health risk (Borai *et al.* 2002; Swietlik *et al.* 2011). There is, however, a paucity in literature with regards to the Cr (VI) quantification in RD, which this study addresses in section 4.5.

Another significant contributor to the identified Cr containing particles is the Cr goethite compound. Interestingly, Cr goethite particles dominated in the 63-38

$\mu\text{m}$  fractions for the first six sampling campaigns, then shifting to the  $<38 \mu\text{m}$  fraction for the two most recent sampling campaigns. The presence of Cr with iron oxide has been observed in RD studies, Taylor and Robertson (2009) reported a large number of  $\text{Fe}_2\text{O}_3$  and  $\text{FeOOH}$  containing Cr, as determined by electron microprobe analysis. The paper suggests that the origin of these Cr containing iron rich particles is vehicular wear. Chromium present in the +3 oxidation state, as is the case in Cr goethite, is not a concern from a health point of view at these concentrations. The prevalence of it which is observed in these samples, however, serves as a reminder that there is a large contribution of metals from anthropogenic sources. In addition, the oxidation of Cr (III) to Cr (VI) in the body should be explored to rule out the possibility of this as a source of potential harm to health.

Aside from one sample containing a small number of  $\text{MgCrO}_4$ , the rest of the particles were assigned as undefined Cr containing particles, indicated by the red bars in figure 4-7. The amount of undefined particles varied sample to sample, but generally speaking a larger portion of undefined particles appeared exist in the 125-63  $\mu\text{m}$  fraction ranging from 3% - 77% of the total Cr containing particles, compared to 2% - 33% for the 63-38  $\mu\text{m}$  fraction and 6% - 42% in the  $<38 \mu\text{m}$  fraction. The identity of these undefined compounds would most likely be  $\text{Cr}_2\text{O}_3$ ,  $\text{Cr}(\text{OH})_3$  or Cr as a free metal, as suggested by Byrne *et al.* (2017). Identification of compounds by the clustering protocol as presented in this section, cannot be applied to these compounds. The reason for this is that they do not contain any other element which can be used for a

ratio with Cr. Oxygen can't be used in ratio with Cr for either  $\text{Cr}_2\text{O}_3$  or  $\text{Cr}(\text{OH})_3$  because it is far too abundant in particles of this nature.

Referring back to the bulk metal concentrations reported in section 4.2 of this chapter, there was a strong seasonal fluctuation in concentrations of Cr, where concentrations were elevated in the summer campaigns across all three fractions of RD. There doesn't appear to be any strong seasonal patterns in the Cr compounds present in RD, however. One possible explanation for this could be that a significantly large amount of sediment is introduced to RD in the winter, effectively diluting the concentrations of metals in RD. The most likely source of this sediment could be rock salt, used to prevent ice forming on roads in cold periods. Salting of roads has been shown to cause elevated NaCl particles resuspended from roads to form  $\text{PM}_{10}$  (Kuipainen *et al.* 2016). This paper also suggests that the action of salting roads promotes abrasion of the road surface, termed the sandpaper effect, which could further dilute metal content of RD.

Figure 4-8 shows Cu compounds in particles that contained any amount of Cu, as determined by CC-SEM-EDX. The largest contributor to the identified particles in figure 4-8 is  $\text{Cu}_3(\text{AsO}_4)_2 \cdot 4\text{H}_2\text{O}$ , which was found most abundantly in the 63-38  $\mu\text{m}$  fraction. Interestingly, there was no  $\text{Cu}_3(\text{AsO}_4)_2 \cdot 4\text{H}_2\text{O}$  observed in the <38  $\mu\text{m}$  samples in any of the first six sampling campaigns. The compound  $\text{Cu}_3(\text{AsO}_4)_2 \cdot 4\text{H}_2\text{O}$  is considered to be damaging to human health (Nelson *et al.* 2011) and has been outlined concern for its ability to leach into ground water (Nordstrom 2002). The only other Cu containing compound, which was found to be present in RD according to literature, is CuS. The

distribution of CuS is fairly sporadic across all 24 samples, ranging from 0% - 22% of the Cu containing particles within samples. Swietlik *et al.* (2015) observed CuS in RD using sequential extraction, and suggested the source to be a product of abrasive actions on tires. Again, this compound is a concern to health, because of the role of Cu as a reactive oxygen species and role in the onset of Alzheimer's disease (Wiseman 2015; Borghesani *et al.* 2017). Referring to figure 4-8, undefined Cu containing particles make up the majority of Cu containing particles for each sample. Similar to the Cr containing particles, the process of determining compounds by a clustering process cannot account for all possible compounds, namely oxides, free metals and organic copper. It is well regarded in literature that the majority of copper in RD exists as organic compounds and as free metal (Banerjee 2003; Murikami *et al* 2008), the data presented here in figure 4-8 seemingly supports this. Similarly to the Cr compounds, there does not appear to be any strong seasonal trends in incidence of Cu compounds despite the fact that there was some seasonal trends observed in bulk Cu concentrations reported in section 4.2.

Pb compounds as determined by the clustering criteria in table 4-7 are reported here in figure 4-9. This figure shows that a significant portion of these Pb containing particles are present as  $\text{PbCrO}_4$ , making up to 50% of the lead containing particles in some samples. As mentioned in the discussion of the distribution of Cr containing particles in this section,  $\text{PbCrO}_4$  particles were more abundant in the larger fraction of RD, this is contrary to the results reported by Barrett *et al.* (2010). Whom also reported a lower contribution of

PbCrO<sub>4</sub> to the total number of Pb containing particles for the grain fractions analysed in this study (16% - 21%).

The compounds Pb<sub>2</sub>SO<sub>4</sub>, PbFe<sub>3</sub>(OH)<sub>6</sub>SO<sub>4</sub>AsO<sub>4</sub> and PbMn<sub>8</sub>O<sub>16</sub> were all quantified using the clustering technique described in this section and presented in figure 4-9. Few of these particles were found sporadically across the samples with no pattern regarding fractions found in or seasonal presence. The study which characterised these compounds did so on heavily contaminated top-soil. It was not expected that these compounds would appear in any considerable quantities in RD. Despite this, PbFe<sub>3</sub>(OH)<sub>6</sub>SO<sub>4</sub>AsO<sub>4</sub> was found in 8 of the 24 samples. This compound would be of significant concern to health if present in considerable quantities, because of the toxicity of As compounds (Gebel 2000). An additional review of arsenic in ambient air in the UK outlines that there is no concentration of arsenic which is permissible in air (DEFEA 2000).

Additionally, PbCO<sub>3</sub> was found to be present in a total of two samples, Sum '13 63-38 µm and Sum '14 63-38 µm. Interestingly, Barrett *et al.* (2010) reported no detectable quantity of PbCO<sub>3</sub> in the <38 µm fraction of RD, but 33% in the 63-38 µm fraction. The PbCO<sub>3</sub> results reported here, however, are likely to underestimate the amount of PbCO<sub>3</sub> present in these samples. The reason for this is that carbon is abundant in all particles and is therefore likely to exist in other compounds within the same particle. This is a similar problem to that which has been discussed with Cr<sub>2</sub>O<sub>3</sub> and Cr(OH)<sub>3</sub> earlier in this section.

Barrett *et al.* (2010) found that the largest contributor to Pb containing particles in Manchester RD was Pb goethite, making up 45% and 51% of these particles in the <38  $\mu\text{m}$  and 63-38  $\mu\text{m}$  fraction respectively. The contribution of Pb goethite to the lead containing particles using the clustering technique described here was found to be significantly lower than this, as reported in figure 4-9. Only 5 samples contained Pb goethite, the most being present in the aut '14 <38  $\mu\text{m}$  sample, with 22%. It is unclear why there is such a large difference in the quantities of Pb goethite between these studies, considering the similarity of the samples used. Aside from the study by Barrett *et al.* (2010) there appears to be a lack of quantification of Pb goethite in RD.

Another large contributor to the lead compounds determined in this study is  $\text{PbMnVO}_4(\text{OH})$  which was observed to be present in 19 of the 24 samples in total, contributing up to 67% of the total Pb containing particles. This compound was observed in RD by Potgieter-Vermaak *et al.* (2012a) using Raman Spectroscopy. As is the case with any Pb containing compound, there are concerns to human health associated with significant exposure.

The unidentified portion of Pb containing compounds as presented in figure 4-9 is relatively low in comparison to the unidentified Cr and Cu containing particles for the majority of samples. The data does, however, show that 5 of the 8 <38  $\mu\text{m}$  fractions are entirely undefined. It is suspected that the majority of these unidentified compounds are likely to be present as oxides, carbonates and organic ligands. Barrett *et al.* (2010) found that PbO and Pb organic ligands made up 13% of the <38  $\mu\text{m}$  fraction of RD each, while  $\text{PbCO}_3$  made up 33% of the 63-38  $\mu\text{m}$  fraction.

The secondary constituents section of this chapter shows the compounds of Cr, Cu, Fe and Pb present in each of the samples. This process of clustering particles has shown that there was a significant amount of Cr (VI) inclusions of particles, particularly in the <38  $\mu\text{m}$  and 125-63  $\mu\text{m}$  fractions, while the 63-38  $\mu\text{m}$  fraction tended to be dominated by Cr goethite particles. It was also observed that the majority of Cu containing particles were likely to be organic ligands or free metals, especially in the <38  $\mu\text{m}$  fraction. Additionally, there was a large amount of copper arsenate particles present in two coarser fractions. Lead containing particles in the finer fraction were largely undefined by the selected Pb compound classes, indicating the presence of PbO or organic ligands of Pb. The two coarser fractions tended to be dominated by PbCrO<sub>4</sub>, however a large portion of the particles were also defined as PbMnO<sub>4</sub>.

In line with the aims of this study, the task will be to link these compounds to the bioaccessible portions of each of these metals, to better understand how the chemical structure of particles informs the potential health issues. Firstly though, the challenge is to show that the compounds quantified in this section are present in RD. A structural technique which will determine the molecular composition of particles will be beneficial. Raman Spectroscopy lends itself ideally for this purpose. The next section details the results obtained from the Raman Spectroscopy analysis, firstly discussing the major components of RD, then the trace metal rich components. Direct comparison of the results reported in the CC-SEM-EDX and the Raman Spectroscopy sections are discussed in section 4.6.

#### 4.4.2 Raman Spectroscopy

Raman Spectroscopy was carried out as described in section 3.3.2. Interpretation of spectra was carried out using the Thermo Scientific Spectral Database as a first estimate then further confirmations was carried out using CrystalSleuth computer program which uses the RRUFF database (RRUFF.info). This section will be structured, first by displaying specimen spectra from RD samples as blue lines, with reference spectra in red and orange lines. These spectra are largely non-representative of the types of spectra which are usually achieved when conducting Raman Spectroscopy on RD, because spectra often include bands from different compounds. These spectra offered a useful matrix appropriate tool for interpretation of noisier, more heterogeneous spectra, because they are representative of the compounds found in any sample. After these spectra are presented, section 4.4.2.7 then discusses the incidence which these particles are observed within each sample.

Firstly, though, the physical appearances of these particles as observed under the Raman microscope are discussed. Figures 4-10 to 4-12 are images from the Raman microscope showing individual particles of the <38  $\mu\text{m}$ , 63-38  $\mu\text{m}$  and 125-63  $\mu\text{m}$  of the win 2014-15 campaign fractions under 10x and 50x objectives. These images are representative of the particles observed in the other sampling campaigns and were selected at random to present the physical appearance of the samples. Figure 4-10 shows the <38  $\mu\text{m}$  fraction of road dust firstly under a 10x objective (top image) and under a 50x objective (bottom image). It is apparent from the top image that particles are uneven in

terms of shape, and that there are several fibres present. The top image in this figure appears to show that most particles are either dark black/brown or bright white. On inspection of the 50x objective image, however, the particles are shown to be various shades of black, grey, brown and yellow, with some orange particles. It is also apparent for the bottom image in figure 4-10 that inclusions exist on particles. This is shown on the white/grey particle directly above the scale bar, where there is a small orange inclusion. The majority of particles in the bottom image of figure 4-10 are out of focus, this is because of the varying depth profile of these particles. This makes it difficult to showcase the inclusions that exist on most of these particles. These observations are largely consistent for the 63-38  $\mu\text{m}$  and 125-63  $\mu\text{m}$  presented in figure 4-11 and 4-12, where the shapes of particles are uneven, colours are only obvious under 50x objective, and inclusions are ubiquitous.

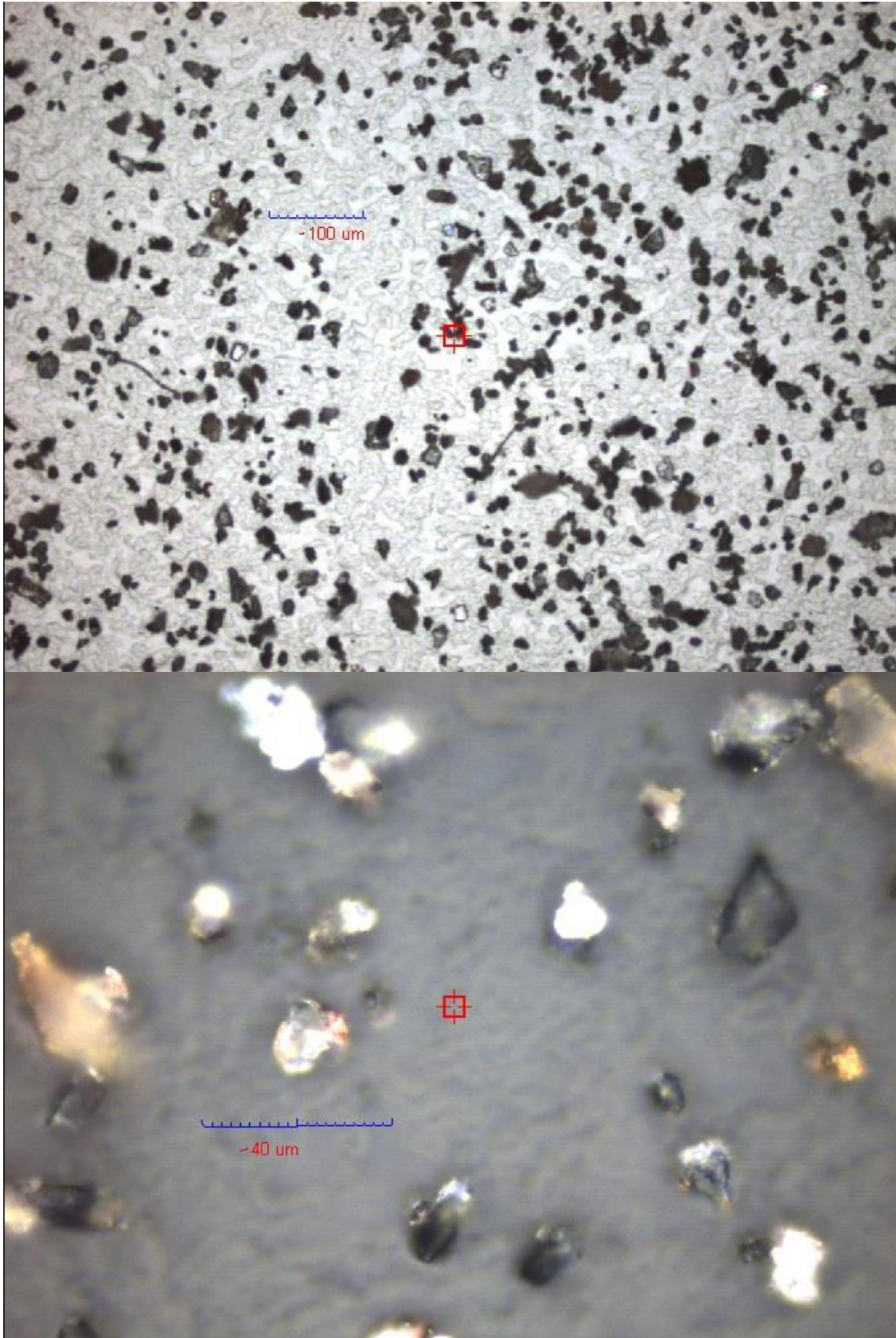


Figure 4-10: Raman microscope images of  $<38\ \mu\text{m}$  sample from win 2014-15 campaign under 10x objective (top image), scale bar  $100\ \mu\text{m}$  and 50x objective (bottom image), scale bar  $40\ \mu\text{m}$ .

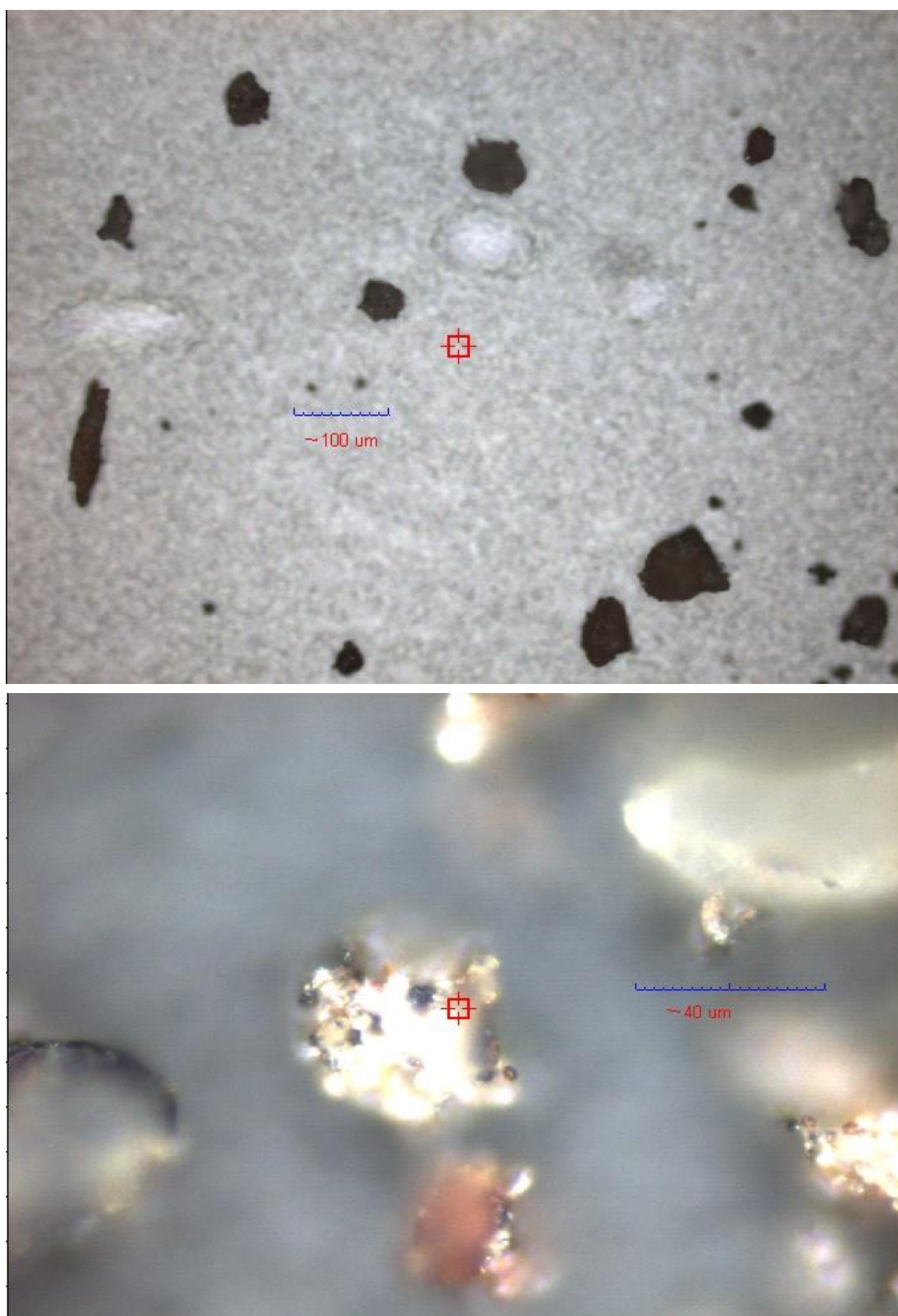


Figure 4-11: Raman microscope images of 63-38  $\mu\text{m}$  sample from win 2014-15 campaign under 10x objective (top image), scale bar 100  $\mu\text{m}$  and 50x objective (bottom image), scale bar 40  $\mu\text{m}$ .

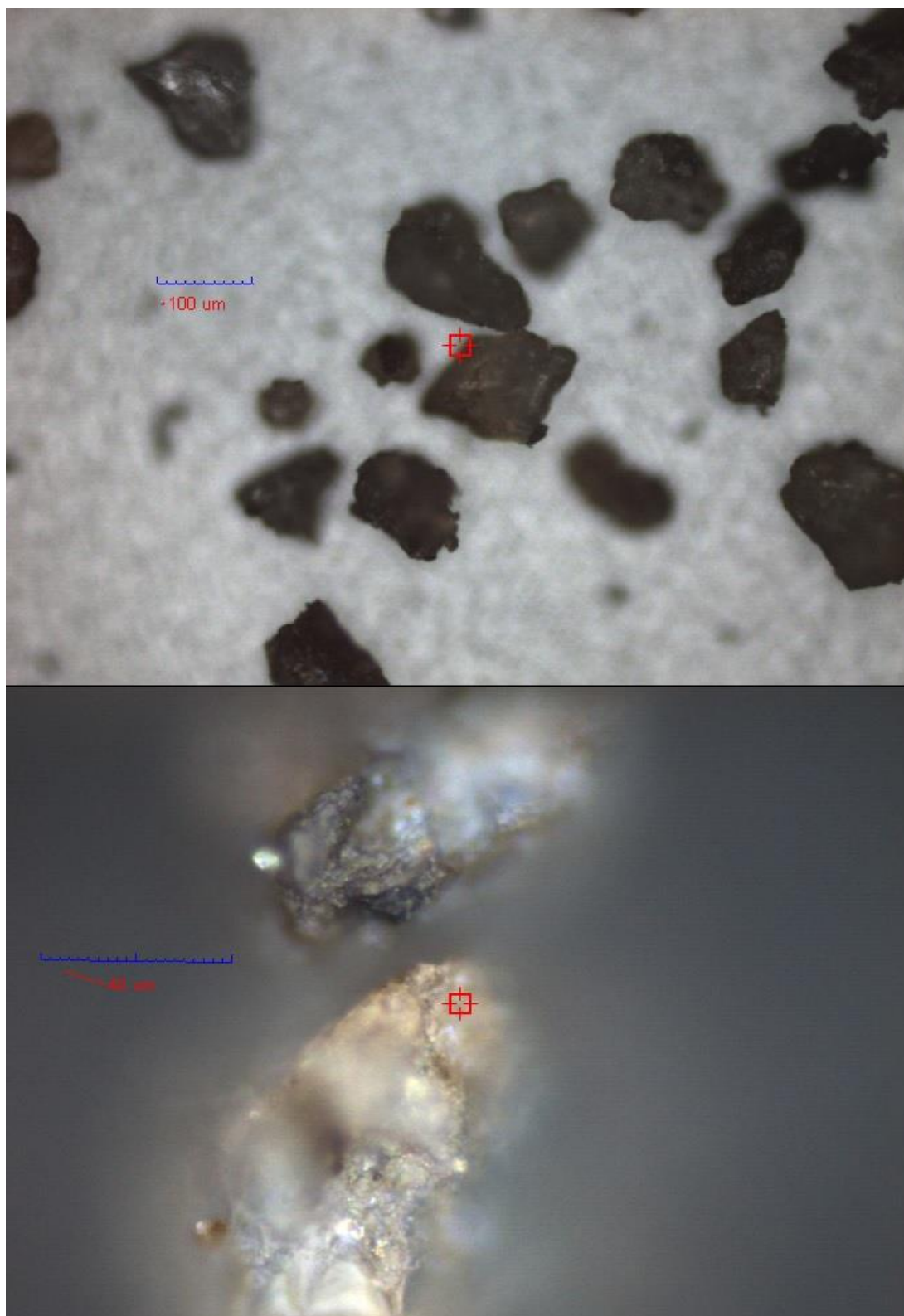


Figure 4-12: Raman microscope images of 125-63  $\mu\text{m}$  sample from win 2014-15 campaign under 10x objective (top image), scale bar 100  $\mu\text{m}$  and 50x objective (bottom image), scale bar 40  $\mu\text{m}$ .

#### 4.4.2.1 Calcium Rich Particles

Figures 4-13 to 4-15 show collected Raman spectra from RD samples as the blue line, along with reference spectra from the RRUFF database as the red and orange lines. These are the calcite ( $\text{CaCO}_3$  – hexagonal crystal structure), aragonite ( $\text{CaCO}_3$  – orthorhombic crystal structure), dolomite ( $\text{CaMg}(\text{CO}_3)_2$ ) and gypsum ( $\text{CaSO}_4 \cdot 2\text{H}_2\text{O}$ ). Each of which were observed with varying degrees of incidence, all of which are designated as calcium rich particles. Each of these particles appear as lustrous white particles which often contain dark inclusions, or are found themselves as inclusions on dark particles. Figure 4-13 shows a specimen calcite particle from RD samples, along with reference spectra for both calcite (red line) and aragonite (orange line). Calcite and aragonite exist as polymorphs of calcium carbonate, a main band for both occurs between  $1082\text{-}1088\text{ cm}^{-1}$ , with smaller bands occurring between  $704\text{-}715\text{ cm}^{-1}$  and  $282\text{-}285\text{ cm}^{-1}$ . It can be challenging to distinguish between aragonite and calcite, especially in samples of this nature where small inclusions interfere with spectra. It has been shown, that calcite is more commonly observed with bands at  $282\text{ cm}^{-1}$  and  $713\text{ cm}^{-1}$ , whereas aragonite is found with bands at  $207\text{ cm}^{-1}$  and  $704\text{ cm}^{-1}$  (White 2009; Lee *et al.* 2014). Despite the fact that specimen spectrum given here in blue clearly shows a calcite particle, there were many times during the analysis that the smaller bands were too weak and it was not possible to distinguish between aragonite and calcite. Accordingly, particles which are either aragonite or calcite will simply be referred to as calcite/aragonite for the rest of this document.

Figure 4-14 shows a specimen dolomite particle observed in RD samples (blue line), along with a reference spectra for dolomite (red line). The key indicator for dolomite is the strong band at  $1097\text{ cm}^{-1}$ . There are a few subtle differences between the two, which will be discussed. Firstly, the smaller bands which occur at  $176\text{ cm}^{-1}$  and  $295\text{ cm}^{-1}$  which are responsible for the Mg-O symmetric stretch and O-Mg-O bending modes respectively (Sun *et al.* 2014) have shoulders in the reference spectra, but not in the specimen. It has been shown in literature that these are not always observed in natural samples (Schmid and Dariz 2016).

The dolomite spectrum is markedly similar to the calcite/aragonite spectra based on the profile. Accordingly, it is important to note band positions when distinguishing between the two, the most pronounced difference is the band at  $1097\text{ cm}^{-1}$  in dolomite compared to a similar band at  $1084\text{ cm}^{-1}$  for calcite/aragonite. The band represents the  $\nu_1(\text{CO}_3)^{2-}$  symmetric stretch mode, this band is shifted by the metal-oxygen bonding which takes place with Mg in dolomite and Ca in calcite/aragonite (Frost *et al.* 2008).

Figure 4-15 shows specimen spectra for gypsum in blue, along with reference spectrum in red. The indicator here for gypsum is the large peak at  $1017\text{ cm}^{-1}$ , evidence of symmetric sulphate stretch in anhydrous gypsum (Schmid and Dariz 2016). The better separation of bands in the specimen spectrum is evidence of a less hydrated particle (Prieto-Taboada *et al.* 2014).

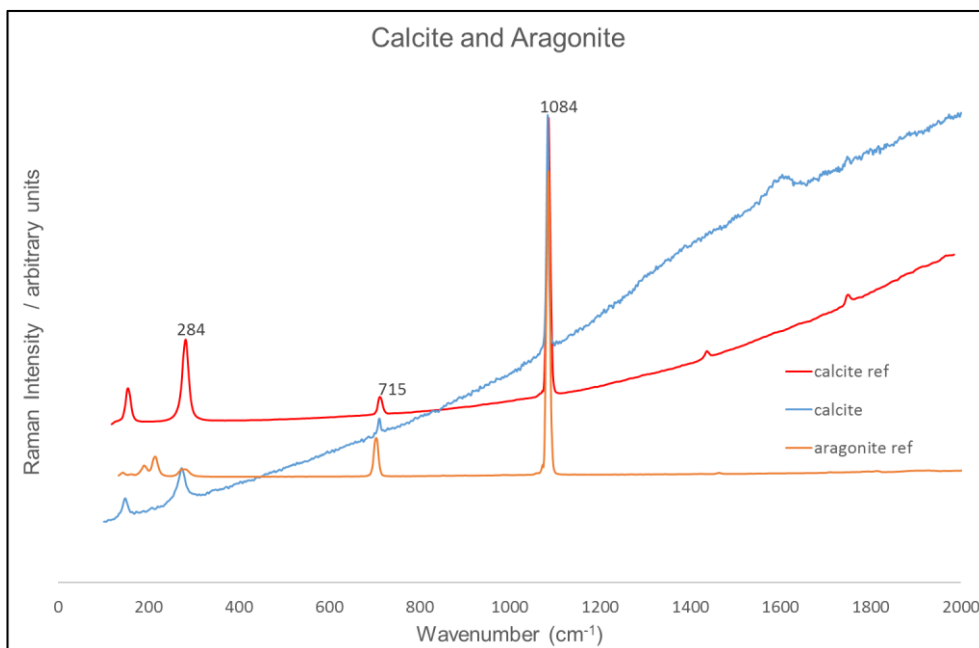


Figure 4-13: Calcite particle, shown here in blue, observed using DXR Raman Spectroscopy. Calcite and aragonite reference spectra from RRUFF database, shown here in red and orange respectively.

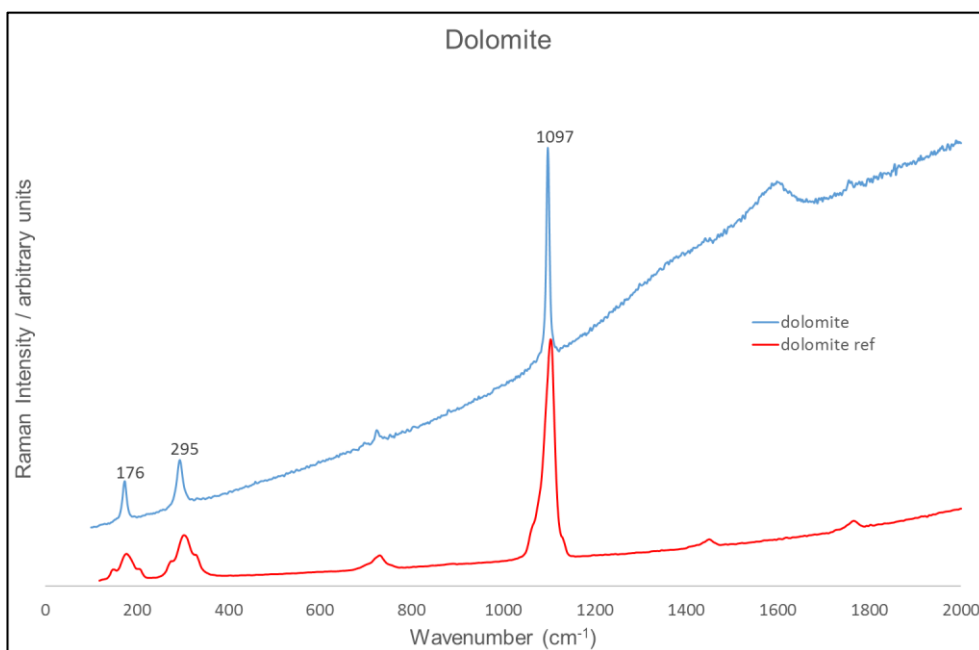


Figure 4-14: Dolomite particle, shown here in blue, observed using DXR Raman Spectroscopy. Dolomite reference spectrum from RRUFF database, shown here in red.

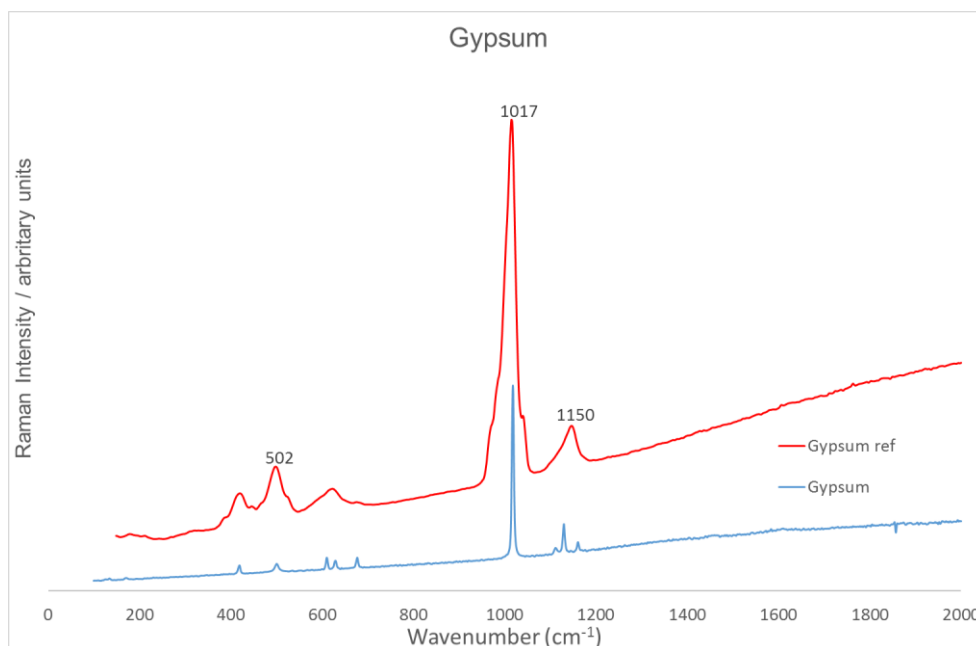


Figure 4-15: Gypsum particle, shown here in blue, observed using DXR Raman Spectroscopy. Gypsum reference spectrum from RRUFF database, shown here in red.

#### 4.4.2.2 Iron Rich Particles

Iron rich compounds were observed using Raman Spectroscopy, the majority of which were iron oxides, a mixture of haematite ( $\text{Fe}_2\text{O}_3$ ) and goethite ( $\text{FeO}(\text{OH})$ ) bands. Iron oxides appear as orange particles and often have a mixture of light, dark and yellow inclusions on. Iron sulphide was also found, present as pyrite ( $\text{FeS}_2$ ), which often appears as dark particles. Comparison of Raman data to literature is difficult, because it is a very uncommon technique as far as RD characterisation is concerned. There are however, a handful of studies, which utilise the technique for iron rich particles. Both Taylor and Robertson (2009) and Potgieter-Vermaak *et al.* (2012a) show iron compounds as oxides in RD. Each of these studies also remark on the difficulty associated with analysing these particles, which are extremely sensitive to laser damage. These studies also both remark on the fact that iron rich

particles from RD exhibit bands from different iron oxide minerals within the same particle spectrum. Taylor and Robertson (2009) indicate the presence of both Haematite and lepidocrocite, whilst Potgieter-Vermaak *et al.* (2012a) show the presence of haematite and magnetite bands from the same particle.

Figure 4-16 shows two different iron rich particles observed in this analysis. It is clear from the spectra that they are two distinct iron oxide compounds present. Contention between reference spectra and different published studies means that it is difficult to elucidate which iron compounds these spectra represent. Many studies use strong bands at 220-227  $\text{cm}^{-1}$  ( $A_{1g}$  symmetrical stretch), 287-295  $\text{cm}^{-1}$  ( $E_g$  symmetrical bend), 400-412  $\text{cm}^{-1}$  ( $E_g$  symmetrical stretch) and 1310-1330  $\text{cm}^{-1}$  (two-phonon interaction) to positively identify haematite (de Faria and Lopes 2007; Colombari *et al.* 2008; Taylor and Robertson 2009; Hernanz *et al.* 2011; Iriarte *et al.* 2017; Kong and Wilson 2017). The blue spectrum in figure 4-16 has been labelled haematite, because of its general similarity to these band positions, with the exception of a band between 400-412  $\text{cm}^{-1}$ . Interestingly there is also a prominent band at 389  $\text{cm}^{-1}$  in this spectrum which has been presented as an indicator of goethite (de Faria and Lopes 2007; Colombari *et al.* 2008).

The green spectrum in figure 4-13 was also identified as an iron oxide particle, because of the orange colour observed on the particle, and because of the bands at positions 255  $\text{cm}^{-1}$  and 680  $\text{cm}^{-1}$ , which have been shown to be within the range of bands synonymous with goethite (de Faria and Lopes 2007; Colombari *et al.* 2008). A band at 423  $\text{cm}^{-1}$  is also observed, which as pointed out in the previous paragraph is associated with haematite. The mixtures of

bands from different iron oxide minerals shown within these two spectra is similar to observations by Taylor and Robertson (2009) and Potgieter-Vermaak *et al.* (2012a).

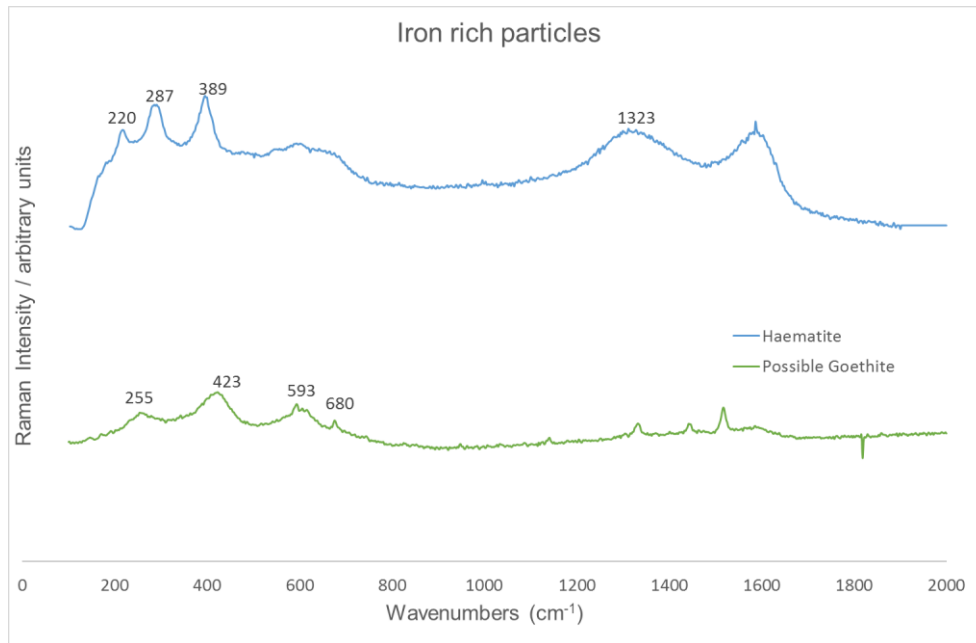


Figure 4-16: Spectra from iron oxide particles observed using DXR Raman Spectroscopy. Blue spectrum has been assigned as a haematite particle based on similarity to haematite particles identified in literature. Green spectrum is designated as possibly goethite because of its similarity to goethite in literature

#### 4.4.2.3 Silica Rich Particles

Silica rich particles make up a significant portion of identifiable particles in RD. The majority of this, especially in the larger grains size fractions is due to the input of quartz. However, there is a large input from subgroups, such as feldspars, pyroxenes and mica.

Figure 4-17 shows a specimen spectrum for quartz in blue, along with a reference spectrum in red. The most prominent band is the stretch at 463 cm<sup>-1</sup> that is a result of the V<sub>2</sub> symmetric bend in the SiO<sub>4</sub> tetrahedral structure. The bands found at 199 cm<sup>-1</sup> and 125 cm<sup>-1</sup> can be attributed to the A<sub>1</sub> symmetry

and rotation of the  $\text{SiO}_4$  tetrahedron respectively (Skulteti *et al.* 2014; Fidirichova *et al.* 2016). The bands are both more commonly found at higher wavenumbers, between  $205\text{-}206\text{ cm}^{-1}$  and  $126\text{-}128\text{ cm}^{-1}$ , (Watenphul and Schmidt 2011; Fidirichova *et al.* 2016), however the wavenumbers at which these bands are present have been shown to lower appropriately in  $\alpha$ -quartz. Figure 4-17 also shows a shoulder on the  $125\text{ cm}^{-1}$  band at  $151\text{ cm}^{-1}$  this could possibly be the presence of the  $A_{1g}$  mode in PbO (Wiechert *et al.* 2005).

Figure 4-18 shows specimen spectra of different feldspar minerals observed in these RD samples. Feldspars characterised by silicate ( $\text{SiO}_4$ ) and aluminate ( $\text{AlO}_4$ ) tetrahedra coordinated with Ca, K, Na and occasionally Ba (Daintith 2008). Those observed in these samples have been characterised as albite ( $\text{NaAlSi}_3\text{O}_8$ ), amazonite ( $\text{KAlSi}_3\text{O}_8$ ) labradorite ( $\text{NaAlSi}_3\text{O}_8$ ), microcline ( $\text{KAlSi}_3\text{O}_8$ ) and sanidine ( $\text{KAlSi}_3\text{O}_8$ ). While some of these feldspars have the same chemical structure, the distinguishing feature is various amounts of sodium where potassium is coordinated and potassium where sodium is coordinated (Boggs 2009), allowing for distinctions to be made using Raman Spectroscopy. The identity of the feldspar particles displayed in figure 4-18 are confirmed by comparing band positions to reference spectra courtesy of the RRUFF database. The main identifiable bands present in the feldspar particles are those at  $469\text{-}480\text{ cm}^{-1}$  and  $507\text{-}515\text{ cm}^{-1}$  which correspond to the coupling of a deformed  $\text{SiO}_4$  symmetrical bend with the (Ca,K,Na)-O stretch (Zhang *et al.* 1996).

Figure 4-19 shows a specimen spectrum for augite (a metal rich alumina silicate compound), along with a reference spectrum. Although the sample

spectrum only provides distinct bands of the very strong bands in the reference spectrum, the particle has nevertheless been classed as augite. The spectrum shows a large background, which is most probably due to fluorescence. Augite belongs to the pyroxene group of silicates, which have a long structure of silicon and oxygen atoms linked by a variety of other elements. The general structure for pyroxenes is  $X_{1-p}Y_{1+p}Z_2O_6$  where  $X$  is Ca, Na,  $Y$  is Al,  $Fe^{2+}$ ,  $Fe^{3+}$ , Li, Mg, Mn and  $Z$  is Al, Si (Boggs 2009). Pyroxenes have two main identifiable bands, one at  $668\text{ cm}^{-1}$  and the other around  $329\text{ cm}^{-1}$ . Similar to the feldspar group they represent the  $SiO_4$  symmetrical bend and the M-O stretch (Tomasisi *et al.* 2015), the complex structure of the pyroxenes causes these bands to shift relative to the feldspar groups.

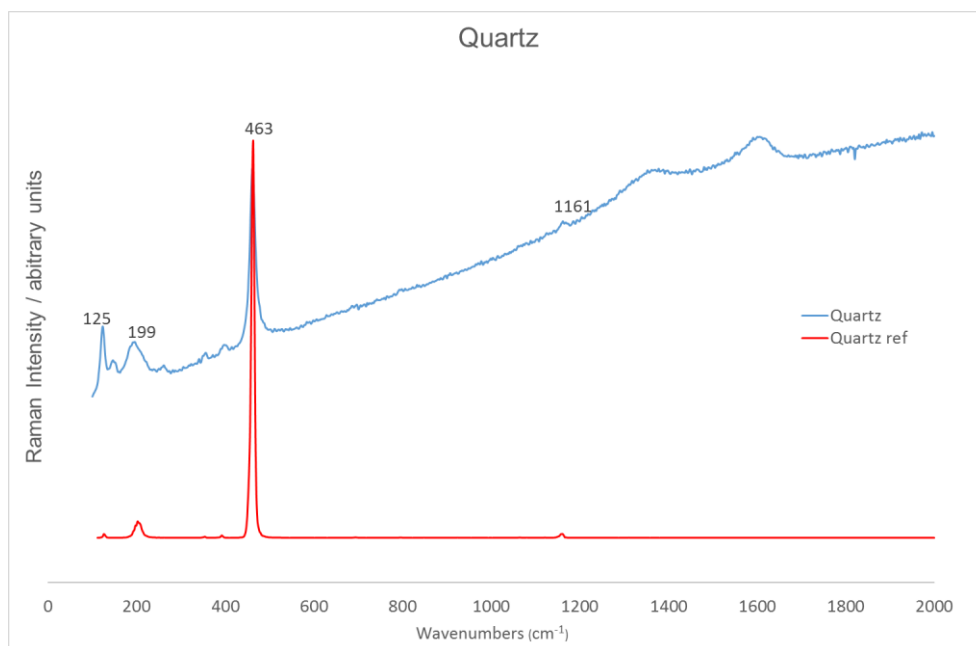


Figure 4-17: Quartz particle, shown here in blue, observed using DXR Raman Spectroscopy. Quartz reference spectrum from RRUFF database, shown here in red.

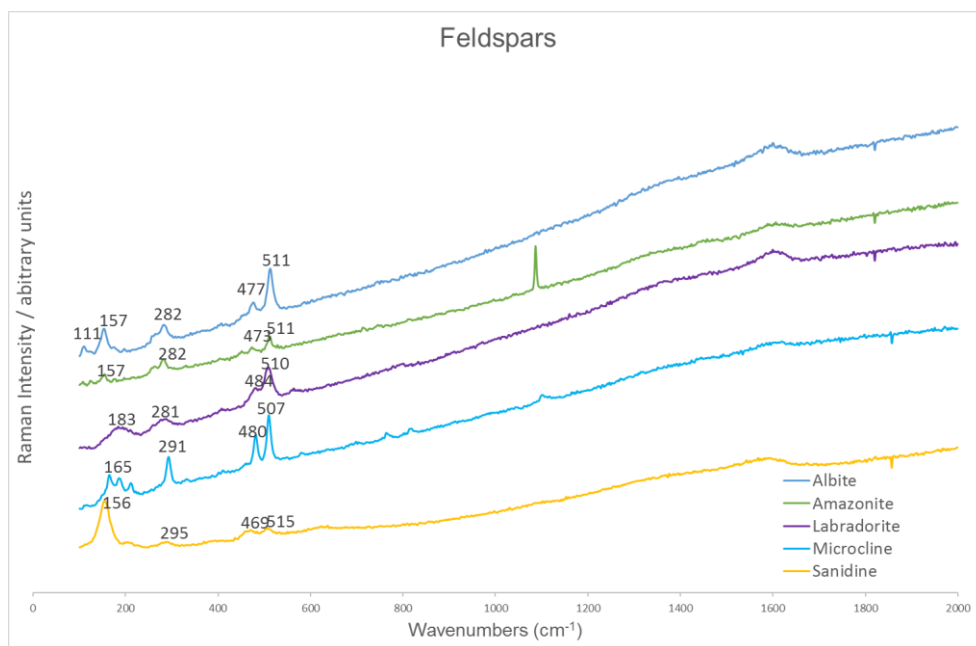


Figure 4-18: Spectra from feldspar group particles observed using DXR Raman Spectroscopy. Blue spectrum has been assigned as an albite, green spectrum has been identified as an amazonite particle, purple spectra has been identified as labradorite particle, light blue spectrum has been identified as a microcline particle and yellow spectrum has been identified as a sanidine particle. All particles are assigned as these compounds based on key band positions matched with spectra from RRUFF database.

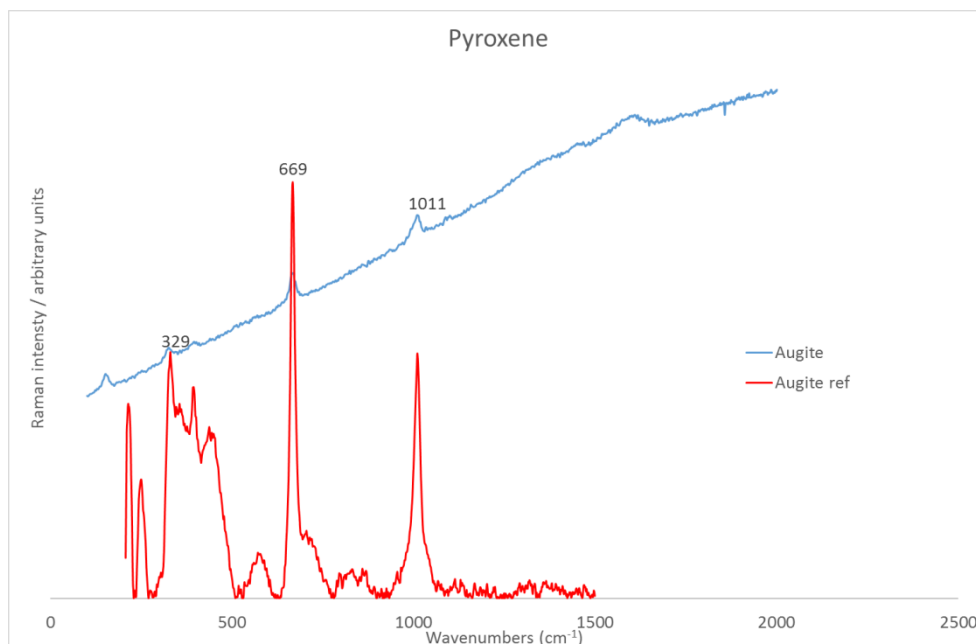


Figure 4-19: Pyroxene particle, shown here in blue, observed using DXR Raman Spectroscopy. Pyroxene reference spectrum from RRUFF database, shown here in red.

#### 4.4.2.4 Titanium Rich

Figure 4-17 shows the Titanium rich particles observed in RD, anatase, brookite and rutile, each of the three types of particle identified are polymorphs of TiO<sub>2</sub>. Brookite represents TiO<sub>2</sub> as an orthorhombic structure, while rutile and anatase are both tetragonal but are differentiated by their crystal structures. Space groups of rutile and anatase can be described as  $P4_2/mnm$  and  $I4_1/amd$  respectively (Liu *et al.* 2015a). These particles are often very stable under laser and produce very little fluorescence resulting in clear spectra, which can be matched to reference spectra easily. Each of the spectra presented in figure 4-20 were corroborated with references from the RRUFF database, further corroborated in literature (Parker and Siegel 1990; Triebold *et al.* 2011; Leal *et al.* 2017). Characteristic bands for rutile occur at 446-449 cm<sup>-1</sup> (E<sub>g</sub>) and 608-611 cm<sup>-1</sup> (A<sub>1g</sub>) (Ahmad *et al.* 2016)

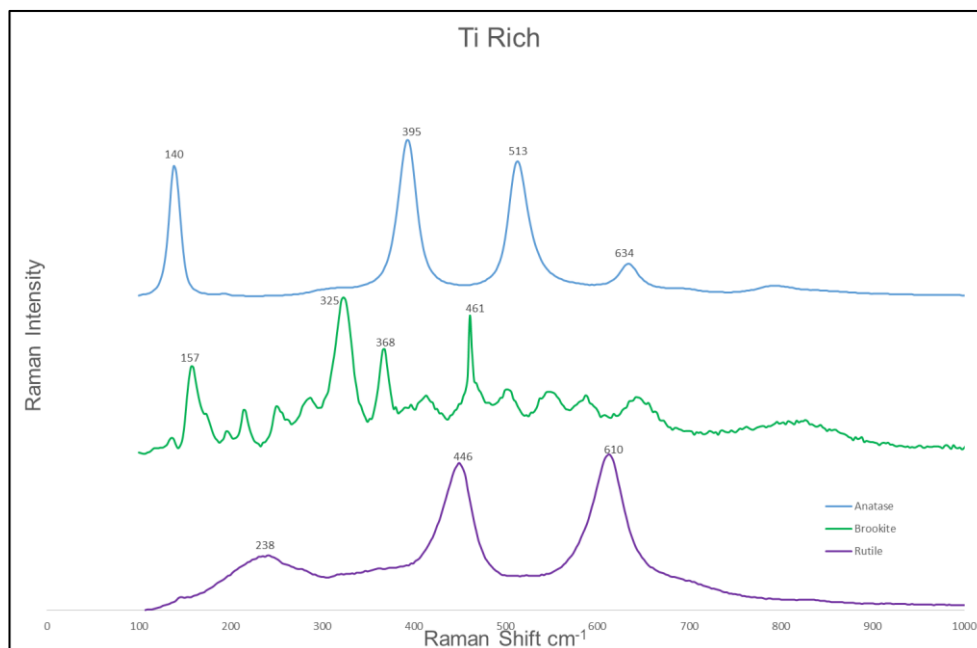


Figure 4-20: Spectra from Ti rich particles observed using DXR Raman Spectroscopy. Blue spectrum has been assigned as a anatase, green spectrum has been identified as a brookite particle, purple spectra has been identified as a rutile particle, All particles are assigned as these compounds based on key band positions matched with spectra from RRUFF database.

#### 4.4.2.5 Other Trace Metal Rich Particles

Figure 4-21 shows the lead chromate  $\text{PbCrO}_4$  as observed in RD samples, in blue, along with reference spectrum in red. The characteristic band here is at  $839 \text{ cm}^{-1}$ , attributed to Cr-O stretching mode (Ravindranath *et al.* 2012) with smaller bands matching the reference spectra at  $363 \text{ cm}^{-1}$  and  $377 \text{ cm}^{-1}$ . It is also observed in this particular specimen spectrum that there is an inclusion peak at  $1088 \text{ cm}^{-1}$ , most likely calcite. Lead chromate is very interesting in the context of this study, because of the presence of Cr (VI) and lead. Where present,  $\text{PbCrO}_4$  particles are very recognisable as large bright yellow crystals.

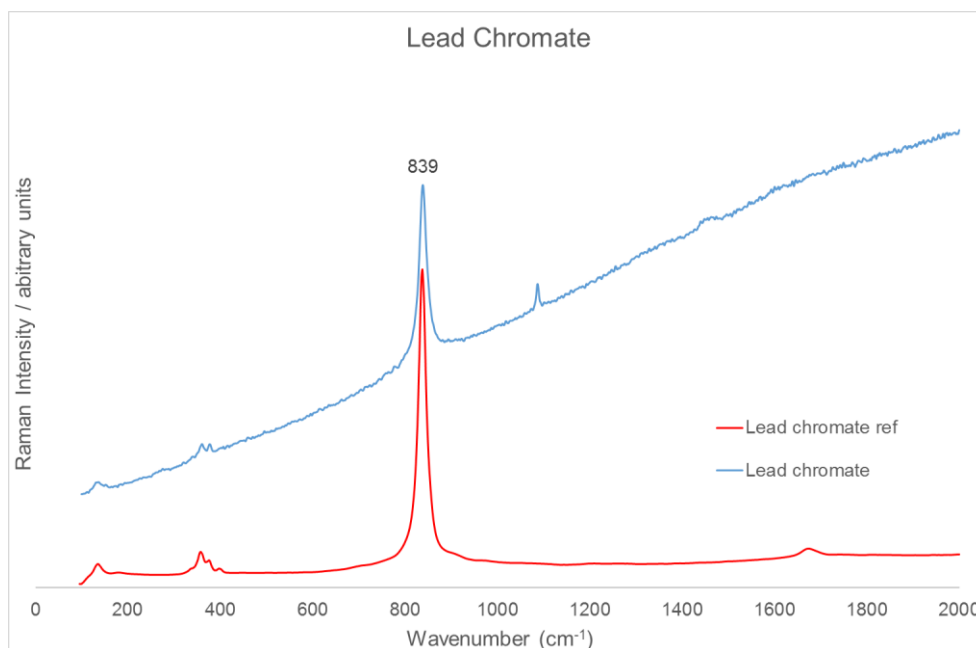


Figure 4-21: Lead chromate particle, shown here in blue observed using DXR Raman Spectroscopy. Lead chromate reference spectrum from RRUFF database, shown here in red.

Figure 4-22 shows copper arsenate ( $\text{Cu}_2(\text{AsO}_4)(\text{OH})\cdot 3\text{H}_2\text{O}$ ), as observed in RD samples. The characteristic band occurs here at  $835\text{-}837\text{ cm}^{-1}$  and is believed to be the  $\nu_1$  ( $\text{AsO}_4$ )<sup>3-</sup> symmetric stretch (Frost *et al* 2010; Frost and Bahfenne 2010), the shoulder band occurring here at  $870\text{ cm}^{-1}$  is believed to be due to the ( $\text{AsO}_4$ )<sup>3-</sup> asymmetric stretch (Frost and Bahfenne 2010).

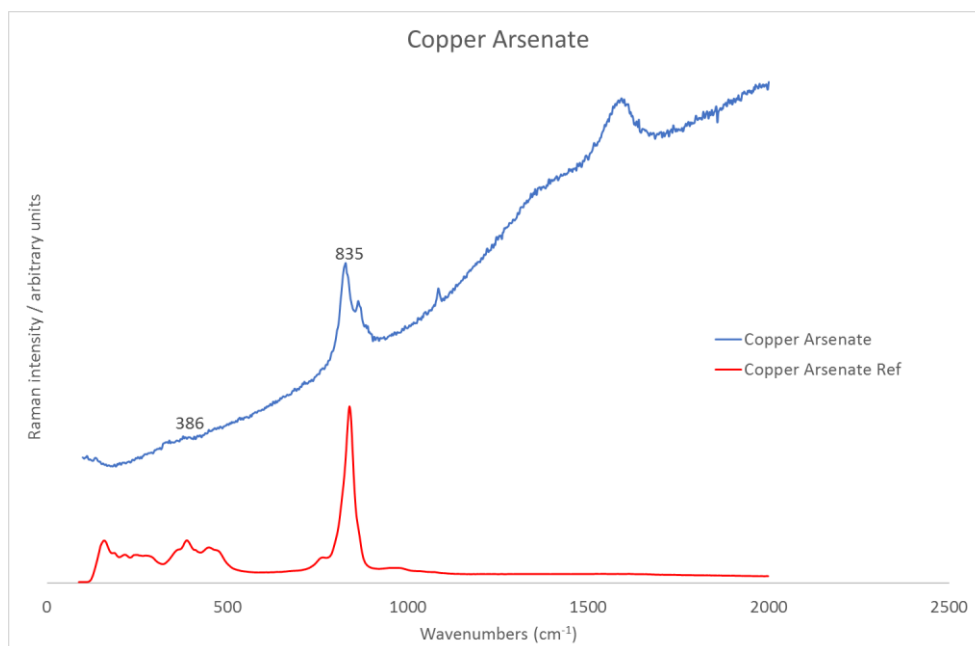


Figure 4-22: Copper arsenate particle, shown here in blue, observed using DXR Raman Spectroscopy. Copper arsenate reference spectrum from RRUFF database, shown here in red.

#### 4.4.2.6 Carbon Inclusions

The majority of spectra collected for each RD sample showed evidence of carbon bands with varying degrees of relative intensity. Figure 4-23 shows an example of this on an anatase particle. The RRUFF database does not have a reference spectra for carbon which matches this, however, there is a large number of journal articles which interpret these bands at  $1360\text{ cm}^{-1}$  and  $1600\text{ cm}^{-1}$  as soot (Sadezky *et al.* 2005; Russo and Ciajolo 2015; Ess *et al.* 2015; Han *et al.* 2017). It is generally accepted that the band observed here at  $1360\text{ cm}^{-1}$  is referred to as the D-band and is attributed to the  $A_{1g}$  vibrational mode, indicative of structural defects within the carbon structure. The band at  $1600\text{ cm}^{-1}$  is referred to as the G-band and is attributed to the  $E_{2g}$  symmetrical stretching mode within carbon rings. It was observed in all of the RD samples

in this study that almost all particles contain some evidence of soot across all size fractions.

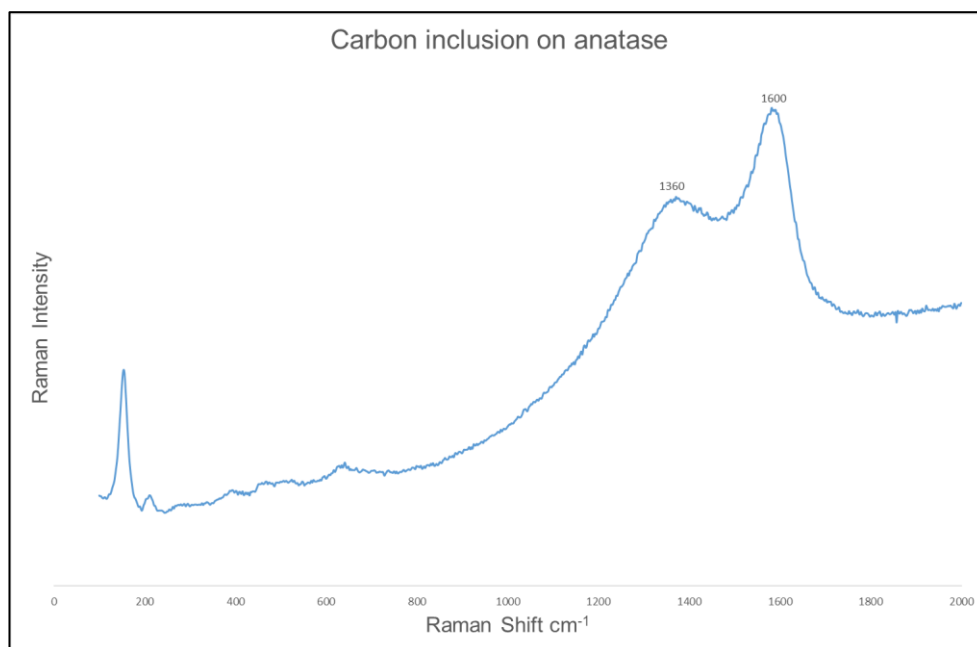


Figure 4-23: Carbon inclusion on anatase shown here in blue, observed using DXR Raman Spectroscopy. Copper arsenate reference spectrum from RRUFF database, shown here in red.

#### 4.4.2.7 Raman Observations of RD Samples

Figure 4-24 shows the particle classes observed in each sampling campaign and fraction, as determined by Raman Spectroscopy. The campaigns are split up by breaks on the x-axis to aid comparison, in the same fashion as demonstrated in the CC-SEM-EDX results section of this chapter. For all samples a minimum of 200 particles were analysed. It is appreciated that this number of particles are much lower than that of the CC-SEM-EDX analysis, but from experience, as well as previously documented data, this number of particles can be deemed as representative of the composition of the RD samples (Potgieter-Vermaak *et al.* 2012b; Jentzsch *et al.* 2013 ). It was

observed that quartz is the most abundant mineral class across all of the samples and 30.3% to 65.6% of the particles analysed showed the presence of the characteristic 463 -464  $\text{cm}^{-1}$  band. The exception was during the Aut '13 campaign in the  $<38 \mu\text{m}$  fraction, where calcite was more abundant. The large incidence of quartz in RD as determined by Raman Spectroscopy was also observed by Potgieter-Vermaak *et al.* (2012a), in one of only two studies published anywhere which use this instrumentation for RD. For each sampling campaign it can be observed that quartz is more abundant in the 125-63  $\mu\text{m}$ , followed by the 63-38  $\mu\text{m}$  fraction, then the  $<38\mu\text{m}$  fraction. Interestingly, if we consider one of the other abundant silicate groups, feldspars, there appears to be a pattern whereby feldspars are more abundant in the finer fraction relative to the larger fraction. This observation is applicable to six of the eight sampling campaigns, the exceptions being Sum '14 and Aut '14. The other two silicate groups, mica and pyroxene are rarer than quartz and feldspar and are observed infrequently but are present in all size fractions in one campaign or another. The observation here of Si concentrations enriched in larger fractions as determined by Raman Spectroscopy further validates the same observation as revealed by the CC-SEM-EDX instrumentation in the previous section of this document. Admittedly, in some incidences, there is a large difference between the absolute abundance of Si rich particles, 70.7% to 86.0% as determined by CC-SEM-EDX compared to 37.9% to 74.6% as determined by Raman Spectroscopy, this is puzzling. One possible explanation for this is that the Raman Spectroscopy gives a signal bands for inclusions on particles, without giving signal bands for the particle itself, whereas the CC-SEM-EDX takes data for an entire particle. For example, if a large Si rich particle were to

have a small Ti rich inclusion on it and the Raman laser is focused on the region where the Ti rich inclusion is, it would seem it is a Ti rich particle, possibly with a weak Si signal. If the same particle was to be analysed using CC-SEM-EDX, however, the output from the instrument would indicate a large atomic fraction of Si with a small amount of Ti. Unfortunately there is no similar study published which can confirm or deny this speculation.

Referring back to the results obtained by the Raman spectroscopy, calcite is the most abundant of the calcium rich particles, ranging from 10.5% to 48.2% abundance. Contrary to the quartz, calcite appears to be generally more abundant in the finer fraction, this being the case in six out of the eight campaigns. A particularly interesting observation regarding the calcites though is the relative abundance of dolomite in the finer fractions, ranging from 5.5-10.6 % in the <38  $\mu\text{m}$  fractions, 3.1-7.4 % in the 63-38  $\mu\text{m}$  fractions and 0-3.8 % in the 125-63  $\mu\text{m}$  fractions. Literature supports this observation, with larger Mg concentrations in finer fractions relative to the same larger fraction (Fujiwara *et al.* 2011). This is interesting in the scope of health, as research has shown the mineral matrix to which anthropogenic metal pollutants are introduced influences the form in which the metals are present, which then ultimately influences the ability for metals to become bioaccessible if entry to the body is gained. Obrist *et al.* (2011) and Grangeon *et al.* (2012) both indicate that the organic and inorganic content of soil dictates the form in which Hg exists when introduced from anthropogenic sources.

Titanium rich particles were present in all RD samples, with abundance ranging from 0.7% to 18.4%. Generally there was a greater abundance

observed in the finer size fraction relative to the larger, with this being the case for seven of the eight campaigns for Ti. This is abundant, in comparison to the CC-SEM-EDX data, where the range was found to be 0.10-0.25%. A similar pattern is observed in terms of elevation of relative abundance in the finer fractions though. Again literature shows that the concentrations of Ti is greater in finer fractions of RD (Fujiwara *et al.* 2011; Potgieter-Vermaak *et al.* 2012a).

Similarly, Iron rich particles were present in all RD samples, with abundance ranging from 0.8% to 12.7% across all samples. In agreement with the calcium rich particles and the Titanium rich particles, Iron rich particles were more abundant in the finer fraction, this being the case for six of the eight sampling campaigns. The analysis here indicated that there a wide spread incidence of iron rich particles, in the form of  $\text{Fe}_2\text{O}_3$  and  $\text{FeOOH}$ , this is indicative of corrosion of high-Cr steel (Nachiappan and Cho 2005). Iron particles in RD have been analysed using Raman Spectroscopy in only two published studies. The most recent of these, which has already been cited in this section with reference to silicon rich particles, where presence of  $\text{Fe}_2\text{O}_3$  and  $\text{Fe}_3\text{O}_4$  were observed (Potgieter-Vermaak *et al.* 2012a). Taylor and Robertson (2009) also used Raman Spectroscopy to characterise Iron particles in RD samples from Manchester.  $\text{Fe}_2\text{O}_3$  and  $\text{FeOOH}$  were characterised, in these particles, it was found that high concentrations of Cr was present (up to 7.5%), as determined using electron microprobe analysis. The paper by Taylor and Robertson (2009) concludes with the assertion that the origin of these iron rich particles is vehicular wear. Interestingly, lead has also been shown to be present in iron rich particles of RD in Manchester. Barrett *et al.* (2010) reported that Pb-

sorbed goethite made up 44.9 % and 51.0 % of total Pb in the <38  $\mu\text{m}$  and 63-38  $\mu\text{m}$  fractions of RD respectively, as determined by XANES.

Only one copper containing particle was found using Raman Spectroscopy. Copper arsenate was found in the aut '13 63-38  $\mu\text{m}$  sample by Raman Spectroscopy. Referring back to the CC-SEM-EDX data, however, copper arsenate was found to be reasonably abundant. Interestingly the sample in which the copper arsenate particle was identified by Raman Spectroscopy was the sample with the largest quantity of copper arsenate particles as determined by CC-SEM-EDX. The only other copper compound defined in the clustering of SEM-EDX data displayed in section 4.4.1.2 was CuS. Copper sulphide was found sporadically in small quantities using the clustering analysis, however none was found using Raman Spectroscopy.

A similar lack in variation in the nature of Cr and Pb containing particles as determined by Raman Spectroscopy is seen. Only  $\text{PbCrO}_4$  was observed using Raman Spectroscopy, no other Pb or Cr containing compounds were observed. The incidence of  $\text{PbCrO}_4$  was too infrequent and sporadic to gain any quantitative data. It is apparent from this data that  $\text{PbCrO}_4$  is present, which is particularly interesting because it represents the carcinogenic oxidation state of Cr (VI).

Despite various studies using Raman Spectroscopy successfully as a quantitative approach (Kazimierski *et al.* 2002; Palermo *et al.* 2012), this study shows that this is extremely difficult in the context of highly heterogeneous samples. This heterogeneous nature also contributes to the difficulty of characterising many compounds which were shown to be present using the

clustering analysis presented in section 4.4.1.2. Additionally, the clustering process was designed to take into account the fact that these compounds may exist as a small particle or inclusion on a larger particle or group of aggregated particles. Raman spectroscopy has difficulty in this respect, where it can be hard to obtain spectra from inclusions, especially when they are small and the larger particle is a strong scatterer, such as a Ti rich particle or quartz.

Based on the analysis carried out so far Cu, Fe and Pb containing compounds should all be considered potentially harmful for human health, because of the reasons outlined at several points in this document. The Cr containing compounds, however, are a little more complex, in the respect that they are of far more concern when present as Cr (VI). Results from the CC-SEM-EDX and Raman Spectroscopy analysis have provided us with this qualitative and somewhat quantitative insight in to presence of Cr (VI) in RD, providing data for 1000 and 200 particles per sample respectively. However, to properly assess the risk to human health, a more representative approach to determine the concentrations at which Cr (VI) is present in RD is needed. The next section of this document will cover the approaches carried out to do this, when applied to RD this poses another novel accomplishment of this study.

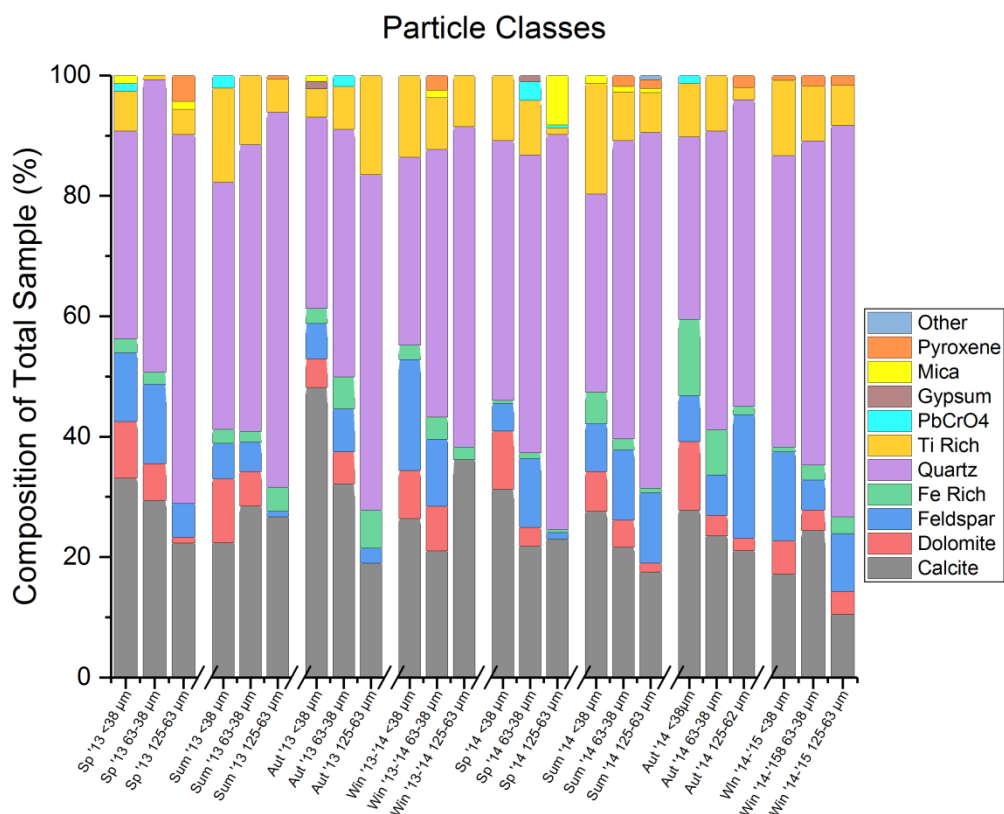


Figure 4-24: Particle classes for each campaign and size fraction as determined by DXR Raman Spectroscopy.

#### 4.5 Chromium (VI) Quantification

Cr (VI) was quantified using the approach outlined in section 3.4. In short, a basic digestion solution (0.5M NaOH, 0.3M Na<sub>2</sub>CO<sub>3</sub>) was used to force native Cr (VI) into solution and precipitate out native Cr (III), all without interconversion between the two. A GFAAS was then used to quantify Cr, as this technique would be able to analyse in the  $\mu\text{g kg}^{-1}$  (ppb) range.

Method development was carried out to ensure that no Cr (III) was present after digestion, up to a spiked content of 500ppb (this was the maximum tested). Tables 4-8 and 4-9 present the results of this method development for aqueous and solid reagents respectively. Each table shows six conditions

under which Cr (VI) and Cr (III) reagents were used to spike a digestion solution to give an appropriate final concentration. Each condition gave a final Cr concentration comparable to the expected concentration of Cr (VI) based on the spiked concentration. It was therefore considered that the method was suitable for precipitating out Cr (III) and solubilising Cr (VI). Table 8 shows that average Cr (VI) recovery using aqueous standards was 109.5% (n=3), roughly in line with pipetting and dilution error. Table 9 shows that average Cr (VI) recovery using solid reagents was 105.1% (n=3).

Table 4-8: Method development results for digestion of aqueous Cr standards at varying concentrations

condition	Spiked Cr(VI) concentration ( $\mu\text{g kg}^{-1}$ )	Spiked Cr (III) concentration ( $\mu\text{g kg}^{-1}$ )	Recovery of total Cr ( $\mu\text{g kg}^{-1}$ )	Cr (VI) recovery (%)
1	50	50	55.9	111.8
2	150	0	168.3	112.2
3	500	500	522.7	104.5
4	0	50	<LOD	<LOD
5	0	150	<LOD	<LOD
6	0	500	<LOD	<LOD

Table 4-9: Method development results for digestion of solid Cr standards at varying concentrations

condition	Spiked Cr(VI) concentration ( $\mu\text{g kg}^{-1}$ )	Spiked Cr (III) concentration ( $\mu\text{g kg}^{-1}$ )	Recovery of total Cr ( $\mu\text{g kg}^{-1}$ )	Cr (VI) recovery (%)
1	22.9	51.5	23.4	102.2
2	68.7	51.5	73.8	107.4
3	229	154.5	242.6	105.9
4	0	51.5	<LOD	<LOD
5	0	154.5	<LOD	<LOD
6	0	463.5	<LOD	<LOD

Once method development proved that this method of Cr(VI) quantification was capable of recovering only native Cr (VI), RD samples were analysed. Table 4-10 shows Cr (VI) concentrations in  $\text{mg kg}^{-1}$  for each the six extractions

of each RD sample. Displaying the data in this form allows the reader a clearer comprehension of how variable the data are, rather than simply displaying median values with standard deviations. This data is also displayed in figure 4-25, which features absolute values of Cr (VI) and total Cr. (note there is an axis break on the y-axis). Referring to the results presented in table 4-10 and figure 4-25, median concentrations ranged from below the limit of detection (<LOD) to 53.0 mg kg<sup>-1</sup>, with individual extractions yielding concentrations of up to 131 mg kg<sup>-1</sup>. Approximately a third (57 of the 144) extractions were found to be <LOD. The Sp '13 <38 µm fraction is a good example of how varied the extractions of a sample could be, this sample had three extractions below detection limit, the other three were 1.32 mg kg<sup>-1</sup>, 84.6 mg kg<sup>-1</sup> and 131 mg kg<sup>-1</sup>. Only one sample had all six extractions above the detection limit, Sum '13 63-38 µm, resulting in a median value of 53.0 mg kg<sup>-1</sup>. One sample had all six extractions below the detection limit, Aut '13 63-38 µm. Based on the heterogeneity of the other samples, however, it may not be appropriate to assume there is little of no Cr (VI) present in this sample.

Table 4-10: Total Cr (VI) concentrations of the 3 different size fractions for each extraction of RD collected over all sampling campaigns, as determined by GFAAS, along with median values based on those extractions. Data is presented here in mg kg<sup>-1</sup>.

Sp '13			
	<38 µm (mg kg <sup>-1</sup> )	63-38 µm (mg kg <sup>-1</sup> )	125-63 µm (mgkg <sup>-1</sup> )
Extract 1	84.6	0.96	6.09
Extract 2	131	<LOD	24.61
Extract 3	1.32	20.4	1.87
Extract 4	<LOD	<LOD	10.1
Extract 5	<LOD	<LOD	2.16
Extract 6	<LOD	28.8	38.6
Median	0.66	0.48	8.08
Sum '13			
	<38 µm (mg kg <sup>-1</sup> )	63-38 µm (mg kg <sup>-1</sup> )	125-63 µm (mgkg <sup>-1</sup> )
Extract 1	1.94	6.13	67.9
Extract 2	<LOD	115	1.79
Extract 3	24.2	105	1.1
Extract 4	5.17	50.9	65.2

Extract 5	<LOD	55.1	<LOD
Extract 6	<LOD	47.3	67.8
Median	0.97	53.0	33.5
Aut '13			
	<38 $\mu\text{m}$ (mg kg <sup>-1</sup> )	63-38 $\mu\text{m}$ (mg kg <sup>-1</sup> )	125-63 $\mu\text{m}$ (mgkg <sup>-1</sup> )
Extract 1	28.8	<LOD	4.86
Extract 2	15.6	<LOD	0.30
Extract 3	1.54	<LOD	<LOD
Extract 4	2.33	<LOD	<LOD
Extract 5	<LOD	<LOD	<LOD
Extract 6	<LOD	<LOD	<LOD
Median	1.94	<LOD	<LOD
Win'13-14			
	<38 $\mu\text{m}$ (mg kg <sup>-1</sup> )	63-38 $\mu\text{m}$ (mg kg <sup>-1</sup> )	125-63 $\mu\text{m}$ (mgkg <sup>-1</sup> )
Extract 1	41.9	1.27	4.80
Extract 2	65.6	0.00	1.07
Extract 3	<LOD	39.8	0.00
Extract 4	<LOD	4.70	36.2
Extract 5	<LOD	2.08	0.63
Extract 6	<LOD	118	0.00
Median	<LOD	3.39	0.85
Sp '14			
	<38 $\mu\text{m}$ (mg kg <sup>-1</sup> )	63-38 $\mu\text{m}$ (mg kg <sup>-1</sup> )	125-63 $\mu\text{m}$ (mgkg <sup>-1</sup> )
Extract 1	0.54	<LOD	10.9
Extract 2	<LOD	11.3	1.82
Extract 3	<LOD	<LOD	<LOD
Extract 4	0.15	3.05	<LOD
Extract 5	<LOD	<LOD	13.7
Extract 6	0.96	<LOD	<LOD
Median	0.08	<LOD	0.91
Sum '14			
	<38 $\mu\text{m}$ (mg kg <sup>-1</sup> )	63-38 $\mu\text{m}$ (mg kg <sup>-1</sup> )	125-63 $\mu\text{m}$ (mgkg <sup>-1</sup> )
Extract 1	<LOD	<LOD	0.67
Extract 2	14.1	<LOD	18.3
Extract 3	<LOD	<LOD	4.22
Extract 4	<LOD	34.2	0.00
Extract 5	4.25	<LOD	2.59
Extract 6	<LOD	1.48	6.34
Median	<LOD	<LOD	3.41
Aut '14			
	<38 $\mu\text{m}$ (mg kg <sup>-1</sup> )	63-38 $\mu\text{m}$ (mg kg <sup>-1</sup> )	125-63 $\mu\text{m}$ (mgkg <sup>-1</sup> )
Extract 1	3.43	0.06	2.83
Extract 2	5.08	3.22	<LOD
Extract 3	<LOD	<LOD	3.83
Extract 4	2.22	3.96	<LOD
Extract 5	<LOD	7.77	0.71
Extract 6	6.35	7.45	<LOD
Median	2.82	3.59	0.36
Win '14- '15			
	<38 $\mu\text{m}$ (mg kg <sup>-1</sup> )	63-38 $\mu\text{m}$ (mg kg <sup>-1</sup> )	125-63 $\mu\text{m}$ (mgkg <sup>-1</sup> )
Extract 1	1.47	2.26	2.21
Extract 2	0.46	4.05	0.83
Extract 3	0.29	0.36	3.82
Extract 4	<LOD	<LOD	0.91
Extract 5	<LOD	<LOD	2.16
Extract 6	<LOD	<LOD	<LOD
Median	0.14	0.18	1.53

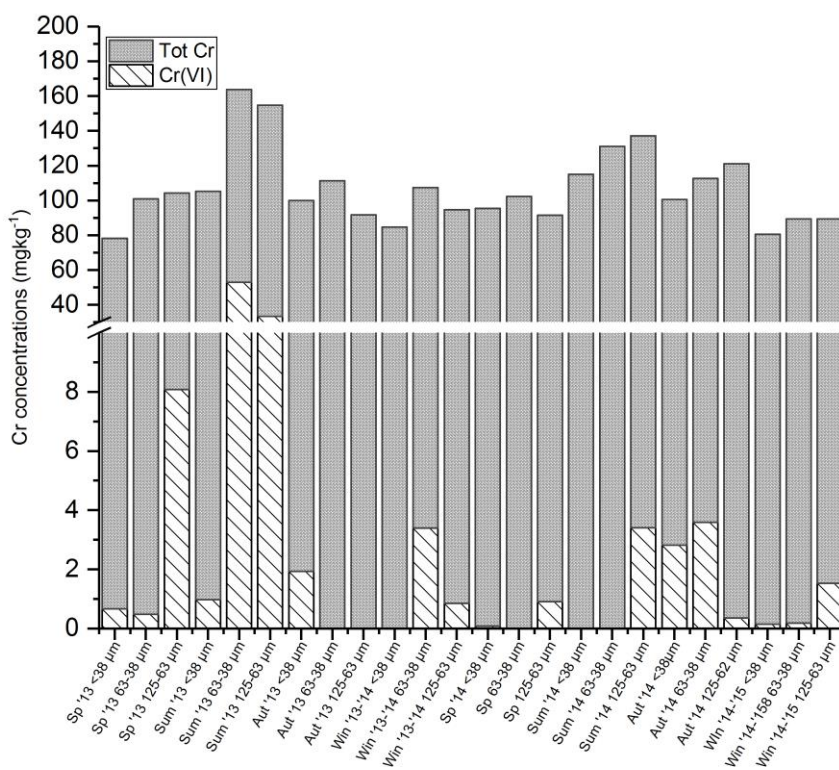


Figure 4-25: Total Cr and Cr (VI) in mg kg<sup>-1</sup> from each sample and fraction. Cr (VI) determined by base extraction and GFAAS, total Cr determined by acid digest and ICP-OES.

Figure 4-26: represents the portion of Cr (VI) present in each sample as a percentage of the total Cr, based on median concentrations. It can be observed that Cr (VI) generally makes up less than 10% of the total Cr within a sample. The two exceptions to this are the Sum '13 63-38 μm and Sum '13 125-63 μm samples which were found to be 47% and 27%, respectively.

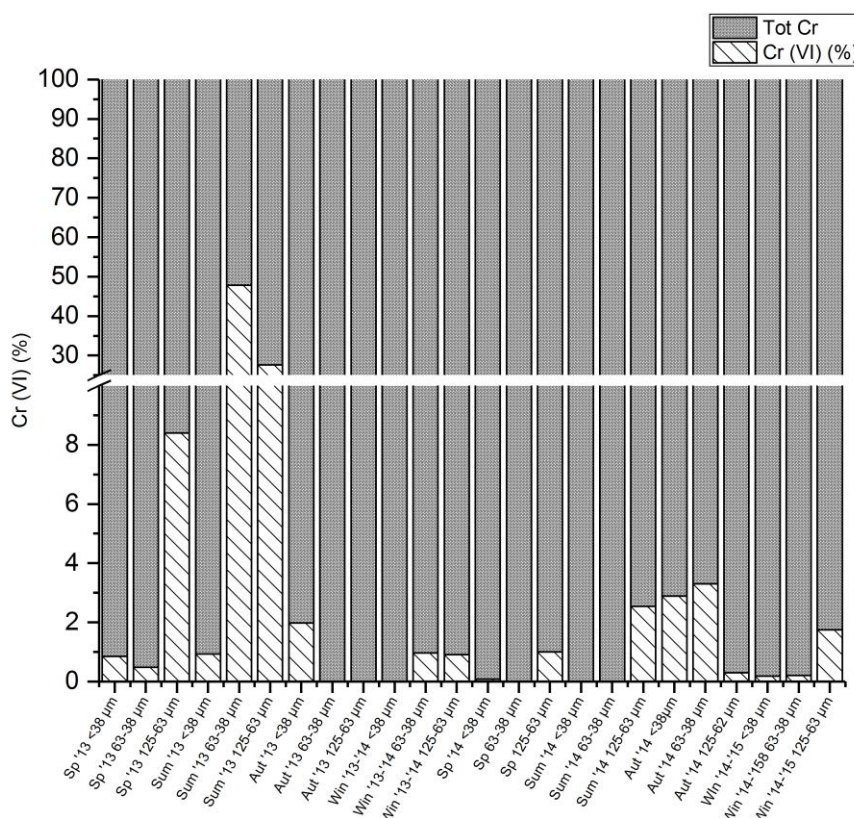


Figure 4-26: Cr (VI) as a portion of total Cr in each sample and fraction. Cr (VI) determined by base extraction and GFAAS, total Cr determined by acid digest and ICP-OES.

As mentioned in experimental section 3.4, there are no available publications regarding the concentrations of Cr (VI) in RD. There are, however, studies which investigated concentrations of Cr (VI) in airborne particulate matter. Swietlik *et al.* (2011) observed mean Cr (VI) concentrations of  $6.0 \text{ ng m}^{-3}$  in total suspended particles (TSP), which was reportedly up to 50% of the total Cr in TSP for the city centre location studied. The study followed the same digestion method as carried out on RD here, using voltammetry as the mode of analysis. Interestingly, this study also reports that there was a large variability in replicates, from  $2.1 \text{ ng m}^{-3}$  to  $98 \text{ ng m}^{-3}$ . Borai *et al.* 2002 found Cr (VI) concentrations in TSP ranging from  $0.93 \pm 0.06 \text{ mg kg}^{-1}$  to  $2.55 \pm 0.13 \text{ mg kg}^{-1}$  for six sampling sites in Egypt, again using the same digestion method,

though using ion chromatography as the analysis method. The study also reports that the Cr (VI) concentrations make up between 19% and 30% of total Cr across all sites examined. The study by Borai *et al.* (2002) reports similar Cr (VI) concentrations to the median values reported in RD for this research, crucially though, Borai *et al.* (2002) report very small variation on the reported values, which is a contrast to both this study and the published data from Swietlik *et al.* (2011).

The aim of this section, was to quantify Cr (VI) present in RD, so that it is possible to gain a more informed view on the potential health effects of Cr. As mentioned in section 2.5 of the literature review and the experimental methodology section 3.4, the toxicity of Cr is highly dependent on the oxidation state in which it is present, where Cr (III) is an essential dietary mineral whereas Cr (VI) is carcinogenic. The results presented in this section, show that Cr (VI) concentrations vary hugely, 0-51 mg kg<sup>-1</sup> based on median concentrations, each with large standard deviations. This data is based on 6 extractions each using 1 g of RD, which is a considerably large mass to use. The CC-SEM-EDX secondary constituents section 4.4.1.2, provided data from Cr containing particles to suggest that Cr (VI) was ubiquitous across all samples. The data collected in this section, however, shows that number of particles containing Cr (VI) does not necessarily equate to a large concentration being present in a sample. Nonetheless, the quantitative analysis in this section does show that in some samples, Cr (VI) can be present in large quantities. This observation is probably best explained by the Raman Spectroscopy, where large particles of PbCrO<sub>4</sub> were characterised in samples.

From a health point of view, we can therefore conclude that the concentration of Cr (VI) in RD which a person can potentially be exposed to can potentially be very high. This large variability makes it difficult to contextualise these results in terms of guidelines. The health and safety executive HSE (2002) recommends airborne Cr (VI) concentrations to not exceed  $50 \mu\text{g m}^{-3}$  in the workplace. Furthermore, DEFRA (2013) acknowledge studies showing that health based guidance values for Cr (VI) should not exceed  $0.9 \mu\text{g kg}^{-1} \text{ BW day}^{-1}$  (where BW is body weight of an individual). This value is better contextualised in the risk assessment section of this document, which brings the metal concentrations observed in this study into context with guideline values to form a risk assessment.

#### **4.6 Key Findings From Sections 4.4 and 4.5: A Short Conclusive Summary**

Sections 4.4 and 4.5 have covered the individual particle characteristics and Cr (VI) concentration in each RD sample collected over the two-year sampling period. This section covers the key findings from these two phases of study in a manner to keep the reader apprised with reference to the original aims of the study, but also to inform the subsequent sections. From the results discussed in sections 4.4 and 4.5, we can conclude:

- CC-SEM-EDX and Raman Spectroscopy techniques produce similar results to show that RD is mainly comprised of silicates, though the concentration of these vary with fraction size, where the finer fraction

appears to be more enriched with metal components. This is reflected in the primary clusters analysis from the CC-SEM-EDX, where trace metal rich particles were the second most abundant class. This plays an important role in the toxicity profile of RD

- CC-SEM-EDX results show that the form in which metals are present in particles varies more with particle size than seasonally.
- The CC-SEM-EDX analysis also concluded that Cr containing particles were largely composed of  $K_2Cr_2O_7$  in the  $<38 \mu m$  fraction, Cr goethite in the  $63-38 \mu m$  fraction and  $PbCrO_4$  and  $Cr_2O_3/Cr(OH)_3/Cr$  as a free metal in the  $125-63\mu m$  fraction.
- This analysis also concluded that Cu particles were mainly organic Cu in all fractions, particularly the  $<38 \mu m$  fraction. Copper sulphide was also observed in most samples across all fraction sizes. Copper arsenate was observed in the  $63-38 \mu m$  and  $125-63\mu m$  fractions. Its presence was also confirmed by Raman Spectroscopy.
- CC-SEM-EDX analysis confirmed presence of Pb particles as mostly  $PbO$ /Organic Pb in the finer fraction of RD, with  $PbMnO_4$  and  $PbCrO_4$  more abundant in the  $63-38 \mu m$  and  $125-63 \mu m$  fractions.
- The Raman Spectroscopy analysis in this study was unable to provide characterisation of all the compounds proposed in the CC-SEM-EDX secondary constituents section 4.4.1.2. It is believed that the difficulty of obtaining spectra from inclusions on particles contributed to this.

- The Raman spectroscopy did, however, show the presence of several, large  $\text{PbCrO}_4$  particles. The sporadic observation of these particles may explain the Cr (VI) distribution observed in the chromium (VI) quantification section 4.5. In that section, concentrations of Cr (VI) varied significantly, even between extractions of the same samples.

The results of this chapter have satisfied the first aim as outlined in chapter 1 of this document, “To gain a comprehensive understanding of the metal composition of individual inhalable and ingestible RD particles”. Moving on to the final sections of this chapter, the challenge is to quantify the leachates of Cr, Cu, Fe and Pb in simulated biological fluids, applying the findings from the single particle analysis to the subsequent findings. This process will then inform the new risk assessment protocol. Firstly though, as outlined in the literature review and experimental methods chapters, the challenge is to assess which size of particles are appropriate for use for the respiratory route of entry to the body. Completion of these goals will satisfy two more of the aims outline in chapter 1, “To elucidate the bioaccessibility of inhalable and ingestible particles” and “Develop an appropriate risk assessment methodology for RD by modifying existing approaches”.

#### **4.7 <math> <38 \mu\text{m}</math> RD Fraction as a Proxy for Inhalable Particulates**

As acknowledged in several sections of this report (literature review section 2.1.6 and experimental methodology section 3.5), there is uncertainty in the scientific community regarding the size of particles which are appropriate for use in studies regarding inhalation of particles. This phase of study intends to address this, along with one of the key aims of the study, to gain a

comprehensive understanding of the metal composition of individual inhalable and ingestible RD particles.

Accordingly, this section approaches the problem by investigating whether a fine fraction of RD (in this case  $<38\ \mu\text{m}$ ) can be considered representative of the  $<10\ \mu\text{m}$  RD particles which have been shown in literature to make up a considerable portion of  $\text{PM}_{10}$ , which is most widely considered inhalable.

#### 4.7.1 Particle Size Analysis

Once particles had been separated, using the method described in section 3.5, it was necessary to justify use of the separation technique by analytically testing for separation efficiency. Particle size was determined using CC-SEM-EDX, this technique is described in detail in section 3.3.2. Analysis of 1500 particles was carried out for each of the two fractions. The smallest measurable diameter was  $0.5\ \mu\text{m}$ , as particles smaller than this are indistinguishable from imperfections in the silver foil surface. Figure 4-27 shows particle size distribution as determined by CC-SEM-EDX for the  $<10\ \mu\text{m}$  and  $<38\ \mu\text{m}$  fractions. The figure divides particles into bins based on particle size, starting with  $0.5\text{-}1.5\ \mu\text{m}$ , then  $1.5\text{-}2.5\ \mu\text{m}$  etc. presented along the x-axis as average particle diameter ( $D_p$ ). The primary y-axes show the number of particles in each bin divided by the total number of particles ( $n_i/n_t$ ). Presenting particle size distribution data in this manner is common for particulate matter (Chen *et al.* 1997; Lin *et al.* 2005; Potgieter-Vermaak *et al.* 2012b; Yue *et al.* 2013) and RD (McKenzie *et al.* 2008). These studies tend to log the number of particles in each bin. It was that felt that logging the number of particles in each bin failed to give a clearer visual representation of the

particle size distribution. The secondary y-axis of figure 4-27 shows a cumulative distribution of particles, by summing the number of particles in each preceding bin, as a percentage of the total number of particles ( $N(D_p)/n_t$ ). The cumulative distribution is included to give an indication of the type of distribution observed. Both the <38  $\mu\text{m}$  and the <10  $\mu\text{m}$  fraction showed somewhat of a lognormal distribution, however there are too many smaller particles to fit this distribution with statistical confidence. It is observed that the number of particles smaller than 1.5  $\mu\text{m}$  dropped off in the <38  $\mu\text{m}$  fraction, but carried on increasing in the <10  $\mu\text{m}$  fraction. It is possible that this was caused by the separation technique failing to remove some particles between 1.5-10  $\mu\text{m}$ , therefore under representing them in the <10  $\mu\text{m}$  fraction. This is unavoidable using a technique, which assumes uniform density of particles.

Geometric median and geometric standard deviation are calculated using equations given by Potgieter-Vermaak *et al.* (2012b). The geometric median particle size in the <10 $\mu\text{m}$  fraction is 1.7  $\mu\text{m}$  (geometric standard deviation 2.3  $\mu\text{m}$ ) and it was found that 94.3% of particles were smaller than 10  $\mu\text{m}$ . In the <38  $\mu\text{m}$  fraction, the geometric median particle size was 3.5  $\mu\text{m}$  (geometric standard deviation 2.3  $\mu\text{m}$ ) with 90.4% of particles smaller than 10  $\mu\text{m}$ . These results show that a good separation efficiency was achieved with this technique, a significant portion of the particles larger than 10  $\mu\text{m}$  have been removed. This is exhibited by performing the Mann-Whitney test, comparing the sizes of particles in the <38  $\mu\text{m}$  and <10  $\mu\text{m}$  sample shows conclusively that the medians of these two data sets are significantly different. A p value of less than  $p=0.05$  is achieved. The distribution of particles observed here in the

<10 $\mu\text{m}$  fraction was similar to that reported by McKenzie *et al.* (2008). In both cases, particles were measured down to a size of 0.5  $\mu\text{m}$ , albeit using different instrumentation. Interestingly results from this study showed a greater exponential skew toward the smallest particles. This could possibly be due to differences in sites or the vacuum collection method used by McKenzie *et al.* (2008). The large number of small particles observed here in the <38  $\mu\text{m}$  fraction supports the concept that RD inherently contains a large number of small particles (Kong *et al.* 2012). This is a crucial observation with respect to the aim of this study; thoracic particles do make up a significant portion of RD.

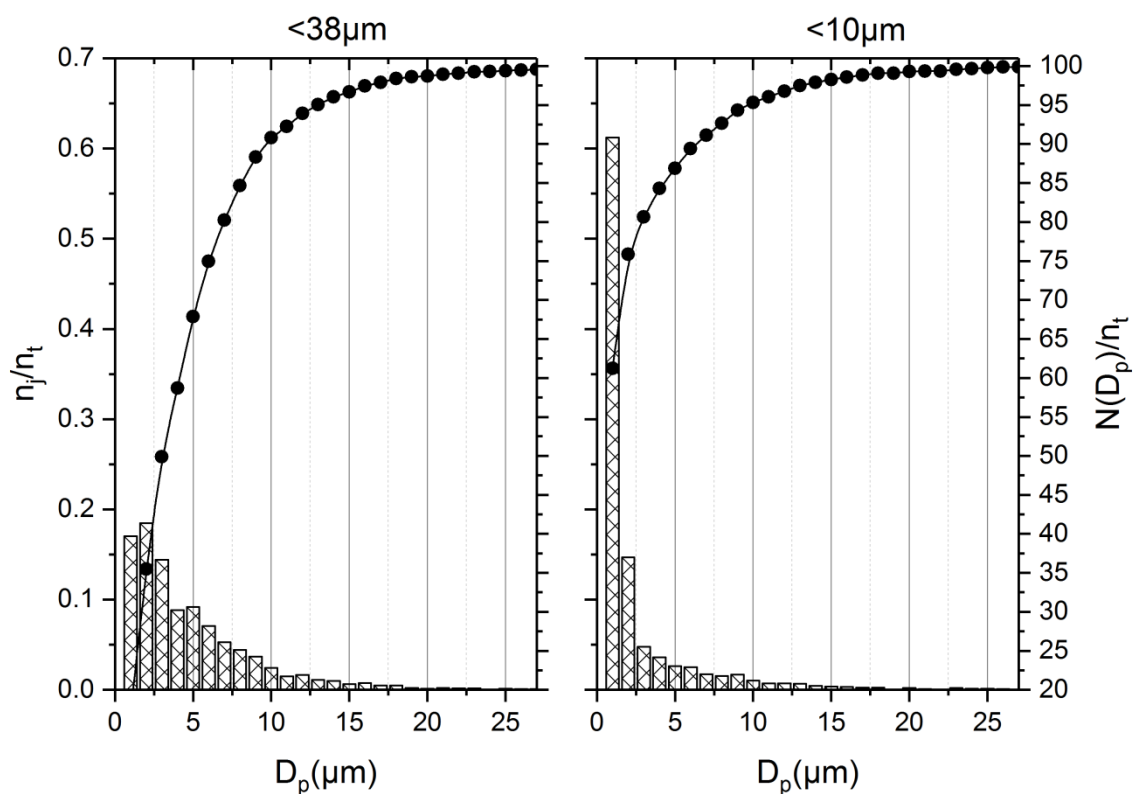


Figure 4-27: Particle size distributions from each fraction.

#### 4.7.2 Elemental Composition

To determine the similarity in chemical composition between the two samples, an elemental profile of the two samples were determined by ICP-OES, as described in section 3.2. The technique used here includes a large suite of metals, this is contrary to the bulk metal analysis results described here in results section 4.2 where only Cr, Cu, Fe and Pb are considered. The reason for this difference in approach is that the use obtaining bulk metal profile here is not to quantify metals as a means to suggest their potential harmful nature, merely as an indicator to show the degree to which these two samples differ. Results from the acid digestion experiment indicated a significant difference in metal concentrations observed between the <38  $\mu\text{m}$  and <10  $\mu\text{m}$  fractions, as displayed in table 4-10. Elemental concentrations were increased in the <10 $\mu\text{m}$  fraction for each element quantified. Table 4-10 also includes the % increase in concentration observed in the <10  $\mu\text{m}$  fraction.

Table 4-10: Acid soluble metal concentrations of the <10 and <38  $\mu\text{m}$  RD fractions.

	Al	As	Cr	Cu	Fe	Mn	Ni	Pb	Sn	Zn
<10 $\mu\text{m}$ (mg/kg)	2127 0 $\pm 7.9$ %	4.97 $\pm 8.6$ %	67.48 $\pm 5.1$ %	722.4 $\pm 0.9$ %	3970 0 $\pm 1.1$ %	618 $\pm 0.8$ %	25.81 $\pm 6.7$ %	329.0 $\pm 0.8$ %	53.55 $\pm 1.4$ %	1124 $\pm 0.9$ %
<38 $\mu\text{m}$ (mg/kg)	1401 0 $\pm 3.6$ %	3.00 $\pm 11\%$	63.68 $\pm 3\%$	457.6 $\pm 1.6$ %	3554 0 $\pm 1.5$ %	578.8 $\pm 1.6$ %	20.97 $\pm 3.8$ %	232.0 $\pm 0.4$ %	46.13 $\pm 1.6$ %	756.4 $\pm 1.6$ %
Increase (%)	51.8	66.3	6.0	57.8	11.7	6.8	23.1	41.8	16.1	48.6

Elemental concentrations in the <10  $\mu\text{m}$  fractions showed the trend Fe>Al>Zn>Cu>Mn>Pb>Cr>Sn>Ni>As. The same pattern was observed in the <38  $\mu\text{m}$  fraction, with the exception of Mn, which was more abundant than copper. Albuquerque *et al.* (2016) concluded a similar pattern of metal

concentration of PM<sub>10</sub>, Zn>Cu>Pb>Mn>Cr>Ni>As, the notable difference being the increased Pb concentration relative to Mn. Other studies investigating metal concentrations of PM<sub>10</sub> also indicated a similar order, again with Pb being more abundant than Mn (Lim *et al.* 2010). It is worth noting that specific metal concentrations, in terms of absolute concentration and relative to other metals are very dependent on site. It is also worth acknowledging that literature quoting concentrations of metals within PM<sub>10</sub> will generally be reported in units of mass per volume (of air), as collection on filters is the most common method of quantification.

Such large differences in metal concentrations between the fractions may appear to conclusively disprove any possibility that the two samples may be comparable. However, it is documented that the largest constituent of RD is Si, and that the concentration of Si increases in larger grain fractions (Cesari *et al.* 2012). It is feasible that the difference between the two samples may be the significantly larger concentration of Si in the <38 µm fraction.

In an attempt to determine whether the influence of Si is indeed preventing the <38 µm and the <10 µm fractions from being considered, we are able to refer back to the SEM-EDX work originally carried out as a means of ascertaining particle size distribution. Using the single particle EDX data and recalculating the percentage weight (%Wt) composition for each particle where C, O and, crucially, Si have been removed, we can compare quantities of each remaining element present in each sample. A full suite of crustal and trace elements quantified by SEM-EDX were included in the %Wt equation to increase accuracy. Distribution for each element also quantified by SEM-EDX was

found to be skewed left (Al, As, Cr, Cu, Fe, Mn, Ni, Pb, Sn and Zn). Therefore, the Mann-Whitney U test was used to compare each of them between the <10 $\mu\text{m}$  and <38 $\mu\text{m}$  fraction, the null hypothesis ( $H_0$ ) being that the samples are statistically not the same. With the exception of Fe, Zn and As, it was found that we could accept the alternative hypothesis for all other elements. In the case of As, the SEM-EDX data indicated too few As containing particles in either fraction to perform a Mann-Whitney U test. Concerning Fe and Zn, the Mann-Whitney U test indicated that these elements were more enriched in the <10 $\mu\text{m}$  fraction.

#### 4.7.3 Mobility in Simulated Biological Fluid

To further test the hypothesis that <38  $\mu\text{m}$  fraction can be used as a proxy for the <10  $\mu\text{m}$  fraction, the two samples were subjected to in vitro testing. Leachate concentrations for both samples are displayed in  $\text{mg kg}^{-1}$  in Table 4-11. Table 4-12 shows bioaccessibility of each element, determined using equation 2-1 in the literature review section of this document, where leached concentrations are those displayed in 4-11 and total concentrations are those displayed in table 4-10 of the previous section.

Table 4-11: ALF leached concentrations ( $\text{mg kg}^{-1}$ ) and RSD (%) for the <10 and <38  $\mu\text{m}$  RD fractions.

	Al	As	Cr	Cu	Fe	Mn	Ni	Pb	Sn	Zn
<10 $\mu\text{m}$ (mg/kg)	3710 $\pm 2.6$ %	5.0 $\pm 4$ 2%	34.6 7 $\pm 6.7$ %	605.9 $\pm 2.7$ %	1236 0 $\pm 8.3$ %	470.2 $\pm 5.9$ %	25.63 $\pm 1.2$ %	248.6 $\pm 5.2$ %	26.92 $\pm 9.9$ %	1131 $\pm 4.9$ %
<38 $\mu\text{m}$ (mg/kg)	2191 $\pm 2.2$ %	3.6 9 $\pm 4$ 9%	21.2 1 $\pm 2.1$ %	252.1 $\pm 2.1$ %	7950 $\pm 2.0$ %	326.4 $\pm 1.3$ %	18.82 $\pm 1.3$ %	145.2 $\pm 2.9$ %	21.08 $\pm 1.6$ %	642.3 $\pm 1.6$ %

Table 4-12: Percentage bioaccessibility for the <10 and <38  $\mu\text{m}$  fractions.

	Al	As	Cr	Cu	Fe	Mn	Ni	Pb	Sn	Zn
<10 $\mu\text{m}$	17.4 $\pm 0.08$	107.9 $\pm 0.1$	51.4 $\pm 0.08$	83.9 $\pm 0.03$	31.1 $\pm 0.08$	76.1 $\pm 0.06$	99.3 $\pm 0.07$	75.6 $\pm 0.05$	50.3 $\pm 0.1$	100.8 $\pm 0.05$
<38 $\mu\text{m}$	15.6 $\pm 0.04$	123.5 $\pm 0.12$	33.3 $\pm 0.04$	55.1 $\pm 0.03$	22.4 $\pm 0.02$	56.4 $\pm 0.02$	89.8 $\pm 0.04$	62.6 $\pm 0.03$	45.7 $\pm 0.02$	84.9 $\pm 0.02$

Standard deviations for each metal in table 4-12 are given as calculated by propagation of errors (Miller and Miller 2005). The results from tables 4-11 and 4-12 do seem to indicate a strong similarity between the leaching behaviour of the two samples across the full range of metals. Considering the data in table 4-12, there is an average difference in bioaccessibility of 13.5% between any given element with respect to fraction size. This presents itself as generally fairly similar, taking into account the highly heterogeneous nature of RD. Further support exists in literature, where replicates within the same RD sample can range from 55.0-65.2% for Cu and 55.0-62.0% for Pb (Pelfrene *et al.* 2017). The results here appear to support the elemental composition results obtained using SEM-EDX. The results here suggesting that it is likely that the forms in which the metals are present in both samples, *i.e* mineralogically or otherwise are the same. It is noted that there are incidences where bioaccessibility is greater than 100%, this is due to the highly heterogeneous nature of RD, as observed in earlier sections in this work. Vastly different leaching behaviour between the two samples would suggest that different minerals or free metals are present in one sample but not the other. In comparison to other studies, the bioaccessibility in ALF results achieved here are in the same order as those collected by Wiseman and Zereni (2014), who

achieved bioaccessibility around an order of magnitude higher across the suite of metals analysed, generally between 60-80% bioaccessible.

Based in the results of section 4.7, it was decided that the <38 µm fraction of RD collected over the sampling campaign could be appropriately used to demonstrate the particles of RD which are likely to be inhaled. The next section in this chapter covers the results for this protocol.

## **4.8 *In Vitro* Analysis**

### **4.8.1 Respiratory Route**

Based on the results of the previous section, only the <38 µm fractions of RD from all sampling campaigns were exposed to artificial lung fluid. This process uses the methodology as described in section 3.6.1. The samples were not exposed to other simulated lung fluids, such as Gamble's solution, as previous work (undergraduate project) has shown that these RD samples leach minimally in Gamble's solution. ALF leaching data (as illustrated in Figure 4-28, total concentrations of leachates are presented in appendix A, table A-4) are presented as the percentage leached relative to that which was available, as determined in the bulk analysis protocol. It is therefore considered as its bioaccessibility (Colombo *et al.* 2008), this is calculated using equation 1 in section 1.1.6. There appears to be a distinct pattern in leaching with Cr, Cu and Fe, where slight peaks in leaching during autumn 2013 and again in summer 2014 are observed. However, Pb showed an initial peak in winter 2013-14, then a second peak in summer 2014. While the peaks in data are somewhat consistent, the campaigns of lower leaching, troughs, for each

metal are less so. There are examples of troughs occurring in each season for various metals, spring being the most common. These observations show the subtle, but valuable difference between using bulk data to estimate health effects rather than *in vitro* studies. The small variation in bioaccessibility % potentially indicates that there may be a subtle change in the nature of pollutants throughout the study. It is probable that the slight seasonal pattern indicates significant meteorological contribution, but also influences from other factors, perhaps changes in types of anthropogenic pollution. In terms of metal content, results indicate that the order of leaching is as follows  $Cu > Pb \gg Fe \approx Cr$ , dividing the metals into two distinct groups of Cu with Pb, and Cr with Fe. The figure shows that there is a significant fluctuation in the amount of each metal which is bioaccessible, with Cr ranging from 15.3-21.1%, Cu from 61.7-78.6%, Fe from 16.8-24.9% and Pb from 57.0-68.7%. In comparison to studies on the bioaccessibility of metals within ALF, the results obtained here are similar. Data from Pelfrene *et al.* (2017) show bioaccessibility of Cr was 8.7%, Cu was 55.0-65.2% and Pb was 55.0-62.0% for three different RD certified reference materials with particle sizes of  $<74 \mu m$ ,  $<90 \mu m$  and  $<100 \mu m$ . Guney *et al.* (2017) publish large variability amongst 6 contaminated urban soils fractioned to  $<20 \mu m$  with bioaccessibility ranging from 23.7-90.1% for Cu, 2.3-67.6% for Fe and 50.3-92% for Pb. The large variance in data between and within all of these studies particularly highlights the variable nature in bioaccessibility in RD.

Referring to the CC-SEM-EDX data on the secondary constituents of particles, in section 4.4.1.2, the  $<38 \mu m$  fractions of samples have been shown to

contain considerable amounts of Cr (VI) and organic Cu and Pb as well as iron oxide. Each of these represents a concern for human health as carcinogens and harmful substances. The Cr content of RD in the <38 $\mu$ m fraction is mostly made up of  $K_2Cr_2O_7$ , which is generally soluble in acidic solutions. This not reflected in this section though, where bioaccessibility is around 20%.

This shows that the bioaccessibility of these PHEs in biological fluids is a complex process and is subject to more than the solubility of these compounds in solution.

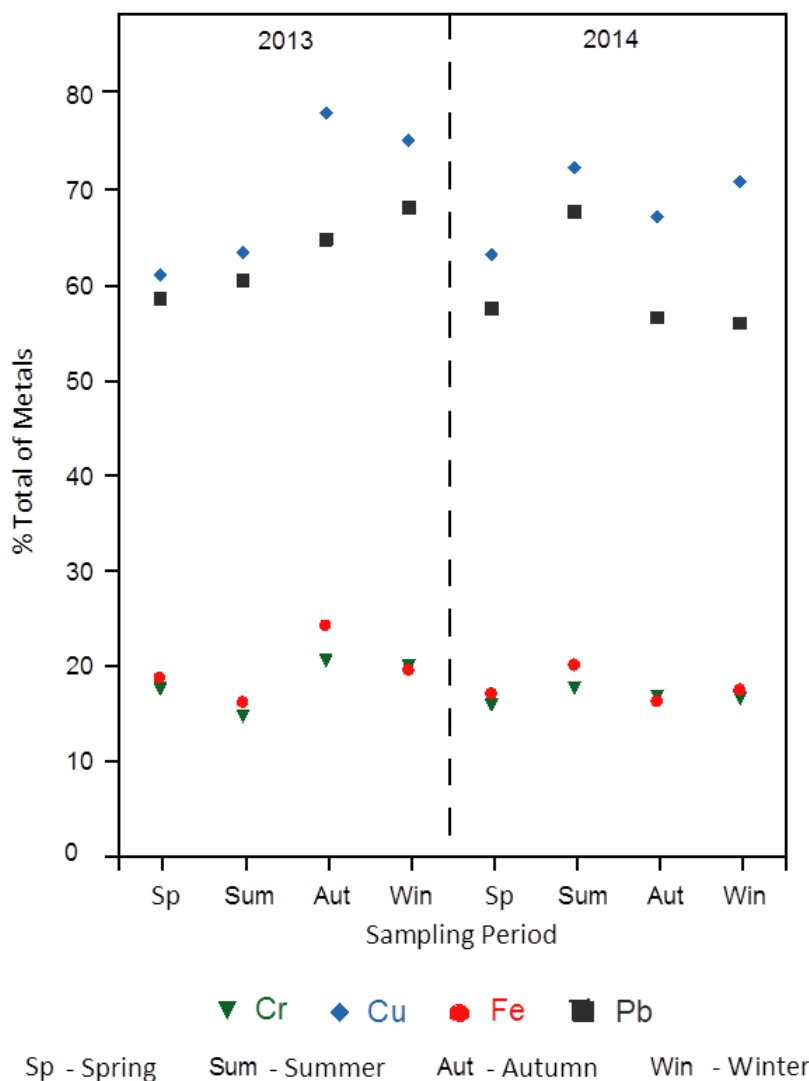


Figure 4-28: Percentage bioaccessibility of the < 38  $\mu$ m fraction of RD using the inhalation route leaching data.

#### 4.8.2 Gastrointestinal Route

The Ingestion leaching data in this study has been handled in the same manner as the inhalation route leaching data, whereby the bioaccessibility of each metal is quoted as a percentage of the bulk total, as determined in this study. Data are presented in Figures 4-29 and 4-30, with tabulated data in appendix A, table A-5 to A-10. Contrary to the inhalation leaching and bulk concentration data, the ingestion leaching data showed no particular temporal trend over the sampling campaign for Cr, Fe and Pb. However, ingestion leaching data for Cu generally appeared to increase from spring through to winter for both GI and GC conditions. Interestingly, the coarser size fraction leached more than the finer fraction in all conditions, with the exception of Cu under gastrointestinal conditions. One would typically expect the finer fraction to leach more due to its smaller surface area to volume ratio. It was observed that for Cr, Fe and Pb the GC conditions yielded higher bioaccessibility, while Cu was more bioaccessible in the GI conditions. In any condition, bioaccessibility for Cr and Fe was <2%, far lower than that of Cu and Pb which ranged from 7.9%-48.7% and 0.5%-21.5%, respectively. A large degree of variability is observed between samples in this study, this is also apparent in the published literature where reported bioaccessibility of Cu and Pb have ranged from 9%-40.9% and 5-25% respectively (Okorie *et al.* 2012; Poggio *et al.* 2009; Gbafa *et al.* 2010). Only Gbafa *et al.* (2010) investigated the bioaccessibility of Cr via the ingestion route: a median bioaccessible value of 0.3% was quoted. There is no literature available on the bioaccessibility of Fe from RD via the ingestion route.

Figure 4-29 shows that bioaccessibility of Pb via GC ingestion route is elevated in the 125-63  $\mu\text{m}$  fraction, this is also somewhat the case for the 63-38  $\mu\text{m}$  fraction. This could possibly be attributed to the increased quantities of  $\text{PbCrO}_4$  and  $\text{PbCrO}_4\cdot\text{PbO}$  particles in these samples, as determined by CC-SEM-EDX data on the secondary constituents of particles outline in section 4.4.1.2.  $\text{PbCrO}_4$  has a small  $K_{\text{sp}}$  value of  $2.3 \times 10^{-13}$  (molar solubility  $4.8 \times 10^{-7}$ ) and is therefore insoluble in water. Under the acidic conditions of the GC solution, however, the solubility would likely increase because of the common ion effect, whereby the weak base, chromate, will hydrolyse to form  $\text{HCrO}_4^-$  ( $K_{\text{b}} = 2.7 \times 10^{-8}$ ,  $\text{p}K_{\text{b}} = 7.57$ ), this will evidently shift the solubility equilibrium to the right with the solubility increases from  $4.8 \times 10^{-7} \text{ mol l}^{-1}$  to  $6.8 \times 10^{-3} \text{ mol l}^{-1}$ . Accordingly, this could account for the increased Pb leachate concentration in the coarser fractions of RD exposed to the GC condition, as the secondary constituent CC-SEM-EDX data has shown that a larger number of  $\text{PbCrO}_4$  particles exist in these fractions. It doesn't, however, explain why the Cr bioaccessibility is so low across all samples and size fractions. This is another example of the complex nature of RD particles in biological fluids which was raised in section 4.8.1.

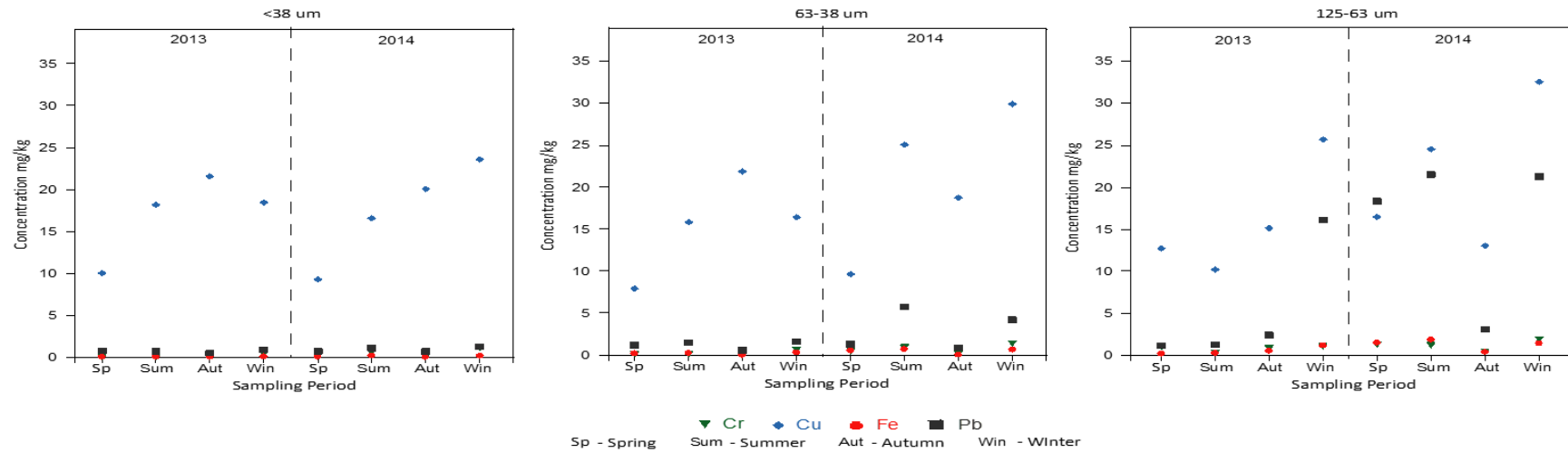


Figure 4-29: Percentage bioaccessibility of each fraction via GC ingestion route leaching

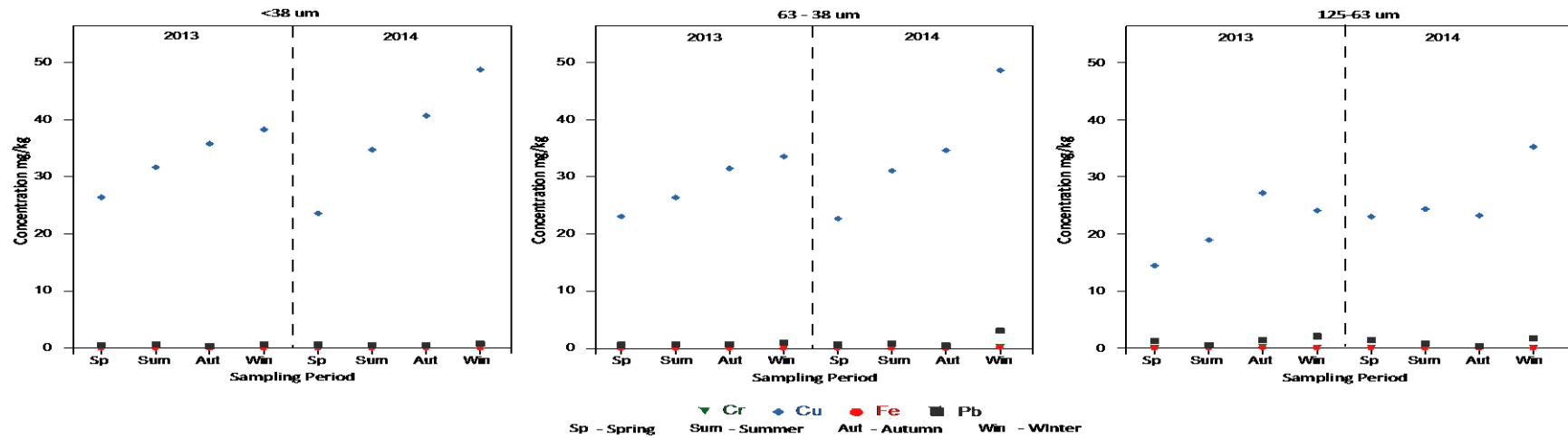


Figure 4-30: Percentage bioaccessibility of each fraction via GI ingestion route leaching

Section 4-8 has allowed for the bioaccessible quantities of Cr, Cu, Fe and Pb to be established. In line with the aims of this study, the task is now to risk assess these concentrations using a novel risk assessment protocol.

#### 4.9 Risk Assessment

Data for the risk assessment portion of this study was handled as stated in Section 3.7. To reiterate, only the ingestion and inhalation routes were included in the risk assessment, non-carcinogenic average daily doses via these routes for each PHE were calculated from equations 4-2 and 4-3. A hazard quotient (HQ) is then calculated for each PHE via each route by dividing ADDs by a reference dose (RfD), bespoke for each element, this is displayed in equation 4-4. Hazard quotients are then summed to produce a hazard index (HI) for each given element. Carcinogenic risk via a lifetime average daily dose (LADD<sub>inh</sub>) was also calculated for Cr inhalation using equation 4-5. The cancer risk is then calculated by multiplying the LADD<sub>inh</sub> by a cancer slope factor (CSF), as displayed in equation 4-6. Parameters for each of these equations are displayed in table 4-13.

Equation 4-2: Average daily dose of a pollutant via ingestion route.

$$ADD_{ing} = \frac{C \times R_{ing} \times CF \times EF \times ED}{BW \times AT}$$

Equation 4-3: Average daily dose of a pollutant via inhalation route.

$$ADD_{inh} = \frac{C \times R_{inh} \times EF \times ED \times ([TSP])}{BW \times AT}$$

Equation 4-4: Hazard index of a pollutant as determined by average daily dose and a reference dose.

$$HI = \frac{ADD}{RfD}$$

Equation 4-5: Lifetime average daily dose for carcinogens via the inhalation route

$$LADD_{inh} = \frac{C \times EF \times ([TSP])}{AT} \times \left( \frac{R_{inh\ child} \times ED_{child}}{BW_{child}} + \frac{R_{inh\ adult} \times ED_{adult}}{BW_{adult}} \right)$$

Equation 4-6: Cancer risk as determined by a lifetime average daily dose and cancer slope factor.

$$Cancer\ risk = LADD_{inh} \times CSF$$

Table 4-13: Parameters for average daily dose and lifetime average daily dose calculations.

Component	Definition (units)	Adult value used	Child value used	Reference
AT	Average Time (days)	365 x ED	365 x ED	This study
BW	Body Weight (kg)	84	21	Potgieter-Vermaak <i>et al.</i> 2012
C	Concentration of contaminant (mg/kg)	Leached metal concentrations	Leached metal concentrations	This study
CF	Conversion factor (kg/mg)	1 x 10 <sup>-6</sup>	1 x 10 <sup>-6</sup>	
ED	Exposure duration (years)	24	6	This study
EF	Exposure frequency (days/year)	350	350	This study
R <sub>ing</sub>	Ingestion rate (mg/day)	200	100	USEPA 1989
R <sub>inh</sub>	Inhalation rate (m <sup>3</sup> /day)	20	5	Du <i>et al.</i> 2014
TSP	RD derived Total suspended particles (kg/m <sup>3</sup> )	5.76 x 10 <sup>-8</sup>	5.76 x 10 <sup>-8</sup>	Brown <i>et al.</i> 2015

The concentration of each metal inserted into the LADD<sub>inh</sub> and ADD<sub>inh</sub> equations were the average leached concentrations for each metal over the two-year sampling campaign. This was considered the best representation of

the average bioaccessible concentration of metal over the chronic exposure duration detailed in Table 4-10. The Cr (VI) quantification results reported in section 4.5 also show that there is uncertainty regarding the amount of Cr (VI) which makes up the total concentration of Cr in RD, therefore the same concentration was used for Cr in the LADD<sub>inh</sub> equation. However, because of the acknowledged contention in literature over the size of particle which is most representative of those which can be ingested, a worst-case scenario approach was adopted. For each metal, the fraction with the highest average concentration over the two-year campaign was selected for the ADD<sub>ing</sub> equation.

Hazard index values for each of the four metals are displayed in Tables 4-14 and 4-15 for adults and children respectively. It can be observed from Tables 4-14 and 4-15 that even with the worst-case scenario approach, there are no metals that present a significant non-carcinogenic risk, but the results do show an elevated risk to children in comparison to adults. Similar approaches to risk assessment on the total concentration of RD have yielded similar insignificant risk (Du *et al.* 2014). However, these studies overestimate the actual exposure. There are results from two studies which risk assess the bioaccessible fraction of an exposure route available, both studies show incomplete data and have not considered appropriate bioaccessibility tests on the two main exposure routes, as in this study (Huang *et al.* 2016; Li *et al.* 2015). Both these studies, show insignificant non-carcinogenic risk.

Table 4-14: HI values for adults.

	Cr	Cu	Fe	Pb
HI	$8.6 \times 10^{-3}$	$1.0 \times 10^{-2}$	$6.2 \times 10^{-4}$	$1.7 \times 10^{-2}$

Table 4-15: HI values for children

	Cr	Cu	Fe	Pb
HI	$1.49 \times 10^{-2}$	$1.82 \times 10^{-2}$	$1.22 \times 10^{-3}$	$3.45 \times 10^{-2}$

While the hazard index equations showed that there was no non-carcinogenic risk due to Cr, Cu, Fe and Pb, the cancer risk as calculated from equations 4-5 and 4-6 produces a figure of  $1.9 \times 10^{-5}$ . This shows that there is a cancer risk associated with the bioaccessible concentrations of Cr in these samples of RD, as the figure is greater than  $1 \times 10^{-6}$  (Ferreira-Baptiste and De Miguel 2005; Chen *et al.* 2014; Singh and Gupta 2016; Samiksha *et al.* 2017; Mastro *et al.* 2017). This cancer risk for chromium exposure here exceeds values quoted in literature for soil and dust (Mastro *et al.* 2017) and RD (Ferreira-Baptiste and De Miguel 2005; Chen *et al.* 2014). Cancer risk due to chromium exposure has been reported higher than the figure obtained in this study on PM<sub>1</sub> samples (Singh and Gupta 2016) as well as PM<sub>10</sub> and PM<sub>2.5</sub> samples (Samiksha *et al.* 2017) both studies reported findings from India. The reason this study reports high Cr carcinogenic risk despite inputting a relatively low Cr concentration, is because of the modification to the LADD<sub>inh</sub> equation used in this study, as motivated in the literature review section 2.8. The other studies reported here use the particle emission factor (PEF) component in the LADD<sub>inh</sub> equation which is believed to underrepresent the number of particles available to inhalation.

#### 4.10 Key Findings from Sections 4.7, 4.8 and 4.9: A Short Conclusive

##### Summary

Sections 4.7, 4.8 and 4.9 have covered the appropriate particles to use for inhalation bioaccessibility studies, then executed this for Cr, Cu, Fe and Pb, along with ingestion bioaccessibility of these metals and a final risk assessment. This section covers the key findings from these phases of study in a manner to keep the reader apprised with reference to the original aims of the study. They also serve to inform the final chapters of this document. Based on the results of sections 4.7, 4.8 and 4.9 section we can conclude:

- The <38  $\mu\text{m}$  fraction of RD can be used as an appropriate proxy for the portion of RD which is inhalable, as determined by the analysis carried out in section 4.7
- The respiratory route is the more efficient route of metal bioaccessibility according to these *in vitro* studies, where Cu and Pb are particularly bioaccessible in ALF.
- A large variation in bioaccessibility of Pb is observed across different fraction sizes via the gastric route. This potentially indicates that the form in which lead is present may play a role on bioaccessibility. CC-SEM-EDX analysis indicates that a larger portion of  $\text{PbCrO}_4$  correlates to greater Pb bioaccessibility in the coarser fraction of RD. This, however, fails to explain other trends we see in the data and ultimately shows the complexity of studies of this nature.

- The risk assessment shows no significant non-carcinogenic risk associated with Cr, Cu, Fe and Pb. It does, however, show a significant chronic carcinogenic risk associated with Cr at these concentrations.

So far, this results section has covered the first three aims outlined in chapter 1, “to gain a comprehensive understanding of the metal composition of individual inhalable and ingestible RD particles”, “to elucidate the bioaccessibility of inhalable and ingestible particles” and “develop an appropriate risk assessment methodology for RD by modifying existing approaches”. This process has produced results which indicate some support for the hypothesis as outlined in chapter 1, “the chemical form in which metals are present in environmental particles is the main factor determining its fate in the environment and humans”, however, evidence is inconsistent and the similarity of the samples analysed up until now make it difficult to conclusively support this hypothesis. The next chapter addresses this shortcoming in the form of a case study, by looking specifically at Hg concentrations in RD from three different international sites.

## Chapter 5.

# Case study: Component-Specific Toxicity of Hg in Various Urban Road Dusts

*One of the principal conclusions drawn from the results presented in chapter 4 is that the bioaccessibility of metals within road dust (RD) is often independent of bulk concentration. It has been shown within this study that the form in which minerals are found has a significant influence on the concentrations which are able to leach into biological fluids. This finding ultimately underlines the necessity to conduct site-specific in-depth analysis of RD, to determine the concentration, chemical structure and speciation of the metals' occurrence in this matrix. Therefore, rather than simply assuming that higher bulk concentrations equate to more significant potential human health concerns, the leaching potential of the metal / element in its specific form (for example as a mineral), should be investigated. To that end, one element, mercury, was selected to display this hypothesis. As this is a case study, this chapter will be presented in the format of a scientific article, containing its own introduction and experimental sections, contrary to chapter 4, which reported on the Oxford Road, Manchester, UK*

*samples only. The case study shows an investigation of the total and bioaccessible mercury concentrations in RD from three international urban sites, where a one-off sampling campaign was conducted*

## 5.1 Introduction

Mercury pollution is of particular interest because of its documented effects to human health and particularly children *in utero* (Maramba *et al.* 2010). Neurological and behavioural disorders are commonly observed as a result of mercury inhalation (Hsi *et al.* 2014; Sondreal *et al.* 2004). Geological studies indicate that the naturally occurring crustal abundance of Hg is 20-60  $\mu\text{g kg}^{-1}$  (Kabata-Pendias and Mukherjee 2007), however there is a significant anthropogenic input worldwide, with major sources including fossil fuel combustion, metal production and mining, cement production and various other industries (Mahub *et al.* 2017). Mercury in these anthropogenically contaminated areas is mostly present as elemental mercury vapour with studies showing a range of 75-99% abundance, with the remainder being present as methyl mercury and the less abundant inorganic mercury (WHO 1990; EC 2001). Accordingly, the Environment Agency (U.K) has set soil guideline values of 1.0  $\text{mg kg}^{-1}$  for elemental mercury in residential soils (Environment Agency 2009). There is, however, evidence to suggest a more realistic guideline for chronic toxicity is 130  $\mu\text{g kg}^{-1}$  (Tipping *et al.* 2010)

Because of these publicised effects, many studies quantify total mercury in RD to assess possible health implications. There is a large body of research on the topic from China, where concentrations in RD have been observed as high as 600  $\mu\text{g kg}^{-1}$  in Xi'an, using Cold Vapour Atomic Absorption Spectroscopy (CVAAS). Han *et al.* (2006) reported concentrations of 120  $\mu\text{g kg}^{-1}$  in Nanjing, using ICP-MS (Hu *et al.* 2011), while Huang *et al.* (2014) report 220  $\mu\text{g kg}^{-1}$  in

Guangzhou using ICP-MS. There have also been several published papers quantifying Hg in other parts of the world. Londonio *et al.* (2012) found Hg concentrations as high as  $1.06 \text{ mg kg}^{-1}$  in Buenos Aires, Argentina using CVAAS. In Matsumoto, Japan, concentrations of Hg in road dust have been observed as high as  $26 \text{ } \mu\text{g kg}^{-1}$  (Ozaki *et al.* 2004) and Rodrigues *et al.* (2014) reported  $2.2 \text{ mg kg}^{-1}$  in southern Portugal using thermal decomposition atomic absorption spectroscopy in conjunction with a gold matrix modifier.

Based on the results of these studies, inferences have been made on the possible detrimental effects to human health. The ability of mercury to become accessible to the human body, however, is seldom considered. It is evident from the literature cited previously, that mercury levels in RD are site-specific. It is hypothesized that not only is bulk concentration site-specific, but that the bioaccessibility is as well, and the leaching profile onto artificial body fluids is not necessarily correlated with the bulk concentration. To test this hypothesis, RD were collected from three different international urban sites, Manchester (U.K), Curitiba (Brazil) and Johannesburg (South Africa). These three sites were selected for their diversity of pollutant sources. Mercury pollution in Johannesburg is well documented because of its notoriety as a by-product of the gold mining industry (Lusilao-Makiese *et al.* 2013; Gichuki and Mason 2013). Bleach production and the textile industry in the 1960s in Manchester has been linked with residual mercury pollution (Vane *et al.* 2009; Ngeutseng *et al.* 2015). The river Mersey in Manchester still has high mercury concentrations present in water and river sediments (Harland *et al.* 2000; Ngeutseng *et al.* 2015). Mercury pollution in Curitiba is most likely to originate

from the coal burning power stations of southern Brazil (Ancora *et al.* 2015; Da Costa *et al.* 2015; Rodriguez-Iruretagoiena *et al.* 2015). Representative aliquots of each RD were acid digested and Hg concentrations were analysed using CVAAS. Simultaneously, aliquots of each RD sample were exposed to artificial lysosomal fluid (ALF), where the resultant leachates were also analysed using CVAAS. Following this method allows for bioaccessibility via the inhalation route to be elucidated. It was deemed appropriate to only study the inhalation route, because it is believed that this is the most appropriate exposure route (Environment Agency 2009), but also because of equipment limitations where the lab work took place in Johannesburg.

## **5.2 Experimental Methodology**

### **5.2.1 Sampling Protocol**

Sampling took place at three urban sites, namely Manchester, Curitiba and Johannesburg. Each site was selected for being well trafficked by motor vehicles and pedestrians and the locations are shown in figures 5-1, 5-2 and 5-3. In line with the aim of this case study, sampling of RD was based on the method described in section 3.1 in order to keep the sampling protocol consistent. Samples were also size fractionated in the manner described in section 3.1, using sieves and a shaker. The sieves available in South Africa were different, however, therefore RD from the Johannesburg site was fractionated into samples <50 $\mu$ m and 100-50 $\mu$ m. Sampling took place in Curitiba during August 2014, during a research visit, and for the purpose of this investigation, it is designated as a winter sampling campaign because of the site location within the southern hemisphere. Similarly, the sampling campaign

in Johannesburg occurred during austral winter. The sample from Manchester was collected in winter 2014-15.

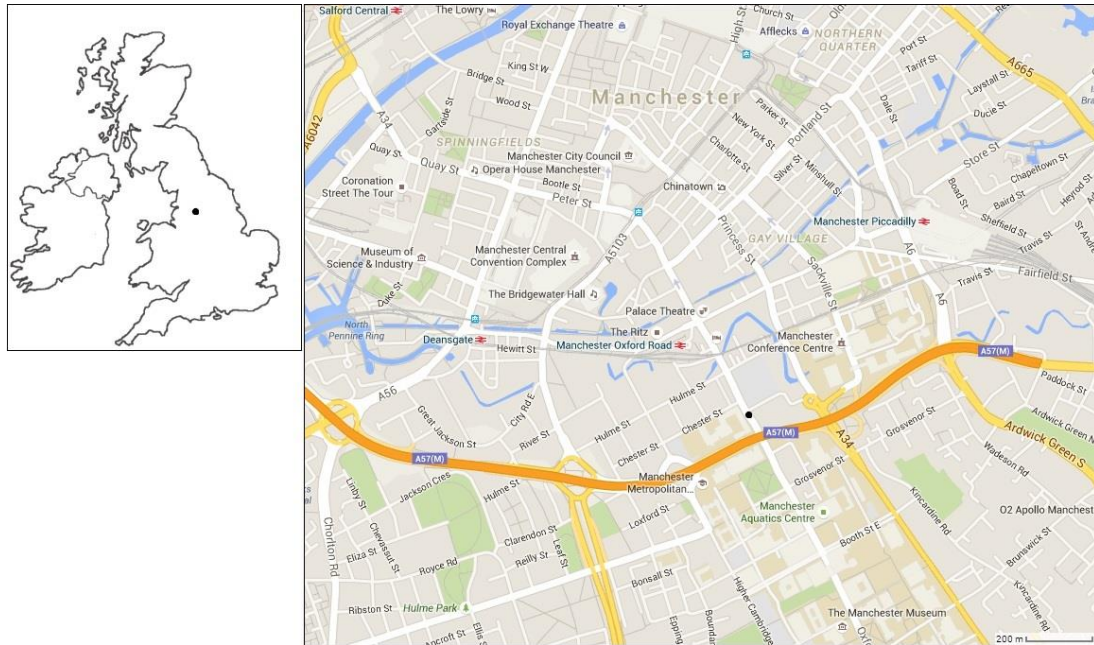


Figure 5-1: Manchester sampling site, indicated by the black dot, within the U.K. and within Manchester.

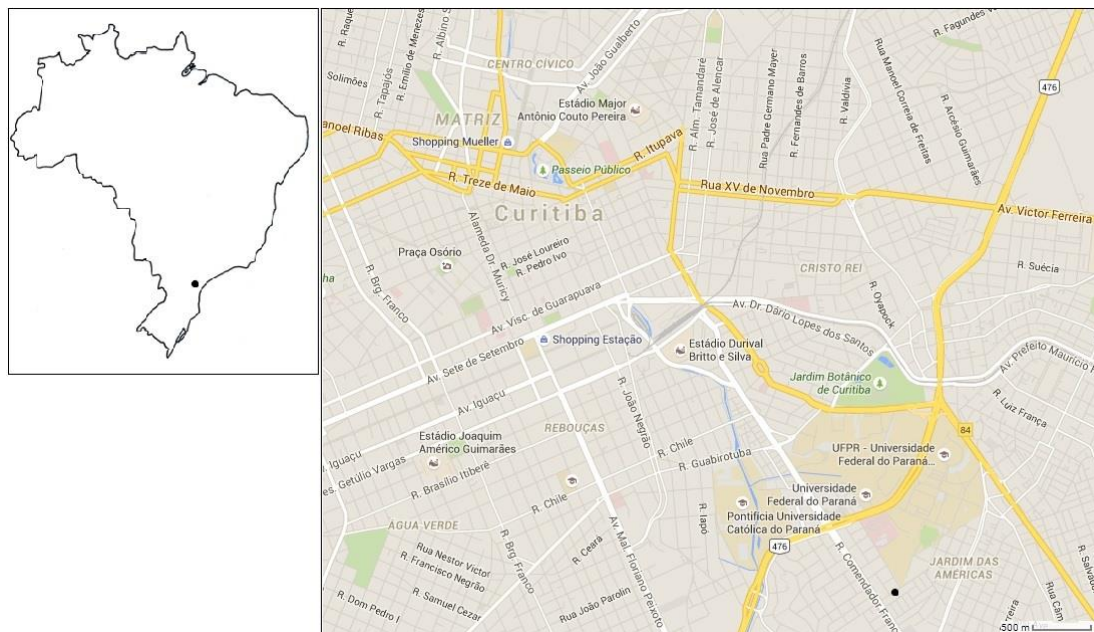


Figure 5-2: Curitiba sampling site, indicated by the black dot, within Brazil and within Curitiba.

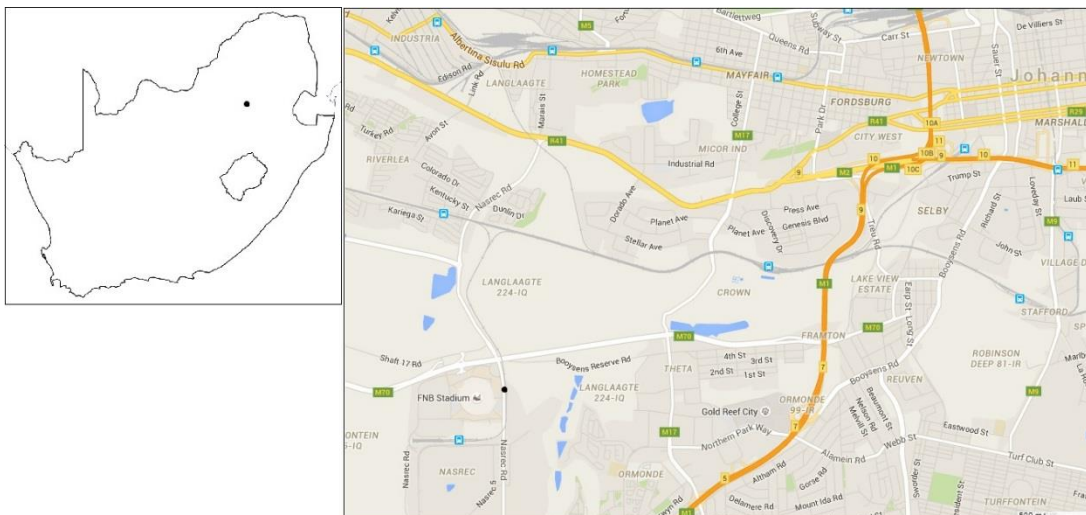


Figure 5-3: Johannesburg sampling site, indicated by the black dot, within South Africa and within Johannesburg.

### 5.2.2 Acid Digestion Technique

Samples were analysed in triplicate for total mercury using an aqua regia and hydrofluoric acid method described in United States Environmental Protection Agency method 3052 (USEPA 1996c). The method suggests exposure of 0.25 g of sample to reagent grade  $\text{HNO}_3$ ,  $\text{HCl}$  and  $\text{HF}$  in the ratio of 9:3:1 (v/v/v) in PTFE vessels. The mixture was then heated using a Perkin Elmer, Multiwave 3000 microwave at 800 W for 30 min, followed by 600 W for 20 min. Samples were then allowed to cool at room temperature before addition of  $\text{HBO}_3$  (6 ml per 1 ml of  $\text{HF}$ ) to precipitate excess fluoride, preventing secondary reactions. Samples were then syringe filtered before analysis using CVAAS. In addition to the samples, a highly enriched mercury containing certified reference material (CRM) (ERMCC580-Esturin sediment) was also digested in triplicate and analysed in the same manner.

### 5.2.3 Bioaccessibility Testing

Bioaccessibility testing was carried out in the same protocol described in section 3.6.1, whereby 15 ml of ALF with 0.15 g aliquots of each RD sample were used. Triplicate aliquots of each RD sample were extracted.

### 5.2.4 Cold Vapour Atomic Absorption Spectroscopy

A PerkinElmer FIMS 400 Flow Injection Mercury System with a PerkinElmer AAnalyst 200 atomic absorption spectrometer and AS-91 auto sampler was used to quantify mercury. The process injects the 500  $\mu\text{l}$  of sample into a reaction vessel, along with 1.1 % (m/v)  $\text{SnCl}_2$  in 3 % (v/v) HCl as a reducing agent, to ensure all Hg is in the 0 oxidation state (Harris 2016). The reaction vessel is then purged with Ar to liberate all gaseous Hg. The mercury vapour and Ar carrier gas continue through the system to a 15 cm quartz tube with a hollow cathode lamp (190 mA lamp current, 0.7 nm slit width, 253.7 nm wavelength of radiation) at one end, and a solar-blind detector at the other. Concentration of samples is determined relative to standards. In each set of analysis, matrix matched standards of 0, 1, 2, 5 and 10  $\mu\text{g L}^{-1}$  were used, both times regression line  $>0.99$  was achieved. To ensure no drift in instrument detection took place, quality control standards of 0.5 and 1  $\mu\text{g L}^{-1}$  were analysed every ten samples, recovery was consistent, between 94% and 99% in all cases. In addition to this, the CRM was analysed at the end of each analyses, giving a mean recovery for the CRM replicates of 99.0%, with RSD (%) of 3.70. Limit of detection for this instrumentation was found to be 0.0152  $\mu\text{g L}^{-1}$  based on the seven blanks of ALF and 0.0095  $\mu\text{g L}^{-1}$  based of seven blanks of the acid digestion solution.

## 5.3 Results

### 5.3.1 Bulk Hg Concentrations

Bulk mercury concentrations are displayed in figure 5-4 as median values with interquartile range and in table 5-1 with median and %RSD. Mercury concentrations for the Curitiba site showed comparable concentrations in the <38  $\mu\text{m}$  and 63-38  $\mu\text{m}$  fractions, with median values of 94  $\mu\text{g kg}^{-1}$  and 95  $\mu\text{g kg}^{-1}$ , respectively. The 125-63  $\mu\text{m}$  fraction was significantly less enriched, with a concentration of 41  $\mu\text{g kg}^{-1}$ . A similar pattern was observed with the Manchester samples, where the <38  $\mu\text{m}$  and 63-38  $\mu\text{m}$  fractions were similar, with medians of 190  $\mu\text{g kg}^{-1}$  and 139  $\mu\text{g kg}^{-1}$ , respectively; again the larger fraction was significantly less enriched with a median concentration of 67  $\mu\text{g kg}^{-1}$ . The Johannesburg sample showed significantly higher concentrations in the finer fraction relative to the coarser fraction, with concentrations of 482  $\mu\text{g kg}^{-1}$  and 117  $\mu\text{g kg}^{-1}$ , respectively. This large difference between the fractions is not observed in the Curitiba or Manchester samples, which implies that the Hg source or RD matrix has an influence on Hg distribution in RD. Each site shows significant enrichment relative to reported worldwide background concentrations of Hg, 20-60  $\mu\text{g kg}^{-1}$  (Kabata-Pendias and Mukherjee 2007).

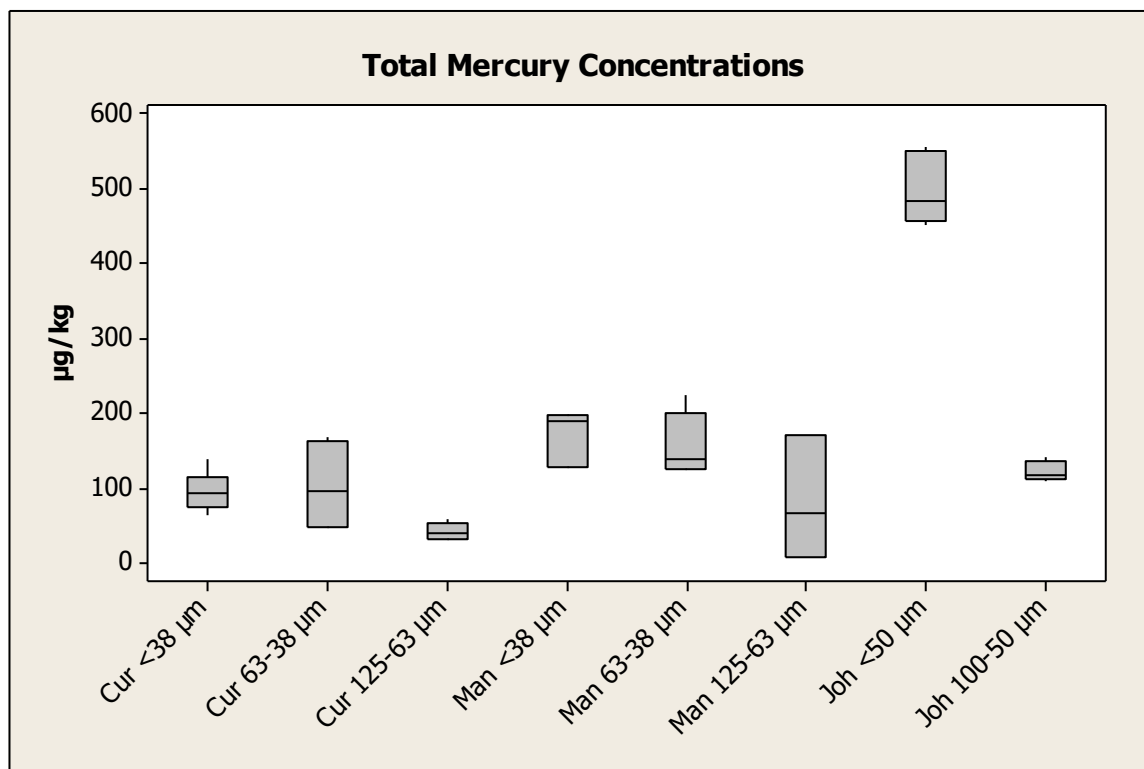


Figure 5-4: Box plots denoting the median acid soluble concentrations of Hg as determined by CVAAS for each sampling location and size fraction (where Cur = Curitiba, Man = Manchester and Joh = Johannesburg).

Table 5-1: Acid soluble concentrations of Hg as determined by CVAAS for each sampling location and size fraction (where Cur = Curitiba, Man = Manchester and Joh = Johannesburg).

	Cur <38 µm	Cur 63-38 µm	Cur 125- 63 µm	Man <38 µm	Man 63-38 µm	Man 125-63 µm	Joh <50 µm	Joh 100-50 µm
Concentration (µg kg <sup>-1</sup> )	93.91	95.44	40.56	189.75	139.49	67.95	482.31	117.37
%RSD	24.62	49.91	22.33	16.78	27.67	102.59	8.61	10.30

Table 5-2 summarises published concentrations of mercury in RD and the fraction size analysed. The concentrations found in the samples in this study were generally in the same range, perhaps slightly less concentrated than those found worldwide. It is noteworthy, however, that all of these studies only included one size fraction which was generally larger than those from this study. This could potentially indicate that finer fractions at each of these sites

could be significantly more enriched than reported if enrichment increases with decreasing size fraction, as demonstrated by this study.

Table 5-2: Literature reported Hg concentrations from international sites, along with appropriate grain size fraction.

Citation	[Hg] $\mu\text{g}/\text{kg}$	Grain size	Location
Han <i>et al.</i> 2006	600	<1000 $\mu\text{m}$	China
Hu <i>et al.</i> 2011	120	<63 $\mu\text{m}$	China
Huang <i>et al.</i> 2014	220	<100 $\mu\text{m}$	China
Londonio <i>et al.</i> 2012	1060	<1000 $\mu\text{m}$	Argentina
Ozaki <i>et al.</i> 2004	26	<2000 $\mu\text{m}$	Japan
Rodrigues <i>et al.</i> 2014	2200	<250 $\mu\text{m}$	Portugal

### 5.3.2 Artificial Lysosomal Fluid Leaching Concentrations of Hg

Leached and total concentrations of Hg are displayed by site in figure 5-5. This figure contains a break on the Y-axis to better present the portion of Hg that leaches. It can be observed from figure 5-5 that the total leaching concentration is significantly higher in the Manchester samples than that of the other two sites. It is also observable that the Hg concentration of the leachates is more enriched in the finer fractions for both the Manchester and the Johannesburg samples. This is not the case for the Curitiba samples, where the 63-38  $\mu\text{m}$  fraction shows the most leaching in terms of absolute concentration. The leached concentrations of Hg in the 125-65  $\mu\text{m}$  fraction of the Curitiba sample is missing from the figure, as the concentrations were found to be below the limit of detection for each replicate.

For the remainder of this results section, Hg concentrations will be referred to in the context of bioaccessibility as a percentage. Bioaccessibility described in detail in section 2.6 of this document, in the context of this case study, it is the

concentration of Hg able to leach into ALF over the total concentration in each sample displayed as a percentage. Bioaccessibility of Hg from each sample is displayed in figure 5-6 and table 5-3. Table 5-3 includes standard deviation, which is determined by propagation of errors (Miller and Miller 2005), a concept which has been described in section 4.7.3 of this document. Leached Hg concentration in the 125-63 $\mu$ m fraction of the Curitiba site was found to be below the limit of detection for each replicate, this has been signified in table 5-3 using the symbol <LOD.

Bioaccessibility results from this study show an interesting trend whereby the Manchester samples, of which 4.87-8.4% leached, are significantly more bioaccessible than those of Curitiba and Johannesburg, 0-0.88% and 0.32-0.33%. This would suggest that Hg is present in a different form in the Manchester samples. Under the slightly acidic conditions of the ALF, a higher bioaccessibility of Hg indicates that there may be more HgS and HgO present. The relative insolubility of Hg in the Curitiba and Johannesburg samples could potentially indicate the prevalence of Hg<sup>0</sup> and Hg-organic species (Bloom *et al.* 2003). In support of this, Malehase *et al.* 2016 have shown that Hg (0) prevails in mine tailings in Johannesburg, which can ultimately pollute RD. In the context of toxicity to humans, literature confirms the toxicity of mercury in the form of organic compounds, inorganic compounds and elemental mercury (Sysalova *et al.* 2017; Mahub *et al.* 2017). There is, however, evidence to suggest the effects of organic and elemental mercury are more potent (Lohren *et al.* 2015).

Referring back to the results of this study, when comparing size fractions within the same sampling location, the <38  $\mu\text{m}$  and 63-38  $\mu\text{m}$  fraction of RD from Curitiba had similar bioaccessibility (0.70 and 0.88%). Similarly, the two size fractions from the Johannesburg samples were comparable in terms of bioaccessibility (0.32 and 0.33%). This would suggest that in both cases, mercury is found in the same form and that corresponding RD matrix has no influence on this. Bioaccessibility in the 125-63  $\mu\text{m}$  Curitiba samples was found to be below the detection limit, which suggests that either the form in which the mercury is present differs from the two finer fractions from the same site or the RD matrix is different within this larger fraction. It is documented that when  $\text{Hg}^{2+}$  or  $\text{Hg}^0$  is introduced to a soil, the organic and inorganic content of the soils plays a significant role in dictating the form in which Hg is then found (Obrist *et al.* 2011; Grangeon *et al.* 2012). It is likely that a similar process occurs within RD and changes in mineral abundance between size fractions can result in this. In support of this possibility, the individual particle analysis section in chapter 4 of this document highlights the fact that changes in mineral abundance do occur between size fractions.

Studies in academic literature on bioaccessibility of Hg via the inhalation route are sparse. There are currently two studies published which explicitly quote concentrations of leachates or bioaccessibility. Both of these studies, however, have different experimental designs to this, which makes comparisons slightly difficult. Huang *et al.* (2014) published bioaccessibility of Hg in lung serum at 20.66%. This study, however, only used the <2.5  $\mu\text{m}$  portion of RD and there is no quoted pH for the lung serum. Rodrigues *et al.*

(2014) quote a bioaccessibility figure of 4.1% for Hg from urban soil <250  $\mu\text{m}$  using Gamble solution.

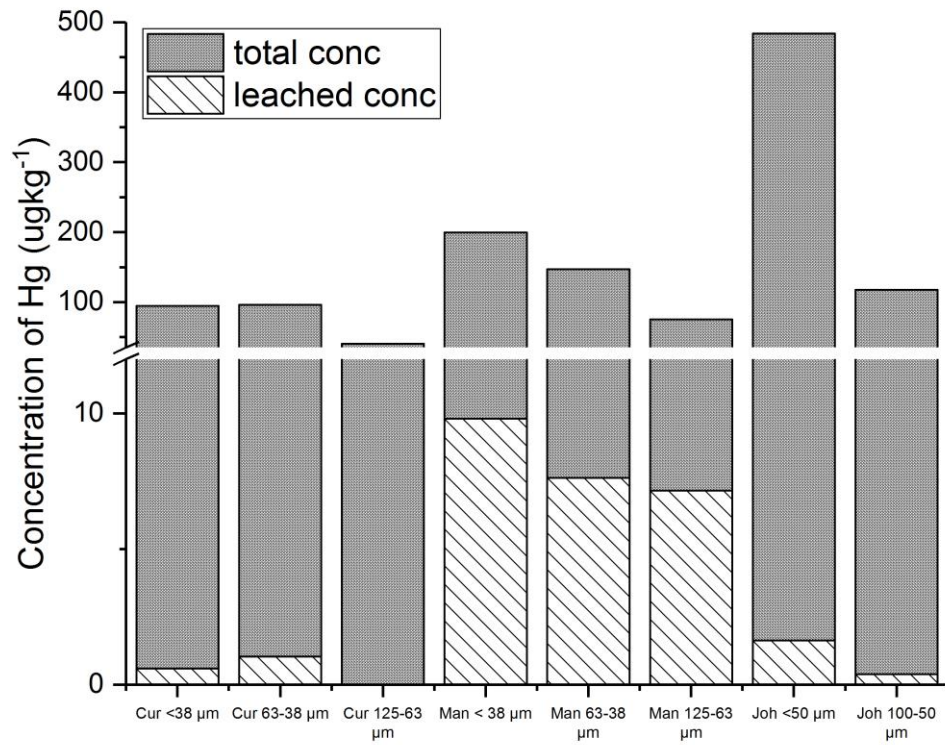


Figure 5-5: Leached and total mercury concentrations as determined by CVAAS.

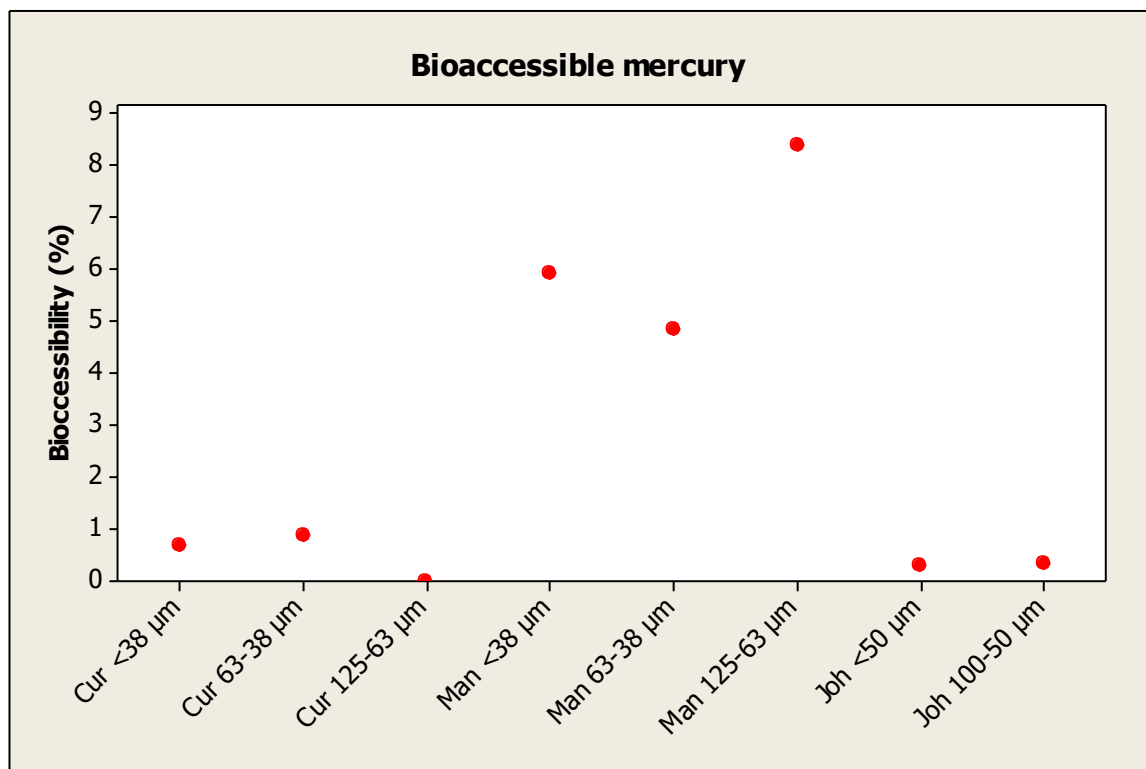


Figure 5-6: Dot plot denoting the bioaccessible concentrations of Hg for each sampling location and size fraction (where Cur = Curitiba, Man = Manchester and Joh = Johannesburg).

Table 5-3: bioaccessibility of Hg for each sampling location and size fraction (where Cur = Curitiba, Man = Manchester and Joh = Johannesburg).

	Cur <38 μm	Cur 63-38 μm	Cur 125-63 μm	Man <38 μm	Man 63-38 μm	Man 125- 63 μm	Joh <50 μm	Joh 100- 50 μm
Bioaccessibility (%)	0.70	0.88	<LOD	5.94	4.87	8.40	0.32	0.33
SD	0.64	0.79		0.29	0.26	0.85	1.00	0.95

## 5.4 Conclusions

The results of this study conclude that the bulk concentration and bioaccessibility of Hg varies significantly site to site. This has been demonstrated by the large observed differences in bulk and bioaccessible concentrations of Hg between the three sites. This is particularly evident while comparing the difference in bioaccessibility between the Manchester site and the other two others. It is that shown in the results section here that

bioaccessibility is up to an order of magnitude greater in the Manchester samples. The results obtained here would suggest that the source of Hg at each site has a large influence ultimately on the bioaccessibility of Hg.

The second interesting conclusion is that the results indicate that the RD matrix present at each site also has an influence on the form which Hg is present and this is manifested in this study by differences in bioaccessibility between size fractions at the Curitiba site. It can be seen in the results section of this case study that the bioaccessibility of Hg in the two finer fractions from the Curitiba site are 0.70% and 0.88%, however the larger size fraction leached no measurable quantity of Hg. It has been demonstrated in several studies that the mineral composition of soils has an influence on the Hg species found. This study is the first to show this influence within RD and indeed within different size fractions of RD from a single site.

The two key conclusions of this case study support the necessity to examine metal concentrations on a site-by-site basis, because it is the form in which a metal is present, which ultimately dictates its potential harm to human health. This case study also presents the importance of examining metals in terms of their mobility in biological fluids, in addition to simply obtaining concentrations. Based on these conclusions, this case study supports the findings from chapter 4 of this document and has successfully completed the final aim from chapter 1, supporting the hypothesis outlined there also.

The next chapter of this document serves as a final summary of this study, bringing together the findings from chapter 4 as well as this one to show how

the original hypothesis has been addressed in line with the aims and objectives.

## Chapter 6.

# Conclusions

*This chapter summarises the findings of this study in the context of the hypothesis, showing how the aims and objectives outlined in chapter 1 have been appropriately addressed.*

It was hypothesised in chapter 1 that the chemical form in which metals are present in environmental particles is the main factor determining its fate in the environment and humans. The aims set out to test this hypothesis were “to gain a comprehensive understanding of the metal composition of individual inhalable and ingestible RD particles”, “to elucidate the bioaccessibility of inhalable and ingestible particles”, “develop an appropriate risk assessment methodology for RD by modifying existing approaches” and “to apply such methodologies to a case study of the human inhalation exposure to Hg in RD in three cities around the world”. Chapters 4 and 5 of this document have addressed these aims, in the process summarising findings along the way, in a conclusive manner. These findings are now reiterated as follows:

- Moisture content of RD is more affected by temperature than rainfall, however there is a relationship between both moisture and temperature. This washout could possibly contribute to the observed lower metal concentrations in winter months. The enrichment observed in the summer months, however, along with the drier and more easily resuspended particle indicates a potentially high risk to human health. The reported seasonal variation in metal concentrations presented in this study is a novel contribution to the field
- Bulk metal concentrations of metals are enriched in the finer fractions of RD. The exception here being Cr, where the concentrations vary little between fraction sizes, but the middle fraction is slightly more concentrated.

- Bulk metal content of RD is site dependant. Based on the comparison of this study with other published literature, it is implied that there is a large influence from anthropogenic sources.
- CC-SEM-EDX and Raman Spectroscopy techniques produce similar results to show that RD is mainly comprised of silicates, though the concentration of these vary with fraction size, where the finer fraction appears to be more enriched with metal components. This is reflected in the primary clusters analysis from the CC-SEM-EDX, where trace metal rich particles were the second most abundant class. This plays an important role in the toxicity profile of RD
- CC-SEM-EDX results show that the form in which metals are present in particles varies with particle size, but not so much seasonally.
- The CC-SEM-EDX analysis also concluded that Cr containing particles were largely composed of  $K_2Cr_2O_7$  in the  $<38 \mu m$  fraction, Cr goethite in the  $63-38 \mu m$  fraction and  $PbCrO_4$  and  $Cr_2O_3/Cr(OH)_3/Cr$  as a free metal in the  $125-63 \mu m$  fraction. This was exhibited using a novel approach to CC-SEM-EDX data analysis.
- This analysis also concluded that Cu particles were mainly organic Cu in all fractions, particularly the  $<38 \mu m$  fraction. Copper sulphide was also observed in most samples across all fraction sizes. Copper arsenate was observed in the  $63-38 \mu m$  and  $125-63 \mu m$  fractions. Its presence was also confirmed by Raman Spectroscopy.

- CC-SEM-EDX analysis confirmed presence of Pb particles as mostly PbO/Organic Pb in the finer fraction of RD, with PbMnO<sub>4</sub> and PbCrO<sub>4</sub> more abundant in the 63-38 μm and 125-63μm fractions.
- The Raman Spectroscopy analysis in this study was unable to provide characterisation of all the compounds proposed in the CC-SEM-EDX secondary constituents section 4.4.1.2. It is believed that the difficulty of obtaining spectra from inclusions on particles contributed to this. Completing Raman Spectroscopy analysis on size segregated RD particles in conjunction with CC-SEM-EDX is presented here as a novel approach.
- The Raman spectroscopy showed the presence of several, large PbCrO<sub>4</sub> particles. The sporadic observation of these particles may explain the Cr (VI) distribution observed in the chromium (VI) quantification section 4.5. In that section, concentrations of Cr (VI) varied significantly, even between extractions of the same samples.
- The <38 μm fraction of RD can be used as an appropriate proxy for most metals in the portion of RD which is inhalable. This data produced in this manner is novel.
- The respiratory route is the more efficient route of metal bioaccessibility according to these *in vitro* studies, where Cu and Pb are particularly bioaccessible in ALF.
- A large variation in bioaccessibility of Pb is observed across different fraction sizes via the gastric route. This potentially indicates that the

form in which lead is present may play a role on bioaccessibility. CC-SEM-EDX analysis indicates that a larger portion of  $\text{PbCrO}_4$  correlates to greater Pb bioaccessibility in the coarser fraction of RD. This, however, fails to explain other trends we see in the data and ultimately shows the complexity of studies of this nature.

- The risk assessment shows no significant non-carcinogenic risk associated with Cr, Cu, Fe and Pb. It does, however, show a significant chronic carcinogenic risk associated with Cr at these concentrations.
- The Hg case study shows a large difference in the bioaccessibility of Hg from three different international samples. It is reasoned that the form in which Hg is present in these three different sites is the reason for the observed differences in bioaccessibility. This is the first study to present findings of this nature from different international sites.

This summary of findings shows a depth of knowledge on the topic of RD has been obtained by this study. To approach the hypothesis directly, results from *in vitro* studies presented in chapter 4 have shown that the bioaccessibility of Cr, Cu, Fe and Pb vary in different RD samples. A novel approach to individual particle analysis, also presented in chapter 4, shows that the compounds in which these metals are found in also vary across these samples. The nature of this data therefore indicates that there is somewhat of a relationship between the form in which these metals are found, and the bioaccessibility thereof. Further proof of this concept is provided in chapter 5, where a case study on Hg in RD showed that the form

in which Hg was present had a profound effect on the bioaccessibility in lung fluid.

Based on this summary, it is the belief of the author that the novel approaches to analysis and data handling have fulfilled the aims of this study to the appropriate level of quality for a PhD thesis. Despite this, there are several aspects of this topic which remain unanswered and require merit future study, for further advancement of this area of science.

Firstly, a different approach to a supplementary technique for the speciation of Cr, Cu, Fe and Pb. Perhaps use of XANES, or a way to improve the resolution of Raman Spectroscopy. This will conclusively prove what species of Cr, Cu, Fe and Pb are present in these RD samples.

Secondly a more robust and in-depth approach to *in vitro* studies could be utilised. It is the opinion of the author that the approach used in this study is appropriate for a good estimation of the bioaccessibility of metals, however lacks certain intricacies to be truly representative of the human body.

# References

Achillios, S., Wolfson, J. M., Fergusson, T., Kang, C. M., Hadjimitsis, D. G., Hadjicaralambous, M., Achillios, C., Christodoulou, A., Nisanzi, A., Papoutsas, C., Themistocleous, K., Athanasatos, S., Perdikou, S., Koutrakis, P. (2016). Spatial variability of fine and coarse particle composition and sources in Cyprus. *Atmospheric Research*, 169, pp. 255-270

Acosta, J. A., Gabarron, M., Faz, A., Martinez-Martinez, S., Zornoza, R., Arocena, J. M. (2015). Influence of population density on the concentration and speciation of metals in the soil and street dust in urban areas. *Chemosphere*, 134, 328-337

Ahmad M. K., Mokhtar, S. M., Soon, C. F., Nafarizal, N., Suriani, A. B., Mohamed A., Mamat, M. H., Malek. M. F., Shimomura, M., Murakami, K. (2016). Raman investigation of rutile-phased TiO<sub>2</sub> nanorods/nanoflowers with various reaction times using one step hydrothermal method. *Journal of Material Science: Materials in Electronics*, 27, pp. 7920-7926

Almeida S. M., Pio, C. A., Freitas, M. C., Reis, M. A., Trancoso, M. A. (2006). Source apportionment of atmospheric urban aerosol based on weekdays/weekend variability: evaluation of road re-suspended dust contribution. *Atmospheric Environment*, 40, 2058-2067

Alomary, A. A., Belhadj, S. (2007). Determination of heavy metals (Cd, Cr, Cu, Fe, Ni, Pb, Zn) by ICP-OES and their speciation in Algerian Mediterranean Sea sediments after a five-stage sequential extraction procedure. *Environmental Monitoring and Assessment*, 135, pp. 265-280.

Amato, F., Pandolfi, M., Escrig, A., Querol, X., Alastuey, A., Pey, J., Perez, N., Hopke, P. K. (2009). Quantifying road dust resuspension in urban environment by multilinear engine: A comparison with PMF2. *Atmospheric Environment*, 43, pp. 2770-2780

Anaf, W., Horemans, B., Van Grieken, R., Da Wael, K. (2012). Chemical boundary conditions for the classification of aerosol particles using computer controlled electron probe microanalysis. *Talanta*, 101, pp. 420-427

AQE, 2017. [http://www.airqualityengland.co.uk/site/statistics?site\\_id=MAN1](http://www.airqualityengland.co.uk/site/statistics?site_id=MAN1). Last accessed 26/04/2018

Aryal, R., Lee, B., Beecham, S., Kandasamy, J., Aryal, N., Parajuli, K. (2015). Characterisation of road dust organic matter as a function of particle Size: A PARAFAC approach. *Water, Air and Soil Pollution*, 226, pp. 24

Ault, A. P., Peters, T. M., Sawvel, E. J., Casuccio, G. S., Willis, R. D., Norris, G. A., Grassian, V. H. (2012). Single-particle SEM-EDX analysis of iron-containing coarse particulate matter in an urban environment: Sources and distribution of iron within Cleveland, Ohio. *Environmental Science and Technology*, 46, pp. 4331-4339

Banerjee, A. D. K. (2003). Heavy metal levels and solid phase speciation in street dusts of Delhi, India. *Environmental Pollution*, 123, pp. 95-105

BARGE/INERIS. (2010). UBM Procedure for the measurement of inorganic contaminant bioaccessibility from solid matrices. <http://www.bgs.ac.uk/berge/ubm.html>. Last accessed 26/04/2018

Barnes, D. G., Dourson, M. (1988). Reference dose (RfD): Description and use in health risk assessments. *Regulatory Toxicology and Pharmacology*, 8, pp. 471-486

Barrett, J. E. S. (2010). Contaminated urban sediments: geochemistry, mineralogy, solid-state speciation and the implications to environmental risk assessment. Unpublished doctoral dissertation. Manchester Metropolitan University, Manchester.

Barrett, J. E. S., Taylor, K. G., Hudson-Edwards, K. A., Charnock, J. M. (2010). Solid-phase speciation of Pb in urban road dust sediment: A XANES and EXAFS study. *Environmental Science and Technology*, 44, pp. 2940-2946

Bavec, S., Biester, H., Gosar, M. (2018). A risk assessment of human exposure to mercury-contaminated soil and household dust in the town of Idrija (Slovenia). *Journal of Geochemical Exploration*, 187, pp. 131-140

Bespalov, V. I., Gurova, O. S., Samarskaya, N. S. (2016). Main principles of the atmospheric air ecological monitoring organization for urban environment mobile pollution sources. *Procedia Engineering*, 150, pp. 2019-2024

Blake, G. R., Hartage, K. H. (1986). Particle density. Methods of soil analysis part 1. Physical and mineralogical methods. *American Society of Agronomy*, Madison, WI

Bloom, N. S., Preus, E., Katon, J., Hiltner, M. (2003). Selective extractions to assess the biogeochemically relevant fractionation of inorganic mercury in sediments and soils. *Analytical Chimica Acta*, 479, pp. 233-248

Boggs, S. (2009). *Petrology of sedimentary rocks*. 2<sup>nd</sup> edition. Cambridge Press. Page 120

Boisa, N., Elom, N., Dean, J. R., Deary, M. E., Bird, G., Entwistle, J. A. (2014a). Development and application of an inhalation bioaccessibility method (IBM) for lead in the PM10 size fraction of soil. *Environment International*, 70, pp. 132-142

Boisa, N., Entwistle, J., Dean, J. R. (2014b). A new simple; low-cost approach for generation of the PM10 fraction from soil and related materials: Application to human health risk assessment. *Analytica Chimica Acta*, 852, pp. 97-104

Boogaard, H., Monage, D. R., Brandenberg, A. P., Meliefst, K., Hoek, G. 2010. Comparison of short-term exposure to particle number, PM10 and soot concentrations on three (sub) urban locations. *Science of the Total Environment*, 408, pp. 4403-4411

Borai, E. H., El-Sofany, E. A., Abdel-Haim, A. S., Soliman, A. A. (2002). Speciation of hexavalent chromium in atmospheric particulate samples by selective extraction and ion chromatographic determination. *Trends in Analytical Chemistry*, 21, pp. 741-745

Borghesani, V., Alies, B., Hureau, C. (2017). Cull binding to various forms of amyloid- $\beta$  peptides: Are they friends or foes? *European Journal of Inorganic Chemistry*. doi:10.1002/ejic.201700776

Bourliva, A., Papadopoulou, L., Aidona, E., Giouri, K., Simeonidis, K., Vourlias, G. (2017). Characterization and geochemistry of technogenic magnetic particles (TMPs) in contaminated industrial soils: Assessing health risk via ingestion. *Geoderma*, 295, pp. 86-97

Bower, J. A., Lister, S., Hazebrouck, G., Perdril, N. (2017). Geospatial evaluation of lead bioaccessibility and distribution for site specific prediction of threshold limits. *Environmental Pollution*, 229, pp. 290-299

Brauer, M., Amann, M., Burnett, R. T., Cohen, A., Dentener, F., Ezzati, M., Henderson, S. B., Kyrzyanowski, M., Martin, R. V., Van Dingenen, R., A Van Donkelaar, Thurston, G. D.

- (2012). Exposure assessment for estimation of global burden of disease attributable to outdoor air pollution. *Environmental Science and Technology*, 46, pp. 652-660
- Bris, F. J., Garnaud, S., Apperry, N., Gonzalez, A., Mouchel, J. M., Chebbo, G., Thévenot, D. R. (1999). A street deposit sampling method for metal and hydrocarbon contamination assessment. *Science of the Total Environment*, 235, pp. 211-230
- Brown, A., Barrett, J. E. S., Robinson, H., Potgieter-Vermaak, S. (2015). Risk assessment to particulate output of a demolition site. *Environmental Geochemistry and Health*, 37, pp. 675-687
- Brunekreef, B., Holgate, S. T. (2002). Air pollution and health. *The Lancet*, 360, pp. 1233-1242
- Buranatrevedh, S. (2014). Health risk assessment of the general populations exposed to metals from an aluminium production plant in Thailand. *Journal of community medicine and health evaluation*, 4, pp. 262
- Byrne, P., Taylor, K. G., Hudson-Edwards, K. A., Barrett, J. E. S. (2017). Speciation and potential long-term behaviour of chromium in urban sediment particulates. *Journal of soils and sediments*, 17, pp. 2666-2676
- Cabouche, J., Esperanza, P., Bruno, M., Alleman, L. Y. (2011). Development of an *in vitro* method to estimate lung bioaccessibility of metals from atmospheric particles. *Journal of environmental monitoring*, 13, pp. 621-630
- Cachada, A., Ferreira da Silva, E., Duarte, A. C., Pereira, R. (2016). Risk assessment of urban soils contamination: The particular case of polycyclic aromatic hydrocarbons. *Science of the total environment*, 551-552, pp. 271-284
- Canlon, C. (2007). Derivation methods of soil screening values in Europe. A review and evaluation of national procedures towards harmonisation. EUR 22805-EN. Joint Research Centre European Commission, Ispra, Italy.
- Cao, S., Duan, X., Zhao, X., Wang, B., Ma, J., Fan, D., Sun, C., He, B., Wei, F., Jiang, G. (2015). Health risk assessment of various metal(loid)s via multiple exposure pathways on children living near a typical lead-acid battery plant, China. *Environmental Pollution*, 200, pp. 16-23
- Casteel, S. W., Cowart, R. P., Weis, C. P., Henningsen, G. M., Hoffman, E., Brattin, W. J., Guzman, R. E., Starost, M. F., Payne, J. T., Stockham, S. L., Becker, S. V., Drexler, J. W., Turk, J. R. (1997). Bioavailability of lead to juvenile swine dosed with soil from the Smuggler Mountain NPL site of Aspen, Colorado. *Fundamental and Applied Toxicology*, 36, pp. 177-187.
- Cavallari, J. M., Eisen, E. A., Fang, S. C., Schwartz, J., Hauser, R., Herrick, R. F. (2008). PM2.5 metal exposures and nocturnal heart rate variability: a panel study of boilermaker construction workers. *Environmental Health*, 7, pp. 36
- Cesari, D., Contini, D., Genga, A., Siciliano, M., Elefante, C., Baglivi, F., & Daniele, L. (2012). Analysis of raw soils and their re-suspended PM10 fractions: Characterisation of source profiles and enrichment factors. *Applied Geochemistry*, 27, pp. 1238–1246.
- Charlesworth, S. Everett, M., McCarthy, R., Ordonez, A., de Miguel, E. A. (2003). Comparative study of heavy metal concentration and distribution in deposited street dusts in a large and a small urban area: Birmingham and Coventry, West Midlands, UK. *Environment International*, 29, pp. 563-573

- Charlesworth, S., De Miguel, E., Ordonez, A. (2011). A review of the distribution of particulate trace elements in urban terrestrial environments and its application to considerations of risk. *Environmental Geochemistry and Health*, 33, pp. 103-123
- Charrier, J. G., McFall, A. S., Richards-Henderson N. K., Anastasio, C. (2014). Hydrogen peroxide formation in a surrogate lung fluid by transition metals and quinones present in particulate matter. *Environmental Science and Technology*, 48, pp. 7010-7017
- Chatterjee, A., Banerjee R. N. (1999). Determination of lead and other metals in a residential area of greater Calcutta. *Science of the Total Environment*, 227, pp. 175-185
- Chen, H., Lu, X., Li, L. Y. (2014). Spatial distribution and risk assessment of metals in dust based on samples from nursery and primary schools of Xi'an, China. *Atmospheric Environment*, 88, pp. 172-182
- Chen, L. C., Hwang, J. S., Lall, R., Thurston, G., Lippman, M. (2010). Alteration of cardiac function in ApoE<sup>-/-</sup> mice by subchronic urban and regional inhalation exposure to ambient PM<sub>2.5</sub>. *Inhalation Toxicology*, 22, pp. 580-592.
- Chen, S.-J., Liao S.-H., Jian, W.-J., Lin, C.-C. (1997). Particle size distribution of ambient aerosol carbons in ambient air. *Environment international*, 23, pp. 475-488
- Chen, X., Zhang, L., Hunag, J., Song, F., Zhang, L., Qian, Z., Trevathan, E., Mao, H., Han, B., Vaughn, M., Chen, K., Liu, Y., Chen, J., Zhao, B. (2016). Long-term exposure to urban air pollution and lung cancer mortality: A 12-year cohort study in Northern China. *Science of the Total Environment*, 571, pp. 855-861
- Cheung, K., Daher, N., Kam, W., Shafer, M. M., Ning, Z., Schauer, J. J., Sioutas, C. (2011). Spatial and temporal variation of chemical composition and mass closure of ambient coarse particulate matter (PM<sub>10-2.5</sub>) in the Los Angeles area. *Atmospheric Environment*, 45, pp. 2651-2662
- Colombo, C., Monhemius, A. J., Plant, J. A. (2008). Platinum, palladium and rhodium release from vehicle exhaust catalysts and road dust exposed to simulated lung fluids. *Ecotoxicology and Environmental Safety*, 71, pp. 722-730
- Columban, Ph., Cherifi, S., & Despert, G. (2008). Raman identification of corrosion products on automotive galvanized steel sheets. *Journal of Raman Spectroscopy*, 39, pp. 881-886.
- Compton, T. R. (2006). *Polymer Reference Book*. Rapra Technology Limited, Ohio. Chapter 1 page 9
- Crosby, C. J., Fullen, M. A., Booth, C. A., Searle, D. E. (2014). A dynamic approach to urban road deposited sediment pollution monitoring (Marylebone Road, London, UK). *Journal of Applied Geophysics*, 105, pp. 10-20
- Dahl, A., Gharibi, A., Swietlicki, E., Gudmundsson, A., Bohgard, M., Ljungman, A., Blomqvist, G., Gustafsson, M., 2009. Traffic generated emissions of ultrafine particles from pavement-tire interface. *Atmospheric Environment*, 40, pp. 1314-1323
- Daintith, J. (2008). *Dictionary of Chemistry*. Oxford Press. 6<sup>th</sup> edition page 221
- Davies, N. M., Feddah, M. R. (2003). A novel method for assessing dissolution of aerosol inhaler products. *International Journal of Pharmaceutics*, 255, pp. 175-187
- de Faria, D. L. A., Lopes, F. N. (2007). Heated goethite and natural hematite: Can Raman spectroscopy be used to differentiate them? *Vibrational Spectroscopy*, 45, pp. 117-121

- De Miguel, E., Llamas, J. F., Chacon, E., Berg, T., Larssen, S., Royset, O., Vadset, M. (1997). Origin and patterns of trace elements in street dust: unleaded petrol and urban lead. *Atmospheric Environment*, 31, pp. 2733-2740
- De Raeve, H., Vandecasteele, C., Demedts, M., Nemery, B. (1998). Dermal and respiratory sensitization to chromate in a cement floorer. *American Journal of Industrial Medicine*, 34, pp. 169-176
- Deacon, A. R., Derwent, R. G., Harrison, R. M., Middleton, D. R., Moorcroft, S. (1994). Analysis and interpretation of measurements of suspended particulate matter at urban background sites in the United Kingdom. *Science of the Total Environment*, 203, pp. 17-36
- DEFRA. (2005). AQEG 2005 Particulate Matter in the UK: Summary. Defra, London
- DEFRA. (2013). ANX appendix G.  
<http://randd.defra.gov.uk/Default.aspx?Module=More&Location=None&ProjectID=18341>.  
Last accessed 26/04/2018
- Denys, S., Cabouche, J., Tack, K., Rychen, G., Wragg, J., Cave, M., Jondreville, C., Feidt, C. (2012). *In vivo* validation of the unified BARGE method to assess the bioaccessibility of arsenic, antimony, cadmium, and lead in soils. *Environmental Science and Technology*, 46, pp. 6252-6260
- Dias da Silva, L. I., Yokoyama, L., Maia L. B., Monteir, M. I. C., Pontes, F. V. M., Carniero, M. C., Neto, A. A. 2015. Evaluation of bioaccessible heavy metal fractions in PM10 from the metropolitan region of Rio de Janeiro city, Brazil, using a simulated lung fluid. *Microchemical Journal*, 118, pp. 266-217
- Dockery, D.W., Pope, C. A., Xu, X., Spengler, J. D., Ware, J. H., Fay, M. E., Ferris, B. G., Speizer, F. (1993). An association between air pollution and mortality in six U.S. cities. *New England Journal of Medicine*, 329, pp. 1753-9
- Dorato, M. A., Engelhardt, J. A. (2005). The no-observed-adverse-effect-level in drug safety evaluations: Use, issues, and definition(s). *Regulatory Toxicology and Pharmacology*, 42, pp. 265-274
- Du, Y., Gao, B., Zhou, H., Ju, X., Hao, H., Yin, S. (2013). Health risk assessment of heavy metals in road dusts in urban parks of Beijing, China. *Procedia Environmental Studies*, 18, pp. 299-309
- Du, Y., Wei, M., Reddy, K. R., Liu, Z., & Jin, F. (2014). Effect of acid rain pH on leaching behavior of cement stabilized lead-contaminated soil. *Journal of Hazardous Materials*, 271, pp. 131-140
- Duggan, M. J., Inskip, M. J., Rundle, S. A., Moorcroft, J. S. (1985). Lead in playground dust and on the hands of schoolchildren. *Science of the Total Environment*, 44, pp. 65-79
- Duong, T. T. T., Lee, B. K. (2011). Determining contamination level of heavy metals in road dust from busy traffic areas with different characteristics. *Journal of Environmental Management*, 92, pp. 554-562
- Elci, L., Divrikli, U., Akdogan, A., Hol, A., Cetin, A., Soylak, M. (2010). Selective extraction of chromium(VI) using a leaching procedure with sodium carbonate from some plant leaves, soil and sediment samples. *Journal of Hazardous Material*, 173, pp. 778-782
- Entwistle, J. A., Hunt, A., Boisa, N., Dean, J. R. (2017). Enhancing the interpretation of *in vitro* bioaccessibility data by using computer controlled scanning electron microscopy (CCSEM) at the individual particle level. *Environmental Pollution*, 228, pp. 443-453

- Environment Agency. (2009). Soil guideline for mercury in soil. Science Report SC050021.
- Ess, M. N., Ferr, D., Kireeva, E. D., Niessner, R., Ouf, F. X., Ivleva, N. P. (2015). *In situ* Raman microspectroscopic analysis of soot samples with different organic carbon content: Structural changes during heating. *Carbon*, 105, pp. 572-585
- European Commission. (2001). Ambient air pollution by mercury (Hg) position paper. [http://ec.europa.eu/environment/air/pdf/pp\\_mercury.pdf#](http://ec.europa.eu/environment/air/pdf/pp_mercury.pdf#). Last accessed 26/04/2018
- European Commission. (2016). Air quality standards. <http://ec.europa.eu/environment/air/quality/standards.htm> 26/04/2018
- Fergusson, J. E., Ryan D. E. (1984). The elemental composition of street dust from large and small urban areas related to city type, source and particle size. *Science of the Total Environment*, 34, pp. 101-116
- Ferreira-Baptiste, L., De Miguel, E. (2005). Geochemistry and risk assessment of street dust in Luanda, Angola: A tropical urban environment. *Atmospheric Environment*, 39, pp. 4501–4512
- Florence, T. M., Batley, G. E., Benes, P. (1980). Chemical speciation in natural waters. *Critical Reviews in Analytical Chemistry*, 9, pp. 219-296
- Fridrichova, J., Bacik, P., Illasova, L., Kozakova, P., Skoda, R., Pulisova, Z., Fiala, A. (2016). Raman and optical spectroscopic investigation of gem-quality smoky quartz crystals. *Vibrational Spectroscopy*, 85, pp. 71-78
- Frost, R. L., Bahfenne, S. (2010). Thermal analysis and hot-stage Raman spectroscopy of the basic copper arsenate mineral: euchroite. *Journal of Thermal Analysis and Calorimetry*, 100, pp. 89-94
- Frost, R. L., Cejka, J., Sejkora, J., Plasil, J., Bahfenne, S., Palmer, S. J. (2010). Raman spectroscopy of the basic copper arsenate mineral: euchroite. *Journal of Raman Spectroscopy*, 41, pp. 571-575
- Frost, R. L., Hales, M. C., Wain, D. L. (2008). Raman spectroscopy of smithsonite. *Journal of Raman Spectroscopy*, 39, pp. 108-114
- Fu, R., Yang, Y., Xu, Z., Zhang, X., Guo, X., Bi, D. (2015). The removal of chromium (VI) and lead (II) from groundwater using sepiolite-supported nanoscale zero-valent iron (S-NZVI). *Chemosphere*, 138, pp. 726-734
- Gbefa, B. K., Entwistle, J. A., Dean, J. R. (2010). Oral bioaccessibility of metals in an urban catchment, Newcastle-upon-Tyne. *Environmental Geochemistry and Health*, 33, pp. 167-181
- Gebel, T. W. (2000). Genotoxicology of arsenical compounds. *International Journal of Hygiene and Environmental Health*, 203, pp. 249-262
- Ghio, A. J., Carraway, M. S., Madden, M. C. (2012). Composition of air pollution particles and oxidative stress in cells, tissues, and living systems. *Journal of Toxicology and Environmental Health*, 15, pp. 1-21
- Godoi, R. H. M., Polezer, G., Borillo, G. C., Brown, A., Valebona, F. B., Silva, T. O. B., Ingberman, A. B. G., Nalin, M., Yamamoto, C. I., Potgieter-Vermaak, S., Neto, R. A. P., de Marchi, M. R. R., Saldiva, P. H. N., Pauliquevos, Y. Godoi, A. F. L. (2016). Influence on the oxidative potential of a heavy-duty engine particle emission due to selective catalytic reduction system and biodiesel blend. *Science of the Total Environment*, 560-561, pp. 179-185

Goix, S., Uzu, G., Oliva, P., Barraza, F., Calas, A., Castet, S., Point, D., Masbou, J., Duprey, J. L., Huayta, C., Chincheros, J., Gardon, J. (2016). Metal concentration and bioaccessibility in different particle sizes of dust and aerosols to refine metal exposure assessment. *Journal of Hazardous Materials*, 317, pp. 552-562

Goldbohm, R. A., Tielemans, E. L. J. P., Heederik, D., Rubingh, C. M., Dekkers, S., Willems, M. I., Kroese, E. D. (2006). Risk assessment for carcinogens based on epidemiological data: A structured approach, illustrated by an example of chromium. *Regulatory Toxicology and Pharmacology*, 44, pp. 294-310

Gondal, M. A., Dastageer, M. A., Al-Adel, F. F., Naqvi, A. A., Habibullah, Y. B. (2015). Detection of highly toxic elements (lead and chromium) in commercially available eyeliner (kohl) using laser induced break down spectroscopy. *Optics and Laser Technology*, 75, pp. 99-104

Gradon, L., Pratsinis, S. E., Podgorski, A., Scott, S. J., Panda, S. (1996). Modeling retention of inhaled particles in rat lungs including toxic and overloading effects. *Journal of Aerosol Science*, 27, pp. 487-503

Grangeon, S., Geudron, S., Asta, J., Sarret, G., Charlet, L. (2012). Lichen and soil as indicators of an atmospheric mercury contamination in the vicinity of a chlor-alkali plant (Grenoble, France). *Ecological Indicators*, 13, pp. 178-183

Gray, J. E., Plumlee, G. S., Morman, S. A., Higuera, P. L., Crock, J. G., Lowers, H. A., Witten, M. L. (2010). *In vitro* studies evaluating leaching of mercury from mine waste calcine using simulated human body fluids. *Environmental Science and Technology*, 44, 4782-4788

Gunawardana, C., Goonetilleke, A., Egodawatta, P., Dawes, L., Kokot, S. (2012). Source characterisation of road dust based on chemical and mineralogical composition. *Chemosphere*, 87, pp. 163-170

Guney, M., Bourges, C. M. J., Chapuis, R. P., Zagury, G. J. (2017). Lung bioaccessibility of As, Cu, Fe, Mn, Ni, Pb, and Zn in fine fraction (< 20 µm) from contaminated soils and mine tailings. *Science of the Total Environment*, 579, pp. 378-386

Hamel, S. C., Buckley, B., Liou, P. J., (1998). Bioaccessibility of metals in soils for different liquid to solid ratios in synthetic gastric fluid. *Environmental Science and Technology*, 32, pp. 358-362

Han, S., Youn, J.S., Jung, Y. W. (2011). Characterisation of PM10 and PM2.5 source profiles for resuspended road dust collected using mobile sampling methodology. *Atmospheric environment* 45, pp. 3343-3351

Han, Y., Wang, J., Dong, Y., Hou, Q., Pan, J. (2017). The role of structure defects in the deformation of anthracite and their influence on the macromolecular structure. *Fuel*, 206, pp. 1-9

Harrison, R. M., Smith, D. G. T., Pio, C. A., Castro L. M. 1997. Comparative receptor modelling study of airborne particulate pollutants in Birmingham, United Kingdom, Coimbra (Portugal) and Lahore (Pakistan). *Atmospheric Environment*, 31, pp. 3309-3321

Haynes (Ed.). (2016). *CRC Handbook of Chemistry and Physics*. 97th edition. CRC Press, Boca Raton

Hein, C., Sander, J. M., Kautenburger, R. (2017). New approach of a transient ICP-MS measurement method for samples with high salinity. *Talanta*, 164, pp. 477-482

Hernanz, A., Gavira-Vallejo, J. M., Ruiz-Lopez, J. F., Martin, S., Maroto-Valiente, A., Balbin-Behrmann, R., Menendez, M., Alcolea-Gonzalez, J. (2011). Spectroscopy of palaeolithic

rock paintings from the Tito Bustillo and El Buxu Caves, Asturias, Spain. *Journal of Raman Spectroscopy*, 43, pp. 1644-1650

Hien, P. D., Binh, N. T., Truong, Y., Ngo, N. T.N. (1999). Temporal variations of source impacts at the receptor, as derived from particulate monitoring data in Ho Chi Minh City, Vietnam. *Atmospheric Environment*, 33, pp. 3133-3142

Hoffman, W., Asgharian, B. (2003). The effect of lung structure and mucociliary clearance and particle retention in human and rat lungs. *Toxicological Sciences*, 73, pp. 448-456

Hopke, P. K., Lamb, R. E., Natusch, D. F. S. (1980). Multielemental Characterization of Urban Roadway Dust. *Environmental Science and Technology*, 14, pp. 164-172

HSE. (2002). <http://www.hse.gov.uk/pubns/indg346.pdf>. Last accessed 30/04/2018

Hsi, H. C., Jiang, C. B., Yang, T. H., Chien, L. C. (2014). The neurological effects of prenatal and postnatal mercury/methylmercury exposure on three-year-old children in Taiwan. *Chemosphere*, 100, pp. 71-76

Hu, X., Zhang, Y., Luo, J., Wang, T., Lian, H., Ding, Z. (2011). Bioaccessibility and health risk of arsenic, mercury and other metals in urban street dusts from a mega-city, Nanjing, China. *Environmental Pollution*, 159, pp. 1251-1221

Huang, J., Li, F., Zeng, G., Liu, W., Huang, X., Ziao, Z., Wu, H., Li, X., He, X., He, Y. 2016. Integrating hierarchical bioavailability and population distribution into potential eco-risk assessment of heavy metals in road dust: A case study in Xiandao District, Changsha city, China. *Science of the Total Environment*, 541, pp. 969-976

Huang, M., Wang, W., Chan, C. Y., Cheung, K. C., Man, Y., B., Wang, X., Wong, M. H. (2014). Contamination and risk assessment (based on bioaccessibility via ingestion and inhalation) of metal(loid)s in outdoor and indoor particles from urban centers of Guangzhou, China. *Science of the Total Environment*, 479-480, pp. 117-124

Iriarte, M., Hernandez, A., Gavira-Vallejo, J. M., Alcolea-Gonzalez, J., Balbin-Behrmann, R. (2017).  $\mu$ -Raman spectroscopy of prehistoric paintings from the El Reno cave (Valdesotos, Guadalajara, Spain). *Journal of Archaeological Science*, 14, pp. 454-460

Jentzsch, P. V., Kampe, B., Ciobota, V., Rosch, P., Popp, J. 2013. Inorganic salts in atmospheric particulate matter: Raman spectroscopy as an analytical tool. *Spectrochimica Acta Part A: Molecular and Biomolecular Spectroscopy*, 115, pp. 697-708

Jordanova, D., Jordanova, N., Petrov, P. (2014). Magnetic susceptibility of road deposited sediments at a national scale – relation to population size and urban pollution. *Environmental Pollution*, 189, pp. 239-251

Kabata-Pendias, A., Mukherjee, A. B. (2007). *Trace elements from soil to human*. Springer-Verlag, Berlin

Kandler, K., Leike, K., Benker, N., Emmel, C., Kupper, M., Muller-Ebert, D., Scheuven, D., Schladitz, A., Schutz, L. (2011). Electron microscopy of particles collected at Praia, Cape Verde, during the Saharan Mineral Dust Experiment: particle chemistry, shape, mixing state and complex refractive index. *Tellus*, 63b, pp. 475-496

Kar, S., Deeb, O., Roy, K. (2012). Development of classification and regression based QSAR models to predict rodent carcinogenic potency using oral slope factor. *Ecotoxicology and Environmental Safety*, 82, pp. 85-95

Kasprzak, K., Sunderman, F. W., Salnikow, K. 2003. *Nickel carcinogenesis*. *Mutation Research/Fundamental and Molecular Mechanisms of Mutagenesis*, 533, pp.67-97

- Kazimierski, P., Tyczkowski, J., Kozanecki, M., Hatanaka, Y., Aoki, T. (2002). Transition from amorphous semiconductor to amorphous insulator in hydrogenated carbon-germanium films investigated by raman spectroscopy. *Chemistry of Materials*, 14, pp. 4694-4701
- Kendal, M., Hamilton, R. S., Watt, J., Williams, I. D. (2001). Characterisation of selected speciated organic compounds associated with particulate matter in London. *Atmospheric Environment*, 35, pp. 2483-2495
- Kennedy, N. J., Hines, W. C. (2002). Inhalability of large solid particles. *Journal of Aerosol Science*, 33, pp. 237-255
- Kereszturi, A., Gyollai, I., Kereszty, Zs., Kiss, K., Szabo, M., Szalai, Z., Ringer, M., Veres, M. (2017). Analyzing raman – infrared spectral correlation in the recently found meteorite Csátalja. *Spectrochimica Acta Part A: Molecular and Biomolecular Spectroscopy*, 173, pp. 637-646
- Khanal, R., Furumai, H., Nakajima, F. (2014). Toxicity assessment of size-fractioned urban road dust using ostracod *Heterocypris incongruens* direct contact test. *Journal of Hazardous Materials*, 264, pp. 53-54
- Kong, D., Wilson, L. D. (2017). Synthesis and characterization of cellulose-goethite composites and their adsorption properties with roxarsone. *Carbohydrate Polymers*, 169, pp. 282-294
- Kong, S., Lu, B., Bai, Z., Zhao, X., Chen, L., Han, B., Li, Z., Ji, Y., Xu, Y., Liu, Y., Jiang, H. (2011). Potential threat of heavy metals in re-suspended dusts on building surfaces in oilfield city. *Atmospheric Environment*, 45, pp. 4192-4204
- Kong, S., Lu, B., Ji, Y., Zhao, X., Bai, Z., Xu, Y., Liu, Y., Jiang, H. (2012). Risk assessment of heavy metals in road and soils dust within PM<sub>2.5</sub>, PM<sub>10</sub>, and PM<sub>100</sub> fraction in Dongying city, Shandong province, China. *Journal of Environmental Monitoring*, 14, pp. 791-803
- Kuipainen, K., Ritola, R., Stojiljkovic, A., Pirjola, L., Malinen, A., Niemi, J. (2016). Contribution of mineral dust sources to street side ambient and suspension PM<sub>10</sub> samples. *Atmospheric Environment*, 147, pp. 178-189
- Kumar, P., Pirjola, L., Ketzler, M., Harrison, R. M. (2013a). Nanoparticle emissions from 11 non-vehicle exhaust sources – A review. *Atmospheric Environment*, 67, pp. 252-277
- Kumar, M., Furumai, H., Kurisu, F., Kasuga, I. (2013b). Tracing source and distribution of heavy metals in road dust, soil and soakaway sediment through speciation and isotopic fingerprinting. *Geoderma*, 211-212, pp. 8-17
- Lammers, L., Naujoks, C., Berr, K., Depprich, R., Kunler, N., Meyer, U., Langenbach, F., Luttenberg, B., Kogler, G., Wiseman, H., Handschel, J. (2012). Impact of DAG stimulation on mineral synthesis, mineral structure and osteogenic differentiation of human cord blood stem cells. *Stem Cell Research*, 81, pp. 193-205
- Landis, M. S., Pancras, J. P., Graney, J. R., White, E. M., Edgerton, E. S., Legge, A., Percy, K. E. (2017). Source apportionment of ambient fine and coarse particulate matter at the Fort McKay community site, in the Athabasca Oil Sands Region, Alberta, Canada. *Science of the Total Environment*, 584-585, pp. 105-117
- Leal, J. H., Cantu, Y., Gonzalez, D. F., Parsons, J. G. (2017). Brookite and anatase nanomaterial polymorphs of TiO<sub>2</sub> synthesized from TiCl<sub>3</sub>. *Inorganic Chemistry Communications*, 84, pp. 28-32
- Leclercq, B., Alleman, L. Y., Perdrix, E., Riffault, V., Happillon, M., Strecker, A., Lo-Guidice, J. M., Garçon, G., Coddeville, P. (2017). Particulate metal bioaccessibility in physiological

fluids and cell culture media: Toxicological perspectives. *Environmental Research*, 156, pp. 148-157

Lee, M. R., Lindgren, P., Sofo, M. R. (2014). Aragonite, breunnerite, calcite and dolomite in the CM carbonaceous chondrites: High fidelity recorders of progressive parent body aqueous alteration. *Geochimica et Cosmochimica Acta*, 144, pp. 126-156

Li, H, Shi, A., Zhang, X. (2015). Particle size distribution and characteristics of heavy metals in road-deposited sediments from Beijing Olympic park. *Journal of Environmental Sciences*, 32, pp. 228-237

Li, H. H., Chen, L. J., Yu, L., Guo, Z. B., Shan, C. Q., Lin, J. Q., Gu, Y. G., Yang, Z. B., Yang Y. X., Shao, J. R., Zhu, X. M., Cheng, Z. (2017). Pollution characteristics and risk assessment of human exposure to oral bioaccessibility of heavy metals via urban street dusts from different functional areas in Chengdu, China. *Science of the Total Environment*, 586, pp. 1076-1084

Li, H., Zhou, D., Zhang, Q., Feng, C., Zheng, W., He, K., Lan, Y. (2013). Vanadium exposure-induced neurobehavioural alterations among Chinese workers. *NeuroToxicology*, 36, pp. 49-54

Li, N., Kang, Y., Pan, W., Zeng, L., Zhang, Q., Luo, J. (2015). Concentration and transportation of heavy metals in vegetables and risk assessment of human exposure to bioaccessible heavy metals in soil near a waste-incinerator site, South China. *Science of the Total Environment*, 521-522, pp. 144-151

Li, N., Kang, Y., Pan, W., Zeng, L., Zhang, Q., Luo, J. (2015). Concentration and transportation of heavy metals in vegetables and risk assessment of human exposure to bioaccessible heavy metals in soil near a waste-incinerator site, South China. *Science of the Total Environment*, 521-522, pp. 144-151

Lima, R. M., Carneiro, L. G., Alfonso, J. C., Cunha, K. M. (2013). Evaluation of solubility in simulated lung fluid of metals present in the slag from a metallurgical industry to produce metallic zinc. *Journal of Environmental Science and Health. Part A Toxic/Hazardous Substances and Environmental Engineering*, 48, pp. 489-494

Lin, C. C., Chen, S. J., Huang, K. L. (2005). Characteristics of Metals in Nano/Ultrafine/Fine/Coarse Particles Collected Beside a Heavily Trafficked Road. *Environmental Science and Technology*, 39, pp. 8113-8122

Liu, E., Yan, T., Birch, G., Zhu, Y. (2014). Pollution and health risk of potentially toxic metals in urban road dust in Nanjing, a mega-city of China. *Science of the Total Environment*, 467-477, pp. 522-531

Liu, Q., Ran, Z., Liu, F., Liu, Z. (2015a). Phase transitions and mechanical stability of TiO<sub>2</sub> polymorphs under high pressure. *Journal of Alloys and Compounds*, 631, pp. 192-201

Liu, X., Zhai, Y., Zhu, Y., Liu, Y., Chen, H., Li, P., Peng, C., Xu, B., Li, C., Zeng, G. (2015b). Mass concentrations and health risk assessment of heavy metals in size-segregated airborne particulate matter in Changsa. *Science of the Total Environment*, 517, pp. 215-221

Liu, Y. Y., Liu, M., Wang, Y. J. (2011). Temporal variation characteristics of PGEs concentrations in road dust. *Chinese Journal of Environmental Science*, 32, pp. 2676

Lohren, H., Blagojevic, L., Fitkau, R., Ebert, F., Schildknecht, S., Leist, M., Schwerdtle, T. (2015). Toxicity of organic and inorganic mercury species in differentiated human neurons and human astrocytes. *Journal of Trace Elements in Medicine and Biology*, 32, pp. 200-208

- Londonio, A., Fujiwara, F., Rebagliati, R. J., Gomez, D., Smichowski, P. (2012). Determination of mercury in size fractionated road dust samples by flow injection-cold vapour-atomic absorption spectroscopy. *Microchemical Journal*, 105, pp. 77-82
- Lopez-Villarrubia, E., Iniguez, C., Peral, N., Garcia, M. D., Ballester, F. (2012). Characterizing mortality effects of particulate matter size fractions in the two capital cities of the Canary Islands. *Environmental Research*, 112, pp. 129-138
- Lu, X., Wu, X., Wang, Y., Chen, H., Gao, P., Fu, Y. (2014). Risk assessment of toxic metals in street dust from a medium-sized industrial city of China. *Ecotoxicology and Environmental Safety*, 106, pp. 154-163
- Lueng, A. O. W., Duzgoren-Aydin, N. S., Cheung, K. C., Wong, M. H. (2008). Heavy metal concentrations of surface dust from e-waste recycling and its human health implications in Southeast China. *Environmental Science and Technology*, 42, pp. 2674-2680
- Luo, X. S., Ding, J., Xu, B., Wang, J. Y., Li, H. B., Yu, S. (2012). Incorporating bioaccessibility into human health risk assessments of heavy metals in urban park soils. *Science of the Total Environment*, 424, pp. 88-96
- Ma, J., Singhirunnusorn, W. (2012). Distribution and health risks assessment of heavy metals in surface dusts of Maha Sarakham municipality. *Procedia Social and Behavioural Sciences*, 50, pp. 280–293
- Ma, Y., Liu, A., Egodawatta, P., McGree, J., Goonetilleke, A. (2017). Quantitative assessment of human health risk posed by polycyclic aromatic hydrocarbons in urban road dust. *Science of the Total Environment*, 575, pp. 895-904
- Mahub, K. R., Krishnan, K., Naidu, R., Andrews, S., Megharaj, M. (2017). Mercury toxicity to terrestrial biota. *Ecological Indicators*, 74, pp. 451-462
- Malehase, T., Daso, A. P., Okonkwo, J. O. (2016). Determination of mercury and its fractionation products in samples from legacy use of mercury amalgam in gold processing in Randfontein, South Africa. *Emerging Contaminants*, 2, pp. 157-165
- Maramba, N. P. C., Reyes, J. P., Francisco-Rivera, A. T., Panganiban, L. C. R., Dioquino, C., Dando, N., Timbang, R., Akagi, H., Castillo, T., Quintoriano, C., Afuang, M., Matsutama, A., Eguchi, T., Fuchigami, Y. (2010). Environmental and human exposure assessment monitoring of communities near an abandoned mercury mine in the Philippines: A toxic legacy. *Journal of Environmental Management*, 81, pp. 135-145
- Marques, M. R. C., Loebenberg, R., Almukainzi, M. (2011). Simulated biological fluids with possible application in dissolution testing. *Dissolution Technology*, 18, pp. 15-28
- Massoud, R., Shihadeh, A. L., Roumie, M., Youness, M., Gerard, J., Saliba, N., Zaarour, R., Abboud, M., Farah, W., Saliba, N. A. (2011). Intraurban variability of PM10 and PM2.5 in an Eastern Mediterranean city. *Atmospheric Research*, 101, pp. 893-901
- Masto, R. E., George, J., Rout, T. K., Ram, L. C. (2017). Multi element exposure risk from soil and dust in a coal industrial area. *Applied Geochemistry*, 176, pp. 100-107
- Mathissen, M., Scheer, V., Vogt, R., Benter, T. (2011). Investigation on the potential generation of ultrafine particles from the tire–road interface. *Atmospheric Environment*, 45, pp. 6172-6179
- Mauderly, J. L. (1994). Toxicological and epidemiological evidence for health risks from inhaled engine emissions. *Environmental Health Perspectives*, 102, pp. 165-171

- McKenzie, E. R., Wong, C. M., Green, P. G., Kayhanian, M., Young, T. M. (2008). Size dependent elemental composition of road-associated particles. *Science of the Total Environment*, 398, pp. 145-153
- Miller, J.N., Miller, J. C. (2010). *Statistics and Chemometrics for Analytical Chemistry*. 6<sup>th</sup> edition. Prentice Hall, New Jersey. pp. 32
- Miu, A. C., Andreescu, C. E., VasIU, R., Olteanu, A. I., 2003. A behavioural and histological study on the effects of long-term exposure of adult rats to aluminium. *International Journal of Neuroscience*, 113, pp. 1197-1211
- Mueller, E. J., Seger, D. L. (1985). Metal fume fever - A review. *The Journal of Emergency Medicine*, 2, pp. 271-274
- Murikami, M., Nakajima, F., Furumai, H. (2008). The sorption of heavy metal species by sediments in soakaways receiving urban road runoff. *Chemosphere*, 70, pp. 2099-2109
- Nachiappan, V., Cho, E. H. (2005). Corrosion of high chromium steel and conventional steels embedded in concrete. *Journal of Performance of Constructed Facilities*, 19, pp. 56-61
- Nelson, H., Shchukarev, A., Sjoberg, S., Lovgren, L. 2011. Composition and solubility of precipitated copper(II) arsenates. *Applied Geochemistry*, 26, pp. 696-704
- Niu, H., Zhang, D., Hu, W., Shi, J., Li, R., Gao, H., Pian, W., Hu, M. 2016. Size and elemental composition of dry-deposited particles during a severe dust storm at a coastal site of Eastern China. *Journal of Environmental Sciences*, 40, pp. 161-168
- Nordstrom, D. K. (2002). Worldwide occurrences of arsenic in ground water. *Science*, 296, pp. 2143-2145
- Norouzi, S., Kahdemi, H., Ayoubi, S., Cano, A. F., Acosta, J. A. (2017). Seasonal and spatial variations in dust deposition rate and concentrations of dust-borne heavy metals, a case study from Isfahan, central Iran. *Atmospheric Pollution Research*, 8(4), pp. 686-699
- O'Brien, P., Kortenkamp, A. (1995). The chemistry underlying chromate toxicity. *Transition Metal Chemistry*, 20, pp. 636-642
- Obrist, D., Johnson, D. W., Lindberg, S. E., Luo, Y., Hararuk, O., Branco, R., Battles, J. J., Dail, D. B., Edmonds, R. L., Monson, R. K., Ollinger, S. V., Pallardy, S. G., Pregitzer, K. S., Todd, D. E. (2011). Mercury Distribution Across 14 U.S. Forests. Part I: Spatial Patterns of Concentrations in Biomass, Litter, and Soils. *Environmental Science and Technology*, 45, pp. 3974-3981
- Okorie, A., Entwistle, J., Dean, J. R. (2012). Estimation of daily intake of potentially toxic elements from urban street dust and the role of oral bioaccessibility testing. *Chemosphere*, 86, pp. 460-467
- Ormstedt, G., Bringfelt, B., Johansson, C. (2005). A model for vehicle-induced non-tailpipe emissions of particles along Swedish roads. *Atmospheric Environment*, 39, pp. 6088-6097
- Ozaki, H., Watanabe, I., Kuno, K. (2004). As, Sb and Hg distribution and pollution sources in the roadside soil and dust around Kamikochi, Chubu Sangaku national Park, Japan. *Geochemical Journal*, 38, pp. 473-484
- Ozilgen, M. (2017). Assessment of the use of zero-emission vehicles and microbial fertilizers in beverage production. *Journal of Cleaner Production*, 165, pp. 298-311

- Padoan, E., Rome, C., Ajmone-Marsan, F. (2017). Bioaccessibility and size distribution of metals in road dust and road side soils along a peri-urban transect. *Science of the Total Environment*, 601-602, pp. 89-98
- Palermo, R. N., Short, S. M., Anderson, C. A., Tian, H., Drennen, J. K. (2012). Determination of figures of merit for near-infrared, raman and powder x-ray diffraction by net analyte signal analysis for a compacted amorphous dispersion with spiked crystallinity. *Journal of Pharmaceutical Innovation*, 7, pp. 56-58
- Pant, P., Harrison, R. M. (2013). Estimation of the contribution of road traffic emissions to particulate matter concentrations from field measurements: A review. *Atmospheric Environment*, 77, pp. 78-97
- Parker J. C., Siegel, R. W. (1990). Raman microprobe study of nanophase TiO<sub>2</sub> and oxidation-induced spectral changes. *Journal of Materials Research*, 5, pp. 1246-1252
- Pelfrene, A., Cave, M. R., Wragg, J., Douay, F. (2017). *In vitro* investigations of human bioaccessibility from reference materials using simulated lung fluids. *Environmental Research and Public Health*, 14, pp. 112-127
- Perez, L., Grize, L., Infanger, D., Kunzli, N., Sommer, H., Alt, G. Schindler, C. (2015). Associations of daily levels of PM<sub>10</sub> and NO<sub>2</sub> with emergency hospital admissions and mortality in Switzerland: Trends and missed prevention potential over the last decade. *Environmental Research*, 140, pp. 554-561
- Poggio, L., Vrscaj, B., Schulin, R., Hepperle, E., Marsan, F. A. (2009). Metals pollution and human bioaccessibility of topsoils in Grugliasco (Italy). *Environmental Pollution*, 157, pp. 680-689
- Pope, C. A., Burnett, R. T., Thun, M.J., Calle, E. E., Krewski, D., Ito, K., Thurston, G. D. (2002). Lung cancer, cardiopulmonary mortality, and long-term exposure to fine particulate air pollution. *Journal of the American Medical Association*, 287, pp. 1132-1141
- Posthuma, L., Eijsackers, H. J. P., Koelmans, A. A., Vijver, M. G. (2008). Ecological effects of diffuse mixed pollution are site-specific and require higher-tier risk assessment to improve site management decisions: A discussion paper. *Science of the Total Environment*, 406, pp. 503-517
- Potgieter-Vermaak, S., Rotondo, G., Novakovic, V., Rollins, S. (2012a). Component-specific toxic concerns of the inhalable fraction of urban road dust. *Environmental Geochemistry and Health*, 34, pp. 689-696
- Potgieter-Vermaak, S., Horemans, B., Anaf, W., Cardell, C., Van Grieken, R. (2012b). Degradation potential of airborne particulate matter at the Alhambra monument: a Raman spectroscopic and electron probe X-ray microanalysis study. *Raman Spectroscopy*, 43, pp. 1570-1577
- Prieto-Taboada, N., Gomez-Laserna, O., Martinez-Arkarazo, I., Olazabel, M. A., Madariaga, J. M. (2014). Raman spectra of the different phases in the CaSO<sub>4</sub>-H<sub>2</sub>O system. *Analytical Chemistry*, 86, pp. 10131-10137
- Quackenboss, J. J., Lebowitz, M. D. (1989). Indoor-outdoor relationships for particulate matter: Exposure classifications and health effects. *Environment International*, 15, pp. 353-360
- Rasmussen, P. E., Subramanian, K. S., Jessiman, B. J. (2001). A multi-element profile of housedust in relation to exterior dust and soils in the city of Ottawa, Canada. *Science of the Total Environment*, 267, pp. 125-140

- Ravindranath, S. P., Kadam, U. S., Thompson, D. K., Irudayaraj, J. (2012). Intracellularly grown gold nanoislands as SERS substrates for monitoring chromate, sulfate and nitrate localization sites in remediating bacteria biofilms by Raman chemical imaging. *Analytica Chimica Acta*, 745, pp. 1-9
- Rees, M., Sansom, L., Rofe, A., Juhasz, A. L., Smith, E., Weber, J., Naidu, R., Kuchel, T. (2009). Principles and application of an *in vivo* swine assay for the determination of arsenic bioavailability in contaminated matrices. *Environmental Geochemistry and Health*, 31, pp. 167-177
- Reis, A. P., Patinha, C., Wragg, J., Dias, A. C., Cave, M., Sousa, A. J., Batista, M. J., Prazeres, C., Costa, C., Ferreira da Silva, E., Rocha, F. (2014). Urban geochemistry of lead in gardens, playgrounds and schoolyards of Lisbon, Portugal: Assessing exposure and risk to human health. *Applied Geochemistry*, 44, pp. 45-53
- Rexeis, M., Hausberger, S. (2009). Trend of vehicle emission levels until 2020 – Prognosis on current vehicle measurements and future emissions legislation. *Atmospheric Environment*, 43, pp. 4689-4698
- Riccio, A., Chianese, E., Monaco, D., Costagliola, M. A., Perretta, G., Prati, M. V., Agrillo, G., Esposito, A., Gasbarra, D., Shindler, L., Brusasca, G., Nanni, A., Pozzi, C., Magliulo, V. (2016). Real-world automotive particulate matter and PAH emission factors and profile concentrations: Results from an urban tunnel experiment in Naples, Italy. *Atmospheric Environment*, 141, pp. 379-387
- Robertson, D. J., Taylor, K. G. (2007). Temporal Variability of Metal Contamination in Urban Road-deposited Sediment in Manchester, UK: Implications for Urban Pollution Monitoring. *Water, Air and Soil Pollution*, 186, pp. 209-220
- Robertson, D. J., Taylor, K. G., Hoon, S. R. (2003). Geochemical and mineral magnetic characterisation of urban sediment particulates, Manchester, UK. *Applied Geochemistry*, 18, pp. 269-282
- Rodrigues, S. M., Coehlo, C., Cruz, N., Monteiro, R. J. R., Henriques, B., Duarte, A. C., Romkens, P. F. A. M., Pereira, E. (2014). Oral bioaccessibility and human exposure to anthropogenic and geogenic mercury in urban, industrial and mining areas. *Science of the Total Environment*, 496, pp. 649-661
- Rohr, A. C., Kamal, A., Morishota, M., Mukherjee, B., Keeler, G. J., Harkema, J. R., Wagner, J. G. (2011). Altered heart rate variability in spontaneously hypertensive rats is associated with specific particulate matter components in Detroit, Michigan. *Environmental Health Perspective*, 119, pp. 474-480
- Royal College of Physicians. (2016). Every breath we take: The lifelong impact of air pollution. <https://www.rcplondon.ac.uk/projects/outputs/every-breath-we-take-lifelong-impact-air-pollution>. Last accessed 30/04/2018
- Russo, C., Ciajolo, A. (2015). Effect of the flame environment on soot nanostructure inferred by Raman spectroscopy at different excitation wavelengths. *Combustion and Flame*, 162, pp. 2431-2441
- Sadezky, A., Muckenhuber, H., Grothe, H., Niessner, R., Poschl, U. (2005). Raman microspectroscopy of soot and related carbonaceous materials: Spectral analysis and structural information. *Carbon*, 43, pp. 1731-1742
- Samiksha, S., Raman, R. S., Nirmalkar, J., Kumar, S., Sirvaiya R. (2017). PM10 and PM2.5 chemical source profiles with optical attenuation and health risk indicators of paved and unpaved road dust in Bhopal, India. *Environmental Pollution*, 222, pp. 477-485

- Schaider, L. A., Senn, D. B., Brabander D. J., McCarthy, K. D., Shine, J. P. (2007). Characterization of zinc, lead, and cadmium in mine waste: Implications for transport, exposure, and bioavailability. *Environmental Science and Technology*, 41, pp. 4164-4171
- Schauer, J. J., Lough, G. C., Shafer, M. M., Christensen, W. F., Arndt, M. F., DeMinter, J. T., Park, J. S. (2006). Characterization of metals emitted from motor vehicles. *Health Effects Issues*, 133, pp. 1-75
- Schmid, T., Dariz, P. (2016). Chemical imaging of historical mortars by Raman microscopy. *Construction and Building Materials*, 114, pp. 506-516
- Shi, G., Chen, Z., Bi, C., Wang, L., Teng, J., Li, Y., Xu, S. (2011). A comparative study of health risk of potentially toxic metals in urban and suburban road dust in the most populated city of China. *Atmospheric Environment*, 45, pp. 764-771
- Shi, G., Chen, Z., Xu, S., Zhang, J., Wang, L., Bi, C., Teng, J. (2008). Potentially toxic metal contamination of urban soils and roadside dust in Shanghai, China. *Environmental Pollution*, 156, pp. 251-260
- Singh, D. K., Gupta, T. (2016). Source apportionment and risk assessment of PM1 bound trace metals collected during foggy and non-foggy episodes at a representative site in the Indo-Gangetic plain. *Science of the Total Environment*, 550, pp. 80-94
- Skulteti, A., Toth, T. M., Fintor, K., Schubert, F. (2014). Deformation history reconstruction using single quartz grain Raman microspectroscopy data. *Journal of Raman Spectroscopy*, 45, pp. 314-321
- Soltani, N., Keshavarzi, B., Moore, F., Tavakol, T., Lahijanzadeh, A. R., Jaafarzadeh, N., Kermani, M. (2015). Ecological and human health hazards of heavy metals and polycyclic aromatic hydrocarbons (PAHs) in road dust of Isfahan metropolis, Iran. *Science of the Total Environment*, 505, pp. 712-723
- Sondreal, E. A., Benson, S. A., Pavlish, J. H., Ralston, N. V. C. (2004). An overview of air quality III: Mercury, trace elements and particulate matter. *Fuel Processing Technology*, 85, pp. 424-440
- Spengler, J. D., Dockery, D. W., Turner, W. A., Wolfson, J. M., Ferris, B. G. (1980). Long-term measurements of respirable sulphates and particles inside homes. *Atmospheric Environment*, 15, pp. 23-30
- Sperling, D., Gordon, D. 2009. *Two billion cars: Driving toward sustainability*. Oxford University Press, Oxford U.K.
- Srimuruganandam, B., Nagendra, S. (2012). Source characterization of PM10 and PM2.5 mass using a chemical mass balance model at urban roadside. *Science of the Total Environment*, 433, pp. 8-19
- Stockfelt, L., Andersson, E. M., Molnar, P., Gidhagen, L., Segersson, D., Rosengren, A., Barregard, L., Sallsten, G. (2017). Long-term effects of total and source-specific particulate air pollution on incident cardiovascular disease in Gothenburg, Sweden. *Environmental Research*, 158, pp. 61-71
- Sturm, R. (2013). Theoretical models for the simulation of particle deposition and tracheobronchial clearance in lungs of patients with chronic bronchitis. *Annals of Translational Medicine*, 1, pp. 3
- Sun, J., Wu, Z., Cheng, H., Zhang, Z., Frost, R. L. (2014). A Raman spectroscopic comparison of calcite and dolomite. *Spectrochimica Acta Part A: Molecular and Biomolecular Spectroscopy*, 117, pp. 158-162

- Sutherland, R. A., Tolosa, C. A. (2000). Multi-element analysis of road-deposited sediment in an urban drainage basin, Honolulu, Hawaii. *Environmental Pollution*, 110, pp. 483-495
- Swietlik, R., Molik, A., Molenda, M., Trojanowska, M., Siwiec, J. (2011). Chromium(III/VI) speciation in urban aerosol. *Atmospheric Environment*, 45, pp. 1364-1368
- Swietlik, R., Trojanowska, M., Strzelecka, M., Bocho-Janiszewska, A. (2015). Fractionation and mobility of Cu, Fe, Mn, Pb and Zn in the road dust retained on noise barriers along expressway – A potential tool for determining the effects of driving conditions on speciation of emitted particulate metal. *Environmental Pollution*, 196, pp. 404-413
- Sysalova, J., Kucera, J., Drtinova, B., Cervenka, R., Zverina, O., Komarek, J., Kamenik, J. (2017). Mercury species in formerly contaminated soils and released soil gases. *Science of the Total Environment*, 584-585, pp. 1032-1039
- Sysalova, J., Szakova, J. (2006). Mobility assessment and validation of toxic elements in tunnel dust samples—Subway and road using sequential chemical extraction and ICP-OES/GF AAS measurements. *Environmental Research*, 101, pp. 287-293
- Tang, Y., Han, G. (2017). Characteristics of major elements and heavy metals in atmospheric dust in Beijing, China. *Journal of Geochemical Exploration*, 176, pp. 114-119
- Tang, Z., Chai, M., Cheng, J., Jin, J., Yang, Y., Nie, Z., Huang, Q., Li, Y. (2017). Contamination and health risks of heavy metals in street dust from a coal-mining city in eastern China. *Ecotoxicology and Environmental Safety*, 138, pp. 83-91
- Tanner, P. A., Ma, H. L., Yu, P. K. N. (2008). Fingerprinting Metals in Urban Street Dust of Beijing, Shanghai, and Hong Kong. *Environmental Science and Technology*, 42, pp. 7111-7117
- Taylor, K., Robertson, D. (2009). Electron microbeam analysis of urban road-deposited sediment, Manchester, UK: Improved source discrimination and metal speciation assessment. *Applied Geochemistry*, 24, pp. 1261-1269
- Thorpe, A., Harrison, R. M. (2008). Sources and properties of non-exhaust particulate matter from road traffic: A review *Science of the Total Environment*, 400, pp. 270-282
- Thorpe, A. J., Harrison, R. M., Boulter, P. G., McCrae, I. S. M. (2007). Estimation of particle resuspension source strength on a major London road. *Atmospheric Environment*, 41, pp. 8007-8020
- Tielemans, E., Schnieder, T., Goede, H., Tscher, M., Warren, N., Kromhout, H., Van Tongeren, M., Van Hemmen, J., Cherrie, J. W. (2008). Conceptual model for assessment of inhalation exposure: defining modifying factors. *The Annals of Occupational Hygiene*, 52, pp. 577-586
- Tipping, E., Lofts, S., Hooper, H., Frey, B., Spurgeon, D., Svedsen, C. (2010). Critical limits for Hg (II) in soils, derived from chronic toxicity data. *Environmental Pollution*, 158, pp. 2465-2471
- Tomasini, E. P., Dubois, C. M. F., Little, N. C., Centeno, S. A., Maier, M. S. (2015). Identification of pyroxene minerals used as black pigments in painted human bones excavated in Northern Patagonia by Raman spectroscopy and XRD. *Microchemical Journal*, 121, pp. 157-162
- Triebold, S., Luvizotto, G. L., Tolosana-Delgado, R., Zack, T., von Eynatten, H. (2011). Discrimination of TiO<sub>2</sub> polymorphs in sedimentary and metamorphic rocks. *Contributions to Mineralogy and Petrology*, 161, pp. 581-596

- Twining, J., McGlenn, P., Loi, E., Smith, K., Giere, R. (2005). Risk ranking of bioaccessible metals from fly ash dissolved in simulated lung and gut fluids. *Environmental Science and Technology*, 39, pp. 7749-7756
- USEPA. (1989). Risk assessment guidance for superfund (RAGS): Part A. <https://www.epa.gov/risk/risk-assessment-guidance-superfund-rags-part>. Last accessed 30/04/2018
- USEPA. (1996a). Superfund soil screening guidance. <https://www.epa.gov/superfund/superfund-soil-screening-guidance>. Last accessed 30/04/2018
- USEPA. (1996b). Method 3060A alkaline digestion for hexavalent chromium. <https://www.epa.gov/sites/production/files/2015-12/documents/3060a.pdf>. Last accessed 30/04/2018
- USEPA. (1997). Exposure factors handbook. EPA/600/P-95/002F. Washington, DC: Environmental Protection Agency, Office of Research and Development. Last accessed 30/04/2018
- USEPA. (2000). Soil screening guidance for radionuclides: Technical background document. <http://www.epa.gov/superfund/health/contaminants/radiation/pdfs/sstbd.pdf>. Last accessed 30/04/2018
- USEPA. (2001). Risk assessment guidance for superfund: Volume III – Part A, Process for conducting probabilistic risk assessment. US Environmental Protection Agency, Washington, D.C. EPA 540-R-02-002. Last accessed 30/04/2018
- Van Vuuren, D. P., Bouwman, L. F., Smith, S. J., Dentener, F. (2011). Global projections for anthropogenic reactive nitrogen emissions to the atmosphere, an assessment of scenarios in the scientific literature. *Current Opinion in Environmental Sustainability*, 3, pp. 359-369
- Vane, C. H., Jones, D. G., Lister, T. R. 2009. Mercury contamination in surface sediments and sediment cores of the Mersey Estuary, UK. *Marine Pollution Bulletin*, 58, pp. 940-946
- Vaughan, J. W., Woodfolk, J. A., Platts-Mills, T. A. E. (1999). Assessment of vacuum cleaners and vacuum cleaner bags recommended for allergic subjects. *Journal of Allergy and Clinical Immunology*, 104, pp. 1079-1083
- Wang, J., Li, S., Cui, X., Li, H., Qian, X., Wang, C., Sun, Y. (2016). Bioaccessibility, sources and health risk assessment of trace metals in urban park dust, Nanjing, Southeast China. *Ecotoxicology and Environmental Safety*, 128, pp. 161-170
- Wang, L., Zhao, J., Duan, B., Zhu, D., Hua, Y., Zhou, W., Liu, G. (2015). Characteristics of street dust in Jiansheng Town, Chongqing City, China. *Environmental Progress and Sustainable Energy*, 35, pp. 794-801
- Wang, W., Huang, M. J., Wu, F. Y., Kang, Y., Wang, H. S., Cheung, K. W., Wong, M. H. (2013). Risk assessment of bioaccessible organochlorine pesticides exposure via indoor and outdoor dust. *Atmospheric Environment*, 77, pp. 525-533
- Wang, Z., Wang, J., Kouketsu, Y., Bodnar, R. J., Gill, B. C., Xiao, S. (2017). Raman geothermometry of carbonaceous material in the basal Ediacaran Doushantuo cap dolostone: The thermal history of extremely negative  $\delta^{13}\text{C}$  signatures in the aftermath of the terminal Cryogenian snowball Earth glaciation. *Precambrian Research*, 298, pp. 174-186
- Watanabe, H., Nakajima, F., Kasuga, I., Furumai, H. (2013). Application of whole sediment toxicology identification evaluation procedures to road dust using a benthic ostracod *Hetrocypris incongruens*. *Ecotoxicology and Environmental Safety*, 89, pp. 245-251

- Watenphul, A., Schmit, C. (2011). Calibration of berlinite ( $\text{AlPO}_4$ ) as Raman spectroscopic pressure sensor for diamond-anvil cell experiments at elevated temperatures. *Journal of Raman Spectroscopy*, 43, pp. 564-570
- Wei, X., Gao, B., Wang, P., Zhou, H., Lu, J. (2015). Pollution characteristics and health assessments of heavy metals in street dusts from different functional areas in Beijing, China. *Ecotoxicology and Environmental Safety*, 112, pp. 186-192
- Weinbruch, S., Worringen, A., Ebert, M., Scheuven, D., Kandler, K., Pfeffer, U., Bruckmann, P. (2014). A quantitative estimation of the exhaust, abrasion and resuspension components of particulate traffic emissions using electron microscopy. *Atmospheric Environment*, 99, pp. 175-182
- Weis, C. P., LaVelle, J. M. (1991). Characteristics to consider when choosing an animal model for the study of lead bioavailability. *Chemical Speciation and Bioavailability*, 3, pp. 113-119
- White, S. N. (2009). Laser Raman spectroscopy as a technique for identification of seafloor hydrothermal and cold seep minerals. *Chemical Geology*, 259, pp. 240-252
- WHO. (1990). Environmental health criteria 101, methylmercury. <http://www.inchem.org/documents/ehc/ehc/ehc101.htm>. Last accessed 30/04/2018
- WHO. (2009). Global health risks, mortality and burden of disease attributable to selected major risks. [http://www.who.int/healthinfo/global\\_burden\\_disease/GlobalHealthRisks\\_report\\_full.pdf](http://www.who.int/healthinfo/global_burden_disease/GlobalHealthRisks_report_full.pdf) WHO . 2014. <http://www.who.int/mediacentre/news/releases/2014/air-pollution/en/>. Last accessed 30/04/2018
- Wiechert, D. U., Grabowski, S. P., Simon, M. (2005). Raman spectroscopic investigation of evaporated PbO layers. *Thin Solid Films*, 484, pp. 73-82
- Wiseman, C. L. S. (2015). Analytical methods for assessing metal bioaccessibility in airborne particulate matter: a scoping review. *Analytica Chimica Acta*, 877, pp. 9-18
- Wiseman, C. L. S., Zereni, F. (2014). Characterizing metal(loid) solubility in airborne PM<sub>10</sub>, PM<sub>2.5</sub> and PM<sub>1</sub> in Frankfurt, Germany using simulated lung fluids. *Atmospheric Environment*, 89, pp. 282-289
- Witt, E. C., Shi, H., Wronkiewicz, D. J., Pavlowsky, R. T. (2014). Phase partitioning and bioaccessibility of Pb in suspended dust from unsurfaced roads in Missouri—a potential tool for determining mitigation response. *Atmospheric Environment*, 88, pp. 90-98
- Woodfolk, J. A., Luczynska, C. M., de Blay, F., Chapman, M. D., Platts-Mills, T. A. (1993). The effect of vacuum cleaners on the concentration and particle size distribution of airborne cat allergen. *Journal of Allergy and Clinical Immunology*, 91, pp. 829-837
- Wragg, J., Cave, M., Basta, N., Brandon, E., Casteel, S., Denys, S., Gron, C., Oomen, A., Reimer, K., Tack, K., Van de Wiele, T. (2011). An inter-laboratory trial of the unified BARGE bioaccessibility method for arsenic, cadmium and lead in soil. *Science of the Total Environment*, 409, pp. 4016-4030
- Wragg, J., Klinck, B. (2007). The bioaccessibility of lead from Welsh mine waste using a respiratory uptake test. *Journal of Environmental Science and Health. Part A, Toxic/Hazardous Substances & Environmental Engineering*, 42, pp. 1223-1231
- Xia, Q., Peng, C., Lamb, D., Mallavarapu, M., Naidu, R., Ng, J. C. (2016). Bioaccessibility of arsenic and cadmium assessed for in vitro bioaccessibility in spiked soils and their

interaction during the Unified BARGE Method (UBM) extraction. *Chemosphere*, 147, pp. 444-450

Yang, T., Liu, Q., Li, H., Zeng, Q., Chan, L. (2010). Anthropogenic magnetic particles and heavy metals in the road dust: magnetic identification and its implications. *Atmospheric Environment*, 44, pp. 1175-1185

Yeung, Z. L. L., Kwok, R. C. W., Yu, K. N. (2003). Determination of multielement profiles of street dust using energy dispersive X-ray fluorescence. *Applied Radiation and Isotopes*, 58, pp. 339-346

Yue, D. L., Hu, M., Wang, Z. B., Wen, M. T., Guo, S., Zhong, L. J., Weidensohler, A., Zhang, Y. H. (2013). Comparison of particle number size distribution and new particle formation between the urban and rural sites in the PRD region, China. *Atmospheric Environment*, 76, pp. 181-188.

Zannoni, D., Valotto, G., Visin, F., Rampazzo, G. (2016). Sources and distribution of tracer elements in road dust: The Venice mainland case of study. *Journal of Geochemical Exploration*, 166, pp. 64-72

Zereni, F., Wiseman, C. L. S., Poprizki, J., Albers, P., Schneider, W., Leopold, K., 2017. Assessing the potential of inorganic anions ( $\text{Cl}^-$ ,  $\text{NO}_3^-$ ,  $\text{SO}_4^{2-}$  and  $\text{PO}_4^{3-}$ ) to increase the bioaccessibility of emitted palladium in the environment: Experimental studies with soils and a Pd model substance. *Environmental Pollution*, 220, pp. 1050-1058

Zereni, F., Wiseman, C. L., Puttmann, W. (2012). *In vitro* investigations of platinum, palladium, and rhodium mobility in urban airborne particulate matter (PM<sub>10</sub>, PM<sub>2.5</sub>, and PM<sub>1</sub>) using simulated lung fluids. *Environmental Science and Technology*, 46, pp. 10326-10333

Zhang, C., Qiao, Q., Appel, E., Huang, B. (2012). Discriminating sources of anthropogenic heavy metals in urban street dusts using magnetic and chemical methods. *Journal of Geochemical Exploration*, 119-120, pp. 60-75

Zhang, J., Fu, Y., Li, J., Wang, J., He, B., Xu S. (2009). Effects of subchronic cadmium poisoning on DNA methylation in hens. *Environmental Toxicology and Pharmacology*, 27, pp. 345-349

Zhang, M., Wruck, B., Barber, A. G., Salje, E. K. H., Carpenter, M. A. (1996). Phonon spectra of alkali feldspars: Phase transitions and solid solutions. *American Mineralogist*, 81, pp. 92-104

Zhang, Y., Li, Q., Liu, X., Zhu, H., Song, A., Jiao, J. (2013). Anti-oxidant and micronutrient-rich formula reduces lead poisoning and related oxidative damage in lead-exposed mice. *Food and Chemical Toxicology*, 57, pp. 201-208

Zhao, H., Xia, B., Fan, C., Zhao, P., Shen, S. (2012). Human health risk from soil heavy metal contamination under different land uses near Dabaoshan mine, southern China. *Science of the Total Environment*, 417-418, pp. 45-54.

Zoitos, B. K., De Meringo, A., Rouyer, E., Bauer, S., Thelohan, J., Law, B., Boymel, P. M., Olson, J. R., Christensen, V. R., Guldborg, M., Koenig A. R., Perander, M. (1997). *In vitro* measurement of fiber dissolution rate relevant to biopersistence at neutral pH: An interlaboratory round robin. *Inhalation Toxicology*, 9, pp. 525-540

# Appendices

## Appendix A: Supplementary Data

	Al	As	Cd	Co	K	Ni	S	Zn
Sp 2013	9210	1.57	1.67	10.2	1150	39.8	1870	560
Sum 2013	14100	0.76	2.15	13.0	2600	49.8	3870	687
Aut 2013	14500	3.26	1.75	14.2	2220	53.5	2900	732
Win 2013/2014	12000	3.12	1.32	11.0	1580	45.0	2650	701
Sp 2014	13400	3.61	1.53	12.9	1750	50.7	2550	720
Sum 2014	13500	4.03	1.65	15.2	1500	63.1	2270	1040
Aut 2014	13500	4.09	1.33	12.8	1990	56.5	2510	878
Win 2014/2015	13400	2.42	1.00	10.9	2000	42.7	3030	610

Table A-1: Mean bulk metal concentrations (mg kg<sup>-1</sup>) in <38µm fraction of RD as determined by ICP-OES

	Al	As	Cd	Co	K	Ni	S	Zn
Sp 2013	9770	1.18	1.68	10.9	1110	43.1	1770	478
Sum 2013	10600	1.07	2.04	11.2	1470	48.6	3100	550
Aut 2013	11800	2.89	1.35	12.4	1530	54.5	2500	584
Win 2013/2014	10700	3.09	3.26	11.1	1290	50.9	2300	579
Sp 2014	9950	2.80	1.26	10.7	1170	47.0	2010	515
Sum 2014	11300	3.15	1.34	12.9	1170	62.2	2090	716
Aut 2014	9850	3.59	1.16	11.3	1200	53.2	2290	708
Win 2014/2015	11800	5.65	0.91	9.38	1720	58.2	2450	583

Table A-2: Mean bulk metal concentrations (mg kg<sup>-1</sup>) in 63-38µm fraction of RD as determined by ICP-OES

	Al	As	Cd	Co	K	Ni	S	Zn
Sp 2013	6070	0.68	1.32	8.28	519	36.9	1120	254
Sum 2013	7130	0.92	1.53	8.82	747	44.3	1720	329
Aut 2013	6450	2.30	0.95	9.35	350	43.3	1480	318
Win 2013/2014	6260	1.79	4.06	7.65	276	39.5	1330	247
Sp 2014	7536	2.83	1.60	7.55	780	37.7	1430	314
Sum 2014	8370	2.48	1.24	9.37	807	49.2	1580	400
Aut 2014	7560	2.78	1.04	8.27	694	48.4	1740	417
Win 2014/2015	8400	1.57	1.36	7.43	918	34.4	1710	332

Table A-3: Mean bulk metal concentrations (mg kg<sup>-1</sup>) in 125-63µm fraction of RD as determined by ICP-OES.

	Cr	Cu	Fe	Pb
Sp 2013	14.1	175	5220	95.8
Sum 2013	16.0	236	5310	131
Aut 2013	20.6	285	7370	153
Win 2013/2014	17.1	260	5760	122
Sp 2014	16.1	210	6000	111
Sum 2014	21.5	431	8130	184
Aut 2014	17.4	343	5720	128
Win 2014/2015	14.3	246	5460	82.7

Table A-4: Mean ALF leachate concentrations (mg kg<sup>-1</sup>) in <38 µm fraction of RD as determined by ICP-OES.

	Cr	Cu	Fe	Pb
Sp 2013	<LOD	74.9	<LOD	0.884
Sum 2013	<LOD	116.9	<LOD	1.36
Aut 2013	<LOD	129.7	<LOD	0.799
Win 2013/2014	0.127	131.2	1.97	1.19
Sp 2014	<LOD	77.1	<LOD	1.14
Sum 2014	<LOD	204	4.55	1.30
Aut 2014	<LOD	20	<LOD	1.14
Win 2014/2015	0.546	167	<LOD	1.06

Table A-5: Mean GI leachate concentrations (mg kg<sup>-1</sup>) in <38 µm fraction of RD as determined by ICP-OES.

	Cr	Cu	Fe	Pb
Sp 2013	<LOD	68.7	1.25	0.970
Sum 2013	<LOD	91.5	0.000	1.30
Aut 2013	0.062	112	5.36	1.47
Win 2013/2014	0.203	115	16.3	1.97
Sp 2014	<LOD	65.2	1.57	0.921
Sum 2014	<LOD	135	18.1	1.66
Aut 2014	<LOD	140	0.000	0.804
Win 2014/2015	0.213	111	59.2	3.38

Table A-6: Mean GI leachate concentrations (mg kg<sup>-1</sup>) in 63-38 µm fraction of RD as determined by ICP-OES.

	Cr	Cu	Fe	Pb
Sp 2013	<LOD	40.0	8.70	1.26
Sum 2013	<LOD	59.8	<LOD	0.624
Aut 2013	0.216	71.6	<LOD	1.80
Win 2013/2014	0.062	64.2	15.7	2.18
Sp 2014	0.029	51.3	7.90	1.35
Sum 2014	<LOD	73.4	<LOD	0.917
Aut 2014	<LOD	76.6	<LOD	0.339
Win 2014/2015	<LOD	54.3	5.00	1.33

Table A-7: Mean GI leachate concentrations (mg kg<sup>-1</sup>) in 125-63 µm fraction of RD as determined by ICP-OES.

	Cr	Cu	Fe	Pb
Sp 2013	0.010	28.5	6.55	1.25
Sum 2013	0.043	67.1	6.82	1.48
Aut 2013	0.084	78.1	11.1	1.15
Win 2013/2014	0.320	63.2	25.9	1.55
Sp 2014	0.089	30.3	13.0	1.36

Sum 2014	0.646	97.3	71.5	2.81
Aut 2014	0.073	101	2.48	1.52
Win 2014/2015	0.917	80.8	38.9	1.82

Table A-8: Mean GC leachate concentrations (mg kg<sup>-1</sup>) in <38 µm fraction of RD as determined by ICP-OES.

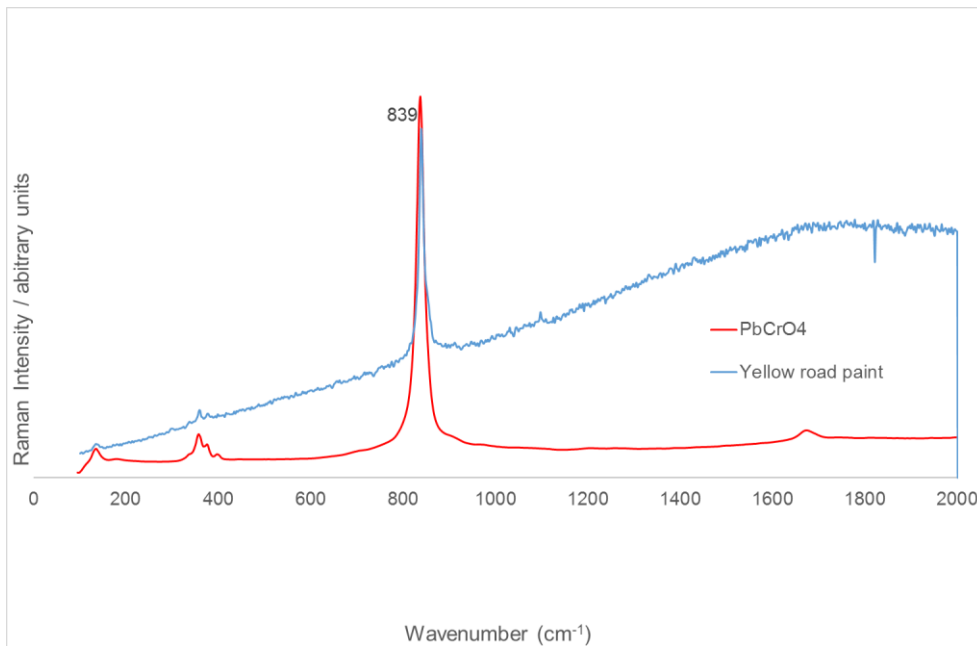
	Cr	Cu	Fe	Pb
Sp 2013	0.085	23.5	54.4	1.74
Sum 2013	0.067	54.8	70.9	2.70
Aut 2013	0.067	77.7	1.97	1.09
Win 2013/2014	0.643	56.3	74.5	2.87
Sp 2014	0.426	27.7	146	1.88
Sum 2014	1.21	109	240	10.7
Aut 2014	0.118	75.9	11.8	1.46
Win 2014/2015	1.24	68.2	169	4.61

Table A-9: Mean GC leachate concentrations (mg kg<sup>-1</sup>) in 63-38 µm fraction of RD as determined by ICP-OES.

	Cr	Cu	Fe	Pb
Sp 2013	0.90	35.3	34.2	1.15
Sum 2013	0.34	32.2	57.0	1.59
Aut 2013	0.72	39.9	107	2.95
Win 2013/2014	1.02	68.5	220	16.6
Sp 2014	1.12	36.7	339	16.9
Sum 2014	1.52	74.1	513	26.0
Aut 2014	0.51	43.0	105	2.90
Win 2014/2015	1.62	50.2	328	16.5

Table A-10: Mean GC leachate concentrations (mg kg<sup>-1</sup>) in 125-63 µm fraction of RD as determined by ICP-OES.

Figure A-1: Yellow road marking spectrum shown here in blue as determined by DXR Raman, along with lead chromate reference spectra.



## Appendix B: Conference Contributions

B.1 Poster presentation at the ECG atmospheric and environmental chemistry forum, University of Leicester 25<sup>th</sup> June 2012

### **Bioaccessibility of the inhalable fractions of urban road dust.**

**Sanja Potgieter-Vermaak<sup>1,2</sup>, Andrew Brown<sup>1</sup>, Judith Barret<sup>1</sup>, Rene Van Grieken<sup>3</sup>**

<sup>1</sup>Division of Chemistry & Environmental Science, Faculty of Science & Environment, Manchester Metropolitan University, Manchester, United Kingdom, s.potgieter@mmu.ac.uk.

<sup>2</sup>Molecular Science Institute, School of Chemistry, university of the Witwatersrand, Johannesburg, South Afrika.

<sup>3</sup>Department of Chemistry, University of Antwerp, Antwerp, Belgium, r.vangrieken@ua.ac.be.

#### Abstract

In-vitro and animal toxicological studies confirmed that the chemical composition of inhaled particles play a major role in its toxic, genotoxic and carcinogenic mechanisms, but the component-specific toxic effects are still not understood. Particle-bound airborne transition metals can also lead to the production of Reactive Oxygen Species in lung tissue; a special concern amongst particularly susceptible cohorts (children and elderly). The bioaccessibility of the fine fraction is evidently of importance for public health. Size-fractionated (<38, 38 – 63, 63 – 125 µm) road dust collected from one of the highest trafficked roads in the United Kingdom and believed to be one of the busiest bus routes in Europe, were characterised for its bulk elemental composition with EDXRF, ICP-OES and ICP-MS and its molecular composition with micro Raman spectroscopy. It was found that the fine fraction (< 38 µm) had the highest Pb (238 ppm) and Cr (171 ppm) concentrations. Concentrations of both Pb and Cr decreased substantially (279 (< 38 µm) – 13 ppm (<1mm); 171 (< 38 µm) – 91 ppm (<1mm), respectively) in the larger fractions. The MRS data showed that the Cr was mostly present as lead chromate and therefore in the Cr(VI) oxidation state. Apart from rather alarmingly high concentrations of oxidative stressors (Cu, Fe, Mn) obtained from the elemental analysis, the carcinogenic potential of the respirable fraction is evident from the MRS data. These same fractions underwent in-vitro testing to assess the mobility of toxic and carcinogenic components by leaching with artificial body fluids. Leachates were analysed for Cr, Cu, Zn, V, Pb, Mn, Cd, Fe, Ni, Al and As concentrations at time intervals from 1 hour to 8 weeks. In general, most of the elements leached in the ppb range and concentrations decreased with increase in particle size. Although the mobility in the artificial body fluids of the various elements varied, up to 19% Cr, 47% Pb and 87% Ni were released.

Keywords: Road dust, respirable, bioaccessibility, artificial body fluid, toxicology.

B.2 Oral presentation at the 5<sup>th</sup> MMU annual research conference, 25<sup>th</sup> April  
2013

**Bioaccessibility of the inhalable fractions of urban road dust.**

**Andrew Brown<sup>1</sup>, Judith Barret<sup>1</sup>, Rene Van Grieken<sup>2</sup> Sanja Potgieter-Vermaak<sup>1,3</sup>**

<sup>1</sup>Division of Chemistry & Environmental Science, Faculty of Science & Environment, Manchester Metropolitan University, Manchester, United Kingdom, 08258722@stu.mmu.ac.uk, s.potgieter@mmu.ac.uk.

<sup>2</sup>Department of Chemistry, University of Antwerp, Antwerp, Belgium, r.vangrieken@ua.ac.be.

<sup>3</sup>Molecular Science Institute, School of Chemistry, University of the Witwatersrand, Johannesburg, South Afrika.

Abstract—An increasing number of studies have indicated the importance of chemical composition of airborne particles. In vitro studies are essential in understanding the component specific toxic effects of metals within inhalable particles; despite this they are seldom considered. Size-fractionated road dust collected from one of the highest trafficked roads in the United Kingdom, were characterised for its bulk elemental composition. It was found that the fine fraction (< 38 µm) was enriched in most heavy metals, including Pb, Cr, Ni, Zn, Mn, Fe and V, amongst others. Concentrations of most of these elements decreased with an increase in particle size. These same fractions underwent in-vitro testing to assess the mobility of toxic and carcinogenic components by leaching with artificial body fluids at time intervals from 1 hour to 8 weeks.

B.3 Poster presentation 30<sup>th</sup> International conference of the society of environmental geochemistry and health, Northumbria University, 1<sup>st</sup>-4<sup>th</sup> July 2014

**In Vitro analysis of particulate output from a demolition site, Manchester**

**Andrew Brown <sup>a\*</sup>, Heather Robinson <sup>a</sup> Sanja Potgieter-Vermaak <sup>a</sup>**

Division of Chemistry & Environmental Science, Faculty of Science & Environment, Manchester Metropolitan University, Manchester.

\* Corresponding author.

A large array of literature underlines the growing concern for the impact of particulate matter from anthropological sources in urban settings on human health<sup>1,2</sup>. Particles of specific interest are those which gather as curb-side sediment poised to be pulverised and perturbed hence suspended by the action of vehicles making use of the road, road dust (RD)<sup>3</sup>. During the winter months 2012-2013 a large building was demolished in the centre of Manchester, the aim of this paper is to assess the changes in elemental composition of inhalable fractions of RD collected 20 metres from the demolition site. The initial sampling takes place in November 2012 approximately two weeks before demolition began, with the second sampling campaign taking place in May 2013, during the final stages of demolition. Consistent methodology was observed, approximately 10 kilograms of RD was collected using a clean polythene dust pan and brush. Samples were air dried and sieve fractioned, analysis took by ICP-OES following a microwave assisted HF digestion. Interestingly, results indicate that the heavy and trace metals were generally lower in concentration for the second sampling campaign, after demolition had taken place. Two notable exception being the silicon and aluminium portions, which increased in concentration by 7.4% and 20% respectively for the smallest fraction (<38µm), 5.9% and 56.7% respectively for the next sized fraction (63-38µm) and 8.6% and 3.8% respectively for the larger fraction (125-63µm). In vitro experimentation carried out on these road dusts using artificial lysosomal fluid indicates that up to 30% of inhalable fraction of aluminium is bioaccessible.

B.4 Poster presentation, 13<sup>th</sup> Quadrennial ICACGP/iGAC Conference on atmospheric chemistry, Federal University of Rio Grande do Norte, 22-26<sup>th</sup> September 2014

**In Vitro analysis of particulate output from a demolition site, Manchester**

**Andrew Brown <sup>a\*</sup>, Heather Robinson <sup>a</sup> Sanja Potgieter-Vermaak <sup>a</sup>**

Division of Chemistry & Environmental Science, Faculty of Science & Environment, Manchester Metropolitan University, Manchester.

\* Corresponding author.

A large array of literature underlines the growing concern for the impact of particulate matter from anthropological sources in urban settings on human health<sup>1,2</sup>. Particles of specific interest are those which gather as curb-side sediment poised to be pulverised and perturbed hence suspended by the action of vehicles making use of the road, road dust (RD)<sup>3</sup>. During the winter months 2012-2013 a large building was demolished in the centre of Manchester, the aim of this paper is to assess the changes in elemental composition of inhalable fractions of RD collected 20 metres from the demolition site. The initial sampling takes place in November 2012 approximately two weeks before demolition began, with the second sampling campaign taking place in May 2013, during the final stages of demolition. Consistent methodology was observed, approximately 10 kilograms of RD was collected using a clean polythene dust pan and brush. Samples were air dried and sieve fractioned, analysis took by ICP-OES following a microwave assisted HF digestion. Interestingly, results indicate that the heavy and trace metals were generally lower in concentration for the second sampling campaign, after demolition had taken place. Two notable exception being the silicon and aluminium portions, which increased in concentration by 7.4% and 20% respectively for the smallest fraction (<38µm), 5.9% and 56.7% respectively for the next sized fraction (63-38µm) and 8.6% and 3.8% respectively for the larger fraction (125-63µm). In vitro experimentation carried out on these road dusts using artificial lysosomal fluid indicates that up to 30% of inhalable fraction of aluminium is bioaccessible.



## Ionic content of road dust

Andrew Brown<sup>a</sup>, J. E. S. Barrett<sup>a</sup>, S. Potgieter-Vermaak<sup>a</sup>  
<sup>a</sup> Division of Chemistry and Environmental Science, Manchester Metropolitan University, Manchester, M1 5GD, UK

### Rationale

Road dust (RD) is defined as particles and sediment, which gathers at roadside locations. Due to proximity to anthropogenic sources, RD is often highly contaminated with toxic substances. Findings by Hien *et al.*<sup>[1]</sup> indicated that resuspended RD can be responsible for up to 74% of PM due to turbulent effects of traffic. Concentrations of ions such as NO<sub>3</sub><sup>-</sup>, SO<sub>4</sub><sup>2-</sup> and NH<sub>4</sub><sup>+</sup> have been closely linked to acute health effects during smog episodes<sup>[2]</sup>, as well as the balance between cations and anions<sup>[3]</sup>. In this study samples of RD were taken to represent winter, spring and summer to assess changes in concentrations of ions seasonally.



### Methodology and Instrumentation



RD was collected from a road traffic island on Oxford Road, Manchester using a dustpan and brush. It was then dried and fractionated to <2000µm, 2000-250µm, 250-125µm, 125-63µm, 63-38µm and <38µm. 1g of each fraction was weighed into a vial along with 20ml of deionised water and shaken for 1 hour using an orbital shaker. A Dionex ICS-2000 was then used to measure concentrations of cations and anions which were water soluble.

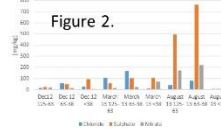
### Results

Results show a general trend of enrichment in the smaller fractions for both anions and cations (figures 2 and 3). It can be observed that the concentration of sodium is increased in the spring months, most likely due to the road salting in the spring months, Calcium, Nitrate and Sulphate ions are all more abundant in the summer months, in agreement with work by Gao *et al.*<sup>[2]</sup>.

Using equations 1 and 2 above, the acidic or basic nature of each fraction can be deduced. Lower A/C ratio for a sample indicates more a more basic sample<sup>[4]</sup>. The samples in this study show increasing acidity from winter to spring to summer, increased acidity has previously been linked with increased airborne particulate matter thus a higher likelihood of acute health effects<sup>[3]</sup>.

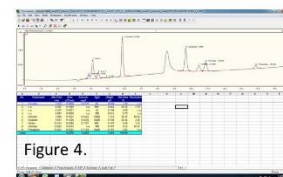
	Al <sup>3+</sup>	Ca <sup>2+</sup>	Mg <sup>2+</sup>	Na <sup>+</sup>	K <sup>+</sup>	NO <sub>3</sub> <sup>-</sup>	SO <sub>4</sub> <sup>2-</sup>	Cl <sup>-</sup>
<b>December 2012</b>								
<38µm	21.71	1.83	36.3	1.4	187.8	31.39	29.39	25.36
63-125µm	27.56	1.46	11.76	2.52	223.26	36.58	30.94	15.16
<125µm	87.04	11.02	38.48	3.06	227.5	68.72	63.32	3.41
<b>March 2013</b>								
<38µm	77.58	1.5	18.56	0.9	130.56	56.42	17.18	14.78
63-125µm	146.24	7.32	10.72	1.62	224.78	35.02	33.9	26.02
<125µm	233.89	10.06	27.28	6.78	312.82	90.2	50.98	86.6
<b>August 2013</b>								
<38µm	31.26	0.88	17.16	2.28	231.26	89.34	89.89	169.2
63-125µm	7.7	1.5	27.84	0.46	391.1	76.12	761.84	117.69
<125µm	204.82	2.06	35.06	22.66	337.18	1.78	878	87.22

Eqn (1): C (Cation microequivalent) =  $\frac{[NH_4^+]}{18} + \frac{[Na^+]}{23} + \frac{[K^+]}{39} + \frac{[Mg^{2+}]}{12} + \frac{[Ca^{2+}]}{20}$   
 Eqn (2): A (Anion microequivalent) =  $\frac{[NO_3^-]}{62} + \frac{[SO_4^{2-}]}{48} + \frac{[Cl^-]}{35.5}$



### Conclusions and future work

It can be observed that ionic nature of RD changes substantially between season, the patterns observed here are in agreement with those seen in literature. Future work on the ionic content of RD will include the quantification of acetate. Peaks were observed using the IC technique described (figure 4). Implementation of these techniques to quantify acetate present in samples of this nature could be very useful if use of ethanol fuelled vehicles continues to increase.



References:  
 [1] Hien, H. Q., Binh, N. T., Truong, V. A. and N. T. 2009. Temporal variations of source impacts on the receptor: as derived from chemical microequivalents in the Chi Minh City, Vietnam. *Atmospheric Environment*, 43, 3133-3142.  
 [2] Gao, J., Tang, H., Cheng, H., Liu, J., Zhang, M., Wang, S., Han, J., Wang, B., Han, J., Peng, C., Wang, T. 2010. The variations of chemical composition of PM2.5 and PM10 and their source during haze pollution events in Beijing, China. *Atmospheric Environment*, 44, 1247-1256.  
 [3] Barone, A., Pardo, A., Van Goolen, R., Jansen, A., Pardo, S., De Wit, A., Pignatelli, B. 2014. Comparison of PM2.5 and PM10 in high and low pollution events: their and its relation to meteorological conditions and air quality indexes. In the 10th European Conference on Applied Environmental Chemistry, 16-18 Oct 2014.  
 [4] Marz, J., Gao, J., Amos, R., Marz, J., Zhang, H., Han, J., Liu, S., Ghosh, T., Nakai, S., Tamura, S. 2009. Ionic composition of TSP and PM10 during dust storms and air pollution episodes at Xi'an, China. *Atmospheric Environment*, 43, 2215-2228.

B.6 Oral presentation at the 9<sup>th</sup> MMU annual research conference, 22<sup>nd</sup>

February 2017

**Bioaccessibility of the inhalable fractions of urban road dust.**

**Andrew Brown<sup>a</sup>, Sanja Potgieter-Vermaak<sup>a</sup>, Judi Barrett<sup>a</sup>**

**<sup>a</sup>School of Science and the Environment, Division of Chemistry and Environmental Science,  
Manchester Metropolitan University**

Urban air quality is of significant importance to the majority of us living or working in our cities worldwide. Short-term events such as the 1952 London smog episode have the ability to dominate headlines because of the 4000 deaths due to acute exposure to air pollution (Whittaker et al, 2004).

However, chronic exposure to air pollution, which we are all subject to provide equally shocking statistics. The European Environment Agency estimates that poor air quality is responsible for 467,000 premature deaths per year amongst Europeans (EEA, 2016). The World Health Organisation estimates that air pollution is responsible for 8% of lung cancer deaths, 5% of cardiopulmonary deaths and 3% of respiratory infection deaths (WHO, 2009).

PM (Particulate matter) is the term used to describe respirable airborne particles that are permanently present in urban areas. The anthropogenic emissions of for PM are numerous, although commonly include industrial and commercial output, vehicular emissions and wear, abrasion of road surfaces etc. Because of the range and nature of sources, PM should be considered unique for any given location.

PM is a topic which has been studied extensively, although recent consensus amongst the scientific community indicates that the micro-chemical structure of PM is responsible for the degree of toxicity (Rohr et al, 2011).

Due to the nature of PM, and particularly respirable PM<sub>10</sub> (<10µm fraction), it can be difficult to analyse with techniques designed to characterise the micro-chemical structure. The work in this study novelly looks into the possibility of using a larger, more abundant size fraction as a proxy for PM<sub>10</sub>, using a water deposition technique to separate road dust. CC-SEM-EDX was used to determine particle size distribution of the separated samples to successfully support the use of water deposition as a separation technique. Samples were then acid digested and analysed using ICP-OES to determine elemental profile, results indicated a large degree of similarity between the <10µm fraction and the original sample from which it was extracted. Finally the observed elemental concentrations were risk assessed using a novel modified version of the Environmental Protection Agency Hazard Index equation to indicate potential toxicity to the public. The most exciting conclusion obtained from this experimentation is the potential for use of larger, more abundant fractions of environmental particles as a proxy for the fine respirable fraction. It will then be possible to collect more representative data on PM<sub>10</sub>, as well as using intra-molecular techniques such as Raman Spectroscopy to draw conclusions on the micro-chemical structure.

## **Appendix C: Publications**

### **C.1 Publications with results which feature in the main text**

# *Risk assessment of exposure to particulate output of a demolition site*

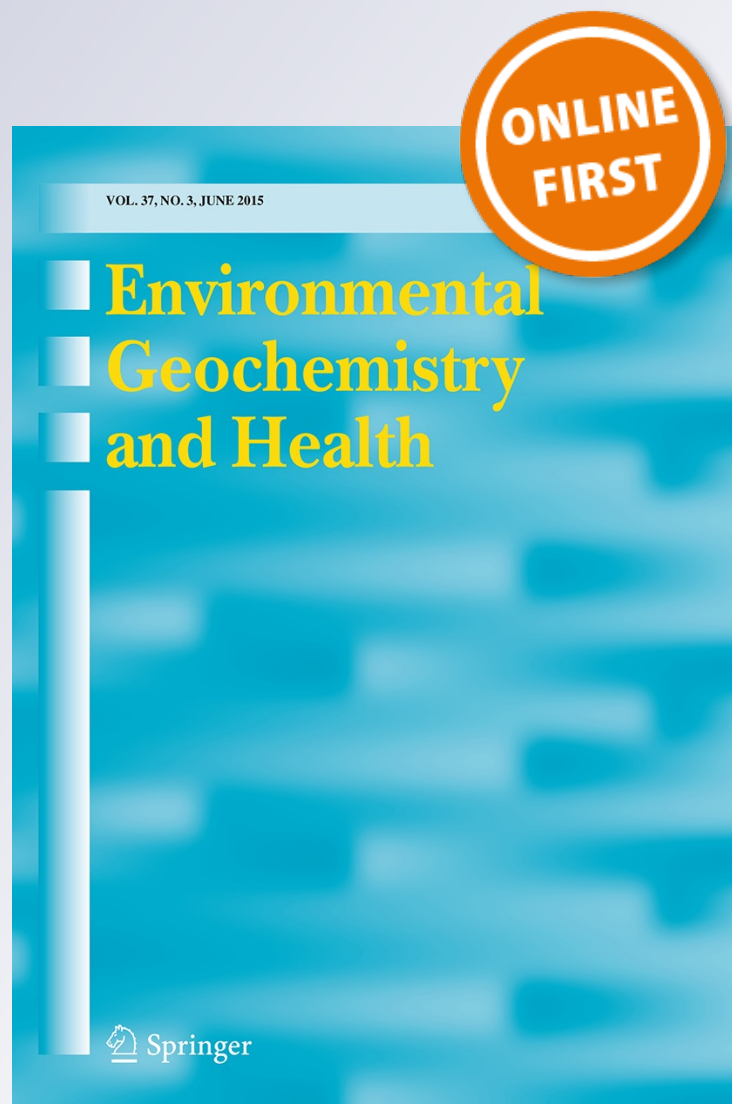
**A. Brown, J. E. S. Barrett, H. Robinson & S. Potgieter-Vermaak**

**Environmental Geochemistry and Health**

Official Journal of the Society for Environmental Geochemistry and Health

ISSN 0269-4042

Environ Geochem Health  
DOI 10.1007/s10653-015-9747-3



**Your article is protected by copyright and all rights are held exclusively by Springer Science +Business Media Dordrecht. This e-offprint is for personal use only and shall not be self-archived in electronic repositories. If you wish to self-archive your article, please use the accepted manuscript version for posting on your own website. You may further deposit the accepted manuscript version in any repository, provided it is only made publicly available 12 months after official publication or later and provided acknowledgement is given to the original source of publication and a link is inserted to the published article on Springer's website. The link must be accompanied by the following text: "The final publication is available at [link.springer.com](http://link.springer.com)".**

# Risk assessment of exposure to particulate output of a demolition site

A. Brown · J. E. S. Barrett · H. Robinson ·  
S. Potgieter-Vermaak

Received: 31 October 2014 / Accepted: 8 July 2015  
© Springer Science+Business Media Dordrecht 2015

**Abstract** Whilst vehicular and industrial contributions to the airborne particulate budget are well explored, the input due to building demolition is relatively unknown. Air quality is of importance to human health, and it is well known that composition of airborne particles can have a significant influence on both chronic and acute health effects. Road dust (RD) was collected before and after the demolition of a large building to elucidate changes in elemental profile. Rainfall and PM<sub>10</sub> mass concentration data aided interpretation of the elemental data. Quantification of Al, As, Ba, Ca, Cd, Cr, Cu, Fe, K, Mg, Mn, Na, Ni, Pb, Rh, S, Si, Sn, Ti, V and Zn was carried out. It was found that only Al, K, Mg, Si and S increased in concentration across all size fractions after the building demolition. Risk assessment was then carried out on elements with applicable reference dose values to

assess the potential health risks due to the demolition. Significant risk to children was observed for chromium and aluminium exposure. PM<sub>10</sub>, monitored 40 metres from the demolition site, indicated no abnormal concentrations during the demolition; however, rainfall data were shown to affect the concentration of PM<sub>10</sub>. The elemental data observed in this study could possibly indicate the role of increased sulphur concentrations (in this case as a result of the demolition) on the buffer capacity of RD, hence leaching metals into rainwater.

**Keywords** Road dust · Demolition · Elemental concentration · Buffer capacity

## Introduction

The contribution to local particulate matter (PM) concentrations originating from building construction and demolition is seldom acknowledged and not considered significant to the PM budget. The literature on the topic is sparse. A study by Deacon et al. (1997) touched upon the possible contribution of a building demolition to mass concentration of PM <10 µm (PM<sub>10</sub>) in the early years of Automatic Urban Air Quality Monitoring Network (AUN), UK. Results indicated that daily maximum exceedances of PM<sub>10</sub> had doubled in a period when demolition of a building had been carried out near a monitoring station in

**Electronic supplementary material** The online version of this article (doi:10.1007/s10653-015-9747-3) contains supplementary material, which is available to authorized users.

A. Brown (✉) · J. E. S. Barrett · H. Robinson ·  
S. Potgieter-Vermaak  
Division of Chemistry and Environmental Science,  
Manchester Metropolitan University,  
Manchester M1 5GD, UK  
e-mail: Andrew.Brown@mmu.ac.uk

S. Potgieter-Vermaak  
School of Chemistry, Molecular Science Institute,  
University of the Witwatersrand, Johannesburg, South  
Africa

**Table 1** Common metal contaminants of RD and their potential effects on human health

Metal	Health concerns	Citation
Al	Neuropathological, neurophysical and neurochemical changes	Miu et al. (2003)
As	Carcinogenic	Zhang et al. (2014)
Ba	Hypertension	Oskarsson (2015)
Cd	Carcinogenic	Zhang et al. (2009)
Cr	Carcinogenic in +6 state	Goldbohm et al. (2006)
Cu	Free radical production	Kadiiska and Mason (2002)
Fe	Causes eye problems	Ugarte et al. (2013)
Mn	Heart conditions	Cavallari et al. (2008)
Ni	Carcinogenic	Kasprzak et al. (2003)
Pb	Affects brain and nervous system	Zhang et al. (2013)
Rh	Cytotoxicity	Iavicoli and Leso (2015)
Si	Causes silicosis	Naghadehi et al. (2014)
Sn	Gastrointestinal conditions	Ostrakhovitch (2015)
V	Affects nervous system	Li et al. (2013)
Zn	Pulmonary effects	Mueller and Seger (1985)

Cardiff, UK. With the exception of a study by Liu et al. (2014) whom only attributed changes in calcium and barium concentrations to construction/demolition work, there is a corresponding paucity in the literature on changes in metal concentrations due to building work. Due to the recognised fact that atmospheric PM poses a threat to human health (e.g. increased mortality amongst the general population as an effect of exposure to PM (Pope et al. 2002; Villeneuve et al. 2002; Meister et al. 2012; Sorenson et al. 2012), the contribution to the PM budget during and after demolition episodes is a concern. In fact, the World Health Organisation suggests that particulate matter is responsible for 8 % of lung cancer deaths, 5 % of cardiopulmonary deaths and 3 % of respiratory infection deaths (WHO 2009). Although vehicular emissions are most commonly cited as a key source of particles (Gunawardana et al. 2012; Dong and Lee 2009 and references therein), some acknowledgement to the role of industrial processes is given. These health effects are still mainly focussed on the PM mass concentrations, and certain aspects regarding the composition and generation of particles remain unaddressed and unaccounted for.

For the purpose of this study, particles of specific interest are those which gather as curb-side sediment ready to be pulverised and suspended by the actions of meteorological conditions or vehicles making use of the road (Abu-Allaban et al. 2003; Atiemo et al.

2012). These particles may be referred to as road dust (RD). Research indicates that road dust accounts for up to 74 % of total suspended particulate matter (TSP) in Ho Chi Minh City, Vietnam (Hien et al. 1999) and 62 % in Lahore, Pakistan (Harrison et al. 1997). This resuspension of RD can enable it to become respired by pedestrians and other road users. The most appealing aspect of RD from an analytical standpoint is the already well-documented abundance of transition metals, many of which are potentially toxic and in some incidences carcinogenic (Unceta et al. 2010). Often, the effects manifest themselves as cardiorespiratory problems, both chronic and acute (see Table 1).

The intention of this study is to investigate the variation in concentration of elemental components of RD before and after the demolition of a large building at an urban site. The selected elements are as follows: Al, As, Ba, Ca, Cd, Cr, Cu, Fe, K, Mg, Mn, Na, Ni, Pb, Rh, Si, Sn, S, Ti, V and Zn. Analysis of these elements is justified by their potential toxicity to humans during overexposure. This research will focus on the resuspendable fraction of RD, which for the purpose this study is defined as particles up to around 140 µm in accordance with the research by Kennedy and Hines (2002). The elemental concentrations will be subject to risk assessment to decipher the possible effects on human health. The risk assessment method used in this paper is based on the US Environmental Protection

Agency (USEPA) model (USEPA 1997), modified for use with sediments as demonstrated on previous studies involving the risks associated with RD (Ma and Singhirunnusorn 2012; Du et al. 2013). This will elucidate whether the anticipated increase in metal concentrations are enough to cause significant increase to likelihood of developing detrimental health effects because of contaminant exposure.

## Experimental methodology

### Sample site

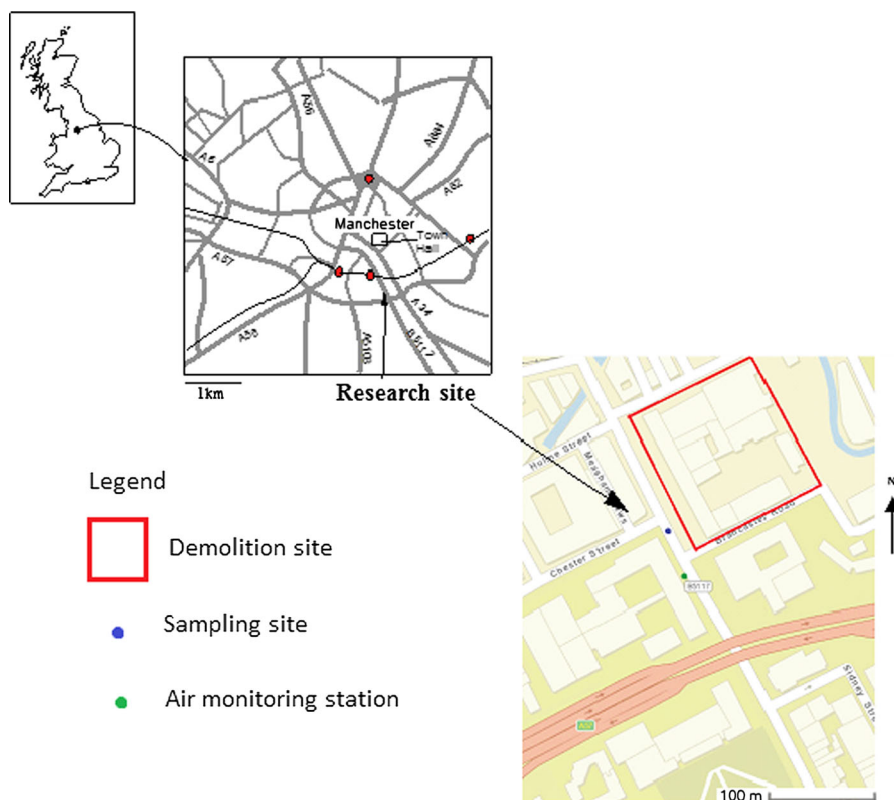
The RD sample site is a traffic island (British National Grid reference: SJ 84229734) in the meridian of Oxford Road, Manchester, UK (Fig. 1). Oxford Road is one of the most highly trafficked roads in Manchester supporting traffic from surrounding settlements of Greater Manchester, with buses and cars being the predominant mode of transport. Another feature present at this section of Oxford Road is the raised train tracks running perpendicular between two of the

main train stations in Manchester. Aside from these vehicles, the roadside area is heavily used by pedestrians, with a large cohort being the student population of the local universities, supporting approximately 75,000 students. The sampling site is situated 20 m west of the 16,600-m<sup>2</sup> demolition site and approximately 40 m north of one of Manchester's air monitoring station. The building subject to demolition was the 'New Broadcasting House', more commonly known as the BBC Building, Manchester, and constructed in the early 1970s (1971–1975). The building is mostly formed of steel reinforced concrete, with bronze-coated window panes and aluminium window frames. The soft demolition took place between November 2012 and May 2013. It was noted that throughout the process, water was used to minimise the spread of dust from the site to surrounding areas.

### Sample collection and processing

Collection of road dust was undertaken at the onset and the completion of the building demolition (November 2012 and May 2013, respectively), using

**Fig. 1** Sediment sampling site on Oxford Road, Manchester, UK



a polyethylene dust pan and brush as recommended by Charlesworth and Lees (1999), and samples were kept in polyethylene bags for transfer to the laboratory. Approximately 10 kg of sample mass was collected from across the site.

After collection, the RD was transferred to the laboratory to be air-dried in paper soil bags at  $25 \pm 5$  °C until a consistent weight was achieved, between 14 and 21 days. Dry samples were fractionated into particles of four grain sizes:  $<38$   $\mu\text{m}$ ,  $63\text{--}38$   $\mu\text{m}$ ,  $125\text{--}63$   $\mu\text{m}$  and  $2000\text{--}125$   $\mu\text{m}$ , where these particles represent the boundaries between 'silts and clays', 'course silts', 'very fine sands' and 'coarse material', respectively (Tucker 1991). Analysis is restricted to the three finest fractions of RD as those are capable of being resuspended. The  $2000\text{--}125$   $\mu\text{m}$  fraction is retained for further unreported analysis, and the  $>2000$   $\mu\text{m}$  fraction is discarded.

#### Digestion of grain-specific fractions

Three replicates of  $0.25 \text{ g} \pm 0.0015 \text{ g}$  for each sample were weighed into a polytetrafluoroethylene microwave vessel and extracted with 1.5 ml of hydrofluoric acid, 5 ml of nitric acid and 2 ml of hydrogen peroxide, all reagent grade. This was then subject to an initial digestion using a 1600-W CEM Mars 5 Microwave, maximum temperature 200 °C. Twelve microlitres of boric acid was then added to assist a further microwave-assisted digestion at a maximum temperature of 80 °C. The aim of the secondary digestion is to precipitate excess fluoride and prevent secondary reactions (Dulski 1996). The samples were then cooled and diluted appropriately having been filtered using 0.45  $\mu\text{m}$  polyethersulfone syringe filters. This method is based on the Environment Agency's EN14385 application note (BS EN 14385, 2004). Use of this method has led to the accreditation of this laboratory by the UK Accreditation Service (UKAS).

#### Geochemical analysis

Digestion analytes of RD samples were analysed for 21 elements (Al, As, Ba, Ca, Cd, Cr, Cu, Fe, K, Mg, Mn, Na, Ni, Pb, Rh, S, Si, Sn, Ti, V and Zn) using a Varian Vista MPX ICP-OES with SeaSpray nebuliser. Initial system stability checks were carried out with a 5-mg/l solution of manganese during the torch alignment, whereby the upper values must be in excess of

300,000 counts per second in both the axial and radial configurations, although sample analysis exclusively used the axial position. A four-point linear calibration was achieved for each element, and a calibration coefficient of  $>0.95$  for all elements was determined. The maximum concentrations of calibration points were 100 mg/l for major elements, 20 mg/l for minor and trace elements and 1000 mg/l for sulphur alone. Multiple wavelength tests were taken to ensure high intensity with little interference was achieved. A total of five blank samples as well as two extractions of MESS-3 certified reference material were also analysed to ensure quality results.

#### PM<sub>10</sub> concentrations

As shown in Fig. 1, there is an air sampling station maintained by Manchester City Council near the demolition site, the site is referred to as MAN1. The monitoring site quantifies airborne particulate matter  $<10$   $\mu\text{m}$  in size (PM<sub>10</sub>) hourly and operates continuously. The site is approximately 40 m south of the demolition site on the opposite side of Oxford Road. The data were archived and available to the public via the Air Quality England website.<sup>1</sup> For the purpose of this study, archived data were reviewed to assess the changes in airborne particulate matter in the direct vicinity of the demolition site. Average PM<sub>10</sub> concentrations were compared over the November to May winter periods for winter 2010–2011, 2011–2012, 2012–2013 (demolition) and 2013–2014.

## Results and discussion

#### Geochemical analysis

The concentrations of the 21 elements analysed in the road dust fractions for both sampling campaigns are summarised in Table 2. It can be observed that the general trend for the major constituents is  $\text{Si} > \text{Ca} > \text{Al}$ ,  $\text{Fe}$ ,  $\text{Mg} > \text{K}$ ,  $\text{Na}$  and  $\text{Ti}$ . These figures are in agreement with the literature from other studies in urban areas (Chen et al. 2012; Cesari et al. 2012 and references therein). It is generally accepted that the large concentrations of these elements are

<sup>1</sup> Air Quality England, [http://www.airqualityengland.co.uk/site/latest?site\\_id=MAN1](http://www.airqualityengland.co.uk/site/latest?site_id=MAN1).

**Table 2** Mean extractable concentrations of the 21 elements, and degree of variance expressed as standard deviation determined for the three finest grain-size fractions collected

from the sample site Oxford Road, Manchester, collected in November 2012 and May 2013

Element	Elemental concentration (mg/kg)					
	<38 $\mu\text{m}$		63–38 $\mu\text{m}$		63–125 $\mu\text{m}$	
	Nov 2012 (%RSD)	May 2013 (%RSD)	Nov 2012 (%RSD)	May 2013 (%RSD)	Nov 2012 (%RSD)	May 2013 (%RSD)
Al	44643.3 (5.7)	53672.0 (4.8)	31967.0 (5.1)	50099.3 (3.3)	34624.3 (3.5)	35948.7 (4.6)
As	11.1 (17.4)	9.1 (28.6)	8.2 (44.5)	4.3 (129.4)	9.6 (60.8)	3.6 <sup>a</sup> (98.0)
Ba	1069.0 (7.6)	853.7 (5.2)	972.7 (9.9)	798.3 (3.3)	685.7 (2.2)	581.7 (4.7)
Ca	110397.0 (8.2)	97071.3 (5.1)	89352.3 (9.9)	89728.0 (2.2)	91271 (3.1)	78188.0 (4.1)
Cd	1.3 <sup>a</sup> (79.7)	0.6 <sup>a</sup> (55.4)	0.8 <sup>a</sup> (138)	0.6 <sup>a</sup> (71.3)	0.7 <sup>a</sup> (19.7)	5.2 (16.5)
Cr	324.7 (5.2)	208.7 (5.1)	311.0 (9.7)	208.7 (3.9)	274.7 (2.9)	181.3 (4.2)
Cu	1076.3 (8.6)	268.3 (9.3)	589.3 (10.6)	273.3 (3.0)	386.0 (3.1)	180.3 (7.8)
Fe	38492.3 (5.6)	31456.3 (4.7)	29294.7 (6.7)	31374.3 (4.8)	28562.3 (3.5)	22501.7 (8.3)
K	15091.3 (9.6)	19636.3 (5.5)	14868.3 (10.4)	16987.7 (2.4)	14662.3 (4.1)	15310.7 (4.2)
Mg	21806.3 (8.5)	27129.7 (5.3)	16550.0 (9.3)	22256.0 (2.1)	14190.3 (3.0)	15621.0 (4.0)
Mn	1250.7 (7.7)	887.7 (5.1)	1118.7 (9.7)	860.0 (2.9)	819.7 (2.5)	730.0 (4.4)
Na	7933.3 (9.3)	5862.7 (6.6)	8194.3 (10.7)	6465.3 (2.4)	7245.3 (5.0)	7696.3 (4.1)
Ni	122.0 (6.7)	70.7 (3.9)	103.0 (7.6)	69.9 (1.6)	63.6 (5.3)	79.9 (4.4)
Pb	384.0 (8.7)	264.0 (5.1)	334.0 (9.7)	247.0 (2.1)	207.0 (3.8)	151.7 (7.9)
Rh	32.9 (29.4)	27.0 <sup>a</sup> (84.3)	23.0 <sup>a</sup> (40.5)	6.5 <sup>a</sup> (11.2)	15.6 <sup>a</sup> (44.5)	34.9 <sup>a</sup> (44.7)
Si	299319.3 (8.3)	321438.0 (2.6)	304412.0 (9.5)	322272.0 (6.7)	417087.3 (5.8)	452857.7 (8.1)
Sn	62.4 (18.9)	13.3 (21.6)	45.9 (11.4)	13.5 (83.6)	22.2 (29.4)	7.4 (47.0)
S	3898.8 (5.4)	11224.8 (6.5)	3494.4 (8.9)	9150.3 (1.5)	2092.8 (4.7)	3349.7 (2.9)
Ti	5112.3 (7.9)	5101.7 (4.7)	5140.3 (9.0)	4481.0 (2.8)	200.3 (21.0)	3349.3 (4.3)
V	115.7 (6.6)	99.7 (6.5)	104.9 (10.7)	95.4 (4.1)	77.4 (0.0)	76.0 (3.6)
Zn	1184.7 (8.5)	767.7 (6.6)	1017.0 (11.0)	624.7 (2.8)	614.0 (3.8)	384.7 (6.4)

$n = 3$ : values are quoted to one decimal place; relative standard deviation (%RSD) to one decimal place in parenthesis

<sup>a</sup> Denotes replicates below detection limit, random numbers below detection limit have been inserted to obtain a value for the average concentration

mainly due to their crustal abundance (Alomary and Belhadj 2007; Gunawardana et al. 2012). In general, trace element concentrations are slightly more subject to variance because the sources are usually of an anthropogenic nature, and henceforth are highly dependent on the local sources of inputs (Amato et al. 2009a). In general, the same trends can be observed in all size fractions for some of the trace elements as reported by Potgieter-Vermaak et al. (2012), i.e.  $\text{Zn} > \text{Cu} > \text{Pb} > \text{Cr}$  for the two smaller fractions and  $\text{Zn} > \text{Cu} > \text{Cr} > \text{Pb}$  for the largest fractions. All trace elements (indicated with cursive font in Table 2) displayed the highest concentration in the finest fraction with a steady decrease in

concentration with increase in particle size (as also reported by Bian and Zhu 2009 and Fujiwara et al. (2011)). In addition, it is noted that the absolute concentrations are lower for the May sampling campaign and the variance in concentration change can be observed in Figs. 2, 3 and 4. Cr, Pb and Ni in particular are of concern to those exposed, because of their severe toxic association (Najafi et al. 2009). There is low confidence in the results for As, Cd, Rh and Sn due to the high %RSDs observed ( $>20\%$ ); therefore, they will not be discussed in any great detail in this article. The high %RSDs are due to the concentrations being close to the detection limit for the instrument used.

**Fig. 2** Percentage increase/decrease in each element in <38  $\mu\text{m}$  fraction relative to initial concentration from November 2012 sample

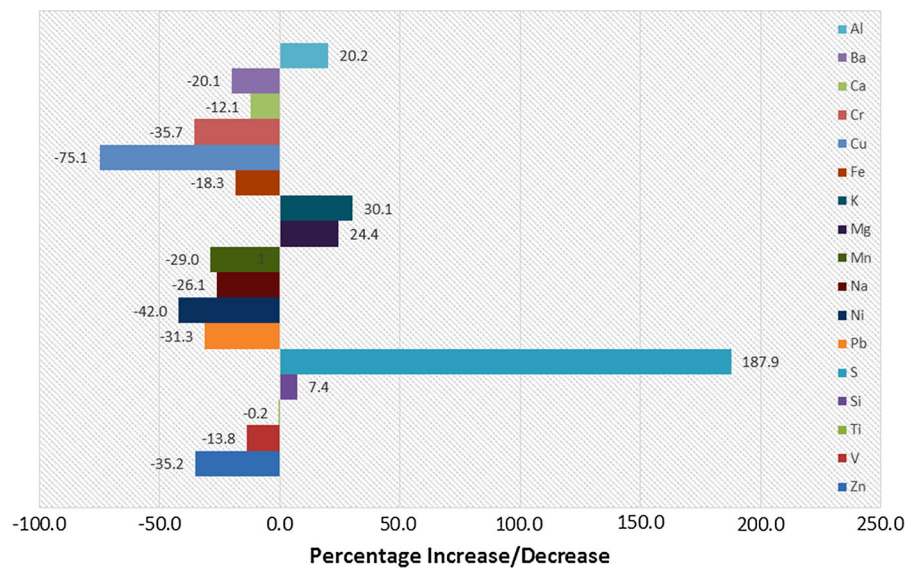
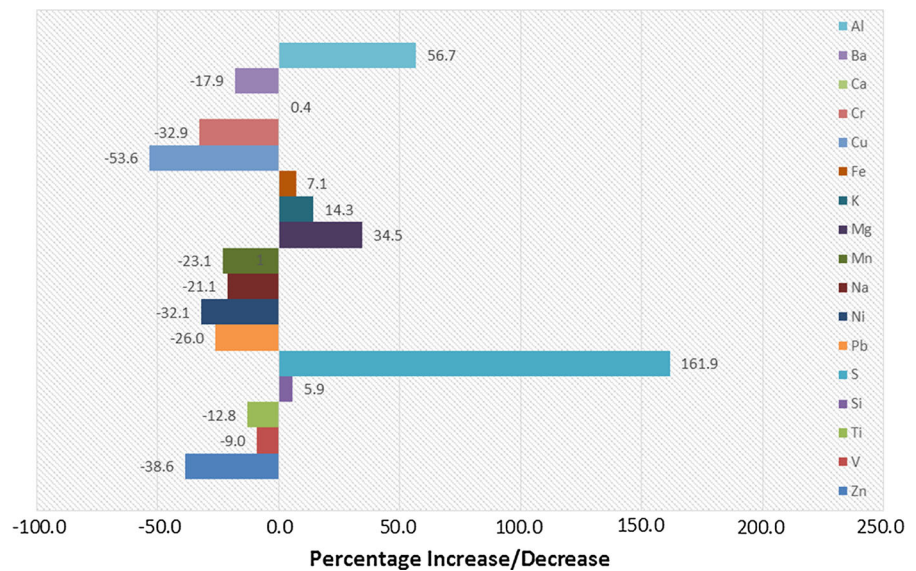


**Fig. 3** Percentage increase/decrease in each element in 63–38  $\mu\text{m}$  fraction relative to initial concentration from November 2012 sample



Change in road dust character over sampling period

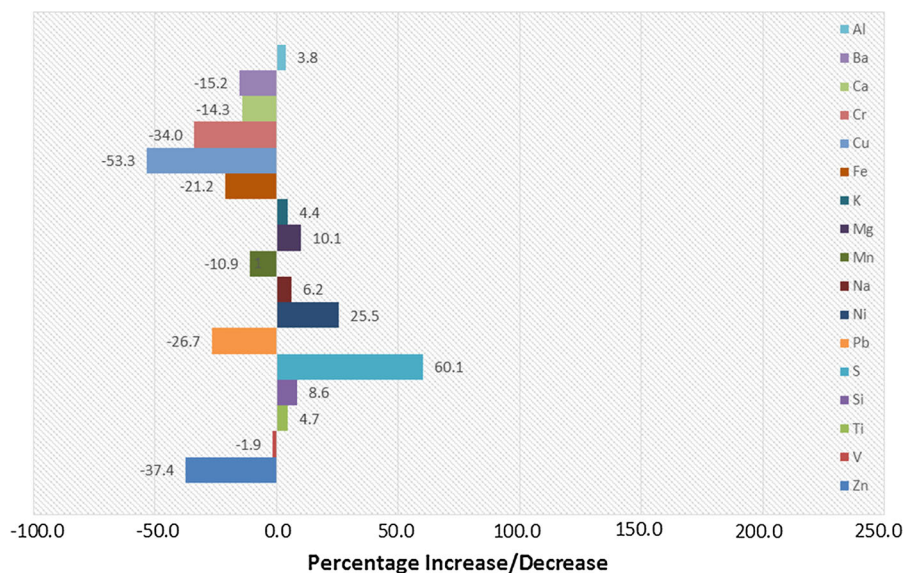
The key aim of this investigation is to assess the change in composition of inhalable particles due to building demolition and assess the risk change on human health. This section discusses the observed changes in the elements in terms of percentage change between the two sampling campaigns (November 2012, May 2013) that covers the period of demolition. The percentage changes in each of the specified

elements from the sampling campaign in November 2012 to May 2013 are presented in Figs. 2, 3 and 4. Each fraction is presented separately.

*Elemental concentration decreases*

It is noted that around 60 % of the elements investigated, namely Ba, Ca, Cr, Cu, Fe, Mn, Na, Ni, Pb, Ti, V and Zn, showed a decrease in their elemental concentrations between the two sampling periods. Interestingly, the average decrease in these elements

**Fig. 4** Percentage increase/decrease in each element in 125–63  $\mu\text{m}$  fraction relative to initial concentration from November 2012 sample



exhibited per fraction was fairly consistent at  $-26 \pm 2.2$  %. Across the three grain-size fractions, the greatest decreases are seen for Cu. Scrutiny of percentage change on a grain-size basis finds that for the  $<38$   $\mu\text{m}$  fraction  $\text{Cu} > \text{Ni} > \text{Cr} > \text{Zn} > \text{Pb}$ , whilst decreases in element concentrations for the 63–38 and 125–63  $\mu\text{m}$  fractions are found to be  $\text{Cu} > \text{Zn} > \text{Cr} > \text{Pb}$ . The behaviour of Ni in the two coarsest fractions is contradictory, whilst exhibiting similar decreases to that of Cr (32–33 %) in the 63 to 38- $\mu\text{m}$  fraction, the concentration Ni is seen to increase (25 %) in 125–63  $\mu\text{m}$  fraction.

A decrease in elemental concentrations of sediments within the literature is often attributed to increased rainfall (Jackson et al. 2007 and references therein). Increased rainfall during the months from December to February might explain the lower concentrations of the ten metals achieved in the May sampling campaign. In addition, it is possible that the significant increase in S observed from the building site, during the sampling period, contributed to the diminishment of most other elemental species. The sulphurous nature of the Manchester RD coupled with the rain events had the potential to lower the pH of the RD and consequently reduce the inherent buffering capacity of the RD (Du et al. 2014), leading to metals being leached from the RD in the surface run-off into the urban water system, similar processes have been observed in soils by Xie et al. (2004). This suggests that increase in the concentration of a contaminant,

such as S, may have led to changes in the intended environmental receptor, with notable decreases in the concentrations of contaminants such as Cr, Cu, Ni, Pb, V and Zn available for inhalation, and corresponding enrichment of urban waters of these potentially harmful elements.

#### *Elemental concentration increases*

S, Si, Mg, K and Al increased in concentration, in all fractions, between the sampling periods. In contrast to the elemental decreases, the average increase for these elements did not stay constant ( $36.5 \% \pm 19.5$  %). Moreover, the average increase for these elements was 54, 40 and 15 % for the  $<38$ , 63–38 and 125–63  $\mu\text{m}$  fractions, respectively. This clearly shows a significant difference in behaviour between the three fractions with reference to elemental concentration increase.

Application of the Mann–Whitney *U* test find that the increases between Nov 2013 and May 2014 sampling campaign were significant ( $>95$  % confidence) for S, K and Al but not Si and Mg. This suggests an additional source of such elements has occurred during between the two sampling campaigns. We could speculate that the large increases in sulphur concentration (187.9 % in the  $<38$   $\mu\text{m}$  fraction, 161.9 % in the 63- to 38- $\mu\text{m}$  fraction and 60.1 % in the 125- to 63- $\mu\text{m}$  fraction) are likely to come from building materials, most likely gypsum. The increased aluminium concentrations (20.2 % in the  $<38$   $\mu\text{m}$

fraction, 56.7 % in the 63- to 38- $\mu\text{m}$  fraction and 3.8 % in the 125- to 63- $\mu\text{m}$  fraction) are also likely to be due to use of aluminium in building materials.

### PM<sub>10</sub> concentrations

Results from the continuous monitoring site are presented in Fig. 5. The monthly averages suggest that at the onset of the demolition (November), the PM mass concentrations were very similar to those observed in the previous 4 years. However, inspection of the data during March–May leads to the conclusion that the spike in mass concentration observed during the previous and subsequent year during this time, is absent during the year of interest. Research into sources of PM<sub>10</sub> in an urban environment by Amato et al. (2009b) indicated that PM<sub>10</sub> concentrations increased by up to ten times, as a result of demolition work. The findings from this study appear to display different results. A possible reason for this could be the nature of the demolition, or perhaps a possibility could be the documented prevailing southerly wind in this area of Manchester (Lapworth and McGregor 2008). It is likely that rainfall affected the concentration of PM<sub>10</sub> during this period. Figure 6 represents monthly rainfall data during the demolition period along with the demolition period PM<sub>10</sub> data. Figure 6 indicates rainfall has an inverse relationship with the concentration of PM<sub>10</sub> during the months of the demolition as would be expected due to washout. The negative correlation of  $-0.55$  ( $p = 0.05$ ) displayed in Fig. 6 further supports this observation. This influence of rainfall on PM is well documented (Shukla et al. 2008 and references therein), and furthermore, research

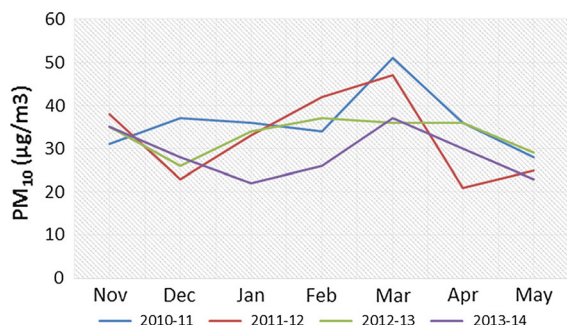


**Fig. 5** Monthly average PM<sub>10</sub> concentrations for winter and spring periods of 2010–2011, 2011–2012, 2012–2013 (demolition took place in this period) and 2013–2014

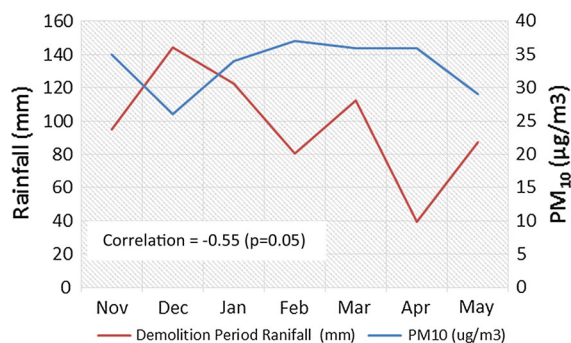


**Fig. 6** Monthly rainfall (mm) and concentration of PM<sub>10</sub> during the demolition period

indicates that SO<sub>2</sub> and NO<sub>2</sub> are washed out of PM by precipitation (Davies 1976; Chang 1984). The wash-out could potentially add to the acidification of urban run-off. All rainfall data are taken from Woodford Meteorological Station 16 km from the sampling site (OS grid reference SJ895825).

### Risk assessment

Risk assessment has been used in many studies to assess the risk of contaminants in RD and road sediments (Du et al. 2013; Ma and Singhirunnusorn 2012; Ferreira-Baptiste and De Miguel 2005). This approach of risk assessment requires the formulation of a conceptual site model to justify the need to assess a particular site. Table 3 presents the heavily trafficked sample site both without and with the addition of the building demolition at the focus of this paper.

The next phase of risk assessment is then to calculate the exposure of an individual to any given pollutant. Equations 1, 2 and 3 represent average daily dose (ADD) exposure via the ingestion, inhalation and dermal routes, respectively (USEPA 1997), ADD expressed in terms of mg/kg day. The components and values used in these equations are presented in Table 4, as some of the components differ between an adult and a child, and ADDs and consequently HIs are different for adults and children. A child is assumed to be aged between 1 and 6 years old, in accordance with USEPA (1989). It is therefore necessary to alter values for body weight, ingestion rate, inhalation rate and skin surface area. The value for exposure duration is specific for this study as it represents the period of demolition, 6 months.

**Table 3** Conceptual site model showing ordinary exposure and sources, as well as exposure and sources due to the building demolition, shown in italics

Source	Exposure medium	Exposure point	Exposure route	Exposed population
Road and rail traffic	Soils and sediments	Oxford Road, Manchester	Ingestion, inhalation and dermal contact	Commuters and recreators
<i>Building demolition</i>	<i>Soils and sediments</i>	<i>Oxford Road, Manchester</i>	<i>Ingestion, inhalation and dermal contact</i>	<i>Commuters and recreators</i>

**Table 4** Parameters for risk assessment model

Component	Definition (units)	Adult value used	Child value used	Reference
<i>C</i>	Concentration of contaminant (mg/kg)	See Table 2	See Table 2	This study
<i>R<sub>ing</sub></i>	Ingestion rate (mg/day)	200	100	USEPA (1989)
<i>EF</i>	Exposure frequency (days/year)	350	350	Du et al. (2014)
<i>ED</i>	Exposure duration (years)	0.5	0.5	This study
<i>BW</i>	Body weight (kg)	84	21	Potgieter-Vermaak et al. (2012)
<i>AT</i>	Average time (days)	365 × ED	365 × ED	Du et al. (2014)
<i>CF</i>	Conversion factor (kg/mg)	1 × 10 <sup>-6</sup>	1 × 10 <sup>-6</sup>	
<i>R<sub>inh</sub></i>	Inhalation rate (m <sup>3</sup> /day)	20	5	Du et al. (2014)
<i>PEF</i>	Particle emission factor (m <sup>3</sup> /kg)	1.32 × 10 <sup>9</sup>	1.32 × 10 <sup>9</sup>	USEPA (2000)
<i>SA</i>	Surface area (cm <sup>2</sup> )	5000	1800	Du et al. (2014)
<i>SL</i>	Skin adherence factor (mg/cm <sup>2</sup> )	1	1	Du et al. (2014)
<i>ABS</i>	Dermal absorption factor	1 × 10 <sup>-3</sup>	1 × 10 <sup>-3</sup>	Du et al. (2014)

**Table 5** HI values for adults for each element from the three exposure routes, using USEPA PEF value

	Al	Ba	Cr	Cu	Pb	Ni	V	Zn
HI	0.147	0.005	0.524	0.008	0.039	0.004	0.014	0.004

$$ADD_{ing} = \frac{C \times R_{ing} \times CF \times EF \times ED}{BW \times AT}$$

$$ADD_{inh} = \frac{C \times R_{inh} \times EF \times ED}{PEF \times BW \times AT}$$

$$ADD_{derm} = \frac{C \times SA \times CF \times SL \times ABS \times EF \times ED}{BW \times AT}$$

A hazard quotient (HQ) can then be calculated by dividing the ADD by a reference dose (Rdf) specific to a chemical. The reference dose acts as a maximum exposure below which the health concerns of the chemical are not a concern. Therefore, a HQ > 1 is not considered a health concern. HQs from each of the three exposure routes can then be summed to give a hazard index value (HI), and again, a value below one is not considered a concern (USEPA 2001).

Tables 5 and 6 present the HI results of the risk assessment model for adults and children, respectively. It is observed that the HI values do not exceed one for any element, with the exception of chromium exposure in children. Full tables showing Rdf, ADD and HQ values for each of the exposure routes can be found in the supplementary section of this paper, listed as Tables S1 and S2, respectively. All Rdf values are taken from the literature (Liu et al. 2015; Cao et al. 2015; Buranatrevedh 2014; HEAST 2011).

One assumption of the ADD calculations used here is the PEF parameter from the inhalation calculation. Despite being commonly used in the literature to assess the risks associated with RD, the PEF value, expressed as m<sup>3</sup>/kg, was derived for the purpose of representing airborne quantities of soil contaminants and relies on the site having a 50 % vegetation

**Table 6** HI values for children for each element from the three exposure routes, using USEPA PEF value

	Al	Ba	Cr	Cu	Pb	Ni	V	Zn
HI	0.575	0.039	1.076	0.062	0.099	0.032	0.102	0.024

**Table 7** HI values for adults for each element from the three exposure routes, using the amended PEF value for the ADD<sub>inh</sub> calculation

	Al	Ba	Cr	Cu	Pb	Ni	V	Zn
HI	0.711	0.005	0.528	0.009	0.039	0.004	0.015	0.004

**Table 8** HI values for children for each element from the three exposure routes, using the amended PEF value for the ADD<sub>inh</sub> calculation

	Al	Ba	Cr	Cu	Pb	Ni	V	Zn
HI	1.132	0.039	1.079	0.062	0.099	0.033	0.103	0.024

coverage (USEPA 2000). The applicability of this PEF value to samples of this nature is therefore questionable, as the physical and morphological characteristics of RD differ greatly to soil, and also the vegetation cover at the site used in this study is 0 %. As previously noted in the introduction section of this paper, RD has been shown to account for 62 % of TSP (Harrison et al. 1997) and 74 % of TSP (Hien et al. 1999). Having monitored TSP concentrations near the demolition site for over a year as part of another study, the average concentration of TSP is 92.9 µg/m<sup>3</sup>, and we can therefore estimate that a lower-bound estimate of the quantity of TSP derived from road dust is 62 %. Replacing the PEF value in the ADD<sub>inh</sub> equation with 62 % of 92.9 µg/m<sup>3</sup> could therefore serve as another estimate of ADD<sub>inh</sub>, it also stands to make the equation used more specific for this study site. To maintain the mg/kg.day units for ADD<sub>inh</sub>, the ADD<sub>inh</sub> equation is altered as displayed below. Here, the units for TSP are in kg/m<sup>3</sup>, all other parameters are the same for the USEPA ADD<sub>inh</sub> equation.

$$ADD_{inh} = \frac{C \times R_{inh} \times EF \times ED \times ([TSP] \times 0.62)}{BW \times AT}$$

A new risk assessment for adults and children table can then be derived using this equation for ADD<sub>inh</sub> whilst keeping the other two ADD equations, the HI results are presented in Tables 7 and 8, respectively. Again, full tables showing ADD and HQ values for

each of the exposure routes can be found in the supplementary section of this paper, listed as Tables S3 and S4, respectively.

As a result of altering the PEF value, it can now be observed that the HI value for each element has increased, most increases are very small and not sufficient to alter the three significant figures quoted. The most noteworthy change is the HI value for aluminium exposure in children, which has increased from 0.575 to 1.13 and is therefore now considered a health concern, along with chromium. The dramatic increase observed in the HI value for aluminium is due to the high HQ value observed for the inhalation route. All HQ values increase by the same factor due to the modified ADD<sub>inh</sub> equation; however, the proximity to one observed for the ADD<sub>inh</sub> in the original equation causes a greater effect on the HI when the equation is modified. The results of this study are comparable with the HI values calculated by Du et al. (2013) with the exception of Al and Cr, which appear to give significantly larger HI values in this study.

## Conclusion

The design of this experimentation was based on the assumption that the concentrations of metals would increase after the demolition of a building. However, in general, this was not observed for all elements and 12 of the 17 elements of interest decreased by an

average of 26 % across all size ranges (Ba, Ca, Cr, Cu, Fe, Mn, Na, Ni, Pb, Ti, V and Zn). A substantial increase in the finer two fractions was however observed (on average 54 and 40 %) for the remaining elements. As alluded to in the results and discussion section, it is likely that the large increase in concentration of sulphur had an influence on the diminished concentrations of other metals that were observed. Perhaps the main concern that can be raised from these results is the effect of the heavy enrichment in sulphur on mobility of metals. While the increase in sulphur causes a reduction in contaminants available for resuspension, it increases the concentrations of contaminants in surface water. Moreover, it will add to the overall burden of urban land contamination due to metal enrichment of water run-offs and soil. Perhaps further investigation on contamination of surface water due to building demolition is required to assess the potential health effects associated. It is observed that rainfall and PM10 were inversely proportional during the demolition. This washout effect was also apparent in the RD; however, to prove this conclusively, it may be necessary to compare rainfall, PM concentration and elemental concentrations over a larger period of time. Thus, one would be able to elucidate whether the elemental washout process occurs independently of the building demolition, or to what extent the building demolition affected the washout. The risk assessment portion of this analysis indicates that the HI for chromium and aluminium is a concern for children exposed at this site, when using the modified PEF value suggested.

## References

- Abu-Allaban, M., Gillies, J. A., Gertler, A. W., Clayton, R., & Proffitt, D. (2003). Tailpipe, resuspended road dust, breakware emission factors from on road vehicles. *Atmospheric Environment*, *37*, 5283–5293.
- Alomary, A. A., & Belhadj, S. (2007). Determination of heavy metals (Cd, Cr, Cu, Fe, Ni, Pb, Zn) by ICP-OES and their speciation in Algerian Mediterranean Sea sediments after a five-stage sequential extraction procedure. *Environmental Monitoring and Assessment*, *135*, 265–280.
- Amato, F., Pandolfi, M., Escrig, A., Querol, X., Alastuey, A., Pey, J., et al. (2009a). Quantifying road dust resuspension in urban environment by multilinear engine: a comparison with PMF2. *Atmospheric Environment*, *43*, 2770–2780.
- Amato, F., Pandolfi, M., Viana, M., Querol, X., Alastuey, A., & Moreno, T. (2009b). Spatial and chemical patterns of PM10 in road dust deposited in urban environment. *Atmospheric Environment*, *9*, 1650–1659.
- Atiemo, S. M., Ofori, G., Aboh, I. J. K., & Oppon, O. C. (2012). Levels and sources of heavy metal contamination in road dust in selected major highways of Accra, Ghana. *X-Ray Spectrometry*, *41*, 105–110.
- Bian, B., & Zhu, W. (2009). Particle size distribution and pollutants in road deposited sediment in different areas of Zhengjiang, China. *Environmental Geochemistry and Health*, *31*, 511–520.
- Buranatrevedh, S. (2014). Health risk assessment of general populations exposed to metals from an aluminium production plant in Thailand. *Journal of Community Medicine and Health Education*, *4*, 262.
- Cao, S., Duan, X., Zhao, X., Wang, B., Ma, J., Fan, D., et al. (2015). Health risk assessments of various metal(loid)s via multiple exposure pathways on children living near a typical lead-acid battery plant, China. *Environmental Pollution*, *200*, 16–23.
- Cavallari, J. M., Eisen, E. A., Fang, S. C., Schwartz, J., Hauser, R., & Herrick, R. F. (2008). PM2.5 metal exposures and nocturnal heart rate variability: a panel study of boilermaker construction workers. *Environmental Health*, *7*, 36.
- Cesari, D., Contini, D., Genga, A., Siciliano, M., Elefante, C., Bagliivi, F., & Daniele, L. (2012). Analysis of raw soils and their re-suspended PM10 fractions: Characterisation of source profiles and enrichment factors. *Applied Geochemistry*, *27*, 1238–1246.
- Chang, T. Y. (1984). Rain and snow scavenging of HNO<sub>3</sub> vapor in the atmosphere. *Atmospheric Environment*, *18*, 191–197.
- Charlesworth, S. M., & Lees, J. A. (1999). The distribution of heavy metals in deposited urban dusts and sediments, Coventry, England. *Environmental Geochemistry and Health*, *21*, 97–115.
- Chen, J., Wang, W., Liu, H., & Ren, L. (2012). Determination of road dust loadings and chemical characteristics using resuspension. *Environmental Monitoring and Assessment*, *184*, 1693–1709.
- Davies, T. D. (1976). Precipitation scavenging of sulfur dioxide in an industrial area. *Atmospheric Environment*, *10*, 879–890.
- Deacon, A. R., Derwent, R. G., Harrison, R. M., Middleton, D. R., & Moorcroft, S. (1997). Analysis and interpretation of measurements of suspended particulate matter at urban background sites in the United Kingdom. *Science of the Total Environment*, *203*, 17–36.
- Dong, T. T. T., & Lee, B. (2009). Characteristics, toxicity, and source appointment of polycyclic aromatic hydrocarbons (PAHs) in road dust of Ulsan, Korea. *Chemosphere*, *74*, 1245–1253.
- Du, Y., Gao, B., Zhou, H., Xinxin, J., Hao, H., & Yin, S. (2013). Health risk assessment of heavy metals in road dusts in urban parks of Beijing, China. *Procedia Environmental Sciences*, *18*, 299–309.
- Du, Y., Wei, M., Reddy, K. R., Liu, Z., & Jin, F. (2014). Effect of acid rain pH on leaching behavior of cement stabilized lead-contaminated soil. *Journal of Hazardous Material*, *271*, 131–140.

- Dulski, T. R. (1996). *A manual for the chemical analysis of metals*. Ann Arbor, MI: America Society for Testing and Materials.
- Ferreira-Baptiste, L., & De Miguel, E. (2005). Geochemistry and risk assessment of street dust in Luanda, Angola: A tropical urban environment. *Atmospheric Environment*, *39*, 4501–4512.
- Fujiwara, F., Rebagliatani, R. J., Dawidowski, L., Gomez, D., Polla, G., & Perenya, V. (2011). Spatial and chemical patterns of sized fractioned road dust collected in a megacity. *Atmospheric Environment*, *45*, 1497–1505.
- Goldbohm, R. A., Tielemans, E. L. J. P., Heederik, D., Rubingh, C. M., Dekkers, S., Willems, M. I., & Kroese, E. D. (2006). Risk assessment for carcinogens based on epidemiological data: A structured approach, illustrated by an example of chromium. *Regulatory Toxicology and Pharmacology*, *44*, 294–310.
- Gunawardana, C., Goonetilleke, A., Egodawatta, P., Dawes, L., & Kokot, S. (2012). Source characterisation of road dust based on chemical and mineral composition. *Chemosphere*, *87*, 163–170.
- Harrison, R. M., Smith, D. G. T., Pio, C. A., & Castro, L. M. (1997). Comparative receptor modelling study of airborne particulate pollutants in Birmingham, United Kingdom, Coimbra (Portugal) and Lahore (Pakistan). *Atmospheric Environment*, *31*, 3309–3321.
- HEAST (2011). Health effect assessment summary tables for superfund. <http://epa-heast.ornl.gov/>
- Hien, P. D., Binh, N. T., Truong, Y., & Ngo, N. T. N. (1999). Temporal variations of source impacts at the receptor, as derived from particulate monitoring data in Ho Chi Minh City, Vietnam. *Atmospheric Environment*, *33*, 3133–3142.
- Iavicoli, I., & Leso, V. (2015). *Handbook on the toxicology of metals* (4th ed., pp. 1143–1174)., Volume II specific metals London: Academic press.
- Jackson, M. T., Sampson, J., & Prichard, H. M. (2007). Platinum and palladium variations through the urban environment: evidence from 11 sampling types from Sheffield. *Science of the Total Environment*, *385*, 117–131.
- Kadiiska, M. B., & Mason, R. P. (2002). In vivo copper-mediated free radical production: An ESR spin-trapping study. *Spectrochimica Acta Part A: Molecular and Biomolecular Spectroscopy*, *58*, 1227–1239.
- Kasprzak, K., Sunderman, F. W., & Salnikow, K. (2003). Nickel carcinogenesis. *Mutation Research/Fundamental and Molecular Mechanisms of Mutagenesis*, *533*, 67–97.
- Kennedy, N. J., & Hines, W. C. (2002). Inhalability of large solid particles. *Journal of Aerosol Science*, *33*, 237–255.
- Lapworth, A., & McGregor, J. (2008). Seasonal variation of the prevailing wind direction in Britain. *Weather*, *63*, 365–368.
- Li, H., Zhou, D., Zhang, Q., Feng, C., Zheng, W., He, K., & Lan, Y. (2013). Vanadium exposure-induced neurobehavioural alterations among Chinese workers. *Neurotoxicology*, *36*, 49–54.
- Liu, E., Yan, T., Birch, G., & Zhu, Y. (2014). Pollution and health risk of potentially toxic metals in urban road dust in Nanjing, a mega-city of China. *Science of the Total Environment*, *476*, 522–531.
- Liu, X., Zhai, Y., Zhu, Y., Liu, Y., Chen, H., Li, P., et al. (2015). Mass concentrations and health risk assessment of heavy metals in size-segregated airborne particulate matter in Changsa. *Science of the Total Environment*, *517*, 215–221.
- Ma, J., & Singhirunusorn, W. (2012). Distribution and health risks assessment of heavy metals in surface dusts of Maha Sarakham municipality. *Procedia Social and Behavioural Sciences*, *50*, 280–293.
- Meister, K., Johansson, C., & Forsberg, B. (2012). Estimated short-term effects of coarse particles on daily mortality in Stockholm, Sweden. *Environmental Health Perspectives*, *120*, 431–436.
- Miu, A. C., Andreescu, C. E., Vasii, R., & Olteanu, A. I. (2003). A behavioural and histological study on the effects of long-term exposure of adult rats to aluminium. *International Journal of Neuroscience*, *113*, 1197–1211.
- Mueller, E. J., & Seger, D. L. (1985). Metal fume fever—A review. *The Journal of Emergency Medicine*, *2*, 271–274.
- Naghadehi, M. Z., Sereshki, F., & Mohammadi, F. (2014). Pathological study of the prevalence of silicosis among coal mines in Iran: A case history. *Atmospheric Environment*, *83*, 1–5.
- Najafi, N. M., Eidizadeh, M., Seidi, S., Ghasemi, E., & Alizadeh, R. (2009). Developing electrodeposition techniques for preconcentration of ultra-traces of Ni, Cr and Pb prior to arc-atomic emission spectrometry determination. *Microchemical Journal*, *93*, 159–163.
- Oskarsson, A. (2015). *Handbook on the toxicology of metals*. Chapter 29—Barium, 4th Ed., pp. 625–634. <http://www.sciencedirect.com/science/article/pii/B978044459453200299>
- Ostrakhovitch, E. A. (2015). *Handbook on the toxicology of metals* (4th ed., pp. 1241–1285)., Volume II specific metals London: Academic press.
- Pope, C. A., Burnett, R. T., Thun, M. J., Calle, E. E., Krewski, D., & Ito, K. (2002). Lung cancer, cardiopulmonary mortality, and long-term exposure to fine particulate air pollution. *Journal of the American Medical Association*, *287*, 1132–1141.
- Potgieter-Vermaak, S., Rotondo, G., Novakovic, V., Rollins, S., & Van Grieken, R. (2012). Component-specific toxic concerns of the inhalable fraction of urban road dust. *Environmental Geochemistry and Health*, *34*, 689–696.
- Shukla, J. B., Misra, A. K., Sundar, S., & Naresh, R. (2008). Effect of rain on removal of gaseous pollutant and two different particulate matters from the atmosphere of a city. *Mathematical and Computer Modelling*, *48*, 832–844.
- Sorenson, M., Hoffmann, B., Hvindberg, M., Ketzler, M., Jensen, S. S., Andersen, Z. J., et al. (2012). Long-term exposure to traffic-related air pollution associated with blood pressure and self-reported hypertension in a Danish cohort. *Environmental Health Perspectives*, *120*, 418–424.
- Tucker, M. E. (1991). *Sedimentary petrology: An introduction to the origin of sedimentary rocks* (2nd ed.). Cambridge: Blackwell Sciences Ltd.
- Ugarte, M., Osborne, N. N., Brown, L. A., & Bishop, P. N. (2013). Iron, zinc and copper in retinal physiology and disease. *Survey of Ophthalmology*, *58*, 585–609.
- Unceta, N., Seby, F., Malherbe, J., & Donard, O. F. X. (2010). Chromium speciation in solid matrices and regulation: a review. *Analytical and Bioanalytical Chemistry*, *397*, 1097–1111.

- USEPA. (1989). *Risk assessment guidance for superfund* (Vol. 1), Human health evaluation manual. EPA/540/1-89/002 Washington, DC: Office of Solid waste and Emergency Response.
- USEPA. (1997). *Exposure factors handbook*. EPA/600/P-95/002F. Washington, DC: Environmental Protection Agency, Office of Research and Development.
- USEPA. (2000). *Soil screening guidance for radionuclides: Technical background document*. <http://www.epa.gov/superfund/health/contaminants/radiation/pdfs/sstbd.pdf>
- USEPA. (2001). *Risk Assessment Guidance For Superfund: Vol. I. Human health evaluation manual (Part D standardized planning, reporting and review of superfund)*. [http://www.epa.gov/swerrims/riskassessment/ragsd/pdf/front\\_2001.pdf](http://www.epa.gov/swerrims/riskassessment/ragsd/pdf/front_2001.pdf)
- Villeneuve, P. J., Goldberg, M. S., Krewski, D., Burnett, R. T., & Chen, Y. (2002). Fine particulate air pollution and all-cause mortality within the harvard six-cities study: variations in risk by periods of exposure. *Annals of Epidemiology*, *12*, 568–576.
- World Health Organisation. (2009). Global health risks, mortality and burden of disease attributable to selected major risks. [http://www.who.int/healthinfo/global\\_burden\\_disease/GlobalHealthRisks\\_report\\_full.pdf](http://www.who.int/healthinfo/global_burden_disease/GlobalHealthRisks_report_full.pdf)
- Xie, S. D., Qi, L., & Zhou, D. (2004). Investigation of the effects of acid rain on the deterioration of cement concrete using accelerated tests established in laboratory. *Atmospheric Environment*, *38*, 4457–4466.
- Zhang, J., Fu, Y., Li, J., Wang, J., He, B., & Xu, S. (2009). Effects of subchronic cadmium poisoning on DNA methylation in hens. *Environmental Toxicology and Pharmacology*, *27*, 345–349.
- Zhang, A., Gao, C., Han, X., Wang, L., Yu, C., Zeng, X., et al. (2014). Inactivation of P15ink4b in chronic arsenic poisoning cases. *Toxicology Reports*, *1*, 692–698.
- Zhang, Y., Li, Q., Liu, X., Zhu, H., Song, A., & Jiao, J. (2013). Anti-oxidant and micronutrient-rich formula reduces lead poisoning and related oxidative damage in lead-exposed mice. *Food and Chemical Toxicology*, *57*, 201–208.

**C.2 Publications with results which do not feature in the main text, but aided conception of the thesis and contributed useful research and data handling skills**



Contents lists available at ScienceDirect

# Science of the Total Environment

journal homepage: [www.elsevier.com/locate/scitotenv](http://www.elsevier.com/locate/scitotenv)

## Composition of PM<sub>2.5</sub> and PM<sub>1</sub> on high and low pollution event days and its relation to indoor air quality in a home for the elderly



Anna J. Buczyńska<sup>a</sup>, Agnieszka Krata<sup>a,b</sup>, Rene Van Grieken<sup>a</sup>, Andrew Brown<sup>c</sup>, Gabriela Polezer<sup>c</sup>, Karolien De Wael<sup>a</sup>, Sanja Potgieter-Vermaak<sup>c,d,\*</sup>

<sup>a</sup> Department of Chemistry, University of Antwerp, Antwerp, Belgium

<sup>b</sup> Faculty of Chemistry University of Warsaw, Biological and Chemical Research Centre University of Warsaw, Warsaw, Poland

<sup>c</sup> Division of Chemistry & Environmental Science, Faculty of Science & Environment, Manchester Metropolitan University, Manchester, United Kingdom

<sup>d</sup> Molecular Science Institute, School of Chemistry, University of the Witwatersrand, Johannesburg, South Africa

### HIGHLIGHTS

- Chemical composition of indoor and outdoor PM<sub>2.5</sub> and PM<sub>1</sub> at a home for the elderly.
- Increased mass concentrations (indoor and outdoor) during high pollution period.
- Increased concentrations of V, Fe and Ni during high pollution event period.
- Cation/anion ratios indicative of an acid aerosol prevailing during high pollution periods.
- Increased risk for the elderly during high pollution events.

### ARTICLE INFO

#### Article history:

Received 5 September 2013

Received in revised form 29 March 2014

Accepted 24 April 2014

Available online 21 May 2014

Editor: P. Kassomenos

#### Keywords:

Indoor air quality  
High pollution event  
PM characterisation  
Acidic aerosol  
Elderly

### ABSTRACT

Many studies probing the link between air quality and health have pointed towards associations between particulate matter (PM) exposure and decreased lung function, aggravation of respiratory diseases like asthma, premature death and increased hospitalisation admissions for the elderly and individuals with cardiopulmonary diseases. Of recent, it is believed that the chemical composition and physical properties of PM may contribute significantly to these adverse health effects. As part of a Belgian Science Policy project (“Health effects of particulate matter in relation to physical–chemical characteristics and meteorology”), the chemical composition (elemental and ionic compositions) and physical properties (PM mass concentrations) of PM were investigated, indoors and outdoors of old age homes in Antwerp. The case reported here specifically relates to high versus normal/low pollution event periods. PM mass concentrations for PM<sub>1</sub> and PM<sub>2.5</sub> fractions were determined gravimetrically after collection via impaction. These same samples were hence analysed by EDXRF spectrometry and IC for their elemental and ionic compositions, respectively. During high pollution event days, PM mass concentrations inside the old age home reached  $53 \mu\text{g m}^{-3}$  and  $32 \mu\text{g m}^{-3}$  whilst outside concentrations were  $101 \mu\text{g m}^{-3}$  and  $46 \mu\text{g m}^{-3}$  for PM<sub>2.5</sub> and PM<sub>1</sub>, respectively.

The sum of nss-sulphate, nitrate and ammonium, dominate the composition of PM, and contribute the most towards an increase in the PM during the episode days constituting 64% of ambient PM<sub>2.5</sub> ( $52 \mu\text{g m}^{-3}$ ) compared to 39% on non-episode days ( $10 \mu\text{g m}^{-3}$ ). Other PM components, such as mineral dust, sea salt or heavy metals were found to be considerably higher during PM episodes but relatively less important. Amongst heavy metals Zn and Pb were found at the highest concentrations in both PM<sub>2.5</sub> and PM<sub>1</sub>. Acid–base ionic balance equations were calculated and point to acidic aerosols during event days and acidic to alkaline aerosols during non-event days. No significant sources of indoor pollutants could be identified inside the old-age home as high correlations were found between outdoor and indoor PM, confirming mainly the outdoor origin of indoor air.

© 2014 Elsevier B.V. All rights reserved.

\* Corresponding author at: Chester Street, School of Science and the Environment, Manchester Metropolitan University, M1 5GD, Manchester, UK.

E-mail addresses: [anna.buczynska@uantwerpen.ac.be](mailto:anna.buczynska@uantwerpen.ac.be) (A.J. Buczyńska), [rene.vangrieken@uantwerpen.ac.be](mailto:rene.vangrieken@uantwerpen.ac.be) (R. Van Grieken), [andrew.brown8@stu.mmu.ac.uk](mailto:andrew.brown8@stu.mmu.ac.uk) (A. Brown), [gabipolezer@gmail.com](mailto:gabipolezer@gmail.com) (G. Polezer), [s.potgieter@mmu.ac.uk](mailto:s.potgieter@mmu.ac.uk) (S. Potgieter-Vermaak).

### 1. Introduction

Numerous epidemiological and clinical studies have been conducted over the last decade and a half and they indicate associations between particulate matter (PM) exposure and various health effects (Strak et al., 2012; Stranger et al., 2009 and references therein; Fuentes-

Leonarte et al., 2009; Jacobs et al., 2012 and references therein). It is shown that increases in PM exposure often lead to increased hospital admissions, especially in susceptible cohorts such as the elderly and individuals with cardiopulmonary diseases (Di Ciaula, 2012). Although earlier studies focused on PM mass concentrations, it is nowadays commonly believed that the chemical and biological compositions of the particulate matter may also contribute significantly to detrimental health effects (Gemenetzis et al., 2006; Bell et al., 2009).

A Belgian Science Policy project (“Health effects of particulate matter in relation to physical–chemical characteristics and meteorology”), which this study was a part of, intended to investigate acute, short-term health effects of PM and its composition in the elderly part of the population (Jacobs et al., 2012). The sampling of air pollution was designed, so that there was a contrast in ambient PM concentrations between the first and second visit of a patient during which a set of clinical measurements was performed. More information may be found in Jacobs et al. (2012). This was possible thanks to the predictions of PM concentrations (4 days in advance) made by Ircel (Belgian Inter-regional Environment Agency). The air particulate matter was sampled both indoors and outdoors of the building. Since this part of the population spends most of their time indoors, monitoring the indoor air and close outdoor environment in place of the personal exposure seems justified. Wichmann et al. (2005) found highly correlated time-series of pairs of personal, indoor and outdoor fixed site PM<sub>2.5</sub> and black smoke concentrations in a small population of elderly cardiovascular patients. The concentration of the PM inside of a building is mainly governed by indoor generation of particles, the concentration of the particles outside, the rate of air exchange and the depositional characteristics of the particles (Gemenetzis et al., 2006). For those reasons this study monitored both environments.

This paper is thus one of a handful reporting on the chemical (elemental composition and water-soluble ion concentrations, including secondary aerosols) and physical (mass concentrations) differences between ambient and indoor concentrations of PM<sub>2.5</sub> and PM<sub>1</sub> during periods of high and low pollution events in old-age home (Czragani Broechem, Belgium). We chose this location as it was characterised by the highest pollution event observed in Antwerp during the course of the project (2007–2010). The sampling campaign covers days before, during and after the event. Thus, in addition to investigation of the relationship between the outdoor and indoor pollutants, a comparison between days with “normal” PM concentrations or so-called non-episode days (NEDs) and episode days (EDs) could be made.

A target value of 25  $\mu\text{g m}^{-3}$  for PM<sub>2.5</sub> entered into force in 2010 under the Ambient Air Quality and Cleaner Air Act for Europe (Council Directive 2008/50/EC) and will enter into force as a limit value in 2015. Although a yearly average indoor PM<sub>2.5</sub> guideline value of 15  $\mu\text{g m}^{-3}$  in Flanders, Belgium exists, we decided to use the 24-h PM<sub>10</sub> indoor air quality guideline value (Stranger et al., 2007) of 40  $\mu\text{g m}^{-3}$ . In this study, the PM<sub>10</sub> concentration was not measured; however, based on our unpublished results from simultaneous PM<sub>10</sub> and PM<sub>2.5</sub> mass measurements in various indoor locations in Belgium, PM<sub>2.5</sub> accounts on average for 73% of PM<sub>10</sub> mass concentration. Therefore, the 24 h PM<sub>2.5</sub> indoor value higher than 29.2  $\mu\text{g m}^{-3}$  stands for an ED in this study and lower than 29.2  $\mu\text{g m}^{-3}$  stands for a NED. This value is not unreasonable taking into account that the WHO guideline values for short term PM<sub>2.5</sub> exposure is 25  $\mu\text{g m}^{-3}$  24-h mean (WHO, 2011).

## 2. Experimental

### 2.1. Sampling location

Broechem is a village (12 km<sup>2</sup>) located in the province of Antwerp, around 10 km to the east of the Antwerp city (N50°10', E4°36') with about 4000 inhabitants. The sampling was performed in the Czragani old-age home, with around 120 inhabitants and 100 workers at the time of the sampling. The old-age home has a surface area of about

6500 m<sup>2</sup> and three floors. The building, built in 1994, is both mechanically and naturally vented. The ground floor (where sampling was performed), was a carpeted open space, it served as a dining room, cafeteria and the reception; the cleaning thereof was performed 6 days per week. The building is situated about 1 km from the highway and 300 m from a major village road.

Local pollution sources include mainly traffic and domestic heating. Other potential sources include the harbour of Antwerp (located to the north of the city), a large petrochemical plant, a municipal waste incinerator, and a non-ferrous plant to the south of Antwerp (Stranger, 2005).

### 2.2. Sampling methodology

PM was collected indoors and outdoors simultaneously by means of impaction (Harvard impactors from Air Diagnostics and Engineering Inc., Naples, ME, USA) and operated at a flow rate of 23 L min<sup>-1</sup> for PM<sub>1</sub> collection and 10 L min<sup>-1</sup> for PM<sub>2.5</sub> collection. Membrane Teflon filters were used (2  $\mu\text{m}$  pore size and 37 mm in diameter) to collect the particles over periods of 24 h. Filter changing took place in the mornings, during which time the flow rate was checked. Indoor sampling took place in the ground floor dining room and the impactors were positioned so that the inlets were as close as possible to the breathing zone of people (about 1 m above the ground). Outdoor sampling was done at the back of the building in order to avoid direct influence from the automobile exhaust emissions originating from a small parking lot in front of the building. Since the building was only 3 storeys high, the ground floor concentrations are assumed representative for all floors. As shown by Gemenetzis et al. (2006) in the study conducted in university rooms in Greece, although a slight decrease in PM<sub>10</sub> and PM<sub>2.5</sub> mass concentrations was observed with an increase in the elevation level, it could be considered as negligibly small up to the 5th floor. The effect of elevation (up to the 40th floor) on indoor particulate concentrations was also studied by Chao and Wong (2002), who reports no significant difference in the PM<sub>10</sub> and PM<sub>2.5</sub> mass concentrations at different levels.

Co-located duplicate samples of PM<sub>2.5</sub> were collected both in indoor and outdoor sites. They were however used only for the determination of the mass concentration and were not subjected to further examinations for elemental and ionic measurements. Thus, the PM mass concentration values are the arithmetic mean of two measurements. The results of the duplicate sampling of PM<sub>2.5</sub> agreed with each other to within 5%, exceeding this difference only four times, with the highest being 16%.

### 2.3. Analysis

The masses of the collected particulates were determined gravimetrically using a microbalance with a resolution of 1  $\mu\text{g}$  (Mettler Toledo MX5, Mettler Toledo, Columbus, USA) in an environmentally controlled laboratory. Filters were conditioned at 20 °C and 50% relative humidity, for at least 24 h before weighing, and stored in Petri dishes until sampling. After sample collection, they were conditioned again, weighed and stored at 4 °C until the analysis.

The filters were analysed firstly by means of X-ray fluorescence (Epsilon-5 XRF, PANAnalytical, The Netherlands) in order to determine the bulk elemental concentrations of selected elements (Al, As, Ca, Cd, Cl, Cr, Cu, Fe, K, Mn, Ni, Pb, S, Sb, Se, Si, Sr, Ti, V, Zn) and afterwards subjected to Ion Chromatographic (IC) analysis (Dionex DX-120, Dionex, USA) for anion (Cl<sup>-</sup>, NO<sub>3</sub><sup>-</sup>, SO<sub>4</sub><sup>2-</sup>) and cation (Ca<sup>2+</sup>, K<sup>+</sup>, Mg<sup>2+</sup>, Na<sup>+</sup>, NH<sub>4</sub><sup>+</sup>) concentrations. Experimental procedures have been described elsewhere (Avigo et al., 2008; Stranger et al., 2009). The IC detection limits (LODs) were estimated from blank filters (three standard deviations of the concentration found in blank) using the average air volume of PM<sub>2.5</sub> and PM<sub>1</sub> samples taken during the sampling campaign. LODs were ranging from 3 ng m<sup>-3</sup> for magnesium to 72 ng m<sup>-3</sup> for sodium

cation in PM<sub>2.5</sub>, and from 1 ng m<sup>-3</sup> to 30 ng m<sup>-3</sup> in PM<sub>1</sub> for the same cations, respectively. Magnesium and calcium ions were generally found in very low amounts. Magnesium was detected above its LOD in 63% of all samples, calcium, in 46%. All other ions were detected in significant amounts in all samples. The precision was better than 3.6% for all analytes (Bencs et al., 2008). For XRF analysis, the detection limits ranged from 0.7 for vanadium to 32 ng m<sup>-3</sup> for aluminium in PM<sub>2.5</sub> and from 0.3 ng m<sup>-3</sup> for vanadium to 13 ng m<sup>-3</sup> for aluminium in PM<sub>1</sub>. Cd, Se and Sb were below the detection limits in all samples; for other elements there were 11% of non-detects. The precision, expressed as relative standard deviation of three repetitions, was generally below 5%; for about 20% of samples it exceeded 15%. Quality check of these analyses was performed by calculating the correlation coefficients between elemental-sulphur and sulphate-sulphur. *R*<sup>2</sup> values of 1 and 0.99 were found for indoor and outdoor PM<sub>2.5</sub>, respectively. The PM<sub>1</sub> correlation coefficients were 0.99 for both indoor and outdoor PM. For chloride the values were somewhat lower, in indoor PM<sub>1</sub> two outliers had to be excluded, the correlations had the *R*<sup>2</sup> equal to 0.98 and 0.95 in PM<sub>2.5</sub> indoors and outdoors, and 0.84 in indoor and 0.97 in outdoor PM<sub>1</sub>.

Identification of the origin of air masses was done for each day of the sampling using 5-day backward trajectories performed with Hysplit model (<http://www.arl.noaa.gov/HYSPLIT.php>) (Draxler and Rolph, 2013). Initial heights of 2 m and 20 m above ground level were investigated.

All statistical calculations were performed using an IBM SPSS Statistics, version 22.0 software package (IBM Corp., Armonk, NY, USA).

### 3. Results and discussion

#### 3.1. Mass concentrations

Descriptive statistics of daily PM<sub>2.5</sub> and PM<sub>1</sub> concentrations for the whole campaign, episode days and non-episode days are summarised in Table 1. Mean outdoor concentrations of 77.0 µg m<sup>-3</sup> and 36.7 µg m<sup>-3</sup> for PM<sub>2.5</sub> and PM<sub>1</sub>, respectively, are reported for episode days. Mean indoor concentrations were 43% and 29% lower for PM<sub>2.5</sub> and PM<sub>1</sub>, respectively (Table 1). PM<sub>1</sub> therefore constitutes 53% of PM<sub>2.5</sub> on average (48 ± 12% for EDs and 55 ± 11% on NEDs) in outdoor air and 64 ± 8% (62 ± 12% for EDs and 65 ± 9% on NEDs) indoors. Maximum PM<sub>2.5</sub> concentrations reached 101 µg m<sup>-3</sup> (46.1 µg m<sup>-3</sup> for PM<sub>1</sub>) outdoors and 53.5 µg m<sup>-3</sup> (31.9 µg m<sup>-3</sup> for PM<sub>1</sub>) indoors. In context to the overall research project investigations, these values are considerably higher than any of those measured during five other campaigns, in different old-age homes in Belgium between years 2007 and 2010. These values are also much higher than some of the values published across the literature, for example: in Birmingham 7.9 µg m<sup>-3</sup> was reported for residential indoor PM<sub>2.5</sub> (Jones et al., 2000), and 9.1 µg m<sup>-3</sup> in Oxford, England (Lai et al. (2004)). A maximum of 56 µg m<sup>-3</sup> was observed for outdoor PM<sub>2.5</sub> in Canada (Cheng et al., 1998), and 66 µg m<sup>-3</sup> (PM<sub>2.5</sub> 12 h day sample) in a study of air quality in offices near a busy street in the centre

of Antwerp (Horemans and Van Grieken, 2010). The outdoor values are also higher than those found in the study of Stranger et al. (2009) reporting on residential indoor air quality in Belgium, although the average indoor concentration and maximum values reported were similar to the ones reported here. Moreover, EDs' PM<sub>2.5</sub> outdoor values exceeded those reported for PM<sub>10</sub> during a yearly study at six different sites in Belgium (urban background to rural; 24-h samples taken once a week) (Vercauteren et al., 2011). However, literature also indicates much higher concentrations elsewhere, especially in Asia, for example, Ye et al. (2003), in a yearly study in Shanghai, reported weekly averages of PM<sub>2.5</sub> equal to 156 µg m<sup>-3</sup>.

Chen et al. (2003) in their study of pollution episodes set the threshold value for EDs and NEDs at 150 µg m<sup>-3</sup>.

Fig. 1 gives the average ambient daily temperature, wind speed and relative humidity during the study. Days with elevated PM concentrations (13, 18, 19 February) are characterised by the lowest temperatures (0.8–1.4 °C) and wind speeds (1.6–2.5 m s<sup>-1</sup>). The only exception is the 20th February where high concentrations of PM were measured despite a maximum temperature of 6.4 °C and a wind speed of 2.8 m s<sup>-1</sup>. Vecchi et al. (2004), noticed typically an increase by 20–35% in both PM<sub>1</sub> and PM<sub>2.5</sub> on days when wind velocity was lower than 2 m s<sup>-1</sup>. In this study the increase of PM concentration registered on episode days was much higher, on average 2.5 to almost 3 times higher, compared to non-episode days. Wintertime increases in ambient pollutant concentrations are frequently attributable to a combination of low level, persistent temperature inversions and increases in emissions related to heating (Ye et al. (2003)). Additionally, lower temperatures occurring during the winter season favour the persistence of particle phase with respect to the gas phase, e.g. NH<sub>4</sub>NO<sub>3</sub> (Vecchi et al. (2004)). Inversion was evident on most days of high pollution events in our study (See Fig. 1S in Supplementary material). Additionally, backward trajectory analyses revealed that anticyclonic circulation of the air masses coincided with the episode days. On the 13th of February, the impact of 120 h trajectories was almost entirely regional (Germany, The Netherlands and Belgium) and between 18th and 20th February the air masses originated in the Arctic region, passing Norway, Sweden, Germany and finally creating an anticyclone over Belgium. As pointed out by Viana et al. (2007a), anticyclonic scenarios lead to the development of thermal inversions, air mass stagnation and accumulation of locally emitted pollutants. During NEDs, air masses seemed to be impacted to a larger extent by cleaner air from the Atlantic Ocean and the North Sea before reaching the sampling location. This is especially visible during the third week of the study, in which air masses travelled very long distances over the Atlantic Ocean before reaching Belgium.

#### 3.2. Indoor–outdoor correlations in PM

The degree of outside PM infiltration was gauged by determining straight-line indoor–outdoor correlations for two fractions PM<sub>2.5</sub>-1 and PM<sub>1</sub>, thus using the value of the correlation coefficient, *R*<sup>2</sup>, as the indicator (Fig. 2). PM<sub>2.5</sub>-1 fraction was obtained by subtracting the concentrations found in PM<sub>2.5</sub> and PM<sub>1</sub>. Mass concentration profiles for PM<sub>2.5</sub>-1 match each other and this correlation is illustrated by an *R*<sup>2</sup> of 0.93. A lower *R*<sup>2</sup> of 0.74 was observed for PM<sub>1</sub>, but after removal of an outlier (13.02.08) the value was close to that of the PM<sub>2.5</sub>-1 as is seen in the insert of Fig. 2. The coefficients for both fractions were considerably higher than those reported for PM<sub>2.5</sub> in residences in California (Geller et al., 2002), where the correlation coefficient was equal to 0.37. This indicates that mass concentration increases on the outside are reflected on the inside and one could deduce that a substantial fraction of indoor particles in our study penetrated from the outdoor environment.

The correlation between PM<sub>1</sub> and PM<sub>2.5</sub> (*R*<sup>2</sup>) was equal to 0.86 when PM outdoors were compared, and 0.97 for the indoor concentrations. The I/O ratios for PM<sub>2.5</sub> were always below 1, and those for PM<sub>1</sub> exceeded 1 only twice (thus 17% of cases, amounting to 1.08 and 1.36).

**Table 1**  
Summary of the PM mass concentrations (µg m<sup>-3</sup>) registered during the study.

	Indoor		Outdoor	
	PM <sub>2.5</sub>	PM <sub>1</sub>	PM <sub>2.5</sub>	PM <sub>1</sub>
Minimum	10.6	5.8	11.4	5.3
Mean	<b>24.8</b>	<b>15.7</b>	<b>43.4</b>	<b>22.1</b>
Median	17.6	11.3	32.8	18.4
Standard deviation	14.6	8.7	27.7	13.1
Maximum	53.5	31.9	100.6	46.1
Event	<b>43.7</b>	<b>27.0</b>	<b>77.0</b>	<b>36.7</b>
Standard deviation	7.2	3.3	20.1	12.0
Non-event	<b>15.4</b>	<b>10.0</b>	<b>26.7</b>	<b>14.8</b>
Standard deviation	2.9	2.0	8.1	5.2

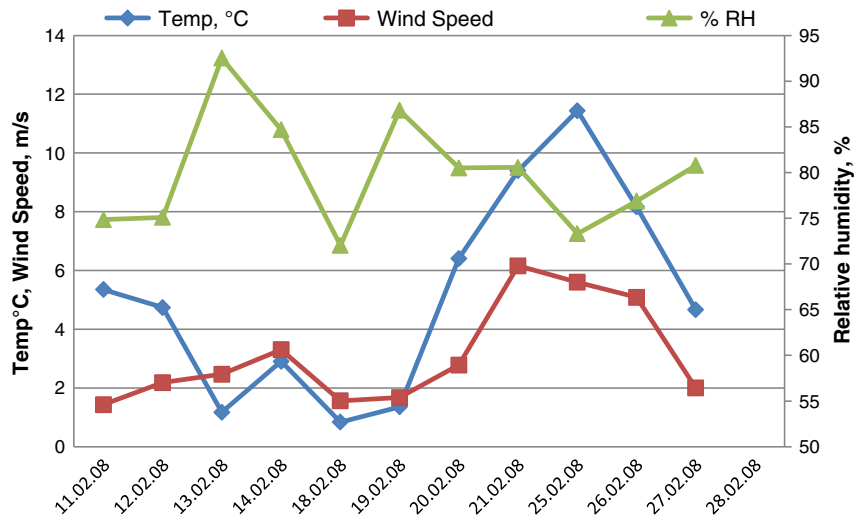


Fig. 1. Ambient meteorological conditions during the sampling campaign.

This, together with high correlations of indoor to outdoor air reported above, suggests no major indoor sources of particulate matter in the studied old-age home. PM1 decreased indoors by 29% on average compared to outdoors and the PM2.5-1 fraction by 57%. These decreases were similar on EDs and NEDs. It thus suggests a more effective indoor penetration of fine particles than of supermicron PM2.5-1 particles. The building, hence, offers a relatively good protection against exposure to supermicron particles and to its components, although larger deposition velocities of these particles on window, door and furniture surfaces could also have played a role.

3.3. Chemical mass closure of PM

Chemical mass closure of the PM2.5, PM1 and PM2.5-1 was calculated using the results obtained from both the IC and XRF analyses (Table 2). PM2.5-1 composition was obtained by subtracting the concentrations found in PM2.5 and PM1; therefore larger uncertainties may be

associated with this fraction. Subsequently, the relative contributions of PM components were calculated to illustrate the differences between EDs and NEDs and outdoor and indoor environments (Fig. 3). As pointed out already by Putaud et al. (2004), relative contributions reflect the differences in the sources and processes controlling the aerosol composition as they are independent of dilution. Additionally, outdoor-to-indoor transport of particles may modify the composition of PM. Meng et al. (2007) found distinct infiltration factors (fraction of ambient PM found indoors) for several components of PM2.5. For those reasons, the contributions of secondary inorganic aerosols, crustal matter, sea salt, smoke and other elements (including heavy metals) to collected PM size fractions were studied in detail. Crustal matter, sea salt, non-crustal K (smoke origin) non-sea salt (nss) SO<sub>4</sub><sup>2-</sup> were assessed using the approaches published previously (Chan et al. (1997), Maenhaut et al. (2002), Sillanpää et al. (2006)). Sea salt content was calculated from Na<sup>+</sup> and Cl<sup>-</sup> concentrations, nss-SO<sub>4</sub><sup>2-</sup> from measured SO<sub>4</sub><sup>2-</sup> and Na<sup>+</sup> and for both calculations, the composition of standard sea water was

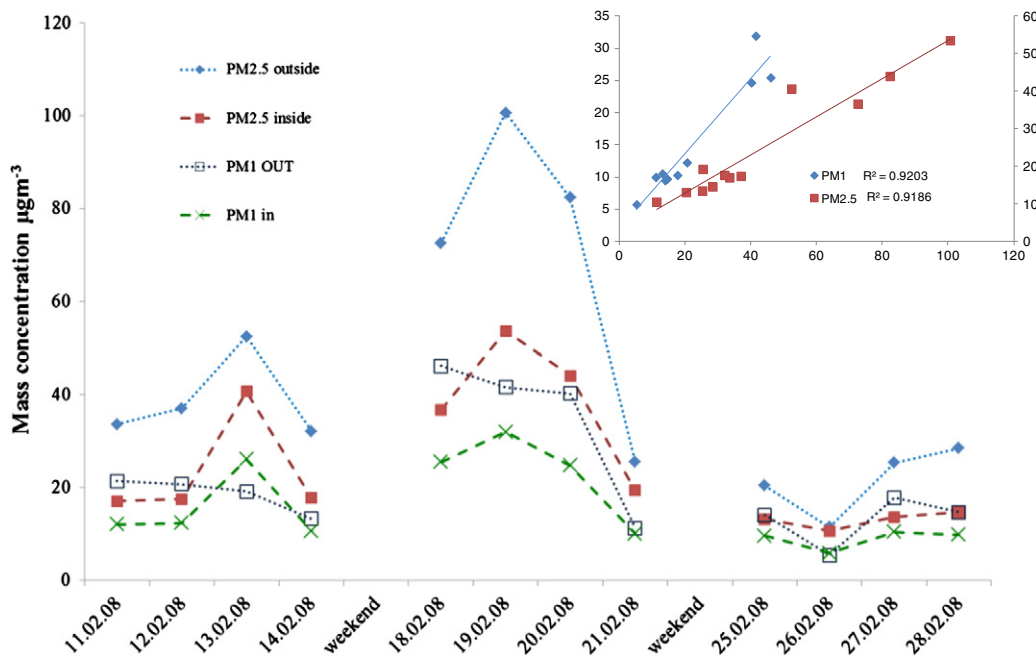


Fig. 2. Indoor:outdoor relationships for PM2.5 and PM1.

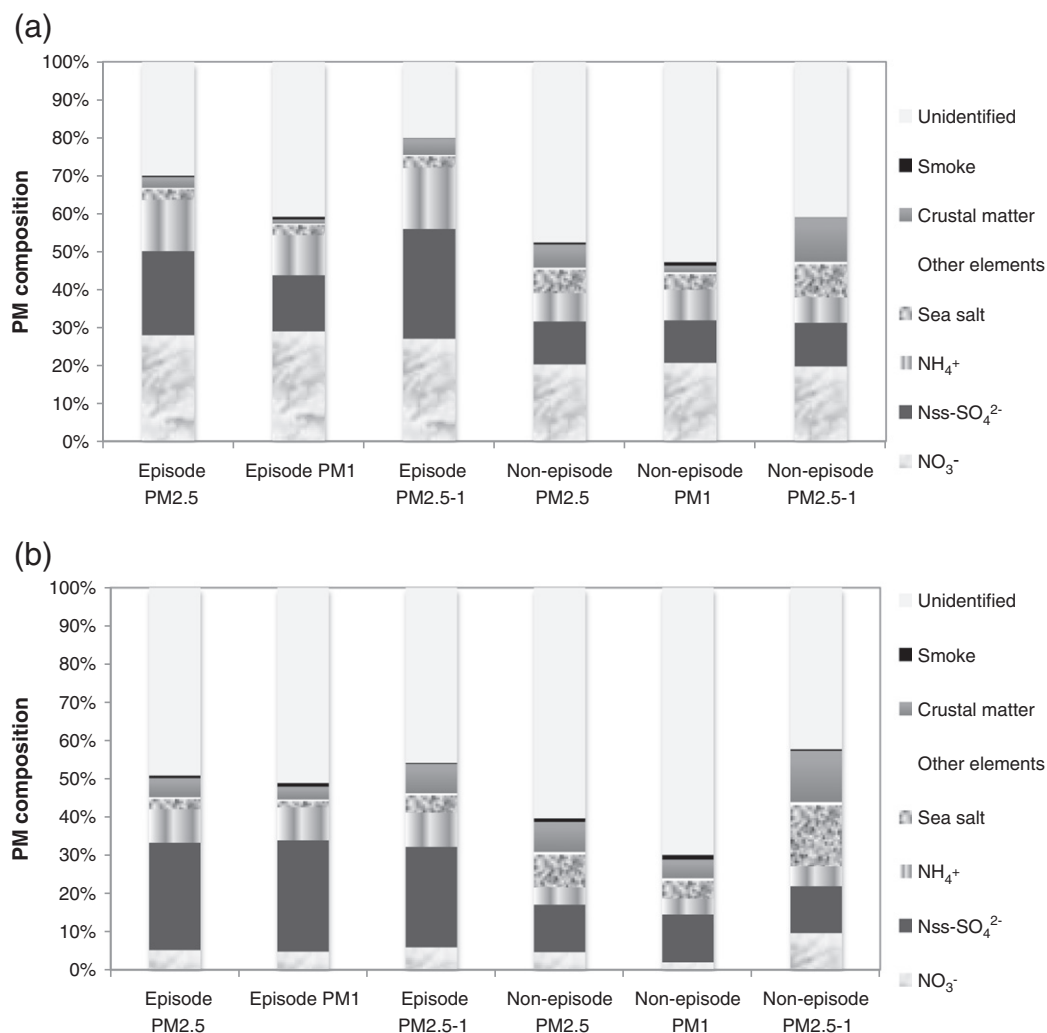
**Table 2**Contribution of PM components to outdoor and indoor PM<sub>2.5</sub>, PM<sub>1</sub> and PM<sub>2.5-1</sub> on EDs and NEDs. Concentration value ( $\mu\text{g m}^{-3}$ ) is accompanied by  $1\sigma$ .

	$\text{NO}_3^-$	$\text{Nss-SO}_4^{2-}$	$\text{NH}_4^+$	Sea salt	Other elements	Crustal matter	Smoke	Unidentified
<i>Outdoors</i>								
ED PM <sub>2.5</sub>	22.9 ± 5.3	18.2 ± 9.5	11.0 ± 3.0	2.3 ± 0.9	0.26 ± 0.11	2.3 ± 0.7	0.30 ± 0.11	24.6 ± 9.4
ED PM <sub>1</sub>	11.3 ± 4.7	5.8 ± 2.5	4.2 ± 1.3	1.1 ± 0.4	0.13 ± 0.06	0.4 ± 0.2	0.27 ± 0.10	16.0 ± 4.8
ED PM <sub>2.5-1</sub>	11.5 ± 3.6	12.4 ± 7.7	6.9 ± 2.9	1.3 ± 0.6	0.13 ± 0.05	1.9 ± 0.5	0.04 ± 0.03	8.6 ± 4.3
NED PM <sub>2.5</sub>	5.4 ± 3.0	3.0 ± 1.5	2.0 ± 0.9	1.6 ± 0.6	0.14 ± 0.08	1.6 ± 1.2	0.14 ± 0.05	12.7 ± 5.9
NED PM <sub>1</sub>	3.1 ± 1.5	1.7 ± 0.4	1.2 ± 0.4	0.6 ± 0.2	0.07 ± 0.04	0.3 ± 0.1	0.14 ± 0.07	7.8 ± 4.2
NED PM <sub>2.5-1</sub>	2.3 ± 2.1	1.4 ± 1.2	0.8 ± 0.6	1.0 ± 0.5	0.07 ± 0.05	1.4 ± 1.1	0.01 ± 0.02	4.8 ± 3.0
<i>Indoors</i>								
ED PM <sub>2.5</sub>	2.2 ± 1.2	12.1 ± 6.9	3.8 ± 1.7	1.2 ± 0.3	0.21 ± 0.08	2.1 ± 0.2	0.30 ± 0.08	21.2 ± 3.7
ED PM <sub>1</sub>	1.3 ± 0.8	7.9 ± 4.0	2.3 ± 1.1	0.4 ± 0.1	0.12 ± 0.03	0.9 ± 0.3	0.25 ± 0.06	13.8 ± 1.6
ED PM <sub>2.5-1</sub>	1.0 ± 0.6	4.2 ± 3.0	1.4 ± 0.7	0.7 ± 0.3	0.09 ± 0.05	1.2 ± 0.3	0.04 ± 0.03	7.4 ± 2.9
NED PM <sub>2.5</sub>	0.7 ± 0.3	1.9 ± 1.0	0.7 ± 0.3	1.3 ± 0.6	0.11 ± 0.05	1.2 ± 0.4	0.14 ± 0.03	9.2 ± 2.3
NED PM <sub>1</sub>	0.2 ± 0.1	1.2 ± 0.9	0.4 ± 0.3	0.5 ± 0.1	0.07 ± 0.03	0.5 ± 0.1	0.12 ± 0.05	7.0 ± 2.4
NED PM <sub>2.5-1</sub>	0.5 ± 0.2	0.7 ± 0.6	0.3 ± 0.2	0.9 ± 0.5	0.04 ± 0.02	0.7 ± 0.3	0.02 ± 0.02	2.3 ± 1.6

taken into account. The concentrations of inorganic secondary species ( $\text{NH}_4^+$ ,  $\text{NO}_3^-$ ) and “other” elements (As, Cr, Cu, Mn, Ni, Pb, Sr, V, Zn) were determined directly from measurements.

Substantial amounts of PM, named “unidentified”, resulted from subtracting the reconstituted mass of each sample from total PM mass determined gravimetrically. Most likely it consists largely of organic (OC) and elemental carbon (EC), which were not measured in this study. Both, percentages of unidentified fraction and absolute values obtained for PM<sub>2.5</sub> (30% on outdoor EDs corresponding to  $24.6 \mu\text{g m}^{-3}$ , and

up to 60% indoors on NEDs, corresponding to  $9.2 \mu\text{g m}^{-3}$ ) are in agreement with the values obtained for OC and EC components in other studies conducted in Belgium and Europe, in which the major component of urban or regional background PM<sub>2.5</sub> and PM<sub>10</sub> appeared to be organic matter (Maenhaut et al. (2002), Putaud et al. (2004), Querol et al. (2004a), Sillanpää et al. (2006)). The OC + EC component is thought to originate mainly from traffic emissions, heating and other combustion related processes. The “unidentified” fraction prevailed in PM<sub>1</sub> with concentrations twice that of the supermicron PM<sub>2.5-1</sub> fraction. A fraction of

**Fig. 3.** Relative contribution of PM components to outdoor (a) and indoor (b) PM<sub>2.5</sub>, PM<sub>1</sub> and PM<sub>2.5-1</sub> on EDs and NEDs.

an unaccounted PM mass may be as well water associated with hygroscopic aerosol components (Maenhaut et al. (2002), Querol et al. (2004b)).

The relative contribution of unidentified species of particulate matter on EDs is significantly lower than on NEDs for both indoor and outdoor PM. This component thus contributed less to the total PM on episode days than on non-episode days, although in absolute values, it was about two times higher on EDs. The increase occurred both in PM1 and PM2.5-1 to a similar extent.

### 3.3.1. Secondary inorganic aerosol species (SIA)

Nss-sulphate constituted 99% of ambient PM 2.5 sulphate on EDs in all studied fractions and about 92% (96% of PM1 sulphate and 80% of PM2.5-1 sulphate) on NEDs. In addition, on EDs the percentage range of nss-sulphate was very narrow – from 98% to 100%, on NEDs, it was more variable. In PM1 it varied between 91% and 97% and in PM2.5-1, between 43% and 97%. The highest relative contribution of sea-sulphate was seen in the third week of the study, when the air masses passed a long distance over the Atlantic Ocean and it was preferably associated with fraction PM2.5-1.

Nss-sulphate, nitrate and ammonium, dominate the composition of PM, constituting 64% of PM2.5 during EDs ( $52 \mu\text{g m}^{-3}$ ) and 39% on NEDs ( $10 \mu\text{g m}^{-3}$ ). Hence, not only an absolute increase in the concentration was seen but also the relative contribution increased by a factor of 1.6 on EDs compared to NEDs. SIA absolute concentrations were 5–6 times higher during EDs compared to NEDs both indoors and outdoors. Ram et al. (2012) reported an increase in concentration by a factor of 2–3 in their study of SIA during fog and haze days. Although the percentage values reported by Ram et al. (2012) were much lower, the same tendency was seen, namely about a 2 fold increase in contribution from clear to foggy days. The episode days in our study were apparently not only influenced by a limited pollutant dilution connected to occurrence of temperature inversions, but also most probably by an increased formation of secondary species due to the preferable meteorological conditions. At lower ambient temperature and wind speed, high RH and  $\text{SO}_2$  and in the presence of higher particle concentration the conversion of gaseous  $\text{SO}_2$  to particle  $\text{SO}_4^{2-}$  is expected to be higher (Ram et al. (2012)).

Amongst secondary species, nitrate prevailed mostly in ambient air, whilst nss-sulphate was the dominant ion in the indoor air. The nitrate indoor/outdoor (I/O) ratio was only 0.14 on the average whilst the nss-sulphate ratio was equal to 0.66 for PM2.5. For PM1, these values were 0.10 and 0.96 for nitrate and nss-sulphate, respectively. The trend of fine particles showing higher I/O ratios for sulphate was also observed by Jones et al. (2000).

The low I/O nitrate ratio indicates a significant decrease of nitrate concentration indoors due to the higher temperature compared to the outdoor air and thus transformation of particle ammonium nitrate to ammonia and nitric acid gases (Parker et al. (2008)) ( $\text{NO}_3^-$  conversion

between particle and the gas phase is strongly temperature dependent). Nitrate appears to be evenly distributed between PM1 and PM2.5-1 on EDs, both in absolute values and relative contributions in ambient (29% and 27%, respectively) and indoor (5% and 6%) concentrations. On NEDs the nitrate prevails in PM1 but its relative contribution is the same in ambient PM1 and PM2.5-1 (20%); in indoor air it constitutes only 2% of PM1 and 10% of PM2.5-1.

Nss-sulphate on the other hand, during episode days is preferentially associated with the supermicron fraction (PM2.5-1), and so is ammonia; the concentration of nss-sulphate in this fraction is 2 times higher than in PM1 and in the case of ammonia 1.6 times higher. The relative contribution follows a similar trend. Indoors, both nss-sulphate and ammonia have a higher concentration in PM1 than in PM2.5-1 which could be attributed to lower infiltration capacity of supermicron particles. As demonstrated earlier, the I/O for sulphate in PM1 was close to 1 on average for all days and much lower in PM2.5. The relative contributions indoors are similar in both size fractions (29% and 26% for EDs and 12% during NEDs). On NEDs slightly higher concentrations of nss-sulphate and ammonia are found in PM1 than PM2.5-1 in indoor as well as ambient air.

The  $\text{NH}_4^+/\text{SO}_4^{2-}$  molar concentration ratios were calculated and were found to be 1.8 and 1.9 for PM2.5 and PM1, respectively, for outdoor concentrations and 0.9 and 0.8 for indoor PM2.5 and PM1 concentrations. The maximum ratio was 3 in PM2.5 and 2.8 in PM1 during one of the episode days. Scatter plots (not shown) of  $\mu\text{equiv}$  concentrations of  $\text{NH}_4^+$  versus  $\text{SO}_4^{2-}$  showed a significant correlation for both outdoor and indoor fractions ( $R^2 = 0.80$  and  $0.72$  for outdoor PM2.5 and PM1, and  $0.98$  for indoor PM2.5 and  $0.99$  for indoor PM1). Generally, at low ammonia concentrations, neutralisation of sulphate is favoured over nitrate; nitrate is stabilised by ammonium at  $\text{NH}_4^+/\text{SO}_4^{2-} > 1.5$ ; this threshold was set at 2 in the study of Squizzato et al. (2013) and references therein. In our study, nitrate dominates over sulphate in ambient air. When the sum of the  $\mu\text{equiv}$  concentrations of  $\text{NO}_3^-$  and  $\text{SO}_4^{2-}$  concentrations were plotted against that of  $\text{NH}_4^+$  (Fig. 4) the  $R^2$  for outdoor values were in the range of 0.97–0.99. The EDs are indicated in red to illustrate their significantly higher concentrations. The slopes of the linear regression lines in all cases suggest an ammonia deficit; therefore invoke the possible role of mineral neutralisation. However, the calcium and magnesium concentrations were very low and one may conclude that an acidic aerosol prevailed. Although Querol et al. (2001) has found the slope value close to 1 for PM2.5 in Barcelona, Spain (1.5 for PM10), others reported ammonium deficits similar to our study, for e.g. Yao et al. (2002) found the slope equal to 1.2–1.4. Taking into account that the average molar concentration ratios, also referred to as a neutralisation ratio (NR) (Bencs et al. (2008), Squizzato et al. (2013)), for  $\text{NH}_4^+/\text{NO}_3^- + \text{nss-SO}_4^{2-}$  are 0.8 and 0.7 outdoors and indoors for PM2.5, and 0.8 for PM1 indoors and outdoors, one can conclude that the ammonium deficit is similar for both environments.

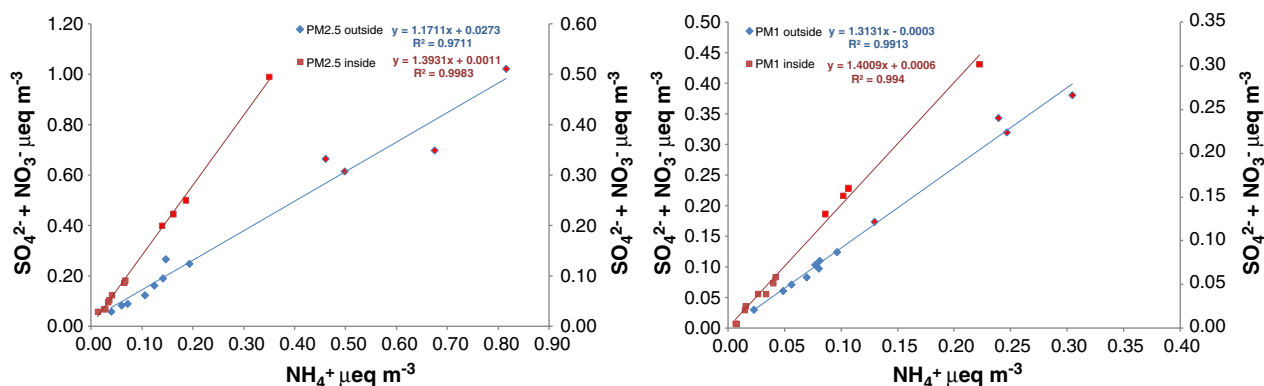


Fig. 4. Correlations between ammonium and the sum of nitrate and sulphate ions in PM1 and PM2.5 (expressed as micro equivalents per  $\text{m}^3$ ).

### 3.3.2. Crustal matter

Crustal matter was calculated using Eq. 1.16 ( $1.90Al + 2.15Si + 1.41Ca + 1.67Ti + 2.09Fe$ ) (Chan et al. (1997), Maenhaut et al. (2002), Sillanpää et al. (2006)). Additionally, enrichment factors were calculated for all elements. Enrichment factor analysis is based on comparison of the specific element's concentration to the concentration of a so-called reference element (Fe in this case) in air relative to their concentration ratio in the Earth's crust (Mason, 1966). The enrichment factor close to one indicates that the crust is the likely source of the element whilst very high EF, points to origin other than crustal. All the abovementioned elements have enrichment factors close to 1 (0.1–2.4), confirming their natural origin. Crustal matter contributes to about 3% ( $2.3 \mu\text{g m}^{-3}$ ) of the total PM<sub>2.5</sub> mass outdoors during episode days and up to 6% ( $1.6 \mu\text{g m}^{-3}$ ) on non-episode days. These values are similar to those found for mineral fraction in Ghent, Belgium, namely 3% for winter PM<sub>2.5</sub> and 4% for summer (Viana et al. (2007a)).

The mineral fraction is preferably associated with the supermicron PM<sub>2.5-1</sub> particles; its concentration in this fraction is higher by a factor of about 4–5, compared to PM<sub>1</sub>. Indoors, this prevalence decreases to a factor of 1.5. Hence, it constitutes 5% of the indoor PM<sub>2.5</sub> on episode days and 8% on NEDs. It is mostly derived from wind-blown soil dust in the outdoor environment or from re-suspension of the floor dust from human activities indoors. It is worth mentioning that the concentration of this fraction in PM<sub>2.5-1</sub> is lower indoors than outdoors ( $I/O = 0.7$ ), whilst in PM<sub>1</sub> it is higher ( $I/O = 2$ , with the exclusion of one detected ( $p < 0.05$ ) outlier of 8). All days were taken into account. Amongst the crust elements analysed, Al outdoors in the PM<sub>1</sub> fraction was often found below the detection limit (9 days out of 12), in indoor PM<sub>1</sub>, only 1 day was below this limit. It may thus lead to some inaccuracies in estimating the contribution of crustal matter outdoors. Other four elements (Ca, Fe, Si, Ti) taken into account for “crustal matter” calculation had concentrations between 2 and 165 times above their respective detection limits in both environments. The inaccuracies are thus not expected to be large. The elevated ratios for indoor PM<sub>1</sub> could be attributed to re-suspension by the movement of people. This was not seen for PM<sub>2.5-1</sub>, perhaps due to much lower outdoor contribution to indoor levels in this fraction than in PM<sub>1</sub>. The indoor PM is a sum of particles generated indoors and those which infiltrated from the outdoor environment. Similarly, Horemans and Van Grieken (2010) found the contribution of soil dust (calculated in the same manner) in PM<sub>1</sub>, collected in offices in Antwerp (Belgium), higher indoors than outdoors during the day and slightly lower during the night, and was explained as being a result of daily office activities, which prevent gravitational settling.

### 3.3.3. Sea salt

Sea salt content was calculated using the concentrations of  $\text{Cl}^-$ ,  $\text{Na}^+$  and a standard composition of sea water. As this approach may have a disadvantage of attributing a part of  $\text{Cl}^-$  which may originate from urban/industrial activities to sea salt, an alternative approach was also tested, which assumes that sea salt contains 30.8% of Na (Maenhaut et al. (2002)). The latter approach may on the other hand overestimate the salt content, since  $\text{Cl}^-$  may be lost from sea salt particles in the atmosphere, especially from the fine PM fraction (Maenhaut et al., 2002; Bencs et al., 2008). Interestingly, during NEDs (and one of the episode days, 13th February, which was influenced by solely regional anticyclonic air masses), the approach using both ions estimated the content of sea salt to be 40% less than the other approach, confirming thus the loss of  $\text{Cl}^-$  ions and overestimation of sea salt content using  $\text{Na}^+$  content only. This did not seem to be the case during the other episode days, where the approach using both the contents of  $\text{Cl}^-$  and  $\text{Na}^+$  ions estimated the salt content to be about 40% higher than when using  $\text{Na}^+$  only. An increase in Cl concentration (both as soluble  $\text{Cl}^-$  and total Cl) was visible during the episode days (except for the 13th of February), in all PM fractions outdoors, whilst  $\text{Na}^+$  concentration remained constant through the whole campaign, with minimal changes

confirming that the increased chloride concentration could not be attributed to sea salt. This can possibly mean that a part of  $\text{Cl}^-$  originated from other sources than sea salt on most days with high pollution and that the sea salt content might be overestimated during those days. Another possibility is as stated by Ye et al. (2003); that the chloride might have originated from the sea salt in large particles but has been displaced by the reaction with nitric acid, followed by the reaction with ammonia to form smaller particles. Higher concentration of pollutants on EDs might have enhanced this process. The fact that the molar ratio of  $\text{Cl}^-/\text{Na}^+$  is not close to unity (if close to one, according to Ye et al. (2003), it may indicate sea salt origin of chloride) further suggests the possible presence of ammonium chloride, which would result in an even more acidic aerosol. Indoors, the chloride concentration was largely reduced compared to respective outdoor values, especially on episode days. I/O ratios of such calculated sea salt were thus 0.5 on EDs and 0.8 on NEDs in both PM<sub>2.5</sub> and PM<sub>1</sub>. Sodium is the only ion that shows the I/O ratio of 1 in both PM fractions. The sea salt contributes to about 3% ( $2.3 \mu\text{g m}^{-3}$ ) of the total ambient PM<sub>2.5</sub> on EDs and 6% on NEDs ( $1.6 \mu\text{g m}^{-3}$ ). It is preferably associated with the supermicron fraction PM<sub>2.5-1</sub>, having about 2 times higher concentration than in fraction PM<sub>1</sub> during NEDs. During EDs these differences are less pronounced (Table 2). Generally, the contribution of this fraction is similar in our study to the results obtained for ambient Ghent PM, where it constituted about 5% ( $1.2 \mu\text{g m}^{-3}$ ) of winter PM<sub>2.5</sub> (Viana et al. (2007a)).

### 3.3.4. Other elements

The fraction “other elements” was calculated similar to the study of Sillanpää et al., 2006, by summation of the Sr, Cr, Ni, Mn, Cu, Zn, As, Pb and V concentrations. For samples below the detection limit, random numbers below the detection limits were generated for the calculation of the averages. This fraction contributes negligibly to the sampled PM, namely 0.3–0.8% of various size ranges (Table 2). Amongst these elements, Sr had the lowest EFs (1.7–2.6), comparable with other soil derived elements. Mn and Cr show medium enrichment, therefore displaying both natural and anthropogenic origins and are followed by slightly higher values for V and Ni. Cu, Zn, As, Pb are highly enriched (EFs > 100), implying mainly anthropogenic origin of those species. The results of concentration measurements and EF calculations are presented in Table 3.

The “other elements” are mostly heavy metals that were present in relatively low concentrations in the outdoor environment and only as

**Table 3**  
The elemental concentrations ( $\text{ng m}^{-3}$ ) of PM<sub>2.5</sub> and PM<sub>1</sub>.

Element	ED	ND	EF <sub>crust</sub>	ED	ND	EF <sub>crust</sub>
	PM <sub>2.5</sub> outdoor			PM <sub>1</sub> outdoor		
As	6	3	433	4	2	1380
Cr	5	3	8	1	<LOD	12
Cu	19	22	101	8	7	135
K	508	259	3	320	165	8
Mn	17	12	4	6	4	5
Ni	9	4	17	5	3	48
Pb	51	31	695	31	17	1660
Sr	2	2	2	1	<LOD	3
V	10	5	12	7	3	39
Zn	137	60	232	63	30	520
	PM <sub>2.5</sub> indoor			PM <sub>1</sub> indoor		
As	5	2	688	3	2	942
Cr	3	2	11	2	1	14
Cu	17	24	156	9	11	163
K	452	212	4	313	152	6
Mn	14	9	4	7	4	4
Ni	6	3	18	4	2	31
Pb	40	22	715	26	15	1124
Sr	3	2	3	1	<LOD	2
V	8.1	3	12	6	3	23
Zn	108	40	250	60	28	398

trace quantities in the indoor air. A few remarks concerning these elements are however of importance. In general, Pb had one of the highest concentrations in this class, ranging from  $15 \text{ ng m}^{-3}$  (NEDs indoor PM1) to  $51 \text{ ng m}^{-3}$  (EDs ambient PM2.5). The National Ambient Air Quality Standard (NAAQS) for Pb (3 months rolling  $0.15 \text{ } \mu\text{g m}^{-3}$ ) is therefore not exceeded, neither was it exceeded under the New European Directive (Directive 2008/50/EC – <http://ec.europa.eu/environment/air/quality/legislation/directive.htm>) where the standard is  $0.5 \text{ } \mu\text{g m}^{-3}$  based on a yearly average. The new directive that came into play on 31.12.2012 (<http://ec.europa.eu/environment/air/quality/standards.htm>) for As ( $6 \text{ ng m}^{-3}$ ) was exceeded during EDs for PM2.5, but it should be noted that our concentrations are reported as 24-h averages and the standard is an annual average. Other elemental concentrations regulated by the new directive are Ni and Cd, both of which were well below the standard. Except for Cu and Cr, all other minors and traces in general exhibited increases in concentration on EDs, ranging from 1.1 to 2.5 times higher than on NEDs. It is also noticeable that V, Fe and Ni showed on average a 1.9 increase in concentration during EDs. These three metals are of interest as Jacobs et al. (2012) reported a significant association between their concentrations and the systolic blood pressure and pulse pressure of the elderly in this (and 5 other) old age homes. During non-episode days the concentration levels of elements in this group are comparable with the levels reported in other studies of outdoor PM2.5 in Antwerp, Belgium (Götschi et al. (2005), Stranger et al. (2009)). On EDs only Cu and Zn exceeded levels reported as winter average for Antwerp (Götschi et al. (2005)) by 1.4 times. In another work by Horemans and Van Grieken, (2010), 12 h (both day and night) PM1 and PM2.5 averages calculated for those

elements inside offices in Antwerp, were much higher than our NEDs' indoor levels. On EDs, Zn, Ni and V were elevated in our study by 1.5–3.5 times.

Elements such as: As, Ni, Pb, V and Zn accumulate to a large extent in the fine fraction as opposed to for example Ti; Fig. 5 shows the fractional distributions (PM1 and PM2.5-1) of these elements with Ti given for comparison. They are characterised by high PM1/PM2.5 ratios of 0.5–0.7 in ambient air and 0.6–0.7 in indoor air. These ratios generally increase for indoor air compared to outdoor air as expected due to the ease of infiltration of fine particles. Additionally, in Fig. 5, sulphur was shown as it exhibits the largest difference in the fractional distribution between EDs and NEDs (about 20%). For other elements a variation below 10% can be seen.

Pearson correlation coefficients (not shown) were calculated for these elements to investigate which of them may originate from a common source. Cr was excluded from correlation analyses as it was detected in about 50% cases only. Amongst other elements, V correlated very well with Ni ( $r = 0.92$ ,  $p < 0.001$  for PM2.5 outdoors) both are considered as originating in Europe from oil combustion (Swietlicki and Krejci (1996)). Their concentration was two times higher on EDs compared to NEDs. Cu did not correlate with other elements from this group; it is fairly correlated with Ca, Si and Ti in ambient PM1 ( $r = 0.66$ – $0.72$ ,  $p = 0.008$ – $0.020$ ); what may suggest some contribution of re-suspended road dust source as Cu is a known tracer for break wear (Viana et al. (2007b), Cyrus et al. (2003)). In PM2.5 these correlations are weaker ( $r = 0.43$ – $0.63$ ) and are only significant for Ca ( $r = 0.62$ ,  $p = 0.028$ ). Other anthropogenic origin elements (Zn, As, Pb) correlated very well with each other ( $r > 0.71$ – $0.95$ ,  $p < 0.01$ ) both in PM1 and PM2.5. Of interest is a very high

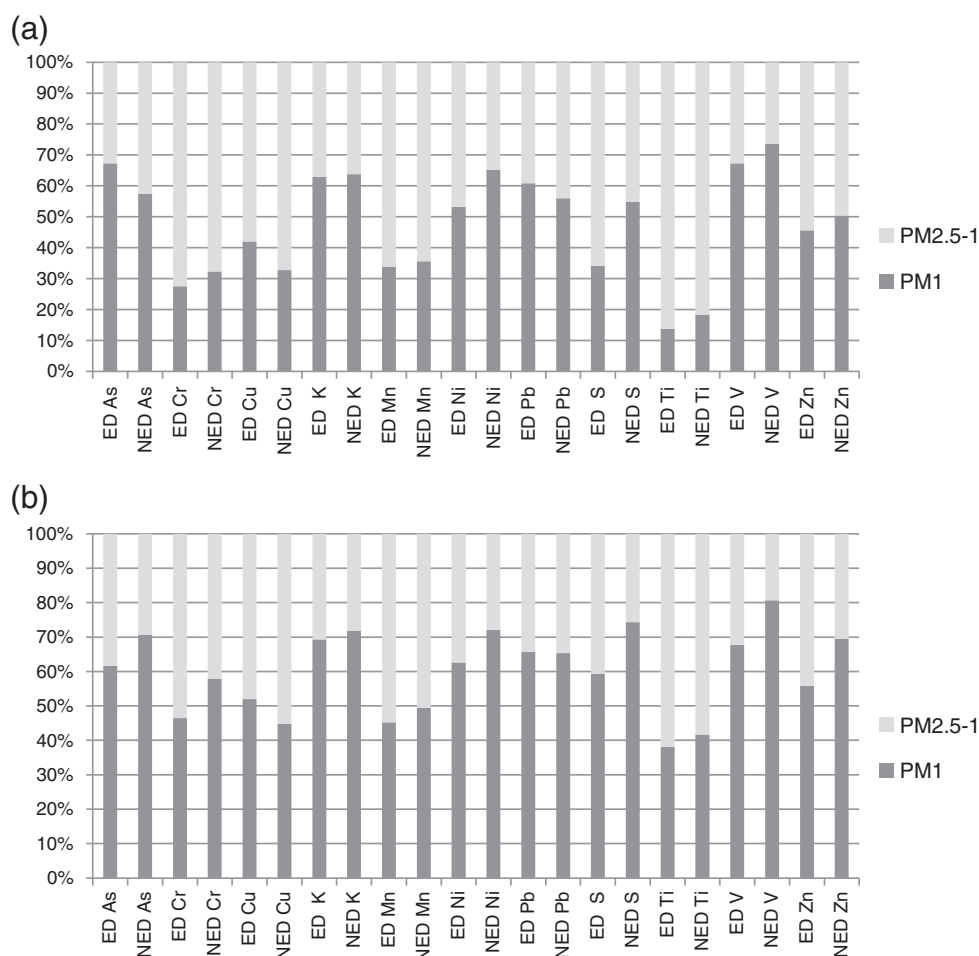


Fig. 5. Partitioning of various elements between PM1 and PM2.5-1 fractions outdoors (a) and indoors (b) during EDs and NEDs.

correlation between Zn, K and Cl ( $r = 0.97\text{--}0.99$ ,  $p < 0.001$ ) in ambient PM1. In PM2.5, the correlation between Zn and K is still high ( $r = 0.99$ ,  $p < 0.001$ ) but with Cl it is slightly weaker ( $r = 0.74\text{--}0.77$ ,  $p < 0.01$ ), probably because of higher contribution of sea salt Cl in this fraction. K is generally associated with biomass combustion (Götschi et al. (2005)) and waste incinerators (Maenhaut et al. (2002)) whilst Zn, is considered to originate from traffic and/or industrial activities such as non-ferrous smelters. Cl, apart from its natural sea salt origin, is thought to originate from industrial emissions of hydrochloric acid and from waste incineration (Götschi et al. (2005)). As already mentioned, the air masses influencing the high pollution days created an anticyclone over the territories of Belgium, The Netherlands and Germany, favouring the accumulation of pollutants not only from local traffic emissions and local industrialised areas (Antwerp) but also from more distant locations such as for example highly industrialised Ruhr region (Stranger, 2005) in Germany.

### 3.3.5. Smoke

The contribution of smoke (or non-crustal K) was calculated as concentration of K – 0.6 of that of Fe (Maenhaut et al. (2002)). This fraction contributes to about 0.5% of PM2.5 ( $0.3 \mu\text{g m}^{-3}$ ), it is preferentially associated with PM1, ranging from 0.7% in ambient PM1 on EDs to 1.2% of indoor PM1 during NEDs. The indoor concentration equals outdoor, as already mentioned elsewhere, due to the high efficiency of fine particles to penetrate the building envelope. The average concentration of this fraction during episode days is twice as high as that on normal days.

### 3.4. Ion balance

In order to evaluate the acid–base balance of aerosols the ion balance equations (Shen et al., 2009; Zhang et al., 2002) were calculated in both PM fractions according to Eqs. (1) and (2) for cations (C) and anions (A), respectively, whereby the concentration for each ion is in  $\mu\text{g m}^{-3}$ . The contribution of  $\text{Mg}^{2+}$  and  $\text{Ca}^{2+}$  were very low, in agreement with Stranger, 2005, thus random numbers were generated for samples which exhibited levels lower than LODs.

$$C(\mu\text{Eq m}^{-3}) = \frac{[\text{NH}_4^+]}{18} + \frac{[\text{Na}^+]}{23} + \frac{[\text{K}^+]}{39} + \frac{[\text{Mg}^{2+}]}{12} + \frac{[\text{Ca}^{2+}]}{20} \quad (1)$$

$$A(\mu\text{Eq m}^{-3}) = \frac{[\text{NO}_3^{2-}]}{62} + \frac{[\text{SO}_4^{2-}]}{48} + \frac{[\text{Cl}^-]}{35.5} \quad (2)$$

The C/A ratios were subsequently calculated. On average, during the episode days all fractions, except for PM2.5 indoors, were slightly acidic ( $C/A = 0.9$ ), whilst on normal days the aerosol particles were on average slightly basic with the C/A values between 1 and 1.3 for different fractions. Statistically significant differences between EDs and NEDs were, however, only found indoors in PM2.5 ( $p = 0.009$ ) and PM1 ( $p = 0.022$ ). During EDs the C/A values in outdoor PM2.5 ranged between 0.82 and 1.08, whilst in PM1, between 0.80 and 0.91. During NEDs in outdoor PM2.5 variation between 0.74 and 1.30 was found and in PM1 between 0.93 and 1.33. Indoors, during EDs PM2.5 C/A values were between 0.90 and 1.02 and in PM1 between 0.89 and 0.91, on NEDs these values ranged from 0.96 to 1.58 in PM2.5 and 0.98 to 1.47 in PM1 (in this fraction two values above 3 were seen). Neutral to alkaline aerosols coincided with the minimas of the registered PM mass (third week of the study, Fig. 2), thus both anions and cations showed lower concentrations than during other days of the study. The highest sea salt content was registered (2 days out of 4) on those days, and a direct influence of North Sea and Atlantic Ocean air masses was noticed.

## 4. Conclusions

A comprehensive insight into the composition of PM2.5 and PM1 on high and low pollution days and outdoor to indoor comparisons of PM sampled in old-age home was provided. This paper is complementary to a study by Jacobs et al., 2012, which investigated acute, short-term health effects of PM and its composition in the elderly part of the population. Extremely high ambient PM2.5 and PM1 values were registered during some days of this study. The investigation of PM composition revealed that although all components were found to be considerably higher during episode days than during non-episode days, it was the secondary inorganic aerosols that contributed the most towards an increase in the PM pollution as their relative contribution was higher by a factor of 1.6. Therefore, the episode days were not only influenced by a limited pollutant dilution connected to occurrence of temperature inversions, but also most probably by an increased formation of secondary inorganic pollutants due to preferable meteorological conditions. The 120 h air mass backward trajectories influencing the high pollution days showed anticyclonic scenarios with no or less direct influences of the North Sea or Atlantic Ocean air masses than during the low pollution days. The anticyclone was formed over the territories of Belgium, The Netherlands and Germany thus facilitating the accumulation of both local and regional pollutants. Natural contribution (mineral dust and sea salt) was relatively less important on EDs than NEDs, the same was true for the “other elements” which included mostly heavy metals and for unaccounted mass which is in our study most probably composed of OC, EC and water. An ammonium deficit for PM was deducted in this study, especially on EDs. On average, the PM fractions on EDs were then slightly acidic ( $C/A = 0.9$ ), whilst on normal days more variations were seen, and C/A ranged from acidic to alkaline ( $C/A > 1\text{--}1.3$ ) in ambient air. Neutral to alkaline aerosols coincided with the minimas of the registered PM mass. Amongst heavy metals Zn and Pb were found at the highest concentrations in both PM2.5 and PM1.

No significant sources of indoor pollutants could be identified inside the old-age home. Generally, the PM1 mass concentration decreased indoors by 29% compared to outdoors, whilst PM2.5-1 fraction by 57%; this decrease was similar on EDs and NEDs. This is in agreement with the fact that fine mode particles penetrate the building envelope easier than supermicron mode. High correlations were found between outdoor and indoor PM, confirming the mainly outdoor origin of air pollution inside the Czagani old-age home.

Supplementary data to this article can be found online at <http://dx.doi.org/10.1016/j.scitotenv.2014.04.102>.

## Conflict of interest

There is no conflict of interest that the author is aware of. Reviewers have been chosen due to their respective areas of expertise and fields that they are currently publishing in.

## Acknowledgements

The work reported in this paper was financed by the Belgian Science Policy under the Science for Sustainable Development programme (SD/HE/01), the Flemish Scientific Fund (FWO:G.0873.11). We thank the direction and staff of the elderly homes for their support. The authors are thankful to the partners of the project Lotte Jacobs, Tim Nawrot and Benoit Nemery for taking care of project organization, Andy Delcoo, Jo Dewulf and Hugo De Backer from Royal Meteorological Institute, Brussels, Belgium for supplying the meteorological data. We acknowledge Dr. Laszlo Bencs for assistance regarding backward trajectory analyses and two reviewers for their constructive comments. The authors gratefully acknowledge the NOAA Air Resources Laboratory (ARL) for the provision of the HYSPLIT transport and dispersion model and/or READY website (<http://www.ready.noaa.gov>) used in this publication.

## References

- Avigo JD, Godoi FL, Janissek PR, Makarovska Y, Krata A, Potgieter-Vermaak S, et al. Particulate matter analysis at elementary schools in Curitiba, Brazil. *Anal Bioanal Chem* 2008;391:1459–68.
- Bell ML, Ebisu K, Peng RD, Samet JM, Dominici F. Hospital Admissions and chemical composition of fine particle air pollution. *Am J Respir Crit Care Med* 2009;179:1115–20.
- Bencs L, Ravindra K, de Hoog J, Rasoazanany EO, Deutsch F, Bleux N, et al. Mass and ionic composition of atmospheric fine particles over Belgium and their relation with gaseous air pollutants. *J Environ Monit* 2008;10:1148–57.
- Chan YC, Simpson RW, Mctainsh GH, Volwles PD, Cohen DD, Bailey GM. Characterisation of chemical species in PM<sub>2.5</sub> and PM<sub>10</sub> aerosols in Brisbane, Australia. *Atmos Environ* 1997;37:3773–85.
- Chao CY, Wong KK. Residential indoor PM10 and PM2.5 in Hong Kong and the elemental composition. *Atmos Environ* 2002;36:265–77.
- Chen SJ, Hsieh LT, Tsai CC, Fang GC. Characterization of atmospheric PM10 and related chemical species in southern Taiwan during the episode days. *Chemosphere* 2003;53:29–41.
- Cheng L, Sandhu HS, Angle RP, Myrick RH. Characteristics of inhalable particulate matter in Alberta cities. *Atmos Environ* 1998;32:3835–44.
- Cyrys J, Stölzel M, Heinrich J, Kreyling WG, Menzel N, Wittmaack K, et al. Elemental composition and sources of fine and ultrafine ambient particles in Erfurt, Germany. *Sci Total Environ* 2003;305:143–56.
- Di Ciaula A. Emergency visits and hospital admissions in aged people living close to a gas-fired power plant. *Eur J Intern Med* 2012;23:53–8.
- Fuentes-Leonarte V, Tenías JM, Ballester F. Levels of pollutants in indoor air and respiratory health in preschool children: a systematic review. *Pediatr Pulmonol* 2009;44:231–43.
- Geller MD, Chang M, Sioutas C, Ostro BD, Lipsett M. Indoor/outdoor relationship and chemical composition of fine and coarse particles in the southern California deserts. *Atmos Environ* 2002;36:1099–110.
- Gemenetzi P, Moussas P, Arditoglou A. Mass concentration and elemental composition of indoor PM2.5 and PM10 in University rooms in Thessaloniki, northern Greece. *Atmos Environ* 2006;40:3195–206.
- Götschi T, Hazenkamp-von Arx ME, Heinrich J, Bono R, Burney P, Fosberg B. Elemental composition and reflectance of ambient fine particles at 21 European locations. *Atmos Environ* 2005;39:5947–58.
- Horemans B, Van Grieken R. Speciation and diurnal variation of thoracic, fine thoracic and sub-micrometer airborne particulate matter at naturally ventilated office environments. *Atmos Environ* 2010;44:1497–505.
- Jacobs L, Buczyńska A, Walgraeve C, Delcloo A, Potgieter-Vermaak S, Van Grieken R, et al. Acute changes in pulse pressure in relation to constituents of particulate air pollution in elderly persons. *Environ Res* 2012;117:60–7.
- Jones NC, Thornton CA, Mark D, Harrison RM. Indoor/outdoor relationship of particulate matter in domestic homes with roadside, urban and rural locations. *Atmos Environ* 2000;34:2603–12.
- Lai HK, Kendall M, Ferrier H, Lindup I, Alm S, Hänninen O. Personal exposures and micro-environment concentrations of PM2.5, VOC, NO<sub>2</sub>, CO in Oxford, UK. *Atmos Environ* 2004;38:6399–410.
- Maenhaut W, Cafmeyer J, Dubtsov S, Chi X. Detailed mass size distributions of elements and species, and aerosol chemical mass closure during fall 1999 at Gent, Belgium. *Nucl Inst Methods Phys Res B* 2002;189:238–42.
- Mason S. Principles of geochemistry. New York: Wiley; 1966. p. 45–6.
- Meng QY, Turpin BJ, Lee JH, Polidori A, Weisel CP, Morandi M, et al. How does infiltration behavior modify the composition of ambient PM2.5 in indoor spaces? An analysis of RIOPA data. *Environ Sci Technol* 2007;41:7315–21.
- Parker JL, Larson RR, Eskelson E, Wood EM, Veranah JM. Particle size distribution and composition in a mechanically ventilated school building during air pollution episodes. *Indoor Air* 2008;18:386–93.
- Pataud J-P, Raes F, Van Dingenen R, Brüggemann E, Facchini M-C, Decesari S, et al. A European aerosol phenomenology-2: chemical characteristics of particulate matter at kerbside, urban, rural and background sites in Europe. *Atmos Environ* 2004;38:2579–95.
- Querol X, Alastuey A, Rodriguez S, Plana F, Ruiz CR, Cots N, et al. PM10 and PM2.5 source apportionment in the Barcelona Metropolitan area, Catalonia, Spain. *Atmos Environ* 2001;35:6407–19.
- Querol X, Alastuey A, Ruiz CR, Artiñano B, Hansson HC, Harrison RM, et al. Speciation and origin of PM10 and PM2.5 in selected European cities. *Atmos Environ* 2004a;38:6547–55.
- Querol X, Alastuey A, Viana MM, Rodriguez S, Artiñano B, Salvador P, et al. Speciation and origin of PM10 and PM2.5 in Spain. *Aerosol Sci* 2004b;35:1151–72.
- Ram K, Sarin MM, Sudheer AK, Rengarajan R. Carbonaceous and secondary inorganic aerosols during wintertime fog and haze over urban sites in the Indo-Gangetic plain. *Aerosol Air Qual Res* 2012;12:359–70.
- Shen Z, Cao J, Arimoto R, Han Z, Zhang R, Han Y, et al. Ionic composition of TSP and PM2.5 during dust storms and air pollution episodes at Xi'an, China. *Atmos Environ* 2009;43:2911–8.
- Sillanpää M, Hillamo R, Saarikoski S, Frey A, Pennanen A, Makkonen U, et al. Chemical composition and mass closure of particulate matter at six urban sites in Europe. *Atmos Environ* 2006;40:S212–23.
- Squizzato S, Masiol M, Brunelli A, Pistollato S, Tarabotti E, Rampazzo G, et al. Factors determining the formation of secondary inorganic aerosol: a case study in the Po Valley (Italy). *Atmos Chem Phys* 2013;13:1927–39.
- Strak M, Janssen NAH, Godri KJ, Gosens I, Mudway IS, Cassee FR, et al. Respiratory health effects of airborne particulate matter: the role of particle size, composition, and oxidative potential. *Environ Health Perspect* 2012;123:1183–9.
- Stranger M. Characterisation of health related particulate and gas-phase compounds in multiple indoor and outdoor sites in Flanders [PhD dissertation] University of Antwerp; 2005.
- Stranger M, Potgieter-Vermaak SS, Van Grieken R. Comparative overview of indoor air quality in Antwerp, Belgium. *Environ Int* 2007;33:789–97.
- Stranger M, Potgieter-Vermaak SS, Van Grieken R. Particulate matter and gaseous pollutants in residences in Antwerp, Belgium. *Sci Total Environ* 2009;407:1182–92.
- Swietlicki E, Krejci R. Source characterisation of the Central European atmospheric aerosol using multivariate statistical methods. *Nucl Inst Methods Phys Res B* 1996;109(110):519–25.
- Vecchi R, Marazzan G, Valli G, Ceriani M, Antoniazzi C. The role of atmospheric dispersion in the seasonal variation of PM1 and PM2.5 concentration and composition in the urban area of Milan (Italy). *Atmos Environ* 2004;38:443–444.
- Vercauteren J, Matheeußen C, Wauters E, Roekens E, Van Grieken R, Krata A, et al. Chemkar PM10: an extensive look at the local differences in chemical composition of PM10 in Flanders, Belgium. *Atmos Environ* 2011;45:108–16.
- Viana M, Maenhaut W, Chi X, Querol X, Alastuey A. Comparative chemical mass closure of fine and coarse aerosols at two sites in south and west Europe: implications for EU air pollution policies. *Atmos Environ* 2007a;41:315–26.
- Viana M, Querol X, Götschi T, Alastuey A, Sunyer J, Forsberg B, et al. *Atmos Environ* 2007b;41:1395–406.
- Wichmann J, Janssen NAH, van der Zee S, Brunekreef B. Traffic-related differences in indoor and personal absorption coefficient measurements in Amsterdam, the Netherlands. *Atmos Environ* 2005;39(38):7384–92.
- World Health Organisation. Air quality in Europe - 2011 report; 2011. <http://www.eea.europa.eu/publications/air-quality-in-europe-2011/download>.
- Yao X, Chan CK, Fang M, Cadle S, Chan T, Mulawa P, et al. The water-soluble ionic composition of PM2.5 in Shanghai and Beijing, China. *Atmos Environ* 2002;36:4223–34.
- Ye B, Ji X, Yang H, Yao X, Chan CK, Cadle S, et al. Concentration and chemical composition of PM2.5 in Shanghai for a 1-year period. *Atmos Environ* 2003;37:499–510.
- Zhang XY, Cao JJ, Li LM, Arimoto R, Cheng Y, Huebert B, et al. Characterization of atmospheric aerosol over XiAn in the south margin of the Loess Plateau, China. *Atmos Environ* 2002;36:4189–99.



## Influence on the oxidative potential of a heavy-duty engine particle emission due to selective catalytic reduction system and biodiesel blend



Ricardo H.M. Godoi<sup>a,\*</sup>, Gabriela Polezer<sup>a</sup>, Guilherme C. Borillo<sup>a</sup>, Andrew Brown<sup>b</sup>, Fabio B. Valebona<sup>a</sup>, Thiago O.B. Silva<sup>a</sup>, Aline B.G. Ingberman<sup>a</sup>, Marcelo Nalin<sup>c</sup>, Carlos I. Yamamoto<sup>d</sup>, Sanja Potgieter-Vermaak<sup>b</sup>, Renato A. Penteado Neto<sup>e</sup>, Mary Rosa R. de Marchi<sup>f</sup>, Paulo H.N. Saldiva<sup>g</sup>, Theotonio Pauliquevis<sup>h</sup>, Ana Flavia L. Godoi<sup>a</sup>

<sup>a</sup> Environmental Engineering Department, Federal University of Parana, Curitiba, PR, Brazil

<sup>b</sup> Division of Chemistry and Environmental Science, School of Science and the Environment, Manchester Metropolitan University, Manchester, UK

<sup>c</sup> LAVIE - Institute of Chemistry, São Paulo State University - UNESP, Araraquara, Brazil

<sup>d</sup> Chemical Engineering Department, Federal University of Parana, Curitiba, PR, Brazil

<sup>e</sup> Vehicle Emissions Laboratory, Institute of Technology for Development (LACTEC), Curitiba, PR, Brazil

<sup>f</sup> Analytical Chemistry Department, Institute of Chemistry, São Paulo State University - UNESP, Araraquara, Brazil

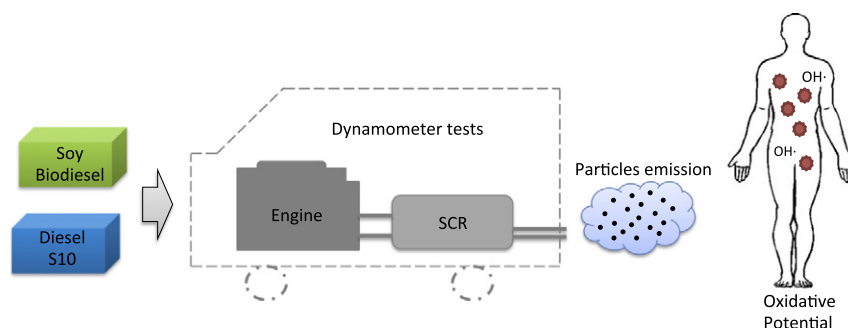
<sup>g</sup> Laboratory of Experimental Air Pollution, Department of Pathology, School of Medicine, University of São Paulo, São Paulo, Brazil

<sup>h</sup> Department of Natural and Earth Sciences, Federal University of São Paulo, Diadema, Brazil

### HIGHLIGHTS

- PM emission from biodiesel burning may be more harmful to human health than diesel.
- Euro V (SCR) engine fuelled with B5 and B20 tested in a bench dynamometer
- Electron Spin Resonance (ESR) to access the oxidative potential of PM emission
- Add biodiesel in the fuel blend increases OP while SCR system reduces it.
- Free radicals generation due biodiesel can cause deleterious effects in health.

### GRAPHICAL ABSTRACT



### ARTICLE INFO

#### Article history:

Received 20 January 2016

Received in revised form 16 March 2016

Accepted 4 April 2016

Available online 19 April 2016

Editor: D. Barcelo

#### Keywords:

Oxidative potential  
Diesel emission  
Biodiesel emission  
Particulate matter

### ABSTRACT

Although the particulate matter (PM) emissions from biodiesel fuelled engines are acknowledged to be lower than those of fossil diesel, there is a concern on the impact of PM produced by biodiesel to human health. As the oxidative potential of PM has been suggested as trigger for adverse health effects, it was measured using the Electron Spin Resonance ( $OP^{ESR}$ ) technique. Additionally, Energy Dispersive X-ray Fluorescence Spectroscopy (EDXRF) was employed to determine elemental concentration, and Raman Spectroscopy was used to describe the amorphous carbon character of the soot collected on exhaust PM from biodiesel blends fuelled test-bed engine, with and without Selective Catalytic Reduction (SCR).  $OP^{ESR}$  results showed higher oxidative potential per kWh of PM produced from a blend of 20% soybean biodiesel and 80% ULSD (B20) engine compared with a blend of 5% soybean biodiesel and 95% ULSD (B5), whereas the SCR was able to reduce oxidative potential for each fuel. EDXRF data indicates a correlation of 0.99 between concentration of copper and oxidative potential. Raman Spectroscopy centered on the expected carbon peaks between  $1100\text{ cm}^{-1}$  and  $1600\text{ cm}^{-1}$  indicate lower molecular disorder for the B20 particulate matter, an indicative of a more graphitic carbon structure. The analytical

\* Corresponding author at: Environmental Engineering Department, Federal University of Parana, 210 Francisco H. dos Santos St., Curitiba, PR 81531-980, Brazil.  
E-mail address: [rhmgodoi@ufpr.br](mailto:rhmgodoi@ufpr.br) (R.H.M. Godoi).

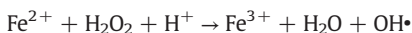
techniques used in this study highlight the link between biodiesel engine exhaust and increased oxidative potential relative to biodiesel addition on fossil diesel combustion. The EDXRF analysis confirmed the prominent role of metals on free radical production. As a whole, these results suggest that 20% of biodiesel blends run without SCR may pose an increased health risk due to an increase in OH radical generation.

© 2015 Elsevier B.V. All rights reserved.

## 1. Introduction

Particulate matter (PM) from anthropogenic sources is of particular concern to human health and has been associated with adverse health effects (Wjst et al., 1993; Kim et al., 2004; Gauderman et al., 2005; Tonne et al., 2007; Ryan et al., 2007). Such effects are linked to particles size, composition, concentration and sources (Davidson et al., 2005; Smekens et al., 2005; Viana et al., 2008; Lee and Hieu, 2011). One particularly notable source of harmful particulate emissions is diesel engines. The PM output from these engines have been linked to cardiopulmonary mortality and morbidity including cancer (Tarkiainen et al., 2003; Nemmar et al., 2007; Peretz et al., 2008; Rivero et al., 2005; Benbrahim-Tallaa et al., 2012). Despite the increase in the health risk being relatively small, the incidence of exposure is high, thus demonstrating its significant importance as the population is exposed (Lim et al., 2012). Accordingly, technologies to reduce emissions associated with diesel vehicles have been implemented (Gill et al., 2012; Borillo et al., 2015). Examples include diesel particulate filters (DPFs), aftertreatment exhaust emission systems (e.g. selective catalyst reduction - SCR). In addition, in light of renewal energy sources, biodiesel is promoted as a sustainable source (Cheng et al., 2008; Hu et al., 2009; Chin et al., 2012).

In short, biodiesel is an ester-based fuel obtained from different vegetable oils, and in some countries, has become accepted as a partial or total substitute for fossil fuels. Introduction of Diesel engines operating with biodiesel is widespread in Brazil, where the majority of this study is based. It is imperative that biofuel emissions are of a higher quality than those of traditional diesel engines for biodiesel to be a suitable alternative. Literature indicates the reduction of PM mass concentration due to use of biodiesel compared to fossil diesel (Lapuerta et al., 2008; Büniger et al., 2012; Guo et al., 2014). Similarly, SCR aftertreatment engines have been shown to reduce the quantity of PM produced and gases (Tadano et al., 2014). However, it has been suggested that despite the reduced mass concentrations of PM, cytotoxicity and pro-inflammatory marker increase with use of biodiesel relative to fossil diesel release (Kooter et al., 2011; Swanson et al., 2011; Gerlofs-Nijland et al., 2013). The effect of engine exhaust particles on oxidative potential is of particular interest for this study because of its well documented association with acute and chronic health effects (Halliwell and Gutteridge, 1999; Valko et al., 2007; Patel et al., 2011). The specific cause of excess free radical production is yet to be proved conclusively (Betha et al., 2012). One possible explanation is the increased quantity of organic matter output from biodiesel fuelled engines, oxidizing once access is gained to the body (Yanamala et al., 2013). The contribution of organic content is again estimated by Jung et al. (2006) who report increased hydroxyl radical (OH•) production as a result of flame soot, compared to carbon black. However these concepts differ from the conventional explanation the influence of metal species. The Fenton reaction describes the production of OH• by the reduction of hydrogen peroxide and simultaneous oxidation of transition metal ions (Shi et al., 2003). Although the example equation features oxidation of iron, this process is observed for other metals such as copper (Kadiiska and Mason, 2002), tin (Lilley et al., 2013), chromium (Lou et al., 2013), even aluminium, despite the fact it only exists in one oxidation state (Kumar and Gill, 2014).



The primary objective of this study is to assess the probable oxidative stress caused by exposure to PM of diesel and biodiesel fuelled

engines using SCR aftertreatment. This was achieved by using the electron spin resonance analysis in order to measure the free radicals generation due to PM emitted by different aftertreatment/fuel settings. Raman spectroscopy and Energy Dispersive X-ray fluorescence spectroscopy (EDXRF) experimentation were carried out to provide a more in-depth understanding of the free radical chemical nature in biodiesel and diesel.

## 2. Experimental section

### 2.1. PM collection

Collection of total PM took place at Institute of Technology for Development, Lactec, Curitiba, Brazil. The engine emissions testing facilities used an engine dynamometer and an engine equipped with a urea SCR aftertreatment system, in accordance with the Euro V standard.

Table 1 shows the characteristics of the tested engine. The tested engine has an individual four-valve cylinder head, cross-flow arrangement; common rail injection system with 1800 bars and engine brake “power brake.” It is used in trucks, minibuses and buses. The engine has a power output of 187 HP (2200 rpm), a peak torque of 720 Nm and follows the European Union regulation no. 715/2007 requirements Euro V with urea-SCR system. The European Union (EU) adopted Euro V engine since 2009 and the Euro VI engine in 2013. In Brazil, due to technological delays, especially according to high sulfur concentration in diesel fuel, the Euro V engine was established in 1 January 2012, through the PROCONVE seventh campaign. Nowadays, around 140,000 trucks and 30,000 buses equipped with SCR systems are being used in Brazil (Anfavea, 2013).

This engine works in conjunction with an AVL SESAM i60 FT dynamometer, 440 kW power output at 6,000 rpm and 2,334 Nm of torque. This set up uses the European Steady Cycle (ESC) test set up in accordance with the European emission regulations directive 1999/96/EC. The ESC uses different engine and dynamometer settings, designed to simulate a variety of different speeds and load weights, to allow collection of PM. The fuels used in this study were a blend of ultra-low sulfur diesel (ULSD) (10 ppm sulfur content) and soybean biodiesel in the following proportions: 5% (B5) and 20% biodiesel (B20). The same biodiesel were used to produce the B5 and B20 blends. The rationale behind this choice is two pronged: Firstly, to show the effect of 5% versus 20% biodiesel additions on emission profiles and secondly, both are representative of current usage all over the world. Total PM for each of these fuels was collected both with and without the SCR treatment, thus a total of four different conditions were analyzed in this study.

**Table 1**  
Characteristics of tested engine.

Specifications	
Configuration	Euro V ‘Heavy Duty’/proconve P7
Valves/cylinder	4
Displacement	4.8 L
Bore × stroke	105 × 137 mm
Combustion system	Direct injection
Injection system	Common rail electronic
Aspiration	TGV intercooler
Power output	187 cv (139.7 kW) 2200 rpm
Peak torque	720 Nm (73 kgf m <sup>-1</sup> ) 1200–1600 rpm
Aftertreatment	SCR

**Table 2**  
Results from the fuel characterization.

Parameters	B20	B5	Standard test methods
Flashpoint (°C)	70.5	68.5	ASTM D93
Total sulfur (mg kg <sup>-1</sup> )	6	1	ASTM D5453
Specific mass (kg m <sup>-3</sup> )	848.1	841.6	ASTM D4052
Colour	Yellow	Yellow	Visual
Aspect	Clear and free from impurities	Clear and free from impurities	ABNT NBR 14954
Viscosity (mm <sup>2</sup> s <sup>-1</sup> )	3.2	3.0	ASTM D445
Cetane number	51.0	53.1	ASTM D6890

The B5 and B20 fuels were previously characterized according to methods and essays described on American (ASTM) and Brazilian (NBR) standardization, results are presented on the Table 2. Total PM was collected on Teflon coated glass fiber filters (T60A20, Pallflex®, Ann Arbor, MI, U.S.A.) with a constant volume sampler (smart sampler, AVL, Graz, Austria) to simulate PM dilution with air. The air dilution must be set such as the exhaust diluted gas temperature measured immediately before the first filter does not exceed 325 K (52 °C). The dilution ratio must not be less than four. The motor data acquisition system was an Engine Computer Aided Test (E-Cat) from Sp Tronic (Guarulhos, Brazil) that can store data of temperature, pressure, rotation, torque and power simultaneously during tests execution. In order to evaluate just the effects of B5 and B20 biodiesel blends and aftertreatment system on oxidative potential, all engine tests were validated to achieve the lower variations on the other experimental parameters, according to directive 1999/96/EC of European Union. Therefore the tests with higher variations were not considered for the present study.

## 2.2. Oxidative potential

Oxidative potential (OP), as predictor for oxidative stress, was measured by Electron Spin Resonance (OP<sup>ESR</sup>) with the spin-trap 5,5-dimethyl-1-pyrroline-*N*-oxide (DMPO) in presence of hydrogen peroxide (H<sub>2</sub>O<sub>2</sub>). The analyses were performed in a Miniscope MS 400 (MT MagnetTech GmbH, Berlin, Germany).

The methodology was based on the one demonstrated by Shi et al. (2003) with adaptations regarding the exclusion of the resuspension and filtering steps, as recommended by Hellack et al. (2014). One filter per each condition ( $n = 1$ ) and two blank filters were cut in the middle and one half inserted in a vial and 0.5 mL of deionized water, 1 mL of 0.05 M DMPO ( $\geq 98\%$  ELSD, Enzo Life Science, Farmingdale, NY, U.S.A.) and 0.5 mL of 0.5 M H<sub>2</sub>O<sub>2</sub> (p.a., Sigma-Aldrich, St. Louis, MO, U.S.A.), both prepared in a Dulbecco's chloride and calcium free phosphate Buffer (PBS) (premium, Sigma-Aldrich, St. Louis, MO, U.S.A.), were added. Vials content were mixed by vortexing (Vortex Genie-2, Scientific Industries, Bohemia, NY, U.S.A.) for 20 s, followed by being placed in a water bath shaker (type 1092, GFL, Burgwedel, Germany) at 37 °C at 150 rpm for 15 min, then vortexed again for 10 s. Finally, capillaries of 50  $\mu$ L (Hirschmann Laborgeraete, Eberstadt, Germany) were placed in the upper layer of the mixture and filled in order to transfer the extracts

to the instrument, in which the analysis was performed. 10  $\mu$ M copper sulfate (CuSO<sub>4</sub>) (p.a., Sigma-Aldrich also, St. Louis, MO, U.S.A.) in PBS was used as the positive control because of its known ability in inducing Fenton type reactions (Hellack et al., 2014). Deionized water was used as the negative control. The controls were mixed with DMPO and H<sub>2</sub>O<sub>2</sub> in the same ratio as for the samples and handled as described above.

The OP<sup>ESR</sup> settings for all measurements were the following: 3390 G magnetic field, 100 G sweep width, 3 scans of 30 s, 2000 mG modulation amplitude and 5E1 gain. The resulting OP<sup>ESR</sup> spectrum consists of four different peaks and the higher its amplitudes are, the higher is the PM elicited OH generation. Results are achieved by calculating the average of its total amplitudes and are expressed as arbitrary units (AU) (Hellack et al., 2014). Those were reported as emission factors in terms of the engine energy output (AU kWh<sup>-1</sup>) in order to show the potential risk of implementing each fuel and exhaust technology.

## 2.3. Bulk elemental profile

Information concerning the bulk elemental concentration is provided by energy-dispersive X-ray fluorescence (EDXRF). The measurements of total PM were performed on a Minipal-4 (PANalytical, Almelo, The Netherlands) equipped with a Silicon Drift Detector (SDD) which is cooled thermo-electrically. For the analysis, a tube voltage of 30 kV, a current of 0.3 mA and an acquisition time of 600 s were selected, in a He-atmosphere, without any further step of sample preparation. The equipment was set to detect a comprehensive list of bulk elements: Si, S, K, Fe, Cu, Ga, Mg, Ca, Ti, Cr, Mn, Co, Ni, Zn, Br, Sr, Ag, Sn, Ba, Pb and Se. The system calibration of the applied EDXRF method was based on thin film reference standards (Micromatter, Seattle, WA, USA) and validated by the measurement of various thin layer standards for each element and a reference material from NIST (2783 air particulate on filter media).

Metals such as Fe, Cr, Co, Mn, Cu and Zn were selected for analysis because of their ability to produce reactive oxygen species (ROS) as part of the Fenton chemistry (Rico et al., 2009; Verma et al., 2010). It was preferred to assess a broad range of elements due to the complex mechanisms that may trigger oxidative stress and the initial stage of OP<sup>ESR</sup> analysis of engine PM emissions (Shi et al., 2003; Pan et al., 2004).

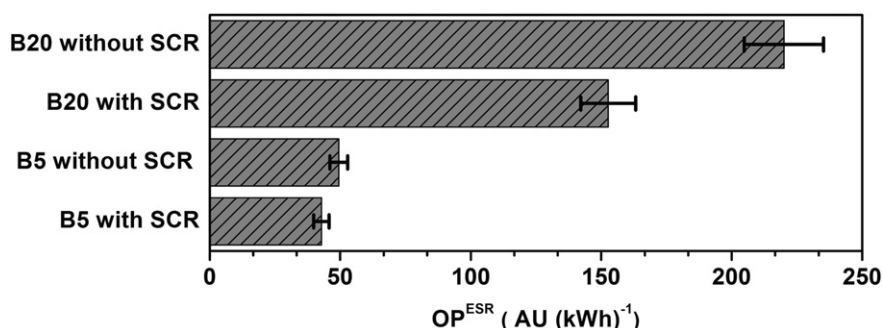


Fig. 1. PM OP<sup>ESR</sup> per kWh and standard deviation for each operational setting of the engine.

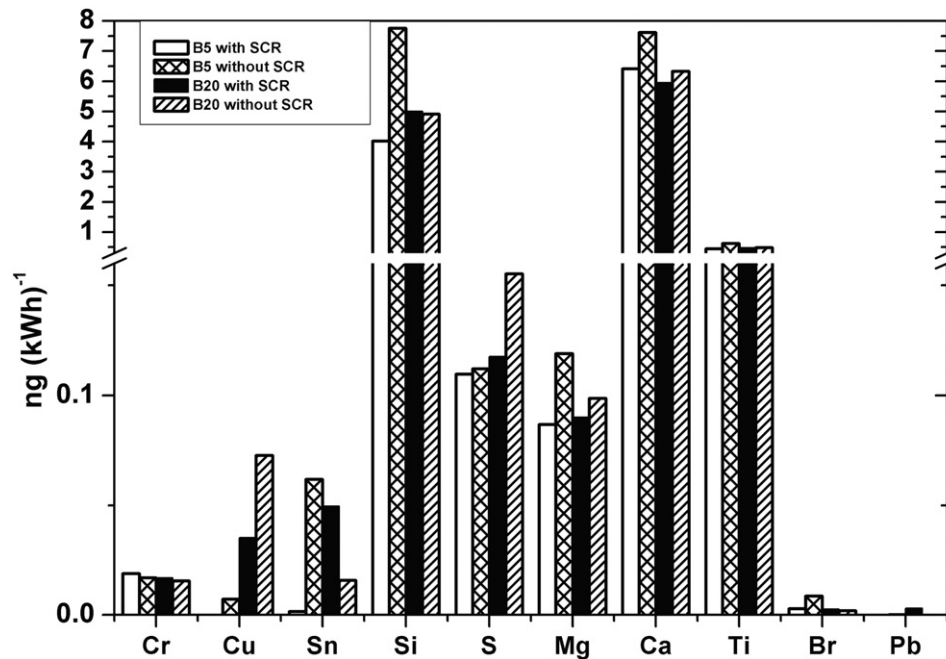


Fig. 2. Detected bulk elemental concentrations in each engine condition as determined by EDXRF.

#### 2.4. Raman spectroscopy

The sampling of individual particles for analysis by Raman Spectroscopy was conducted using a May Impactor connected to the diluter, allowing control of the time and rate of air sampling. The May Impactor consists of seven sampling stages that segregate the particles by aerodynamic diameter (May, 1945). For the analysis, particles with diameter  $<0.25 \mu\text{m}$  were sampled, which were impacted on surface-enhanced Raman spectroscopy substrates made of a thin gold film. The SERS substrates used to collect the soot were 2D photonic crystals (PC) measuring  $1 \times 1 \text{ cm} \times 90 \text{ nm}$  in thickness. PC was prepared using a holographic setup following the methodology developed by Menezes et al. (2006). A LabRAM Jobin-Yvon-HORIBA micro-Raman, equipped with a 632.8 nm He-Ne laser and  $50\times$  white light objective, was used for obtaining the Raman spectra (Soewono and Rogak, 2011). Several spots were analyzed to ensure representative results and minimize variance.

The amorphous carbon character of the soot collected can be described by their respective Raman spectra. Literature proposes 2 models to fit the rather broad Raman features, two-band and five-band model. The two-band model does not take into account the various D bands describing the  $\text{sp}^2/\text{sp}^3$  character and therefore we opted for the five-band fitting proposed by Sadezky et al. (2005) (G, D1, D2, D3, and D4 at about 1580, 1350, 1500, 1620, and  $1200 \text{ cm}^{-1}$ ). The G band is designated to the E2g symmetry stretching mode of the  $\text{sp}^2$  graphitic lattice. The D1 band according to the classic approach is assigned to the breathing mode of  $\text{sp}^2$  atoms and is called the defect band (Ferrari, 2007). The D3 band has been assigned to defects outside the plane of aromatic layers like tetrahedral carbons, while the D4 band is assigned to  $\text{sp}^3$  or  $\text{sp}^2\text{-sp}^3$  bonded atoms and is normally only present in disordered amorphous C. The D2 band's assignment is still debatable and is only present if there is disorder.

### 3. Results and discussion

#### 3.1. Oxidative potential

The resulting signals were well ranged between the negative and positive controls and were normalized to give units of  $\text{AU kWh}^{-1}$ . The

results are presented in Fig. 1. AU is used for Arbitrary Units. The standard deviation of positive control analyzed in five consecutive days prior and after the experiment analyses was calculated in order to check the equipment stability, resulting in a value of 6.9%.

The results achieved for this study show that use of B20 increases the  $\text{OP}^{\text{ESR}}$  of PM per kWh compared to B5 fuel. For each fuel, we can observe that the use of SCR reduces  $\text{OP}^{\text{ESR}}$ , a 30.6% and 13.5% decrease was observed for B20 and B5 respectively.

As outlined in the introduction, one of the primary motivations for this study is to assess the potential harm when using biodiesel blends and aftertreatment of the exhaust. In this study, the major impacts in PM emission factor variations is the use of biodiesel blend, due to its known property of reducing PM mass emission (USEPA, 2002; Xue et al., 2011; Gerlofs-Nijland et al., 2013). In order to assess the impact on human health due to different engine settings, it is relevant to evaluate the results in terms of engine operational metrics (Gerlofs-Nijland et al., 2013). This was achieved by representing the results in terms of the recommended unit in the European emission regulations directive

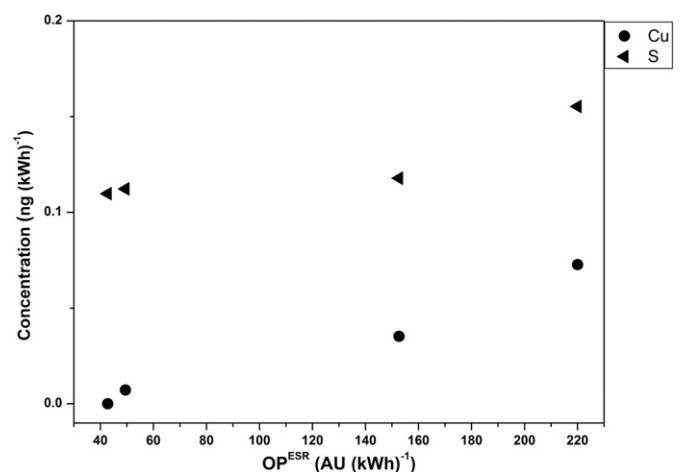


Fig. 3. Correlation between concentration of Cu and S and  $\text{OP}^{\text{ESR}}$ .

**Table 3**  
Pearson correlation between concentration of metals and OP<sup>ESR</sup>.

Si	S	Cu	Mg	Ca	Ti	Cr	Br	Sn	Pb
−0.29	0.89	0.99	−0.22	−0.57	−0.34	−0.81	−0.62	−0.11	0.26

1999/96/EC (kWh), showing that the implementation of soy biodiesel can actually enhance the OP<sup>ESR</sup> risk.

The toxicity impact of biodiesel blending and aftertreatment technologies is contrary to studies previously conducted. Kooter et al. (2011) used the dithiothreitol (DTT) catalytic reduction of oxygen to measure the OP of diesel and pure plant oil biodiesel blends PM emissions in terms of kWh. The results showed that B0 and B20 had more or less the same OP. Gerlofs-Nijland et al. (2013) assessed the OP of diesel and rape-seed methyl-ester biodiesel blend by means of DTT and ascorbic acid consumption rate per distance driven and found that the use of B50 reduced or maintained the OP. However, when OP was analyzed in mass unit basis, some studies revealed that biodiesel can lead to PM with higher OP (Cheung et al., 2009; Gerlofs-Nijland et al., 2013). Moreover, in the majority of these studies, there was no coherence among results of different analyses of toxicity assessment (e.g.: cytotoxicity, cytokines release, oxidative stress and mutagenicity). As mentioned, the health risks are eventually determined by the amount inhaled, and OP per kWh is therefore a more useful metric to assess the health impacts.

In relation to the SCR technology, the results showed that its use reduces the OP<sup>ESR</sup> of emitted particles per kWh. Biswas et al. (2009) found a significant reduction in the OP of exhaust particles per distance driven from a heavy-duty engine when equipped with SCR technology. The authors suggest that the OP of particles is affected by catalytic surfaces and the semi volatile organics absorbed on the surface of soot particles. Moreover, among oxidant catalyzers, filter catalyzers or SCR all seems to have variables degrees of influence in changing the composition and reactivity of PM.

At the present moment, there is no single method to assess the overall OP activity of PM. Various assays to measure OP are sensitive to different groups of compounds. The DTT consumption rate is based on the ability of active reductants compound associated with PM to transfer electrons from DTT to oxygen, and are known to be sensitive to organic compounds, especially quinones emitted from diesel exhaust (Ayres et al., 2008). Ascorbic acid depletion analysis and ESR, on the other hand, are particularly sensitive to the presence of transition metals (Ayres et al., 2008; Yang et al., 2014). Furthermore, different results among several studies may be a consequence of different study configurations (Gerlofs-Nijland et al., 2013). Different factors such as, engine technology, fuel type and the use of catalyzers and filters may affect the composition and thus, the toxicity of the engine exhaust mixture, which complicates the comparison among experiments. An example would be the increased, equal or decreased toxicity potential reported from biodiesel emission studies (Bünger et al., 2000; Cheung et al., 2009; Jalava et al., 2010; Kooter et al., 2011; Swanson et al., 2011; Gerlofs-Nijland et al., 2013).

OP<sup>ESR</sup> has been suggested to be a feasible analysis for continued PM monitoring, due to its correlation with health effects, simplicity and versatility to be used with standard monitoring filters (Hellack et al., 2014). The present study showed variations among the different engine settings (SCR aftertreatment and biodiesel blends) in terms of the OP<sup>ESR</sup>

with the spin trap DMPO in the presence of H<sub>2</sub>O<sub>2</sub>. Therefore, there is a need of further investigations of the potential health effects of emissions of soy biodiesel usage. Besides this technique may be revealed as a tool for assessing PM properties beyond mass in engine testing and monitoring.

### 3.2. Bulk elemental concentrations

Among the analyzed elements only Cr, Cu, Sn, Si, S, Mg, Ca, Ti, Br and Pb presented detectable mass. Fig. 2 presents the bulk elemental concentrations as determined by EDXRF. It can be observed that there are only two samples that indicated detectable presence of lead, these low lead concentrations were expected as use of lead in fuels has been outlawed. As these values appear insignificant, the lead data will not be considered further in this discussion. Liati et al. (2013) indicate that Cr, Cu, Si, Sn and Ti are common in diesel output, originating from various components of the engine, while Ca, Mg and S emission are commonly related to lubricating oil additives. This appears to be consistent with the Cr and Ti data obtained from this study. EDXRF analysis indicates fairly consistent concentrations of Cr and Ti independent of fuel type or use of SCR, thus implying that the source is the engine components rather than the fuel. This is perhaps not the case with the Cu, as a large variation in concentration can be observed between B5 and B20. The Sn, Si, Ca and Mg data appears to show no pattern and is therefore very difficult to discern the potential sources. It can be observed that there is no relationship between the concentration of these metals and the use of SCR. This is illustrated in Fig. 2. Interestingly, sources for metals in biodiesel can include leaching from storage containers. Yaakob et al. (2014) indicate that copper is particularly susceptible to this. The Cu results presented could indicate evidence of this.

As indicated in the previous section, OP<sup>ESR</sup> assumed the order: B20 without SCR > B20 with SCR >> B5 without SCR > B5 with SCR. This same pattern also existed for the concentration of copper and sulfur in each sample. Fig. 3 plots OP<sup>ESR</sup> against concentration of these elements to show correlation between its concentrations and OP. The spearman correlation between oxidative potential and bulk elemental concentrations of all detected elements is presented in Table 3. It can be observed that there is a strong correlation ( $R = 0.99$ ) between concentration of copper and OP<sup>ESR</sup>, the ability of copper to oxidize and produce radicals is documented in literature, the results in this study could be indicative of the role of copper on OP<sup>ESR</sup>. Furthermore, there is evidence in literature, which suggests a link between copper and OP<sup>ESR</sup> (Shi et al., 2003; Hellack et al., 2014; Janssen et al., 2014). Another good correlation ( $R = 0.88$ ) was obtained for sulfur. Shi et al. (2003) suggest that other inorganic components than metals, such as sulfate may affect the oxidant activity of PM. Cheng et al. (2008) found higher levels of sulfate in a biodiesel car emission than a petrodiesel one, despite the zero sulfur level in the biodiesel fuel, what was suggested to be due to lube oil sulfur. What is also interesting is the strong negative correlation present between chromium and OP<sup>ESR</sup>. The pattern observed here with chromium is contrary to that observed in literature where chromium in both the common +3 and +6 oxidation states are observed to increase OP (Khan et al., 2012; Lou et al., 2013). Results for other elements, such as Si, Mg, Ca, Ti and Br also indicated negative correlation with OP<sup>ESR</sup>. However, it is important to note that a low or negative correlation with OP<sup>ESR</sup> does not eliminate the potential toxicity of these elements as there are many other potential pathways of PM toxicity (Biswas et al., 2009).

**Table 4**  
Average band positions, FWHM, and Intensity ratios of some of the Raman bands identified for the different fuels with and without SCR.

	D1	WD1	D2 + G	W G + D2	D3	WD3	ID3/IG + D2	ID1/IG + D2
B20 with SCR	1328 ± 1	192 ± 8	1600 ± 3	68 ± 2	1532 ± 7	157 ± 10	1.93 ± 0.42	4.83 ± 0.77
B20 without SCR	1327 ± 0.1	170 ± 3	1599 ± 1	70 ± 3	1524 ± 5	163 ± 12	1.72 ± 0.20	3.72 ± 0.50
B5 with SCR	1326 ± 4	172 ± 14	1599 ± 3	68 ± 13	1523 ± 3	174 ± 10	1.86 ± 0.33	4.20 ± 0.58
B5 without SCR	1327 ± 1	152 ± 12	1602 ± 1	67 ± 12	1531 ± 93	139 ± 21	1.80 ± 0.8	3.83 ± 0.49

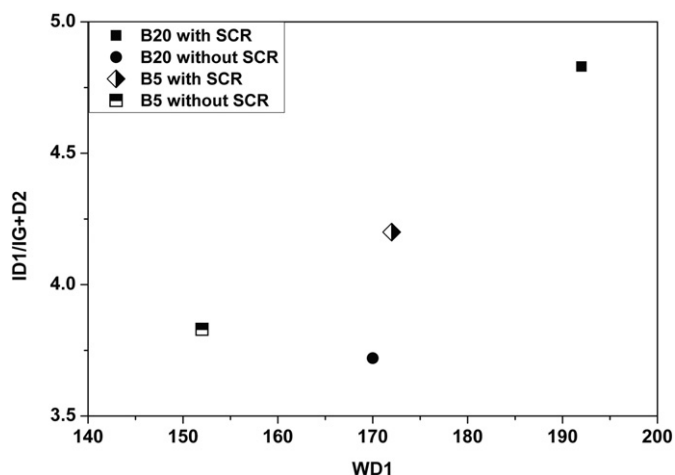


Fig. 4. The FWHM of the D1 band versus ID1/IG + D2 ratio for both fuels investigated and with and without SCR.

### 3.3. Raman spectroscopy

The deconvolution was performed by using WIRE® software. The best fit was obtained by Lorentzian-Gaussian-shaped bands for all identified bands. The D2 band could not be deconvoluted from the G band and the combined G + D2 band is observed and fitted around  $1600\text{ cm}^{-1}$ . To avoid confusion this band will be referred to as the G + D2 band, to indicate that we are not referring to the graphitic band on its own. In this study the band positions were assigned as follows: G + D2 between  $1597$  and  $1604\text{ cm}^{-1}$ , D1 between  $1326$  and  $1333\text{ cm}^{-1}$ , D3 between  $1520$  and  $1539\text{ cm}^{-1}$ , and D4 between  $1167$  and  $1196\text{ cm}^{-1}$ . These values are in fair agreement with those published by Soewono and Rogak (2011). Table 4 provides some more data on the deconvoluted spectra.

Discrimination of amorphous character of the particles can be discerned from the FWHM of the D1 band. It is observed that in general the B20 had more amorphous character due to a wider D1 band, in accordance with Soewono and Rogak (2011), but in contrast to Song et al. (2006) and Lapuerta et al. (2008). It is also observed that an increase in biodiesel content suggests an increase in disorder. This has also been observed by Xu et al. (2013) and explained as the production of heavier polycyclic hydrocarbons during the pyrolysis process, which could coalesce to form amorphous structures. Furthermore, the use of the SCR seems to increase the amorphous nature of the soot as illustrated in Fig. 4. This is also in agreement with the D3/G + D2 intensity

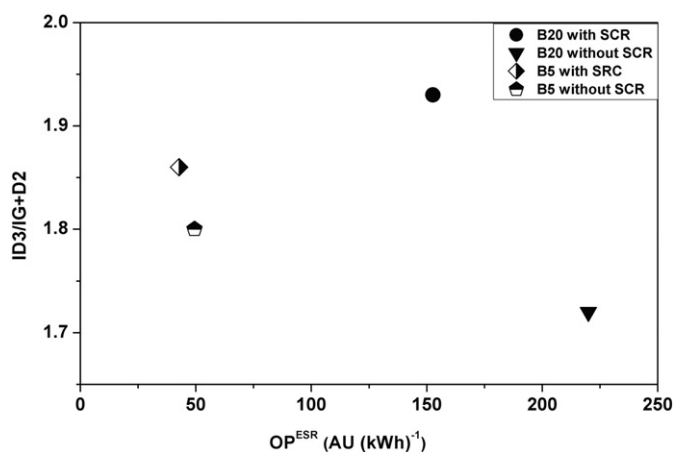


Fig. 5. The oxidation potential versus ID3/IG + D2 ratio for both fuels investigated and with and without SCR.

ratios, indicating the presence of tetrahedral carbons. This contradicts the findings of Soewono and Rogak (2011), reporting ID/IG ratios of similar proportions than those reflected in Table 4 for B20 and B5 (3.2–5.2), where aftertreatment had the opposite effect.

There is an apparent inverse correlation between the  $OP^{ESR}$  and disorder. It seems as the  $OP^{ESR}$  increases for B20 so does the disorder decrease, which is also the case for the B5 although to a much lesser extent, as illustrated in Fig. 5.

However, overall the highest graphitic structure (B20 without SCR) showed the highest  $OP^{ESR}$ , which agrees with the study of Jung et al. (2006), outlining a ten-fold increase in  $OH\cdot$  production for more graphitic structures (USEPA, 2002).

## 4. Conclusions

The primary objective of this study is to assess the probable oxidative stress caused by exposure to PM of diesel and biodiesel fuelled engines using SCR aftertreatment system. This study assessed a substantial increase (~4.5 times) in  $OP^{ESR}$  when proportional of biodiesel is rise from 5% to 20%. The use of an SCR aftertreatment system suppressed the  $OP^{ESR}$  in all fuel evaluated.

The Raman results suggest that an increase in biodiesel content will lead to an increase in disorder of the amorphous carbons emitted when the engine is run with SCR, while the opposite is true when it is run without SCR. The highest graphitic content showed the highest  $OP^{ESR}$ , which was displayed by B20 without SCR. EDXRF data shows that concentrations of copper under each fuel condition were strongly correlated with OP. The highest  $OP^{ESR}$  reported to the highest Cu concentration, which was again displayed by the B20 blend run without SCR.

These results, therefore, suggest that 20% biodiesel blends run without SCR may pose an increased health risk due to an increase in OH radical generation. However, these results will have to be supplemented by additional studies including 100% of Biodiesel and pure fossil diesel to make conclusive statements in this regard.

The current results have paramount importance to inform the potential impact of Biodiesel blends on emission profiles and related health risks. This information may be of interest to the policy makers mainly for countries that already set the use of Biodiesel as USA and E.U. and for countries that have not yet adopted the use of Euro V emission standards like China, India, Australia, or Russia, as well as those already adopting it.

## Acknowledgement

The authors would like to thank Dr. Cassee from Center for Environmental Health Research, National Institute for Public Health and the Environment (RIVM) by the support with  $OP^{ESR}$  analysis. This work was supported financially by the National Council for Scientific and Technological Development (CNPq), Process Number 402391/2009-8.

## References

- Anfavea, 2013. National Association of Automobile Manufacturers—Brazil. Brazilian Automotive Industry Yearbook (<http://www.anfavea.com.br/Anuario.html>, Accessed Sep 2013).
- Ayres, J.G., Borm, P., Cassee, F.R., Castranova, V., Donaldson, K., Ghio, A., Harrison, R.M., Hider, R., Kelly, F., Kooter, I.M., Marano, F., Maynard, R.L., Mudway, I., Nel, A., Sioutas, C., Smith, S., Baeza-Squiban, A., Cho, A., Duggan, S., Froines, J., 2008. Evaluating the toxicity of airborne particulate matter and nanoparticles by measuring oxidative stress potential—a workshop report and consensus statement. *Inhal. Toxicol.* 20, 75–99.
- Benbrahim-Tallaa, L., Baan, R.A., Grosse, Y., Lauby-Secretan, B., El Ghissassi, F., Bouvard, V., Guha, N., Loomis, D., Straif, K., 2012. Carcinogenic of diesel-engine and gasoline-engine exhausts and some nitroarenes. *Lancet Oncol.* 13, 663–664.
- Betha, R., Pavagadhi, S., Sethu, S., Hande, M.P., Balasubramanian, R., 2012. Comparative in vitro cytotoxicity assessment of airborne particulate matter emitted from a stationary engine fuelled with diesel and waste cooking oil-derived biodiesel. *Atmos. Environ.* 61, 23–29.
- Biswas, S., Verma, V., Schauer, J.J., Cassee, F.R., Cho, A.K., Sioutas, C., 2009. Oxidative potential of semi-volatile and non volatile particulate matter (pm) from heavy-duty vehicles retrofitted with emission control technologies. *Sci. Total Environ.* 43, 3905–3912.

- Borillo, G.C., Tadano, Y.S., Godoi, A.F.L., Santana, S.S.M., Weronka, F.M., Penteado Neto, R.A., Rempel, D., Yamamoto, C.I., Potgieter-Vermaak, S., Potgieter, J.H., Godoi, R.H.M., 2015. Effectiveness of selective catalytic reduction systems on reducing. *Sci. Total Environ.* 49, 3246–3251.
- Bünger, J., Krahl, J., Baum, K., Schröder, O., Müller, M., Westphal, G., Ruhnau, P., Schulz, T.G., Hallier, E., 2000. Cytotoxic and mutagenic effects, particle size and concentration analysis of diesel engine emissions using biodiesel and petrol diesel as fuel. *Arch. Toxicol.* 74 (8), 490–498.
- Bünger, J., Krahl, J., Schroder, O., Schmidt, L., Westphal, G.A., 2012. Potential hazards associated with combustion of bio-derived versus petroleum-derived diesel fuel. *Crit. Rev. Toxicol.* 42, 732–750.
- Cheng, C.H., Cheung, C.S., Chan, T.L., Lee, S.C., Yao, C.D., Tsang, K.S., 2008. Comparison of emissions of a direct injection diesel engine operating on biodiesel with emulsified and fumigated methanol. *Fuel* 87, 1870–1879.
- Cheung, K.L., Polidori, A., Ntziachristos, L., Tzamkiozis, T., Samaras, Z., Cassee, F.R., Gerlofs, K., Sioutas, C., 2009. Chemical characteristics and oxidative potential of particulate matter emissions from gasoline, diesel, and biodiesel cars. *Sci. Total Environ.* 43, 6334–6340.
- Chin, J., Batterman, S.A., Northrop, W.F., Bohac, S.V., Assanis, D.N., 2012. Gaseous and particulate emissions from diesel engines at idle and under load: comparison of biodiesel blend and ultralow sulphur diesel fuels. *Energy Fuel* 26, 6737–6748.
- Davidson, C.I., Phalen, R.F., Solomon, P.A., 2005. Airborne particulate matter and human health: a review. *Aerosol Sci. Technol.* 39, 737–749.
- Ferrari, A., 2007. Raman spectroscopy of graphene and graphite: disorder, electron-phonon coupling, doping and nonadiabatic effects. *Solid State Commun.* 143, 47–57.
- Gauderman, W.J., Avol, E., Lurmann, F., Kuenzli, N., Gilliland, F., Peters, J., McConnell, R., 2005. Childhood asthma and exposure to traffic and nitrogen dioxide. *Epidemiology* 16, 737–743.
- Gerlofs-Nijland, M.E., Totlandsdal, A.I., Tzamkiozis, T., Leseman, D.L., Samaras, Z., Låg, M., Schwarze, P., Ntziachristos, L., Cassee, F.R., 2013. Cell toxicity and oxidative potential of engine exhaust particles: impact of using particulate filter or biodiesel fuel blend. *Sci. Total Environ.* 47, 5931–5938.
- Gill, S.S., Turner, D., Tzolakis, A., York, A.P.E., 2012. Controlling soot formation with filtered EGR for diesel and biodiesel fuelled engines. *Sci. Total Environ.* 46, 4215–4222.
- Guo, J., Ge, Y., Hao, L., Tan, J., Li, J., Feng, X., 2014. On-road measurements of regulated pollutants from diesel and cng buses with urea selective catalytic reduction system. *Atmos. Environ.* 99, 1–9.
- Halliwell, B., Gutteridge, J.M.C., 1999. *Free Radicals in Biology and Medicine*. Oxford University Press.
- Hellack, B., Yang, A., Cassee, F.R., Janssen, N.A., Schins, R.P., Kuhlbusch, T.A., 2014. Intrinsic hydroxyl radical generation measurements directly from sampled filters as a metric for the oxidative potential of ambient particulate matter. *J. Aerosol Sci.* 72, 47–55.
- Hu, Y., Griffiths, K., Norton, P.R., 2009. Surface science studies of selective catalytic reduction of NO: progress in the last ten years. *Surf. Sci.* 603, 1740–1750.
- Jalava, P.L., Tapanainen, M., Kuusalo, K., Markkanen, A., Hakulinen, P., Happonen, M.S., Pennanen, A.S., Ihalainen, M., Yli-Pirilä, P., Makkonen, U., Teinilä, K., Mäki-Paakkanen, J., Salonen, R.O., Jokiniemi, J., Hirvonen, M.R., 2010. Toxicological effects of emission particles from fossil- and biodiesel-fueled diesel engine with and without doc/poc catalytic converter. *Inhal. Toxicol.* 22, 48–58.
- Janssen, N.A.H., Yang, A., Strak, M., Steenhof, M., Hellack, B., Gerlofs-Nijland, M.E., Kuhlbusch, T., Kelly, F., Harrison, R., Brunekreef, B., Hoek, G., Cassee, F., 2014. Oxidative potential of particulate matter collected at sites with different source characteristics. *Sci. Total Environ.* 472, 572–581.
- Jung, H., Guo, B., Anastasio, C., Kennedy, I.M., 2006. Quantitative measurements of the generation of hydroxyl radicals by soot particles in a surrogated lung fluid. *Atmos. Environ.* 40, 1043–1052.
- Kadiiska, M.B., Mason, R.P., 2002. In vivo copper-mediated free radical production: an spin-trapping study. *Spectrochim. Acta Part A* 58, 1227–1239.
- Khan, F.H., Ambreen, K., Fatima, G., Kumar, S., 2012. Assessment of health risks with reference to oxidative stress and DNA damage in chromium exposed population. *Sci. Total Environ.* 430, 68–74.
- Kim, J.J., Smorodinsky, S., Lipsitt, M., Singer, B.C., Hodgson, A.T., Ostro, B., 2004. Traffic-related air pollution near busy roads – the east bay children’s respiratory health study. *Am. J. Respir. Crit. Care Med.* 170, 520–526.
- Kooter, I.M., Van Vugt, M.A.T.M., Jedynska, G., Tromp, P.C., Houtzager, M.M.G., Verbeek, R.P., Kadijk, G., Mulderij, M., Krul, C.A.M., 2011. Toxicological characterisation of diesel engine emissions using biodiesel and closed soot filter. *Atmos. Environ.* 45, 1574–1580.
- Kumar, V., Gill, K.D., 2014. Oxidative stress and mitochondrial dysfunction in aluminium neurotoxicity and its amelioration: a review. *Neurotoxicology* 41, 154–166.
- Lapueta, M., Rodriguez-Fernandez, J., Agudelo, J.R., 2008. Diesel particulate emissions from used cooking oil. *Bioresour. Technol.* 99, 731–740.
- Lee, B.K., Hieu, N.T., 2011. Seasonal variation and sources of heavy metals in atmospheric aerosols in a residential area of Ulsan, Korea. *Aerosol Air Qual. Res.* 11, 679–688.
- Liati, A., Schrieder, D., Eggenschwiler, P.D., Dasilva, Y.A.R., 2013. Metal particle emission in the exhaust stream of diesel engines: and electron microscope study. *Sci. Total Environ.* 47, 14495–14501.
- Lilley, T.M., Ruokolainen, L., Meierjohann, A., Kanerva, M., Stauffer, J., Laine, V.N., Atosuo, J., Lilius, E.M., Nikinmaa, M., 2013. Resistance to oxidative damage but not immunosuppression by organic tin compounds in natural populations of Daubenton’s bats (*Myotis daubentonii*). *Comp. Biochem. Physiol. Part C: Toxicol. Pharmacol.* 157, 298–305.
- Lim, S.S., Vos, T., Flaxman, A.D., et al., 2012. A comparative risk assessment of burden of disease and injury attributable to 67 risk factors and risk factor in 21 regions, 1990–2010: a systematic analysis for the global burden of disease study 2010. *Lancet* 380, 2224–2260.
- Lou, J., Jin, L., Wu, N., Tan, Y., Song, Y., Gao, M., Liu, K., Zhang, X., He, J., 2013. DNA damage and oxidative stress in human b lymphoblastoid cells after combined exposure to hexavalent chromium and nickel compounds. *Food Chem. Toxicol.* 55, 533–540.
- May, K.R., 1945. The cascade impactor: an instrument for sampling coarse aerosols. *J. Sci. Instrum.* 22 (10), 187.
- Menezes, J.W., Cescaio, L., Carvalho, E.J., Braga, E.S., 2006. Recording different geometries of 2D hexagonal photonic crystals by choosing the phase between two-beam interference exposures. *Opt. Express* 14 (19), 8578–8583.
- Nemmar, A., Al-Maskari, S., Ali, B.H., Al-Amri, I.S., 2007. Cardiovascular and lung inflammatory effects induced by systemically administered diesel exhaust particles in rats. *Am. J. Physiol. Lung Cell. Mol. Physiol.* 292, I664–I670.
- Pan, C.J.G., Schmitz, D.A., Cho, A.K., Froines, J., Fukuto, J.M., 2004. Inherent redox properties of diesel exhaust particles: catalysis of the generation of reactive oxygen species by biological reductants. *Toxicol. Sci.* 81 (1), 225–232.
- Patel, H., Eo, S., Kwon, S., 2011. Effects of diesel particulate matter on inflammatory responses in static and dynamic culture of human alveolar epithelial cells. *Toxicol. Lett.* 200, 124–131.
- Peretz, A., Kaufman, J.D., Trenga, C.A., Allen, J., Carlsten, C., Aulet, M.R., Adar, S.D., Sullivan, J.H., 2008. Effects of diesel exhaust inhalation on heart rate variability in human volunteers. *Environ. Res.* 107, 178–184.
- Rico, D., Martin-Gonzalez, M., Diaz, S., De Lucas, D., Gutierrez, J., 2009. Heavy metals generate reactive oxygen species in terrestrial and aquatic ciliated protozoa. *Comp. Biochem. Physiol. Part C: Toxicol. Pharmacol.* 149, 90–96.
- Rivero, D.H., Soares, S.R., Lorenzi-Filho, G., Saiki, M., Godleski, J.J., Antonangelo, L., Dolhnikoff, M., Saldiva, P.H., 2005. Acute cardiopulmonary alterations induced by fine particulate matter of Sao Paulo, Brazil. *Toxicol. Sci.* 85, 898–905.
- Ryan, P.H., Lemasters, G.K., Biswas, P., Levin, L., Hu, S., Lindsey, M., Bernstein, D.I., Lockey, J., Villareal, M., Khurana, Hershhey, G.K., Grinshpun, S.A., 2007. A comparison of proximity and land use regression traffic exposure models and wheezing in infants. *Environ. Health Perspect.* 115, 278–284.
- Sadezky, A., Muckenhuber, H., Grothe, H., Niessner, R., Pöschl, U., 2005. Raman microspectroscopy of soot and related carbonaceous materials: spectral analysis and structural information. *Carbon* 43, 1731–1742.
- Shi, T., Schins, R.P., Knaapen, A.M., Kuhlbusch, T., Pitz, M., Heinrich, J., Borm, P.J., 2003. Hydroxyl radical generation by electron paramagnetic resonance as a new method to monitor ambient particulate matter composition. *J. Environ. Monit.* 5, 550–556.
- Smekens, A.; Godoi, R.H.M.; Berghmans, P.; Van Grieken, R., 2005. Characterisation of soot emitted by domestic heating, aircraft and cars using diesel or biodiesel. *J. Atmos. Chem.*, Volume 52, Issue 1, pp 45–62.
- Soewono, A., Rogak, S., 2011. Morphology and raman spectra of engine-emitted particulates. *Aerosol Sci. Technol.* 45.
- Song, J., Alam, M., Boehman, A.L., Kim, U., 2006. Examination of the oxidation behaviour of biodiesel soot. *Combust. Flame* 146, 589–604.
- Swanson, K.J., Kado, N.Y., Funk, W.E., Pleil, J.D., Madden, M.C., Ghio, A.J., 2011. Release of the pro-inflammatory markers by bees-2b cells following in vitro exposure to biodiesel extracts. *Open Toxicol.* J. 3, 8–15.
- Tadano, Y.S., Borillo, G.C., Godoi, A.F.L., Cichon, A., Silva, T.O.B., Valebona, F.B., Errera, M.R., Penteado Neto, R.A., Rempel, D., Martin, L., Yamamoto, C.I., Godoi, R.H.M., 2014. Gaseous emissions from a heavy-duty engine equipped with SCR after treatment system and fuelled with diesel and biodiesel: assessment of pollutant dispersion and health risk. *Sci. Total Environ.* 500–501, 64–71.
- Tarkiainen, T.H., Timonen, K.L., Vanninen, E.J., Alm, S., Hartikainen, J.E., Pekkanen, J., 2003. Effect of acute carbon monoxide exposure on heart rate variability in patients with coronary artery disease. *Clin. Physiol. Funct. Imaging* 23, 98–102.
- Tonne, C., Melly, S., Mittleman, M., Coull, B., Goldberg, R., Schwartz, J., 2007. A case-control analysis of exposure to traffic and acute myocardial infarction. *Environ. Health Perspect.* 115, 53–57.
- USEPA, 2002. Comprehensive analysis of biodiesel impacts on exhaust emissions. Draft Technical Report, EPA420-02-001.
- Valko, M., Leibfritz, D., Moncol, J., Cornin, M.T.D., Mazur, M., Telser, J., 2007. Free radicals and antioxidants in normal physiological functions and human disease. *Int. J. Biochem. Cell Biol.* 39, 44–84.
- Verma, V., Shafer, M.M., Schaur, J.J., Sioutas, C., 2010. Contribution of transition metals in the reactive oxygen species activity of pm emissions from retro-fitted heavy duty vehicles. *Atmos. Environ.* 44, 5165–5173.
- Viana, M., Kuhlbusch, T.A.J., Querol, X., Alastuey, A., Harrison, R.M., Hopke, P.K., Winarwarter, W., Vallius, M., Szidat, S., Prévôt, A.S.H., Hueglin, C., Bloemen, H., Wählin, P., Vecchi, R., Miranda, A.L., Kasper-Giebl, A., Maenhaut, W., Hitznerberger, R., 2008. Source apportionment of particulate matter in Europe: a review of methods and results. *J. Aerosol Sci.* 39, 827–849.
- Wjst, M., Reitmeir, P., Dold, S., Wulff, A., Nicolai, T., von Loeffelholz-Colberg, E.F., von Mutius, E., 1993. Road traffic and adverse-effects on respiratory health in children. *Br. Med. J.* 307, 596–600.
- Xu, Z., Li, X., Guan, C., Huang, Z., 2013. Characteristics of exhaust diesel particles from different oxygenated fuels. *Fuel* 27, 7579–7586.
- Xue, J., Grift, T.E., Hansen, A.C., 2011. Effect of biodiesel on engine performances and emissions. *Renew. Sustain. Energy Rev.* 1098–1116.
- Yaakob, Z., Narayanan, B.N., Padikkaparambil, S., Unni, S., Akbar, P.M., 2014. A review of the oxidation stability of biodiesel. *Renew. Sustain. Energy Rev.* 35, 136–153.
- Yanamala, N., Hatfield, M.K., Farcas, M.T., Schwegler-Berry, D., Hummer, J.A., Shurin, M.R., Birch, M.E., Gutkin, D.W., Kisin, E., Kagan, V.E., Bugarski, A.D., Shvedova, A.A., 2013. Biodiesel versus diesel exposure: enhanced pulmonary inflammation, oxidative stress, and differential morphological changes in the mouse lung. *Toxicol. Appl. Pharmacol.* 272, 373–383.
- Yang, A., Jedynska, A., Hellack, B., Kooter, I., Hoek, G., Brunekreef, B., Kuhlbusch, T.A.J., Cassee, F.R., Janssen, N.A., 2014. Measurement of the oxidative potential of pm<sub>2.5</sub> and its constituents: the effect of extraction solvent and filter type. *Atmos. Environ.* 83, 35–42.



## Human exposure to hydrogen sulphide concentrations near wastewater treatment plants



Ana Flavia Locateli Godoi<sup>a</sup>, Anderson Marlon Grasel<sup>a</sup>, Gabriela Polezer<sup>a</sup>, Andrew Brown<sup>b</sup>, Sanja Potgieter-Vermaak<sup>b,c</sup>, Débora Camargo Scremim<sup>a</sup>, Carlos I. Yamamoto<sup>d</sup>, Ricardo Henrique Moreton Godoi<sup>a,\*</sup>

<sup>a</sup> Environmental Engineering Department, Federal University of Parana, 210 Francisco H. dos Santos St., Curitiba, PR 81531-980, Brazil

<sup>b</sup> Division of Chemistry and Environmental Science, Manchester Metropolitan University, Manchester M1 5GD, UK

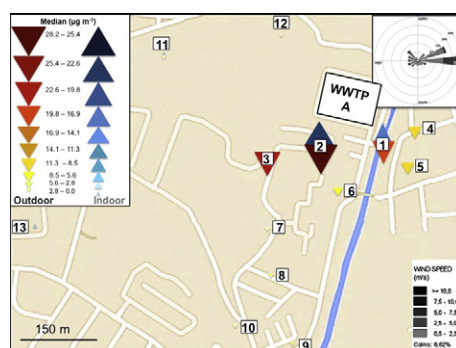
<sup>c</sup> Molecular Science Institute, University of the Witwatersrand, Johannesburg, South Africa

<sup>d</sup> Chemical Engineering Department, Federal University of Paraná/UFPR, Curitiba, PR, Brazil

### HIGHLIGHTS

- First time quantification of hydrogen sulphide levels at wastewater treatment plants in Curitiba, Brazil.
- Indoor and outdoor levels above the WHO guideline values.
- Indoor/outdoor ratios pointing to H<sub>2</sub>S accumulation inside residences.
- Life-time risk analysis indicates a significant non-carcinogenic risk.

### GRAPHICAL ABSTRACT



### ARTICLE INFO

#### Article history:

Received 23 March 2017

Received in revised form 13 July 2017

Accepted 23 July 2017

Available online 17 August 2017

Editor: D. Barcelo

#### Keywords:

Hydrogen sulphide

Air pollution

Odour

Anaerobic wastewater treatment

Health risk

### ABSTRACT

The hydrogen sulphide (H<sub>2</sub>S) levels from wastewater treatment plants (WWTPs) in Curitiba, Brazil have been quantified for the first time. H<sub>2</sub>S generated by anaerobic decomposition of organic matter in WWTPs is a cause for concern because it is an air pollutant, which can cause eye and respiratory irritation, headaches, and nausea. Considering the requirement for WWTPs in all communities, it is necessary to assess the concentrations and effects of gases such as H<sub>2</sub>S on populations living and/or working near WWTPs. The primary objective of this study was to evaluate the indoor and outdoor concentration of H<sub>2</sub>S in the neighbourhood of two WWTPs located in Curitiba, as well as its human health impacts. Between August 2013 and March 2014 eight sampling campaigns were performed using passive samplers and the analyses were carried out by spectrophotometry, presenting mean concentrations ranging from 0.14 to 32 µg m<sup>-3</sup>. Eleven points at WWTP-A reported H<sub>2</sub>S average concentrations above the WHO recommendation of 10 µg m<sup>-3</sup>, and 15 points above the US EPA guideline of 2 µg m<sup>-3</sup>. At WWTP-B the H<sub>2</sub>S concentration was above US EPA guideline at all the sampling points. The I/O ratio on the different sampling sites showed accumulation of indoor H<sub>2</sub>S in some instances and result in exacerbating the exposure of the residents. The highest H<sub>2</sub>S concentrations were recorded during the summer in houses located closest to the sewage treatment stations, and towards the main wind direction, showing the importance of these factors when planning a WWTP. Lifetime risk assessments of hydrogen sulphide exposure showed a significant non-carcinogenic adverse health risk for local residents and workers, especially those close to anaerobic

\* Corresponding author.

E-mail address: [rhmgodoi@ufpr.br](mailto:rhmgodoi@ufpr.br) (R.H.M. Godoi).

WWTPs. The data indicated that WWTPs operated under these conditions should be recognized as a significant air pollution source, putting local populations at risk.

© 2017 Elsevier B.V. All rights reserved.

## 1. Introduction

Human activities have contributed significantly to increased emissions of air pollutants at global, regional and local scales. It is important to know the source and concentration of pollutants for better pollution control and to assess the potential effects on human health.

H<sub>2</sub>S is a colourless gas with a strong odour of rotten eggs produced under anaerobic conditions by organic matter decomposition from both natural (petroleum, volcanic) and anthropogenic sources (oil refining, wood pulp production, tanning industry) (WHO, 2000). Anaerobic wastewater treatment plants (WWTPs) and the degradation processes in landfills are significant sources of H<sub>2</sub>S (Redondo et al., 2008; Capelli et al., 2009; Muñoz et al., 2010). Of the ten largest WWTPs existing in the world, eight are operational as anaerobic treatment facilities (Reynolds, 2012). Under anaerobic conditions, the biological reduction of sulphate to sulphide essentially occurs in the submerged part of sewers (Parande et al., 2006). Hydrogen sulphide emission is a physicochemical process involving both the water and air phases of sewer networks and is dependent on pH, temperature, hydraulic conditions of the water phase (Yongsiri et al., 2005). Only H<sub>2</sub>S can be transferred to the air–water interface, resulting in an increase in the emission of H<sub>2</sub>S from wastewater to the sewer atmosphere (Fu and Shen, 1990).

Unpleasant odours from WWTPs may cause acute social and economic conflicts due to poor quality of life and economic depreciation of the neighbouring real estate (Stellacci et al., 2010). Nuisance complaints about the odour emitted by WWTPs are registered in different parts of the world (Aristu, 2009; Billings, 2012; Wall, 2011). Besides the obvious unpleasant odour, the dominant cause for concern regarding H<sub>2</sub>S pollution is its documented toxicity to humans. H<sub>2</sub>S pollution effects are dose-related and can be detrimental to the nervous, cardiovascular and respiratory systems. Acute high-level concentration exposure can lead to eye damage, olfactory paralyzing perception, respiratory irritation, as well as pulmonary oedema, convulsions and even death (WHO, 2000). The long-term exposure to low-level concentrations also affects human health negatively, e.g., causing nausea, headaches and respiratory problems (Lebrero et al., 2011).

As the nuisance H<sub>2</sub>S odour threshold has been reported to be in the ranges 0.7–200 µg m<sup>-3</sup>, it is recommended to maintain levels at or below the lower limit to avoid community complaints (WHO, 1981). It has been established that daily inhalation exposure to H<sub>2</sub>S has to be below 2.0 µg m<sup>-3</sup> to ensure lifetime risk abatement (USEPA, 2003). Having said that, the World Health Organisation recognises the fact that information on the effects that long-term low dosage exposure to ambient H<sub>2</sub>S is scanty (WHO, 2000). It therefore remains of interest to evaluate the air quality in terms of its H<sub>2</sub>S content close to WWTPs.

This paper aims to provide data on the indoor and outdoor concentration of H<sub>2</sub>S in the neighbourhoods of two WWTPs in Curitiba, Brazil. This provided baseline data that could serve as a reference point for future research. The data obtained were used in a risk-assessment protocol to estimate the likely effect on human health of the residents over a lifetime of exposure. This information can be used to aid local governmental policies, provide baseline data that could inform future changes in operation, as well as assist in future planning for new plants.

## 2. Experimental

As there have been complaints regarding unpleasant odours at and around the plant, the investigators decided to start the analysis of the

air quality by monitoring H<sub>2</sub>S levels, as it is also the main pollutant from degradation processes causing nuisance odours.

### 2.1. Sampling methodology

To protect the identity of the WWTPs, they will be referred as WWTP “A” and WWTP “B”. These plants treat wastewater volumes of 560 L s<sup>-1</sup> and 1680 L s<sup>-1</sup> for A and B, respectively. Both wastewater treatment plants (WWTP) process mainly domestic Municipal wastewater through a conventional setup. The preliminary treatment aims to remove bulky and large solids, thus preconditioning the effluent for the following treatment steps, including screening, flocculation, and flow equalization. In sequence, within the named primary treatment, sedimentation and/or flotation are employed to remove effluent’s suspended and colloidal fractions. At the secondary treatment, the organic matter is removed through a biological process called Fluidized Bed Anaerobic Reactor (FBAR, or RALF in Portuguese), a Brazilian version of the Upflow Anaerobic Sludge Blanket – UASB. The hydraulic retention time at this step is only 8–10 h, resulting in 65–75% organic matter removal efficiency. With the tertiary treatment, using iron chloride, some nutrients such as nitrogen and phosphorous, residual suspended solids, inorganics, and refractory organics that may have escaped from previous stages, are removed. Finally, the disinfection removes pathogens by chlorination. The sludge produced at the secondary step is also treated through thickening, dewatering, drying, and digestion in order to reduce its volume as well as to biologically stabilize the final product, which is usually then sent to landfills (although it also may be used as fertilizer).

H<sub>2</sub>S was sampled using radial diffusion passive samplers (Radiello®, Fondazione Salvatore Maugeri, Padova, Italy). This sampler comprises a zinc acetate impregnated polyethylene adsorbing cartridge, surrounded by a cylindrical microporous diffusive body mounted on a supporting plate. When H<sub>2</sub>S contacts the zinc acetate, it is converted to stable zinc sulphide, which is later extracted and assayed by sulphide ion (Pavilonis et al., 2013). Sampling took place for seven consecutive days. The temperature was recorded every 20 min during the weekly sampling campaigns.

Sampling was performed in houses and schools near the two WWTPs, which are located in two different residential areas in Curitiba.

Eight sampling campaigns were carried out, as listed in Table 1. Samplings locations were assigned as A1 to A13 for WWTP “A”, and B1 to B5 for WWTP “B”. Besides point A1 that was assessed during all campaigns, locations of WWTP “A” were evaluated in campaigns 1 to 4, and points of WWTP “B” in campaigns 5 to 8. Residential accommodation near the WWTPs has little or no insulation between the roof and walls, allowing easy diffusion of H<sub>2</sub>S into the house.

The sampling points were chosen based on three basic criteria: location with respect to the pollution source (WWTP) and the main wind direction, electrical support, and security against vandalism and theft. Table 2 presents the sampling points distances from the WWTPs.

Cartridges were installed at a height of 1.5 m inside residences, after permission was gained from residents. To enable a comparison between inside and outside air quality, samplers were positioned on the outside of the residences at an average height of 2.0 m. Radiello shelters (specifically designed for the diffusion tubes) were used to protect the samplers from precipitation. The Radiello samplers were exposed to air for a period of 15 days, after which the cartridge was removed from the diffusive body, sealed in its original tube and stored below 4 °C for analysis.

**Table 1**  
Collection period, season and sampling locations for each campaign.

Campaigns No.	Collection period	Season	Sampling locations ID	
			Indoor	Outdoor
1	06–20 August 2013	Winter	A1, A2, A11, A13	A1 to A12
2	20–27 August 2013	Winter	A1, A2, A11, A13	A1 to A12
3	13–18 December 2013	Summer	A1, A2, A11, A13	A1 to A12
4	06–13 February 2014	Summer	A1, A2, A11, A13	A1 to A12
5	17–24 February 2014	Summer	A1, B1, B2, B3, B5	A1, B1, B3, B4
6	28 Feb–06 March 2014	Summer	A1, B1, B2, B3, B5	A1, B1, B3, B4
7	19–24 March 2014	Summer	A1, B1, B2, B3, B5	A1, B1, B3, B4
8	24–31 March 2014	Summer	A1, B1, B2, B3, B5	A1, B1, B3, B4

## 2.2. Analytical methodology

Cartridges were desorbed with 10 mL of ultrapure water followed by 0.5 mL of ferric chloride-amine solution. After stirring for 2 min, the samples were left to react at room temperature for 30 min.

The leachate solutions of H<sub>2</sub>S samples were analysed using a spectrophotometer (Cary 50 Bio UV/Visible Spectrophotometer, Varian Inc., Australia) at a wavelength of 665 nm. The detailed extraction procedure is described in Fogo and Popowsky (1949). A calibration curve was prepared with eight points in triplicate using standard methylene blue solution (Sigma-Aldrich, St. Louis, MO). The calibration curve had linear correlation coefficient R<sup>2</sup> > 0.995, indicating that 99.5% of the points can be described by the regression line. The analytical detection limit (3 µg L<sup>-1</sup>) was determined as 3 \* S.D./S, where S.D. is the standard deviation of six blank samples measurements and S is the method sensitivity given by the slope of calibration curve. Procedural blanks were prepared as follows: unexposed cartridges from the same batch to those that were exposed were submitted to the same analysis protocol than the exposed cartridges.

## 2.3. Health risk assessment for H<sub>2</sub>S exposition

The data obtained was subjected to a health risk assessment using the Risk Assessment Information System (RAIS, 2013), which is based on a method created by the United States Environmental Protection Agency (USEPA, 1989; USEPA, 2013). The input parameters were similar to those quoted in Godoi et al. (2013). RAIS models both carcinogenic and non-carcinogenic (hazardous quotient - HQ) adverse health risks.

However, only HQ assessment was carried out for H<sub>2</sub>S as it is not a carcinogen. The hazard quotient equations are listed below:

$$HQ = \frac{CDI_{HQ}}{RFC_i} (a) CDI_{HQ} \left( \frac{mg}{m^3} \right) = \frac{C \left( \frac{\mu g}{m^3} \right) \times ET \left( \frac{hours}{day} \right) \times EF \left( \frac{days}{year} \right) \times ED (years)}{ED (years)} \times \frac{1 \text{ day}}{24 \text{ hours}} \times \frac{1 \text{ year}}{365 \text{ days}} \times \frac{1000 \mu g}{1 \text{ mg}} (b) \quad (1)$$

The input values were H<sub>2</sub>S concentrations in µg m<sup>-3</sup> (C), exposure durations (ED - years), exposure frequency (EF - days/year), exposure time (ET - hours/day), and lifetime (LT - years). Besides that, the models use the Reference concentration of inhalation (RFC<sub>i</sub>) value in mg m<sup>-3</sup> for H<sub>2</sub>S provided on the US EPA website (USEPA, 1989; USEPA, 2013).

Furthermore, different cohorts were identified; each with different input values (Table 3). Cohort 1 represents residents, who live and work in the area. Cohort 2 denotes a resident that lives in the area but studies or works away from WWTPs and Cohort 3 characterizes a person that works near WWTPs but resides quite a distance from the plant.

The HQ assumes that there is a level of exposure, below which it is unlikely that an adverse non-carcinogenic health effect will be experienced. As the HQ is the ratio of the exposure level at a site to the reference dose, an HQ < 1 indicates that there is no significant risk of non-carcinogenic effects. On the other hand, an HQ > 1 means that there is a chance of non-carcinogenic effects occurring, with a probability that tends to increase as the value of HQ increases.

## 3. Results and discussion

### 3.1. Indoor and outdoor H<sub>2</sub>S concentrations

The indoor and outdoor concentrations (illustrated in Fig. 1 and 2) showed that in general, both sampling areas showed similar results. As both plants operate under anaerobic conditions and have no effluent gas treatment system this result is not surprising. The waste water treatment process, as discussed in the introduction, can explain the relatively high concentrations observed.

H<sub>2</sub>S indoor and outdoor concentration values for WWTP "A", summarized in Fig. 1, ranged from 0.14 µg m<sup>-3</sup> to 32 µg m<sup>-3</sup>. With just a few exceptions, mean concentrations of H<sub>2</sub>S were mostly above levels recommended by USEPA (2.0 µg m<sup>-3</sup>) suggesting potential adverse effects on human health. For sampling sites <200 m from the plant, the

**Table 2**  
Sampling points distances from WWTP's.

Sampling Point	Distance from WWTP (m)
A1	101
A2	75
A3	179
A4	137
A5	172
A6	206
A7	345
A8	430
A9	565
A10	575
A11	481
A12	281
A13	790
B1	94
B2	70
B3	92
B4	99
B5	99

**Table 3**  
Exposure considerations for assess each cohort health risk due to H<sub>2</sub>S.

	Cohort 1	Cohort 2	Cohort 3
EF (days/year)	350	350	225
ET(hours/day)	24	15	8
ED (years)	1	1	1

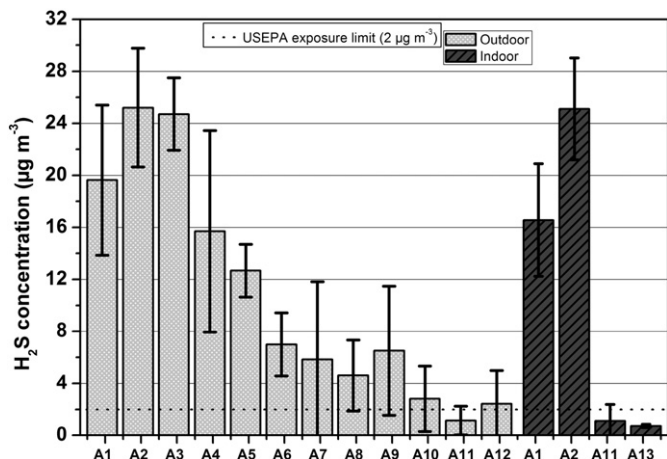


Fig. 1. Average and standard deviation of H<sub>2</sub>S concentrations between the 4 campaigns (except for A1 that had 8 campaigns) for each sampling point at WWTP "A".

concentration is substantially higher and ranged from 8 to 30  $\mu\text{g m}^{-3}$ . Moreover, 89% of the samples collected in close proximity of the WWTP "A" had concentrations above 0.7  $\mu\text{g m}^{-3}$  and therefore could result in complaints from the community due to odour nuisance.

H<sub>2</sub>S concentration values ranged from 4.5  $\mu\text{g m}^{-3}$  to 18  $\mu\text{g m}^{-3}$  at the WWTP "B" sampling sites and are illustrated in Fig. 2. Average indoor and outdoor concentrations were above USEPA recommended levels (indicated in Fig. 2) for all the sampling sites. All the sampling sites for WWTP "B" were at similar distances from the plant and differed only in their geographical position to the plant. It is expected that the different concentrations are due to the predominant wind direction rather than distance as was the case with WWTP "A". It is noticeable that high outdoor concentrations relate to high indoor concentrations and once again suggests possible adverse health effects in residents.

The results obtained in our study are comparable with data reported by Stuetz et al. (1999) in the United Kingdom and Delgado et al. (1999) in Spain. All of whom found concentrations ranging from 5 to 15  $\mu\text{g m}^{-3}$ , near a WWTP. Zarra et al. (2008) in Italy, observed levels below those observed in this study but linked the presence of odorous compounds in ambient air with decreased tourism and economic activity. On the other hand, much higher concentrations were reported by Kim et al. (2013) in South Korea (around 80  $\mu\text{g m}^{-3}$ ) and Dincer and Muezzinoglu (2007) in Turkey (ranging from 39 to 700  $\mu\text{g m}^{-3}$ ).

A recent survey revealed that complaints about the odour emitted by WWTPs are reported all over the world (Heaney et al., 2011; Giuliani et

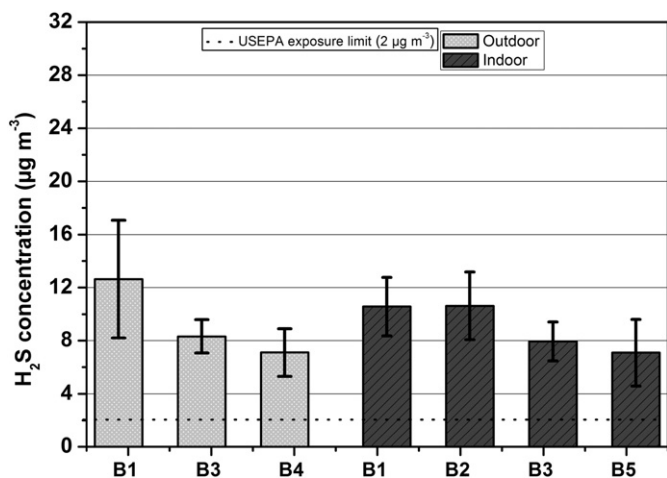


Fig. 2. Average and standard deviation of H<sub>2</sub>S concentrations between the 4 campaigns for each sampling point at WWTP "B".

al., 2013; Bruno et al., 2007) suggesting that the problem is not exclusive to tropical, undeveloped, or developing countries. Our results indicated concentrations several orders of magnitude above the background level, which is accepted as 0.3  $\mu\text{g m}^{-3}$  for H<sub>2</sub>S in air and above the threshold of perception of the odour, which is 0.7  $\mu\text{g m}^{-3}$  (WHO, 1981).

To observe the influence and relationship of the geographical location of the sampling sites from the WWTP on the level of pollution, the sampling sites as well as the wind direction at each WWTP are displayed in Fig. 3 and 4. The level of pollution is indicated by the size of the triangle so that hot spots can easily be observed. The more distant sites (A7–A13) at WWTP "A" were observed to have the lowest H<sub>2</sub>S concentrations and ranged between 0 and 2.8  $\mu\text{g m}^{-3}$ . The intermediate distance sampling sites (A4 and A5) had concentrations between 8.5 and 11  $\mu\text{g m}^{-3}$  and those nearest to the plant had the highest level of H<sub>2</sub>S pollution, as expected and eluded to in the previous paragraph. However, despite being the closest point, site A1 does not exhibit the highest median H<sub>2</sub>S concentration, suggesting the competing role of wind direction. As discussed previously, this was also evident for WWTP "B", where downwind sites showed the highest observed concentrations (Fig. 4).

To attempt a direct comparison between the two plants some of the measurement campaigns were run simultaneously. Table 4 presents the H<sub>2</sub>S results obtained at sampling points A1 and B1 to B5, all at a distance  $\leq 100$  m, albeit in different geographical orientations.

Overall, the concentration levels across the 4 campaigns, where sampling was taking place simultaneously at the two plants, correlated reasonably well with each other with correlation coefficients ( $R^2$ ) ranging from 0.6–0.91. The poorest correlation was observed between campaigns 6 and 7, and the best between campaigns 6 and 8. If the data is separated into indoor and outdoor concentrations, the correlations changed. The indoor correlations improved and ranged between 0.69 (campaigns 7 and 8) and 0.99 (campaigns 5 and 7), as well as the outdoor correlations which varied between 0.4 (campaigns 5 and 7) and 0.96 (campaigns 6 and 8). Since the general tendency is good correlations for indoor concentrations but poorer correlations for outdoor concentrations, it is reasonable to postulate that indoor concentrations seemed to be buffered and less subject to fluctuations. This is of great concern for residents spending a lot of time indoors. If WWTP "A" is correlated with WWTP "B", it is found that the indoor correlation coefficient was 0.17 and for outdoor 0.56, therefore reporting little correlation. On inspecting the concentration values this phenomenon is seen due to concentrations at WWTP "B" dropping during campaigns 7 and 8. Taking into consideration that WWTP "B" has a higher volume throughput in comparison with WWTP "A", it would be expected to produce higher concentrations. This is not observed from the data, but rather the contrary, whereby average concentrations at A and B are 16.7 and 9.2  $\mu\text{g m}^{-3}$ , respectively. This led us to deduce that concentration levels at each plant, and therefore the exposure levels, are determined by the microenvironment of the plant.

### 3.2. Evaluation of climate interference in H<sub>2</sub>S concentrations

Fig. 5 indicates the role of climatic conditions, by plotting outdoor concentrations of H<sub>2</sub>S in WWTP "A" for sampling campaigns 1 and 2 (winter season), and 3 (summer season). The WWTP "B" had no campaign running during the winter season thus has no comparable climate data.

Higher atmospheric temperatures increase the microbiological reaction rates during the treatment, resulting in increased H<sub>2</sub>S production. Although hydrogen sulphide production can be attributed to the presence of sulphide ions, organic matter, and dissolved oxygen, and/or variations in pH, retention time, stream velocity and surface area, as well wind direction and speed, rain, and problems with the treatment system, it is believed that temperature is the main contributor (Bentzen et al., 1995). The data displayed in Fig. 5 certainly indicates increased H<sub>2</sub>S generation during the summer campaign and concentrations that

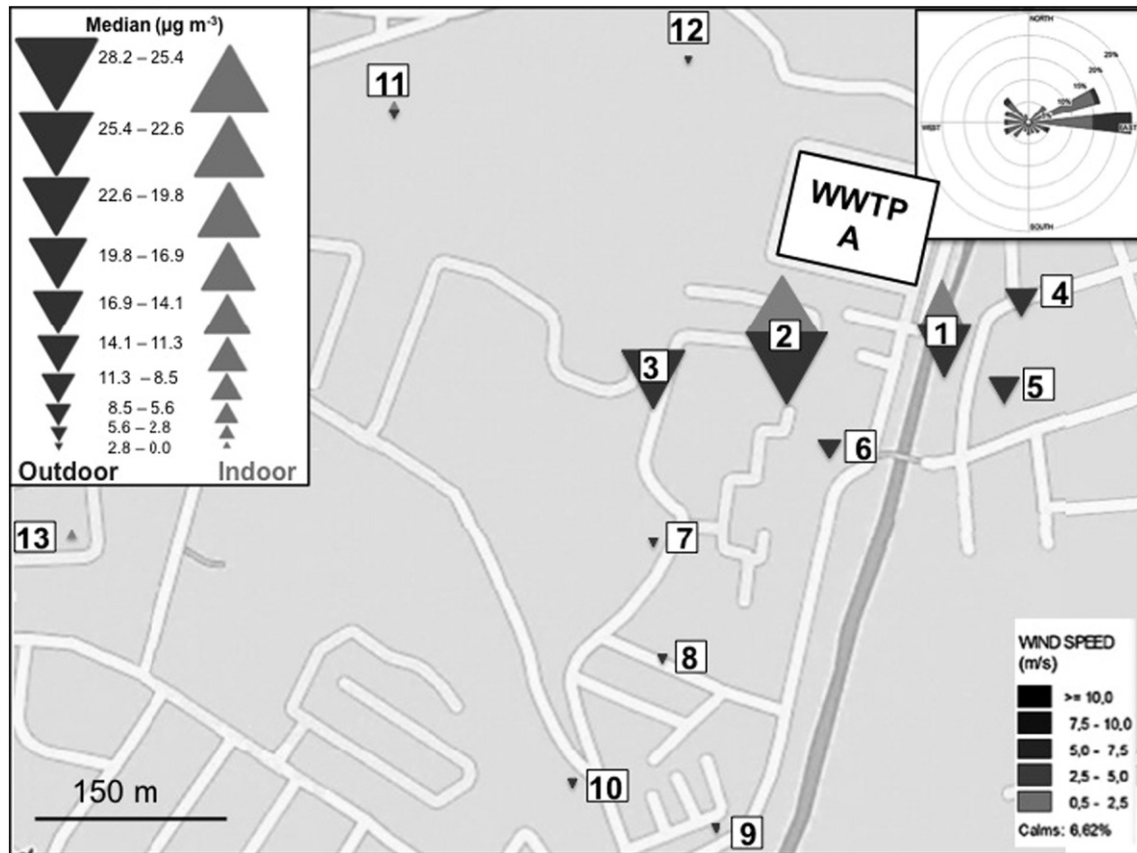


**Fig. 3.** Geographic distributions of indoor (up light grey triangles) and outdoor (down dark grey triangles)  $H_2S$  median concentrations for each sampling site in WWTP “A” area. The larger the size of the triangles the higher the concentrations.

were on average 3.7 times higher (from 0.1 times at A3 – 11.4 times at A12) than during the two winter campaigns were reported. The only exception is at A6 where the winter concentration was 0.3 times higher during the winter campaign. The increase in  $H_2S$  generation, however, does not seem linear with an increase in air temperature in all cases and clearly, other factors must play a role. Even though the temperature difference between the two winter campaigns are only 3 degrees, the concentration differences are noticeable (sites A4, A7–A12 reported on average 37% higher values at 16 °C and sites A1–A3, A5–A6 reported on average 28% higher values at 13 °C). To verify these observations, Pearson correlations between the  $H_2S$  concentration and air temperature for each sampling point were calculated and are reported in Table 5. In general, strong positive correlations ( $>0.9$ ) are observed except for points A2 and A3 with correlations 0.7 and 0.51, respectively. A6 showed a strong negative correlation, which has been eluded to previously.

### 3.3. Indoor-to-outdoor ratios of $H_2S$ air levels

Although several indoor pollutants have endogenous sources, such as gas cookers emitting  $NO_x$ 's, indoor  $H_2S$  is expected to be dominated by the infiltration of outdoor air. The type and the amount of pollutants carried into houses depend on the occurrence of emission sources in the immediate neighbourhood (Zabiegala, 2006). I/O ratio data obtained from the different sampling sites were summarized to provide a general impression of the relationship between indoor and outdoor concentrations. I/O ratio is defined as:

$$\frac{I}{O} \text{ ratio} = \frac{C_{in}}{C_{out}} \quad (2)$$

Where  $C_{in}$  and  $C_{out}$  are the indoor and outdoor  $H_2S$  concentrations respectively. When the I/O ratio  $\gg 1$  one can conclude that endogenous emission sources are mainly responsible for the indoor air quality. If however, the I/O ratio  $\approx 1$ , both internal and external sources influence the indoor air quality to the same degree. For an I/O ratio  $\ll 1$  the quality of outdoor air dominates the quality of indoor air. Fig. 6 shows the I/O ratios for sampling sites A1, A2, A11, B1 and B3 over the campaign period.

The data in Fig. 6 display I/O ratios that are below 1 and therefore indicative of outdoor penetration dominating the indoor  $H_2S$  levels in 60% of the sites investigated over all the campaigns. Forty percent of the ratios displayed values higher than 1, which could point to possible indoor sources. The lowest I/O ratios were recorded in campaigns 1 and 2 which took place during the winter, indicating that an indoor source is unlikely and infiltration from outside minimal. Point A2, however, showed a different profile in comparison to A1 and A11 with I/O ratios substantially higher and even above one. A2 has then also previously separated itself from the others as the site with the highest  $H_2S$  concentration over all sites and campaigns. Since data discussed earlier in this paper suggested that the main contributing factor for it, is its geographical location being directly down-wind from the plant it is possible to conclude that low housing quality at this site can be one of the reasons for its higher ratio. The summer campaigns (3–8) had I/O ratios above or close to one, suggesting a bigger or dominant influence of outdoor  $H_2S$  in comparison with the winter campaigns. Since all the sites investigated for their indoor and outdoor  $H_2S$  levels displayed a ratio larger than one in at least one of the campaigns, it is important to remark that the residents in a 500 m radius of the two plants are just as much at risk in their homes than outside.

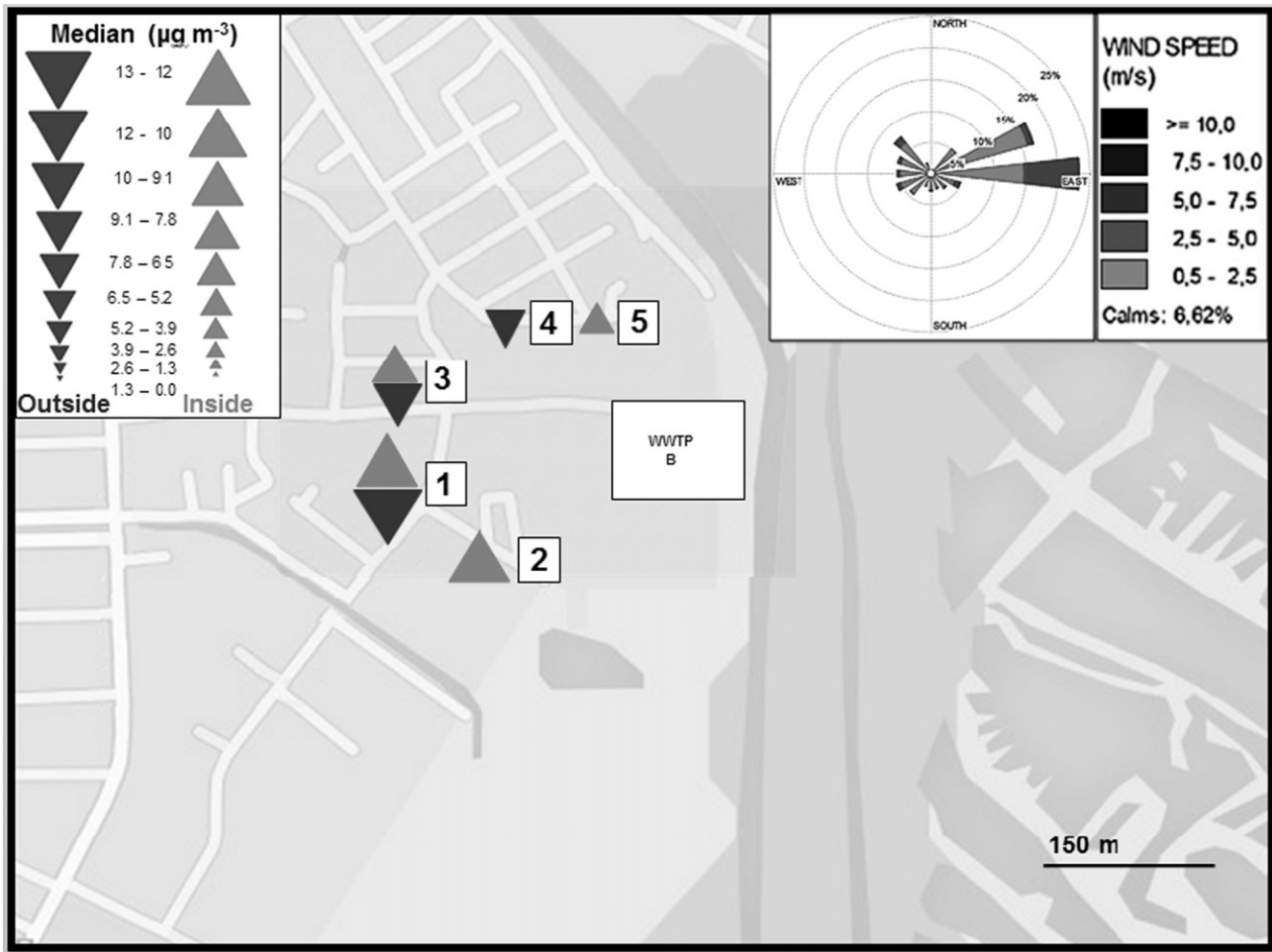


Fig. 4. Geographic distributions of indoor (up light grey triangles) and outdoor (down dark grey triangles) H<sub>2</sub>S median concentrations for each sampling site in WWTP “B” area. The size of triangles represents concentrations.

3.4. Health risk results

In a toxicological review (EPA/635/R-03/005) a no adverse effect level (NOAEL) adjusted for weekly human exposure of 0.64 mg m<sup>-3</sup> are given. The NOAELhec equates to an RfC (response factor concentration) of 0.002 mg m<sup>-3</sup>. Purely based on these values, without further consideration of body weight, exposure duration, etc., it seems as though a number of the investigated sites are above this level. Hence, simulations were performed with the RAIS calculator to identify the lowest concentration of H<sub>2</sub>S that may cause adverse effects on human health, or when HQ is equal to one. For cohort 1 (residents living and working in the area) an H<sub>2</sub>S concentration of 2.1 µg m<sup>-3</sup> reported to

an HQ equivalent to one, while for cohorts 2 (resident living in the area of monitoring but works outside the area) and 3 (resides away from the area, but work in the area), H<sub>2</sub>S concentrations of 3.4 µg m<sup>-3</sup> and 9.7 µg m<sup>-3</sup>, respectively would result in an HQ equal to one. Concentrations above these values could then statistically point to potential adverse effects to human health. Table 6 presents the percentage of

Table 4  
Indoor and Outdoor H<sub>2</sub>S concentrations (µg m<sup>-3</sup>) of 4 summer campaigns during which sampling took place simultaneously at the two plants investigated.

	Campaign 5	Campaign 6	Campaign 7	Campaign 8
A1 - IN	16.1	18.8	11.8	17.1
A1 - OUT	15.3	23.9	11.1	19.6
B1 - IN	12.2	13.3	9.0	7.7
B1 - OUT	16.1	17.8	6.6	9.8
B2 - IN	13.9	12.5	10.5	5.6
B3 - IN	10.9	7.3	7.3	6.3
B3 - OUT	8.8	10.3	8.1	6.0
B4 - OUT	8.7	9.1	5.6	4.8
B5 - IN	8.2	11.0	4.5	4.7

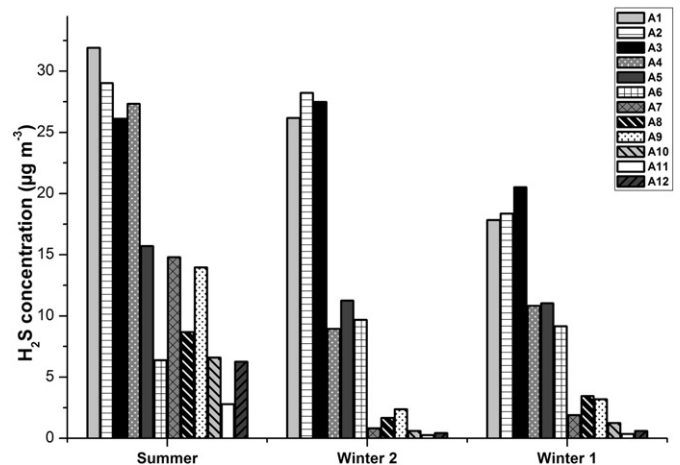


Fig. 5. The seasonal variance in H<sub>2</sub>S concentration between the 12 outdoor sites at WWTP “A” during the summer (air temperature of 28 °C), and winter campaigns 1 and 2 (air temperature of 13 °C and 16 °C, respectively).

**Table 5**

Pearson correlation of outdoor air temperature and H<sub>2</sub>S concentration for each sampling point from A1 to A12 OUT.

A1	A2	A3	A4	A5	A6	A7	A8	A9	A10	A11	A12
0.90	0.70	0.51	0.96	0.99	-0.95	0.97	0.91	0.97	0.96	0.98	0.98

samples at each WWTP that exceeded the threshold values calculated using the RAIS calculator.

It is observed that at WWTP “A” the maximum percentage exceeding these threshold values is 62% for cohort 1, while it is 100% at B plant for both cohorts 1 and 2. It seems that the higher threshold value (cohort 3) is exceeded at sampling sites closest to the plants.

It is evident from the risk assessment that those who reside and work in the area of WWTP “A” (cohort 1) are at risk irrespective of the distance from the source. To put this into perspective: the intake/dose for a worst-case scenario (continuous daily full lifetime exposure) at the point source with the highest concentration (A1 outside) was calculated and value of 9.62  $\mu\text{g kg body weight}^{-1} \text{ day}^{-1}$  was determined. This is based on a person living and working at the plant, of average weight 70 kg, an inhalation rate of 22  $\text{m}^3 \text{ day}^{-1}$ , and 100% retention of air and absorption. At points A9 and A10 (565 and 575 m away from the plant respectively) the hazardous quotient exceeds one but at A11 (481 m) and A13 (790 m) this is not the case. This is probably due to A9 and A10’s geographical location being down-wind from the plant. Those living in the area but working elsewhere (cohort 2), also are at risk, even at relatively distant locations such as point A9 at 565 m. The people living elsewhere but works at or close to the plant (cohort 3) will be at risk at distances close to the plant, such as 180 m.

The risk profile is different for the sites investigated at plant B, as these were all at a similar distance from the plant. For both cohorts 1 and 2, a risk is identified at all sampling points. For cohort 3, the risk is only significant at B1 and B2, both down-wind from the plant and therefore reporting much higher concentrations.

Health risk exposure (HQ values) of this study are comparable to those reported in a study conducted in Tianjin, China (Niu et al., 2014) and poses the question as to how the health of the workers and residents could be addressed.

#### 4. Conclusions

The results indicated that the anaerobic process operated WWTPs are most likely the source of H<sub>2</sub>S pollution in the two residential areas, as there is no other obvious source of H<sub>2</sub>S nearby the sampling points. The odour complaints made by the community were quantified for the first time. The concentrations ranged from 0.14  $\mu\text{g m}^{-3}$  to 32  $\mu\text{g m}^{-3}$

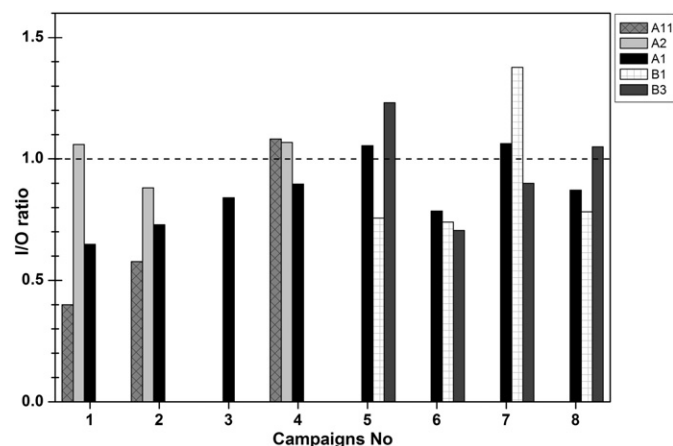


**Fig. 6.** Indoor/Outdoor (I/O) concentration ratios for each campaign at sampling sites A11, A2, A1, B1, and B3.

**Table 6**

Percentage of samples at WWTP “A” and “B” exceeding the concentration limit of non-carcinogenic risk.

Concentrations above ( $\mu\text{g m}^{-3}$ )	WWTP “A” (%)	Risk for sampling points	WWTP “B” (%)	Risk for sampling points
2.1	62	A1 to A10, A12	100	B1 to B5
3.4	55	A1 to A9	100	B1 to B5
9.7	43	A1 to A5	39	B1 and B2

at plant A and 4.5  $\mu\text{g m}^{-3}$  to 18  $\mu\text{g m}^{-3}$  at plant B, which exceeded the nuisance odour level in 89% of the cases. In addition, the measured concentration levels exceeded the USEPA recommended value at 15 of the 18 points analysed. It appears that a better control of the microbiological processes within the UASB combined with the constant use of the gas scrubber should reduce H<sub>2</sub>S emissions considerably.

These H<sub>2</sub>S concentrations observed are indicative of the potential to cause chronic adverse health effects, such as eye irritation, headaches, and nausea (Kourtidis et al., 2008). These concentrations seemed to be influenced by geographical location, distance from the plant, weather conditions and indoor/outdoor environments. I/O ratios indicated that indoor pollution levels are mainly due to infiltration, but in some of the cases there may be an indoor source due to I/O ratios higher than 1. The health risk has been quantified using a risk calculator and indicated that up to 100% of the locations analysed reported hazardous quotients above 1 (this is the case for plant B and cohorts who reside and work in the area).

These findings are alarming from a social and public health point of view, as adverse health effects inevitably lead to increase hospital admissions, loss of working time, as well as government expenses. However, the authors recognise that wastewater treatment plants are essential and primarily to improve environmental and human health. What this investigation alerts to is that health issues can arise at WWTPs using anaerobic technology without stringent control, optimisation of the process and abatement of H<sub>2</sub>S using gas scrubbers for example. The data displayed in this paper can assist in establishing a directive in developing countries, so that emissions of this particular pollutant can be limited. In addition, it could inform where mitigation of the pollutant is most important and may lead to the development of remedial processes at the existing plants.

#### Acknowledgements

The authors acknowledge Coordination for the Improvement of Higher Level - or Education - Personnel - CAPES (1281049)- for financial support.

#### References

- Aristu, I., 2009. Zaragoza and dozens of municipalities continue to suffer odour problems. Herald. Spanish Report on Internet Newspaper [http://www.heraldo.es/noticias/argon/zaragoza\\_decenas\\_municipios\\_siguen\\_sufriendo\\_problemas\\_olores.html](http://www.heraldo.es/noticias/argon/zaragoza_decenas_municipios_siguen_sufriendo_problemas_olores.html) (accessed 10.07.2014).
- Bentzen, G., Smit, A.T., Bennett, D., Webster, N.J., Reinholt, F., Sletholt, E., Hobsont, J., 1995. Controlled dosing of nitrate for prevention of h<sub>2</sub>s in a sewer network and the effects on the subsequent treatment processes. *Water Sci. Technol.* 31, 293–302.
- Billings, R., 2012. Sewage Odours Prompt Study of Plant. Portland Press Herald [http://www.pressherald.com/2012/11/02/sewage-odours-prompt-study-of-plant\\_2012-11-03/](http://www.pressherald.com/2012/11/02/sewage-odours-prompt-study-of-plant_2012-11-03/) (accessed 28.05.2014).
- Bruno, P., Caselli, M., Gennaro, G., Solito, M., Tutino, M., 2007. Monitoring of odour compounds produced by solid waste treatment plants with diffusive samplers. *Waste Manag.* 27, 539–544.
- Capelli, L., Sironi, S., Rosso, R.D., Céntola, P., 2009. Predicting odour emissions from wastewater treatment plants by means of odour emission factors. *Water Res.* 43, 1977–1985.
- Delgado, S., Alvarez, M., Rodriguez-Gomez, L.E., Aguiar, E., 1999. H<sub>2</sub>S generation in a reclaimed urban wastewater pipe: case study: Tenerife (Spain). *Water Res.* 33, 539–547.
- Dincer, F., Muezzinoglu, A., 2007. Odour determination at wastewater collection systems: olfactometry versus H<sub>2</sub>S analyses. *Clean: Soil, Air, Water.* 35, 565–570.

- Fogo, J.K., Popowsky, M., 1949. Spectrophotometric determination of hydrogen sulphide. *Anal. Chem.* 21, 732–734.
- Fu, X., Shen, W., 1990. *Physical-Chemistry*. 4. China Higher Education Publisher, pp. 247–248.
- Giuliani, S., Zarra, T., Naddeo, V., Belgiorno, V., 2013. Measurement of odour emission capacity in wastewater treatment plants by multisensor array system. *Environ. Eng. Manag. J.* 12, 173–176.
- Godoi, R.H.M., Godoi, A.F.L., de Quadros, L.Q., Polezer, G., Silva, T.O.B., Yamamoto, C.I., Van Grieken, R., Potgieter-Vermaak, S., 2013. Risk assessment and spatial chemical variability of PM collected at selected bus stations. *Air Qual. Atmos. Health* 6, 725–735.
- Heaney, C.D., Wing, S., Campbell, R.L., Caldwell, D., Hopkins, B., Richardson, D., Yeatts, K., 2011. Relation between malodour, ambient hydrogen sulphide, and health in a community bordering a landfill. *Environ. Res.* 111847–111852.
- Kim, K.H., Jo, S.H., Song, H.C., Pandey, S.K., Song, H.N., Oh, J.M., Sunwoo, Y., Choi, K.C., 2013. Diagnostic analysis of offensive odourants in a large municipal waste treatment plant in an urban area. *Int. J. Environ. Sci. Technol.* 10, 261–274.
- Kourtidis, K., Kelesis, A., Petrakakis, M., 2008. Hydrogen sulphide (H<sub>2</sub>S) in urban ambient air. *Atmos. Environ.* 42, 7476–7482.
- Lebrero, R., Bouchy, L., Stuetz, R., Muñoz, R., 2011. Odour assessment and management in wastewater treatment plants: a review. *Environ. Sci. Technol.* 41, 915–950.
- Muñoz, R., Sivret, E.C., Parcsi, G., Lebrero, R., Wang, X., Suffet, I.H., Stuetz, R.M., 2010. Monitoring techniques for odour abatement assessment. *Water Res.* 44, 5129–5149.
- Niu, Z.G., Xu, S.Y., Gong, Q.C., 2014. Health risk assessment of odours emitted from urban wastewater pump stations in Tianjin, China. *Environ. Sci. Pollut. Res.* 2, 10349–10360.
- Parande, A.K., Ramsamy, P.L., Ethirajan, S., Rao, C.R.K., Palanisamy, N., 2006. Deterioration of reinforced concrete in sewer environments. *Proc. Inst. Civ. Eng.-Municipal Eng.* 159, 11–20.
- Pavilonis, B.T., O'Shaughnessy, P.T., Altmaier, R., Metwali, N., Thorne, P.S., 2013. Passive monitors to measure hydrogen sulphide near concentrated animal feeding operations. *Environ. Sci. Process Impacts.* 15, 1271–1278.
- RAIS, 2013. RAIS Risk Exposure Models for Chemicals User's Guide. [http://rais.ornl.gov/tools/rais\\_chemical\\_risk\\_guide.html](http://rais.ornl.gov/tools/rais_chemical_risk_guide.html).
- Redondo, R., Machado, V.C., Baeza, M., Lafuente, J., Gabriel, D., 2008. On-line monitoring of gas-phase bioreactors for biogas treatment: hydrogen sulphide and sulphide analysis by automated flow systems. *Anal. Bioanal. Chem.* 391, 789–798.
- Reynolds, J., 2012. The largest wastewater treatment plants around the globe. *Engineering News Record* [http://enr.construction.com/infrastructure/water\\_dams/2012/extras/0328/slideshow.asp?slide=1](http://enr.construction.com/infrastructure/water_dams/2012/extras/0328/slideshow.asp?slide=1) (accessed 31.05.2014).
- Stellacci, P., Liberti, L., Notarnicola, M., Haas, C.N., 2010. Hygienic sustainability of site location of wastewater treatment plants: A case study. I. Estimating odour emission impact. *Desalination* 253, 51–56.
- Stuetz, R.M., Fenner, R.A., Engin, G., 1999. Assessment of odours from sewage treatment works by an electronic nose, H<sub>2</sub>S analysis and olfactometry. *Water Res.* 33, 453–461.
- USEPA, United States Environmental Protection Agency, 1989. Risk Assessment Guidance for Superfund Volume I Human Health Evaluation Manual (Part A).
- USEPA, United States Environmental Protection Agency, 2003. Toxicological review of hydrogen sulphide. EPA-635/R-03/005.
- USEPA, United States Environmental Protection Agency, 2013. Risk Assessment Guidance for Superfund (RAGS), Volume I: Human Health Evaluation Manual (Part F, Supplemental Guidance for Inhalation Risk Assessment).
- Wall, P., 2011. In Case You Didn't Notice: Sewage Odours Are Drawing Fewer Complaints. *The New York Times* [https://cityroom.blogs.nytimes.com/2011/10/13/in-case-you-didnt-notice-sewage-odors-are-drawing-fewer-complaints/?\\_r=0](https://cityroom.blogs.nytimes.com/2011/10/13/in-case-you-didnt-notice-sewage-odors-are-drawing-fewer-complaints/?_r=0).
- WHO, World Health Organization, 1981. Hydrogen sulphide. *Environmental Health Criteria* 19. <http://www.inchem.org/documents/ehc/ehc/ehc019.htm>.
- WHO, World Health Organization, 2000. Air Quality Guideline for Europe. Ed 2. Regional Publications, European Series, No. 91, Copenhagen.
- Yongsiri, C., Vollertsen, J., Hvitved-Jacobsen, T., 2005. Influence of wastewater constituents on hydrogen sulfide emission in sewer networks. *J. Environ. Eng.* 131, 1676–1683.
- Zabiegala, B., 2006. Organic Compounds in Indoor Environments. *Pol. J. Environ. Stud.* 15, 383–393.
- Zarra, T., Naddeo, V., Belgiorno, V., 2008. Measurement, management and control of odours in wastewater treatment plants by portable GC-MS. *Chem. Eng. Trans.* 15, 63–70.

### C.3 Publications under review

#### Hazard assessment of bioaccessible metals in urban road dust: A temporal study

Andrew D. Brown<sup>a\*</sup>, Judith E. S. Barrett<sup>a</sup>, Michael Bennett<sup>a</sup>, Sanja Potgieter-Vermaak<sup>a,b</sup>

\*Corresponding author

<sup>a</sup> School of Science and the Environment, Manchester Metropolitan University, Manchester, U.K., M1 5GD

<sup>b</sup> Molecular Science Institute, University of the Witwatersrand, Johannesburg, South Africa

#### Abstract

Road dust (RD) is a significant contributor to airborne particulate matter worldwide. It is also highly contaminated with potentially toxic metals from anthropogenic sources, particularly in urban areas. The aim of this study is to identify the risk associated with the bioaccessible portion of these metals, by carrying out *in vitro* analysis modelling both the inhalation and ingestion routes of exposure. Crucially, this paper also probes the potential link between water-soluble ions in RD and the bioaccessibility of metals. Metal leaching ranges from 17-78% and from 0-48% for the inhalation and ingestion routes respectively. The data from the water-soluble ion analysis indicate that all metals leach more when the cation/anion ratio is more acidic. Despite the high bulk concentrations of metals and the significant bioaccessibility, the results from the risk assessment show no significant risk with the metal concentrations observed in this study. The most interesting observations of this study are the inconsistent leaching behaviour of all metals and the inconsistencies between bulk metal concentration and bioaccessibility. The results seemingly indicate that the sources of pollutants changed throughout the study.

#### Keywords

Road dust, bioaccessibility, temporal, *in vitro*, risk assessment

#### Highlights

Road dust is of significant concern to human health  
This study features temporal sampling of RD over two years  
This study involves *in vitro* analysis to model human gastric and ingestion of RD  
This study critically risk assesses bioaccessible concentrations of metals  
Results show dynamic nature of health implications regarding road dust

#### Introduction

Air quality is of significant importance to the majority of the world's population. The World Health Organisation estimates that, in 2012, 3 million premature deaths were caused by ambient air pollution worldwide (WHO 2016). The potentially harmful effects of poor air quality are well documented and often attributed to vehicular emissions (Mauderly 1994; Deacon et al. 1997; Ghio et al. 2012). In recent years, however, both increasingly stringent laws and public scrutiny of exhaust emissions have led to significant advancements in reduction of particulate output from modern vehicles (Dahl et al. 2006). Accordingly, more emphasis is being placed on other major contributors to airborne particulates, possibly the most significant being road dust (RD) (Rexeis and Hausberger 2009; Kumar et al. 2013).

Road Dust often consists of numerous components from a range of sources bespoke for any given area, crustal soil and particles from abrasive action on vehicles and road surfaces are typically the main constituents (Pant and Harrison 2013; Tanner et al. 2008). Because of the anthropogenic contributors to RD, it is highly enriched with potentially harmful metals such as As, Cr, Hg, Mn, Ni, Pb, V, Zn (Lueng et al. 2008; Zhao et al. 2012; Luo et al. 2012; Schauer et al. 2006). It is well documented that a significant portion of airborne particles are derived from RD which has been

resuspended by the action of meteorological conditions or turbulence caused by traffic (Almeida et al. 2006; Tanner et al. 2008; Thorpe and Harrison 2008). Hien et al. (1999) reported findings from Ho Chi Minh City, Vietnam, indicating that resuspended road dust accounts for 74% of the total suspended particulate matter. Similarly, Harrison et al. (1997) calculated the amount to be 62% in Lahore, Pakistan. Landis et al. (2017) concluded that RD is respectively the largest and second largest contributor to particulate matter with an aerodynamic diameter  $<10\mu\text{m}$  ( $\text{PM}_{10}$ ) and particulate matter with an aerodynamic diameter  $<2.5\mu\text{m}$  ( $\text{PM}_{2.5}$ ). As a result of the toxic nature of RD, combined with its ubiquitous nature, particularly in urban areas, it has been characterised extensively globally, with health implications associated with any metals present (Han et al. 2011; Chen et al. 2012). To gain a more accurate interpretation of what is actually accessible to the body, it is necessary to carry out *in vitro* studies. Currently there is little literature available which considers both the gastrointestinal and respiratory routes of entry.

Ingestion of particles, especially by children, is usually assumed to happen via the hand to mouth process described by Duggan et al. (1985), where particles of up to  $250\mu\text{m}$  adhere to the hands when in direct contact with soil. Other studies quote particle sizes appropriate for hand to mouth process at up to  $125\mu\text{m}$  (Hamel et al. 1998; Casteel et al. 1997). This seems to be unlikely to be appropriate when considering ingestion of RD, but has been used in the literature to justify characterisation of metals within particles  $<250\mu\text{m}$  (Okorie et al. 2012; Rodrigues et al. 2014). Other studies on gastrointestinal bioaccessibility of RD restrict themselves to smaller particles, assuming exposure takes place through direct ingestion or via mucociliary cleansing (Gradon et al. 1996). Accordingly, RD particles  $<63\mu\text{m}$  are commonly used although  $<22\mu\text{m} \pm 13.25\mu\text{m}$ ,  $<10\mu\text{m}$  and  $<2.5\mu\text{m}$  have also been published (Li et al. 2017; Wang et al. 2016; Zereni et al. 2017; Kong et al. 2011).

Contention in literature also exists as to the size of particles which can be used appropriately for modelling the inhalation route of exposure. Many studies opt for particles in the range of  $\text{PM}_{10}$  and  $\text{PM}_{2.5}$  for assessing bioaccessibility of metals in lung fluid, as it is believed that particles of this size are more likely to be inhaled (Dias da Silva et al. 2015; Zereni et al., 2012). One distinct limitation, however, is the liquid to solid ratio (mL/g), which is far higher than recommended elsewhere (Twining et al. 2005; Wragg and Klinck 2007; Hamel et al. 1998). To overcome this, the use of larger RD particles for assessing bioaccessibility of metals via the inhalation route has been very common, with RD  $<63\mu\text{m}$ ,  $<37\mu\text{m}$  and  $<20\mu\text{m}$  being used (Potgieter-Vermaak et al. 2012; Guney et al. 2017; Schaidler et al. 2007). RD particles as large as  $38\mu\text{m}$  have been shown to be representative of the  $<10\mu\text{m}$  fraction, because RD is simply crustal material contaminated with anthropogenic matter to form aggregates (Brown et al. 2017). Despite the inability of large particles to enter the deep lungs where the more acidic lung fluid environment exists (Davies and Feddah 2003), RD aggregates can be broken down by meteorological conditions or vehicular turbulence (Thorpe et al. 2007).

This study aims to build upon and combine in a novel fashion investigations into bioaccessibility of four specific metals for both the gastrointestinal and inhalation routes of entry, thus giving a total exposure for bioaccessible metals. Four metals of particular interest for their abundance as environmental pollutants and their acknowledged impact on health, Cr, Cu, Fe and Pb are selected for this study. Cr and Pb are very commonly found in a wide range of studies addressing the impact of metal pollutants on health (Gondal et al. 2015; Fu et al. 2015; Liu et al. 2014). Cu and Fe are both heavily implicated in the Fenton reaction (Godoi et al. 2016) as well as having significant crustal and anthropogenic input to RD (Brown et al. 2015). Modelling of the gastrointestinal route in this study will be based on the Unified BARGE Method (UBM) (BARGE/INERIS, 2010), using three size fractions of RD,  $125\text{--}63\mu\text{m}$ ,  $63\text{--}38\mu\text{m}$  and  $<38\mu\text{m}$ . The use of three different fractions is merited by the general uncertainty in the literature mentioned above; the outcomes of this study could potentially elucidate any difference in enrichment and behaviour between the fractions. The inhalation route in this study will use artificial lysosomal fluid (ALF) (Colombo et al. 2008), with a residence time of 24 h (Zereni et al. 2012; Wragg and Klinck 2007; Gray et al. 2010). Only the  $<38\mu\text{m}$  fraction was used for the inhalation route experimentation. In conjunction with the two dissolution techniques, water soluble ions in the RD samples were also quantified to investigate the link between cation/anion ratio (C/A) and bioaccessibility of metals (Buczynska et al. 2014). Finally, the bioaccessible portions of various metals are risk assessed based on the USEPA (1997) method, modified for RD (Brown et al. 2015).

## **Experimental**

### **Study site**

Road dust was collected from Oxford Road, Manchester, UK, one of the main routes into the city, passing along two of the largest universities in the UK supporting over 70,000 students. Oxford Road is widely believed to be one of the busiest bus routes in Europe, as well as being heavily laden with cars and taxis, giving it the potential to be a highly anthropogenically polluted area. The M60 raised motorway and Manchester Oxford Road railway station lie adjacent to Oxford Road further enhancing this. Figure 1. Shows the location of the study site within the U.K.



Figure 1. Road dust sampling site

### Sample handling

Sampling was carried out on a traffic island, Oxford Road, Manchester, UK using a plastic dustpan and brush, a similar process to that carried out by Charlesworth and Lees (1999). One sampling site was deemed to be representative of the 550 m stretch of road by rigorous analysis and statistical testing carried out previously on Oxford Road (Barrett 2010). Sampling took place seasonally over two years, starting in spring 2013 and ending in winter 2014/15, giving a total of 8 sampling campaigns. These sampling campaigns will be designated as Sp for spring (March to May), Sum for summer (June to August), Aut for autumn (September to November), and Win for winter (December to February). 10 kg of RD was collected from the sampling site in each campaign and air dried at a temperature of  $21^{\circ}\text{C} \pm 3^{\circ}\text{C}$  for 14 days. The resulting sediment was separated into different grain size fractions using standard sieve methods. Stainless steel woven wire mesh sieves (200 mm diam; 50 mm depth: to ISO 3310-1:2000; BS 410-1:2000) were used. The three grain-size fractions analysed in this study,  $<38 \mu\text{m}$ ,  $63\text{-}38 \mu\text{m}$  and  $125\text{-}63 \mu\text{m}$  were attained using sieves of mesh sizes 0.125 mm (US std 120), 0.063 mm (US std 240) and 0.038 mm (US std 400).

## Bulk metal analysis

To calculate the bioaccessibility of metals within a sample, it is necessary to quantify the total metals present. 500 mg  $\pm$  10 mg of each sample was analysed for its acid soluble metal content by digestion in *aqua regia* (7.5ml HCl, 2.5 ml HNO<sub>3</sub>); three extractions were carried out per sample. This process was facilitated with a 1600W CEM Mars 5 Microwave equipped with Teflon digestion tubes. Analysis was carried out using a Varian Vista MPX ICP-OES with SeaSpray nebulizer. Initial system stability checks were carried out with a 5 mg/l solution of manganese during the torch alignment whereby the upper values must be in excess of 300,000 counts per second, sample analysis exclusively used the axial position. A four point linear calibration was achieved for each element, a calibration coefficient of  $>0.99$  for all elements was determined. Five replicates were carried out per sample.

## Bioaccessibility via Inhalation

Analysis of the leachates was carried out using the same instrumentation and parameters as the bulk metal analysis method described above, calibration standards were matrix matched using ALF. ALF was prepared according to Colombo *et al.* (2008), 0.15 g  $\pm$  0.0015 g of each RD sample were incubated at 37°C with 15ml of ALF for 24 hours. On removal from the incubator shaker, samples were allowed to cool to room temperature for 10 minutes before being filtered using 0.2 $\mu$ m Whatman® PVDF syringe filters into clean universal vials. The samples were then acidified using spectral grade HNO<sub>3</sub> (310 $\mu$ l), to achieve a 2% w/v acid solution and stored at 4 °C until analysis could be performed. Analysis of the leachates was carried out using the same instrumentation and parameters as the both the ingestion route leachates and the bulk metal analysis method described above, calibration standards were matrix matched using ALF.

## Bioaccessibility via ingestion

Gastrointestinal dissolution of metals was quantified using the UBM. The method is best described by BARGE/INERIS (2010) and has been shown to be comparable to *in vivo* studies (Denys *et al.* 2012). The process involves simulating the gastric route alone (GC) and the gastrointestinal route (GI). The GC route exposes RD to simulated fluids in just the mouth and stomach compartments, simulated saliva and simulated gastric fluid respectively. The GI route has the additional exposure to the intestinal compartment, modelled with simulated duodenal fluid and bile. The organic and inorganic constituents of each of the four solutions were produced the day before exposure, they were then combined and heated to 37°C before addition of RD. A calibrated pH meter was used to ensure the pH of each solution stayed within the strict range as described by BARGE/INERIS (2010). The entire process was scaled down, using 0.3g of RD, rather than 0.6g as described by BARGE/INERIS (2010), the quantity of each solution used was also halved to keep the stated liquid to solid ratio. The process of reducing the quantities in this manner has been shown not to affect the quantity of metals leached (Xia *et al.*, 2016). Analysis of the leachates was carried out using the same instrumentation and parameters as the bulk metal analysis method described above, calibration standards were matrix matched using ALF

## Water soluble ions

Extraction methods of water soluble ions from RD vary significantly in the literature and are often not supported with references or evidence of method development. A similar gap in the literature is also present with respect to water soluble ion extraction from soils. A variety of extraction times are published, ranging from 5-120 minutes (Zissimos *et al.* 2014; Endovitsky *et al.* 2016; Behrooz *et al.* 2017). There is, however, published work detailing the optimised soil:water ratio, 1.5-5:100 (g/ml) was preferred (Reis *et al.* 2014).

Accordingly, several different techniques were investigated here to ensure the efficiency and repeatability of extractions. It was found that use of an orbital shaker improved extraction efficiency of chloride, nitrate, phosphate, sulphate, sodium, ammonium, potassium, magnesium and calcium relative to an ultrasonic bath. 1g of RD in 20ml of deionised water was preferred over lower quantities of RD as samples showed greater standard deviation with the lower mass, supporting the work of Reis *et al.* (2014). Extraction time was also varied, although there was relatively little increase in quantities of ions extracted after 40 min, 1 h was selected as the optimum.

## Risk assessment

The risk assessment method used in this paper is based on the USEPA model (USEPA 1997), whereby the risk of detrimental health effects caused by a pollutant on an individual was calculated based on severity of exposure. Equations 1 and 2 show calculations for average daily dose of a pollutant via the ingestion, inhalation and dermal absorption routes. The parameters and values for each equation are displayed in table 1.

$$ADD_{ing} = \frac{C \times R_{ing} \times CF \times EF \times ED}{BW \times AT}$$

Equation 1: Average daily dose of a pollutant via ingestion route

$$ADD_{inh} = \frac{C \times R_{inh} \times EF \times ED \times ([TSP])}{BW \times AT}$$

Equation 2: Average daily dose of a pollutant via inhalation route

Table 1: Parameters for average daily dose calculations

<i>Component</i>	<i>Definition (units)</i>	<i>Adult value used</i>	<i>Child value used</i>	<i>Reference</i>
<i>C</i>	Concentration of contaminant (mg/kg)	This study	This study	
<i>R<sub>ing</sub></i>	Ingestion rate (mg/day)	200	100	USEPA 1989
<i>EF</i>	Exposure frequency (days/year)	350	350	Du et al. 2014
<i>ED</i>	Exposure duration ( years)	24	6	Du et al. 2014
<i>BW</i>	Body Weight (kg)	84	21	Potgieter-Vermaak et al. 2012
<i>AT</i>	Average Time (days)	365 x ED	365 x ED	Du et al. 2014
<i>CF</i>	Conversion factor (kg/mg)	1 x 10 <sup>-6</sup>	1 x 10 <sup>-6</sup>	
<i>R<sub>inh</sub></i>	Inhalation rate (m <sup>3</sup> /day)	5	20	Du et al. 2014
<i>TSP</i>	RD derived Total suspended particles (kg/m <sup>3</sup> )	5.76 x 10 <sup>-8</sup>	5.76 x 10 <sup>-8</sup>	Brown et al. 2015
<i>ABS</i>	Dermal absorption factor	1 x 10 <sup>-3</sup>	1 x 10 <sup>-3</sup>	Du et al. 2014

The inhalation methodology was adapted for use with sediments as demonstrated by Brown et al. (2015), whereby the particle emission factor (PEF) has been changed to be more applicable to urban road dusts. Whilst use of the PEF value as proposed by USEPA (2000) has been common in literature (Buranatrevedh 2014; Liu et al. 2015; Cao et al. 2015), it was designed to model resuspension of soils from sites where vegetation makes up 50% of the surface. A novel feature of this analysis is that the risk assessment was performed on the bioaccessible portion of RD as

determined by the leaching studies. Once values are inserted into Equations 1 and 2,  $ADD_{ing}$  and  $ADD_{ing}$  can be calculated. Hazard quotients (HQ) for each route of exposure can then be derived by dividing each ADD of each metal by a reference dose (RfD). The RfD value represents the threshold for which the health effects of any given pollutant can be observed (Buranatrevedh 2014; Liu et al. 2015; Cao et al. 2015). HQ values for each exposure route are then combined to obtain a hazard index value (HI). A HI greater than 1 are indicative that significant risks of non-carcinogenic health effects due to a pollutant may be observed (USEA 2001).

## Results and discussion

### Bulk metal analysis

The bulk analysis results are displayed in Figures 2, 3 and 4 for each metal of interest within the <38  $\mu\text{m}$ , 63-38 $\mu\text{m}$  and 125-63 $\mu\text{m}$  fractions, respectively. Generally, the median concentrations of metals follow  $\text{Fe} > \text{Cu} > \text{Pb} > \text{Cr}$ , this occurs across all size fractions and sampling campaigns with the exception of summer 2014, autumn 2014 and winter 2014/2015 in the 125-63 $\mu\text{m}$  fraction, where Cr is more abundant than Pb. From the box plots displayed in Figures 2, 3 and 4 it appears that the median concentrations show an increasing trend towards summer and a decreasing trend towards winter. This is consistent across all three fractions of RD studied. Similar studies into temporal variation of metal concentrations in RD are limited; however, both Norouzi et al. (2017) and Liu et al. (2011) indicated strong seasonal variance in metal concentrations throughout the year. Contrary to the results obtained here, both studies observed increased metal concentrations towards winter followed by a decrease towards summer. This can be rationalised, as acknowledged by both studies, by the influence of precipitation. The studies by Norouzi et al. (2017) and Liu et al. (2011) note increased wet summers and dry winters, contrary to the Manchester study site which experiences wet winters and relatively dry summers (Brown et al. 2015). Referring to the data presented here, a degree of variance is observed temporally within a fraction as well as between fractions. This presents an interesting unexplained trend, all samples were handled in the same manner and the instrumental analysis was all carried out on the same day.

Chromium concentrations in this study range from 77.6-132.0 mg/kg. These results are comparable with those quoted in literature, although generally towards the higher end of ranges quoted. Concentrations have been observed ranging from 3.7-94 mg/kg in China (Liu et al. 2014; Tang and Han 2017), 17-34 mg/kg in Angola (Ferreira-Baptiste and De Miguel 2005). Copper concentrations in this study range from 154.0-502.5 mg/kg. Copper in RD has been studied extensively in the UK, the results obtained in this study are relatively low in comparison to Birmingham and Coventry, where concentrations of 16.4-6,688.4 mg/kg and 49.3-815 mg/kg respectively are reported (Charlesworth et al. 2003). In comparison to other continents, however, the results obtained in this study are relatively high. Concentrations ranging from 4.5-172 mg/kg in China (Liu et al. 2014; Tang and Han 2017), 18-118 mg/kg in Angola (Ferreira-Baptiste and De Miguel 2005) have been published. Iron concentrations in this study range from 19,700-38,480 mg/kg, this is quite typical of global concentrations. Concentrations in the order of 8,381-35,400 mg/kg in China (Luo et al. 2012; Tang and Han 2017), 8,000-20,100 mg/kg in Angola (Ferreira-Baptiste and De Miguel 2005). The observed concentrations in this study are significantly higher than those reported by Robertson et al. (2003) at a site less than a kilometre away (7,664-17,214 mg/kg). Lead concentrations in this study range from 77.3-267.1 mg/kg, this is generally in line with those reported in literature, ranging from 10-270 mg/kg in China (Liu et al. 2014; Tang and Han 2017), 74-1,856 mg/kg in Angola (Ferreira-Baptiste and De Miguel 2005). Contrary to concentrations of Cu, lead concentrations in Manchester are higher relative to those reported in Birmingham and Coventry by Charlesworth et al. (2003) (0-146.3 mg/kg and 0-199.4 mg/kg respectively). Despite this, concentrations in this study are observed to be slightly lower than those reported at a nearby site in Manchester by Robertson et al. (2003) (120-645 mg/kg). The large variability in absolute concentrations of metals in RD across both the globe and even within a relatively small city such as Manchester intriguing from a health standpoint. It is most likely that the variances can be attributed to the different anthropogenic sources in any given site. Comparison between these results and those gathered by Robertson et al. (2003) show how quickly a pollutant, such as lead can diminish, and a new one, iron, can present itself. This study ultimately highlights the importance to examine metal contamination at a local level.

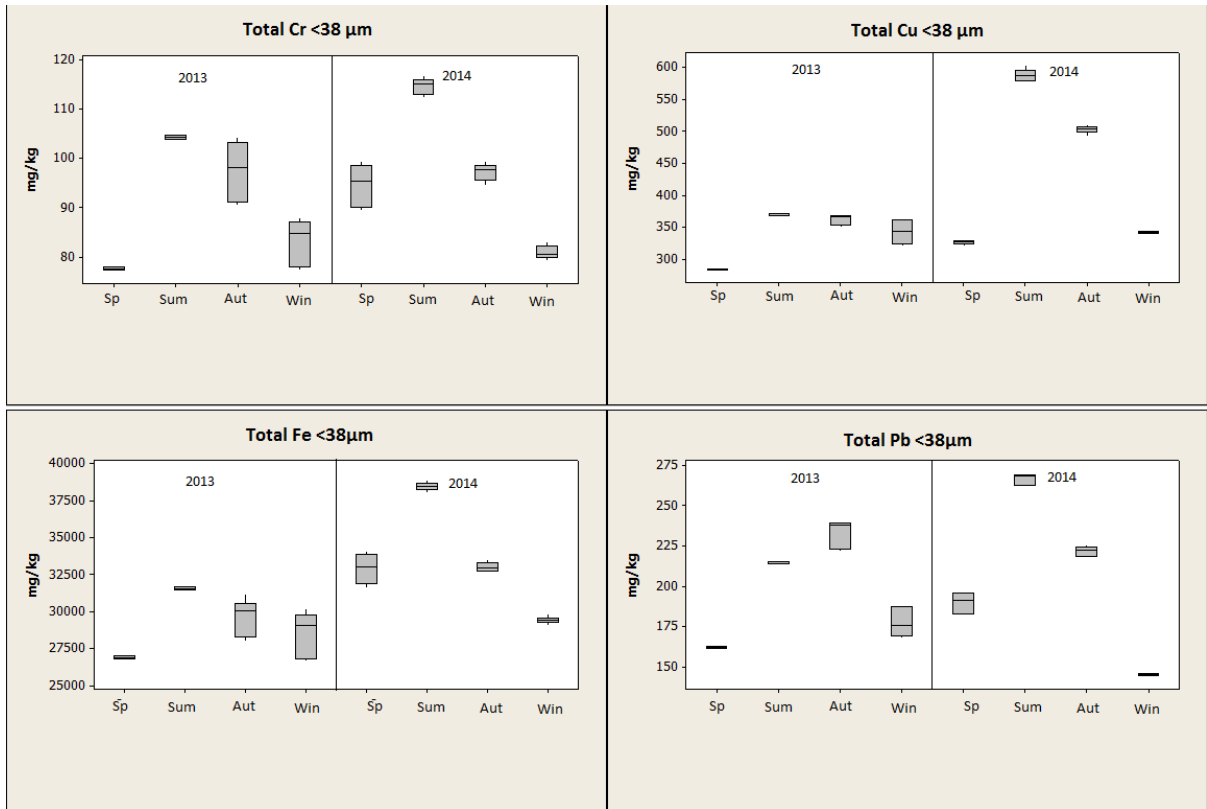


Figure 2: Box plots denoting the acid soluble concentrations of Cr, Cu, Fe and Pb in <38µm fraction as determined by ICP-OES for the two-year sampling campaign (where Sp = spring, Sum = summer, Aut = autumn, Win = winter)

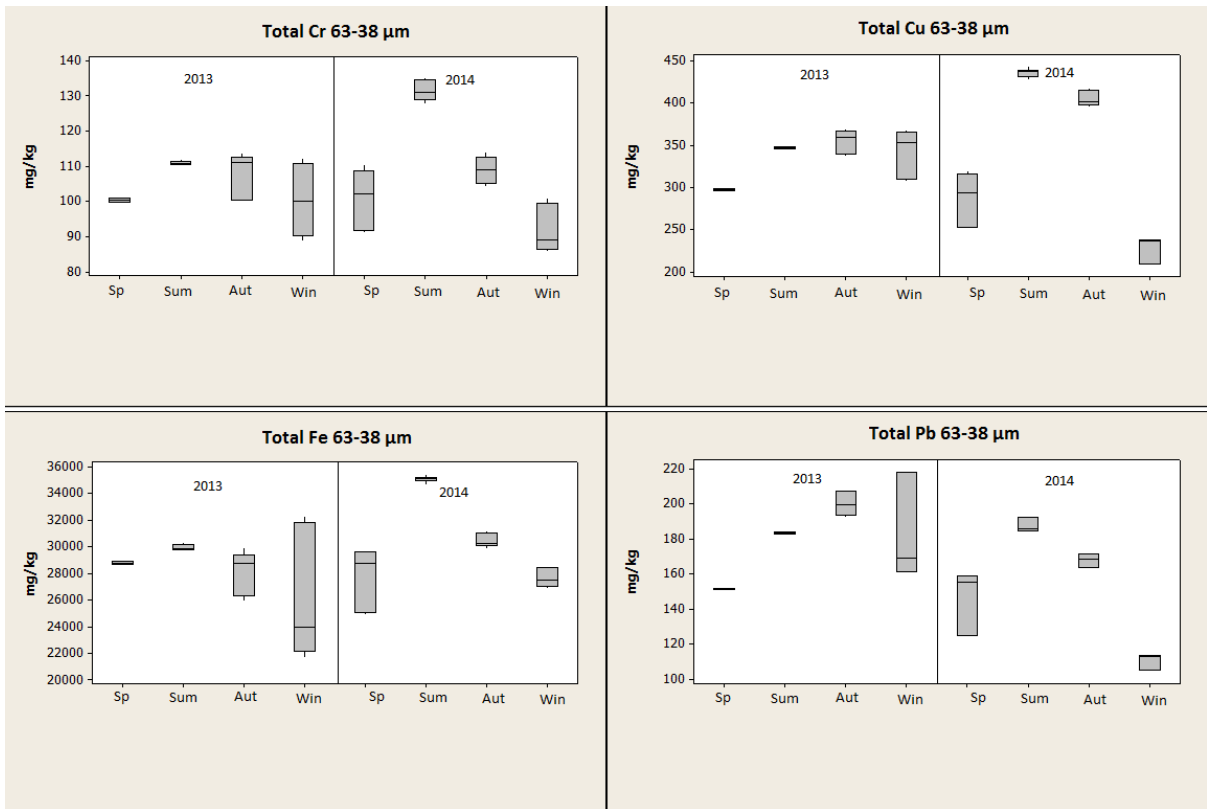


Figure 3: Box plots denoting the acid soluble concentrations of Cr, Cu, Fe and Pb in 63-38 $\mu$ m fraction as determined by ICP-OES for the two-year sampling campaign (where Sp = spring, Sum = summer, Aut = autumn, Win = winter)

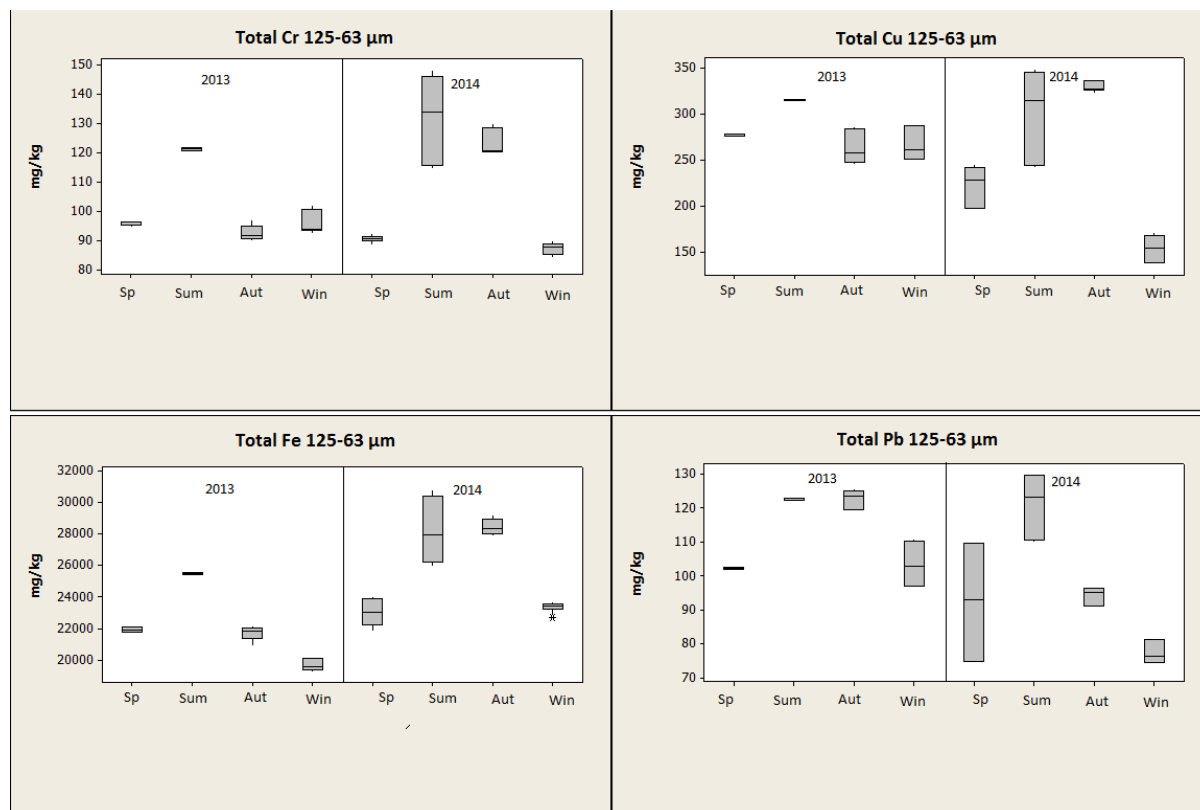


Figure 4. Box plots denoting the acid soluble concentrations of Cr, Cu, Fe and Pb in 125-63 $\mu$ m fraction as determined by ICP-OES for the two-year sampling campaign (where Sp = spring, Sum = summer, Aut = autumn, Win = winter)

### Bioaccessibility via Inhalation

As mentioned in the introduction section of this study, only the <38 $\mu$ m fraction of RD was considered for the inhalation route leaching portion of the study because of the ability for the <38 $\mu$ m fraction to act as a proxy form inhalable particles (Brown et al. 2017). ALF leaching data (as illustrated in Figure 5.) are presented as the percentage leached relative to that which was available, as determined in the bulk analysis protocol. It is therefore considered as its bioaccessibility (Colombo et al. 2008), this is calculated using equation 3. There appears to be a distinct pattern in leaching with Cr, Cu and Fe, where peaks in leaching during autumn 2013 and again in summer 2014 are observed. However, Pb shows an initial peak in winter 2013-14, then a second peak in summer 2014. While the peaks in data are somewhat consistent, the campaigns of lower leaching, troughs, for each metal are less so. There are examples of troughs occurring in each season, spring being the most common. These observations show the subtle, but valuable difference between using bulk data to estimate health effects rather than *in vitro* studies. The apparent independence between bulk concentration of each of these metals and bioaccessibility shows that the nature of pollutants changed throughout the study. It is probable that the slight seasonal pattern indicates significant meteorological contribution, but also influences from other factors, perhaps changes in types of anthropogenic pollution.

In terms of metal content, results indicate that the order of leaching is as follows Cu>Pb>>Cr=Fe, dividing the metals into two distinct groups of Cu with Pb, and Cr with Fe. The figure shows that there is a significant fluctuation in the amount of each metal which is bioaccessible, with Cr ranging from 15.3-21.1%, Cu from 61.7-78.6%, Fe from 16.8-24.9% and Pb from 57.0-68.7%. In comparison to studies on the bioaccessibility of metals within ALF, the results obtained here are similar. Data from Pelfrene et al. (2017) show bioaccessibility of Cr was 8.7%, Cu was 55.0-65.2% and Pb was 55.0-62.0% for three different RD certified reference materials with particle sizes of <74 $\mu$ m, <90 $\mu$ m and

<100µm. Guney *et al.* (2017) publish large variability amongst 6 contaminated urban soils fractionated to <20µm with bioaccessibility ranging from 23.7-90.1% for Cu, 2.3-67.6% for Fe and 50.3-92% for Pb. The large variance in data between and within all of these studies particularly highlights the variable nature in bioaccessibility in RD.

$$\text{Bioaccessibility (\%)} = \frac{[\text{leached}]}{[\text{total}]} \times 100$$

Equation 3. Calculation for bioaccessibility (%)

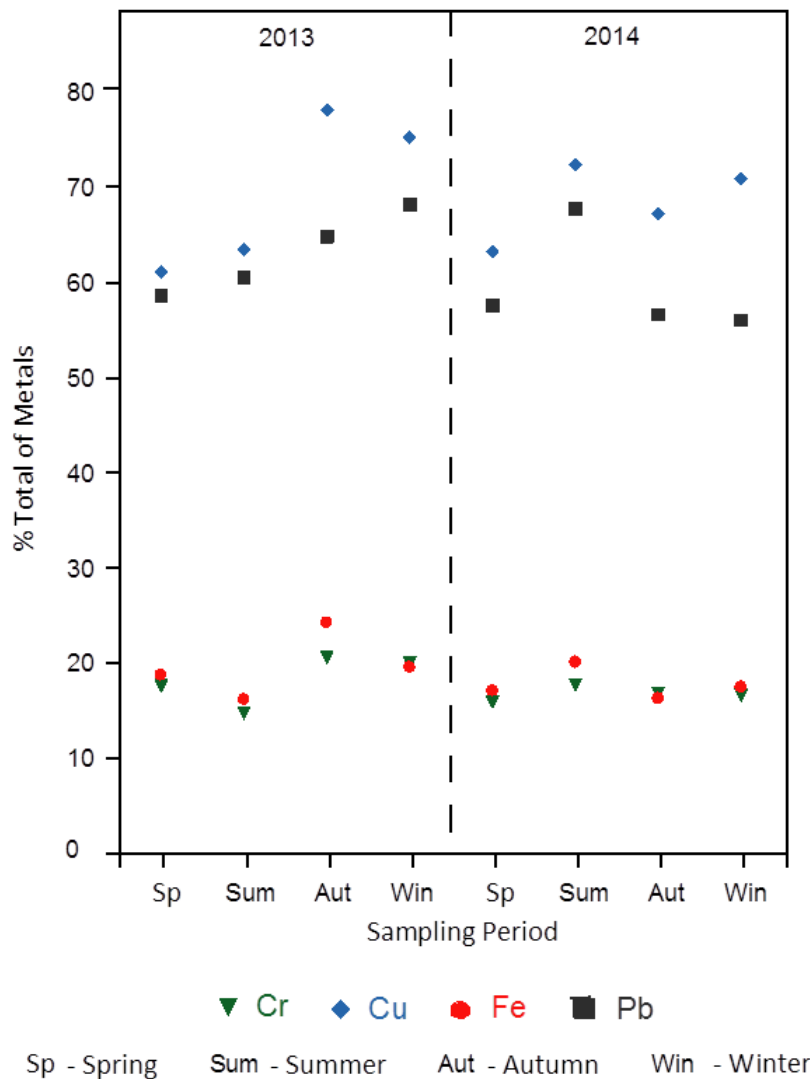


Figure 5: Percentage bioaccessibility, inhalation route leaching

### Bioaccessibility via Ingestion

The Ingestion leaching data in this study has been handled in the same manner as the inhalation route leaching data, whereby the bioaccessibility of each metal is quoted as a percentage of the bulk total, as determined in this study. Boxplots of the data are presented in Figures 6 and 7. Contrary to the inhalation leaching and bulk concentration data, the ingestion leaching data showed no particular temporal trend over the sampling campaign for Cr, Fe and Pb. However, ingestion leaching data for Cu generally appeared to increase from spring through to winter for both GI and GC conditions. Interestingly, the coarser size fraction leached more than the finer fraction in all conditions, with the exception of Cu under gastrointestinal conditions. One would typically expect the finer fraction to leach more due to its smaller surface area to volume ratio. It was observed that for Cr, Fe and Pb the

GC conditions yielded higher bioaccessibility, while Cu was more bioaccessible in the GI conditions. In any condition, bioaccessibility for Cr and Fe was <2%, far lower than that of Cu and Pb which ranged from 7.9%-48.7% and 0.5%-21.5%. A large degree of variability is observed between samples in this study, this is also apparent in the published literature where reported bioaccessibility of Cu and Pb have ranged from 9%-40.9% and 5-25% respectively (Okorie et al. 2012; Poggio et al. 2009; Gbafa et al. 2010). Only Gbafa et al. (2010) investigated the bioaccessibility of Cr via the ingestion route: a median bioaccessible value of 0.3% was quoted. There is no literature available on the bioaccessibility of Fe from RD via the ingestion route.

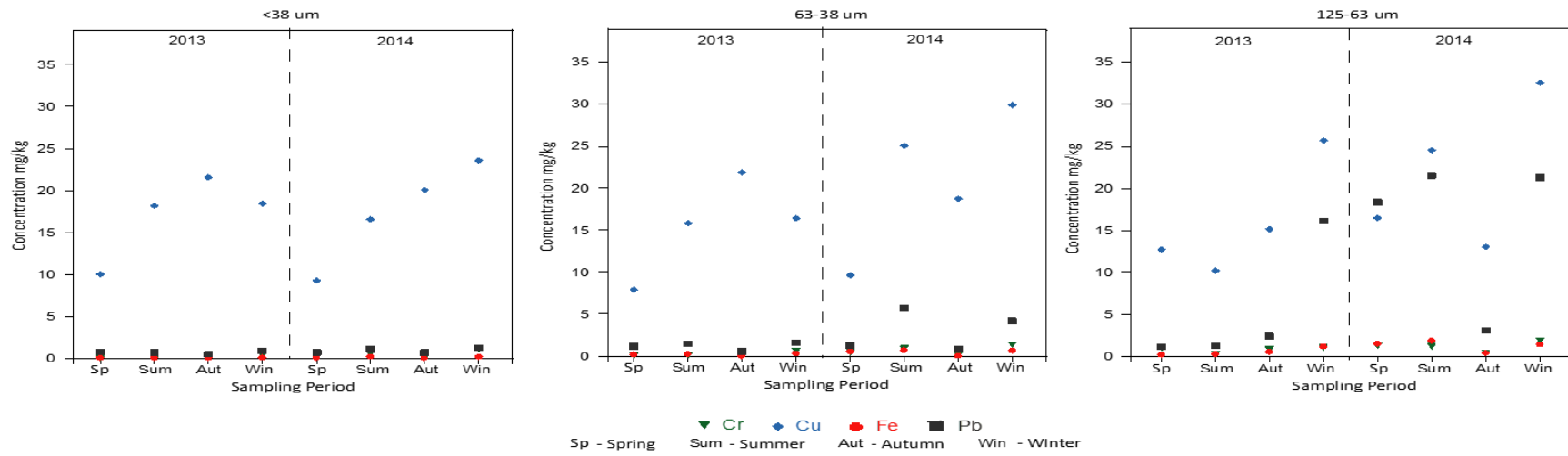


Figure 6: Percentage bioaccessibility, GC ingestion route leaching

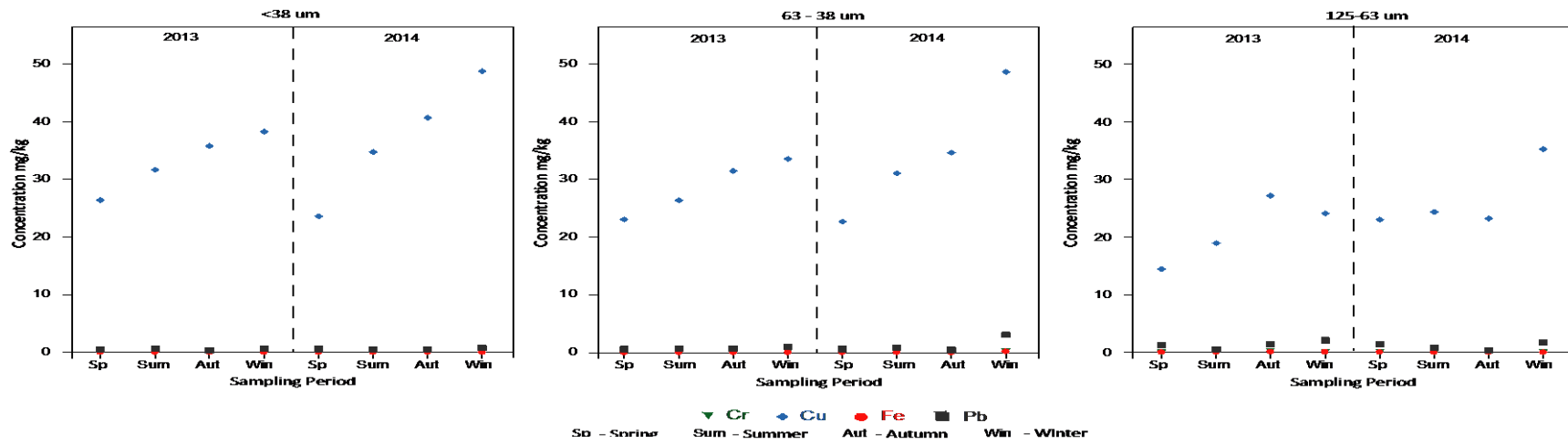


Figure 7: Percentage bioaccessibility, GI ingestion route

## Water soluble ions

Concentrations of  $\text{Na}^+$ ,  $\text{NH}_4^+$ ,  $\text{K}^+$ ,  $\text{Mg}^{2+}$ ,  $\text{Ca}^{2+}$ ,  $\text{Cl}^-$ ,  $\text{NO}_3^{2-}$ ,  $\text{SO}_4^{2-}$  and  $\text{PO}_4^{3-}$  were determined by IC, as described in Section 2.6. Cation/Anion (C/A) ratios were then calculated for each size fraction using molar equivalents (Buczynska et al. 2014). These calculations are presented in Equations 3 and 4. It is accepted that the C/A ratio provides an insight into the acidity of the material, whereby a lower C/A value indicates a more acidic sample (Ram et al. 2012)

$$C = \frac{[\text{Na}^+]}{23} + \frac{[\text{NH}_4^+]}{18} + \frac{[\text{K}^+]}{39} + \frac{[\text{Mg}^{2+}]}{12} + \frac{[\text{Ca}^{2+}]}{20}$$

Equation 4

$$A = \frac{[\text{Cl}^-]}{35.5} + \frac{[\text{NO}_3^{2-}]}{62} + \frac{[\text{SO}_4^{2-}]}{48} + \frac{[\text{PO}_4^{3-}]}{95}$$

Equation 5

Boxplots for the C/A data are shown in Figure 8. Aside from the  $<38\mu\text{m}$  fraction in the first two sampling campaigns, the C/A ratio data are similar in terms or range for each of the three size fractions in all campaigns.

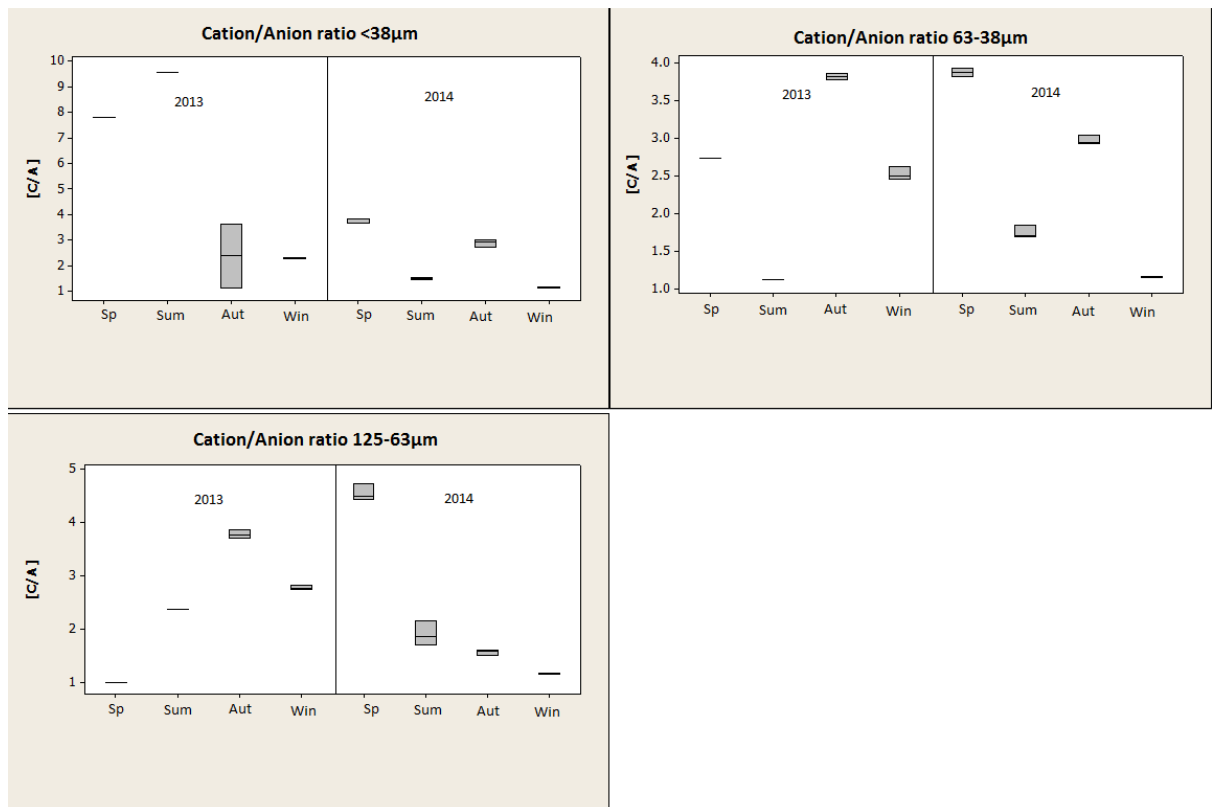


Figure 8: Cation/Anion ratio for each fraction

A regression line using C/A in the  $<38\mu\text{m}$  fraction as the predictor variable and inhalation bioaccessibility for each metal in the  $<38\mu\text{m}$  as the response was plotted. Negative correlations were observed for all metals. If the null hypothesis is true, then ratio of variance

between the two samples is close enough to 1 to be considered random variation. An F-test was carried out on the data, where if the F value exceeded the F critical value of 3.787 for a one-tailed test ( $p=0.05$ ), the null hypothesis can be rejected. F values of each sample are displayed along with correlation coefficients ( $R^2$ ) are displayed in Table 2. The results displayed in Table 2 shows that there is a significant linear relationship between the concentration of Cr and Cu leached, and C/A. This suggests that the more acidic the water soluble ions in an RD sample, the more readily some metals leach. This has been proposed by Huang et al. (2016), but no data were presented to prove this.

	Cr	Cu	Fe	Pb
$R^2$	-0.43	-0.64	-0.27	-0.095
F value	4.52	10.70	2.26	0.63

Table 2: Correlation coefficients between C/A and inhalation of metals in <38um fraction

### Risk assessment

Data for the risk assessment portion of this study was handled as stated in Section 2.7. Hazard index values for each of the four metals are displayed in Tables 3 and 4 for adults and children respectively. The concentration of each metal inserted into the  $ADD_{inh}$  equations were the average leached concentrations for each metal over the two-year sampling campaign. This was considered to be the best representation of the average bioaccessible concentration of metal over the chronic exposure duration detailed in Table 1. However, because of the acknowledged contention in literature over the size of particle which is most representative of those which can be ingested, a worst case scenario approach was adopted. For each metal, the fraction with the highest average concentration over the two-year campaign was selected for the  $ADD_{ing}$  equation. It can be observed from Tables 3 and 4 that even with the worst case scenario approach, there are no metals that present a significant non-carcinogenic risk, but the results do show an elevated risk to children in comparison to adults. Similar approaches to risk assessment on the total concentration of RD have yielded similar insignificant risk (Brown et al. 2015, Du et al. 2014). However, these studies overestimate the actual expose. There are results from two studies which risk assess the bioaccessible fraction of an exposure route available, both studies show incomplete data and have not considered appropriate bioaccessibility tests on the two main exposure routes, as in this study (Huang et al. 2016; Li et al. 2015). Both these studies, show insignificant non-carcinogenic risk. Cheque

	Cr	Cu	Fe	Pb
HI	$8.6 \times 10^{-3}$	$1.0 \times 10^{-2}$	$6.2 \times 10^{-4}$	$1.7 \times 10^{-2}$

Table 3. HI values for adults

	Cr	Cu	Fe	Pb
	$1.49 \times 10^{-2}$	$1.82 \times 10^{-2}$	$1.22 \times 10^{-3}$	$3.45 \times 10^{-2}$

Table 4. HI values for children

### Conclusions

One of the key aims of this study was to risk assess the bioaccessible portion of metals at this study site. Whilst the results suggest that there is little concern for health of those exposed, this model over simplifies the vulnerability of an individual to pollutants, it fails to consider those of poor health or elderly. Furthermore, this approach to risk assessment oversimplifies complex process of human exposure to urban pollutants. This is particularly apparent when considering all the data presented here, large variability between total concentrations of metals, not to mention the bioaccessibility thereof indicative of the dynamic

nature of sources and the effect of meteorological conditions. Perhaps the most interesting aspect of the results presented here is the apparent link between acidity of RD and elevated leaching via the inhalation route.

## References

- Almeida S. M., Pio, C. A., Freitas, M. C., Reis, M. A., Trancoso, M. A., 2006. Source apportionment of atmospheric urban aerosol based on weekdays/weekend variability: evaluation of road re-suspended dust contribution. *Atmospheric environment* 40, 2058-2067
- BARGE/INERIS., 2010. UBM Procedure for the Measurement of Inorganic Contaminant Bioaccessibility from Solid Matrices. <http://www.bgs.ac.uk/barge/ubm.html>
- Barrett, J. E. S. (2010). Contaminated urban sediments: geochemistry, mineralogy, solid-state speciation and the implications to environmental risk assessment. Unpublished doctoral dissertation. Manchester Metropolitan University, Manchester
- Behrooz, R., Esmaili-Sari, A., Bahramifar, N., Kaskaoutis, D. G., Saeb, K., Rajaei, F. 2017. Trace-element concentrations and water-soluble ions in size-segregated dust-borne and soil samples in Sistan, southeast Iran. *Aeolian research* 25, 87-105
- Brown, A., Barrett, J. E. S., Robinson, H., Potgieter-Vermaak, S. 2015. Risk assessment to particulate output of a demolition site. *Environmental geochemistry and health* 37, 675-687
- Buczynska, A. J., Krata, A., Van Grieken, R., Brown, A., Polezer, G., De Wael, K., Potgieter-Vermaak, S. 2014. Composition of PM<sub>2.5</sub> and PM<sub>1</sub> on high and low pollution event days and its relation to indoor air quality in a home for the elderly. *Science of the total environment* 490, 134-143
- Buranatvedh, S., 2014. Health risk assessment of the general populations exposed to metals from an aluminium production plant in Thailand. *Journal of community medicine and health evaluation* 4, 262
- Cao, S., Duan, X., Zhao, X., Wang, B., Ma, J., Fan, D., Sun, C., He, B., Wei, F., Jiang, G., 2015. Health risk assessment of various metal(loid)s via multiple exposure pathways on children living near a typical lead-acid battery plant, China. *Environmental pollution* 200, 16-23
- Casteel, S. W., Cowart, R. P., Weis, C. P., Henningsen, G. M., Hoffman, E., Brattin, W. J. Guzman, R. E., Starost, M. F., Payne, J. T., Stockham, S. L., Becker, S. V., Drexler, J. W., Turk, J. R., 1997. Bioavailability of lead to juvenile swine dosed with soil from the Smuggler Mountain NPL site of Aspen, Colorado. *Fundamental and Applied Toxicology*, 36, 177-187.
- Charlesworth, S. M., Lees, J. A. (1999). The distribution of heavy metals in deposited dusts and sediments, Coventry, UK. *Environmental Geochemistry and Health*. 21, 97-115.
- Charlesworth, S. Everett, M., McCarthy, R., Ordonez, A., de Miguel, E. A comparative study of heavy metal concentration and distribution in deposited street dusts in a large and a small urban area: Birmingham and Coventry, West Midlands, UK. *Environment international* 29, 563-573
- Colombo, C., Monhemius, A. J., Plant, J. A. (2008). Platinum, palladium and rhodium release from vehicle exhaust catalysts and road dust exposed to simulated lung fluids. *Ecotoxicology and Environmental Safety*. 71, 722-730
- Chen, J., Wang, W., Liu, H., Ren, L. (2012). Determination of road dust loadings and chemical characteristics using resuspension. *Environmental Monitoring and Assessment*. 184, 1693-1709.
- Dahl, A., Gharibi, A., Swietlicki, E., Gudmundsson, A., Bohgard, M., Ljungman, A., Blomqvist, G., Gustafsson, M., 2009. Traffic generated emissions of ultrafine particles from pavement-tyre interface. *Atmospheric environment* 40, 1314-1323

- Davies, N. M., Feddah, M. R., 2003. A novel method for assessing dissolution of aerosol inhaler products. *International journal of pharmaceutics* 255, 175-187
- Deacon, A. R., Derwent, R. G., Harrison, R. M., Middleton, D. R., Moorcroft, S. 1994. Analysis and interpretation of measurements of suspended particulate matter at urban background sites in the United Kingdom. *Science of the total environment* 203, 17-36
- Denys, S., Cabouche, J., Tack, K., Rychen, G., Wragg, J., Cave, M., Jondreville, C., Feidt, C., 2012. In Vivo Validation of the Unified BARGE Method to Assess the Bioaccessibility of Arsenic, Antimony, Cadmium, and Lead in Soils. *Environmental science and technology* 46, 6252-6260
- Dias da Silva, L. I., Yokoyama, L., Maia L. B., Monteir, M. I. C., Pontes, F. V. M., Carniero, M. C., Neto, A. A., 2015. Evaluation of bioaccessible heavy metal fractions in PM<sub>10</sub> from the metropolitan region of Rio de Janeiro city, Brazil, using a simulated lung fluid. *Microchemical journal* 118, 266-217
- Du, Y., Wei, M., Reddy, K. R., Liu, Z., & Jin, F. (2014). Effect of acid rain pH on leaching behavior of cement stabilized lead-contaminated soil. *Journal of Hazardous Material*, 271, 131–140.
- Duggan, M. J., Inskip, M. J., Rundle, S. A., Moorcroft, J. S., 1985. Lead in Playground Dust and on the Hands of Schoolchildren. *Science of the Total Environment*, 44, 65-79.
- Endovitski, A. P., Batukaev, A. A., Minkina, T. M., Kalinitchenko, V. P., Mandzhieva, S. S., Sushkova, S. N., Mischenko, N. A., Bakoyev, S. V., Zarmaev, A. A., Jusupov, V. U. Ions association in soil solution as the cause of lead mobility and availability after application of phosphogypsum to chernozem. *Journal of chemical research – in press*
- Ferreira-Baptiste, L., & De Miguel, E. 2005. Geochemistry and risk assessment of street dust in Luanda, Angola: A tropical urban environment. *Atmospheric Environment*, 39, 4501–4512
- Fu, R., Yang, Y., Xu, Z., Zhang, X., Guo, X., Bi, D. 2015. The removal of chromium (VI) and lead (II) from groundwater using sepiolite-supported nanoscale zero-valent iron (S-NZVI). *Chemosphere* 138, 726-734
- Gbefa, B. K., Entwistle, J. A., Dean, J. R., 2010. Oral bioaccessibility of metals in an urban catchment, Newcastle upon Tyne. *Environmental geochemistry and health* 33, 167-181
- Ghio, A. J., Carraway, M. S., Madden, M. C . 2012. Composition of air pollution particles and oxidative stress in cells, tissues, and living systems. *Journal of Toxicology and Environmental Health*, 15 1-21
- Godoi, R. H. M., Polezer, G., Borillo, G. C., Brown, A., Valebona, F. B., Silva, T. O. B., Ingberman, A. B. G., Nalin, M., Yamamoto, C. I., Potgieter-Vermaak, S., Neto, R. A. P., de Marchi, M. R. R., Saldiva, P. H. N., Pauliquevos, Y. Godoi, A. F. L. 2016. Influence on the oxidative potential of a heavy-duty engine particle emission due to selective catalytic reduction system and biodiesel blend. *Science of the total environment* 560-561, 179-185
- Gondal, M. A., Dastageer, M. A., Al-Adel, F. F., Naqvi, A. A., Habibullah, Y. B., 2015. Detection of highly toxic elements (lead and chromium) in commercially available eyeliner (kohl) using laser induced break down spectroscopy. *Optics and laser technology* 75, 99-104
- Gradon, L., Pratsinis, S. E., Podgorski, A., Scott, S. J., Panda, S., 1996. Modeling retention of inhaled particles in rat lungs including toxic and overloading effects. *Journal of aerosol science* 27, 487-503
- Gray, J. E., Plumlee, G. S., Morman, S. A., Higuera, P. L., Crock, J. G., Lowers, H. A., Witten, M. L., 2010. In vitro studies evaluating leaching of mercury from mine waste calcine using simulated human body fluids. *Environmental science and technology* 44, 4782-4788

- Guney, M., Bourges, C. M. J., Chapuis, R. P., Zagury, G. J., 2017. Lung bioaccessibility of As, Cu, Fe, Mn, Ni, Pb, and Zn in fine fraction (< 20 µm) from contaminated soils and mine tailings. *Science of the total environment* 579, 378-386
- Hamel, S. C., Buckley, B., Liou, P. J., 1998. Bioaccessibility of metals in soils for different liquid to solid ratios in synthetic gastric fluid. *Environmental Science & Technology*, 32, 358-362.
- Han, S., Youn, J.S., Jung, Y. W. (2011). Characterisation of PM10 and PM2.5 source profiles for resuspended road dust collected using mobile sampling methodology. *Atmospheric Environment*. 45, 3343-3351.
- Harrison, R. M., Smith, D. G. T., Pio, C. A., Castro L. M. (1997). Comparitive receptor modelling study of airborne particulate pollutants in Birmingham, Unite Kingdom, Coimbra (Portugal) and Lahore (Pakistan). *Atmospheric Environment*. 31, 3309-3321
- Hien, P. D., Binh, N. T., Truong, Y., Ngo, N. T.N. (1999). Temporal variations of source impacts at the receptor, as derived from particulate monitoring data in Ho Chi Minh City, Vietnam. *Atmospheric Environment*. 33, 3133-3142
- Huang, J., Li, F., Zeng, G., Liu, W., Huang, X., Ziao, Z., Wu, H., Li, X., He, X., He, Y. 2016. Integrating hierarchical bioavailability and population distribution into potential eco-risk assessment of heavy metals in road dust: A case study in Xiandao District, Changsha city, China. *Science of the total environment* 541, 969-976
- Kong, S., Lu, B., Bai, Z., Zhao, X., Chen, L., Han, B., Li, Z., Ji, Y., Xu, Y., Liu, Y., Jiang, H., 2011. Potential threat of heavy metals in re-suspended dusts on building surfaces in oilfield city. *Atmospheric environment* 45, 4192-4204
- Kumar, P., Pirjola, L., Ketznel, M., Harrison, R. M., 2013. Nanoparticle emissions from 11 non-vehicle exhaust sources – A review. *Atmospheric environment* 67, 252-277
- Landis, M. S., Pancras, J. P., Graney, J. R., White, E. M., Edgerton, E. S., Legge, A., Percy, K. E. 2017. Source appointment of ambient fine and coarse particulate matter at the fort Mckay community site, in the Athabasca Oil Sands Region, Alberta, Canada.
- Li, N., Kang, Y., Pan, W., Zeng, L., Zhang, Q., Luo, J., 2015. Concentration and transportation of heavy metals in vegetables and risk assessment of human exposure to bioaccessible heavy metals in soil near a waste-incinerator site, South China. *Science of the total environment* 521-522, 144-151.
- Li, H. H., Chen, L. J., Yu, L., Guo, Z. B., Shan, C. Q., Lin, J. Q., Gu, Y. G., Yang, Z. B., Yang Y. X., Shao, J. R., Zhu, X. M., Cheng, Z. 2017. Pollution characteristics and risk assessment of human exposure to oral bioaccessibility of heavy metals via urban street dusts from different functional areas in Chengdu, China. *Science of the total environment* 586, 1076-1084
- Liu, E., Yan, T., Birch, G., Zhu, Y. 2014. Pollution and health risk of potentially toxic metals in urban road dust in Nanjing, a mega-city of China. *Science of the total environment* 476-477, 522-531
- Liu, X., Zhai, Y., Zhu, Y., Liu, Y., Chen, H., Li, P., Peng, C., Xu, B., Li, C., Zeng, G. (2015) Mass concentrations and health risk assessment of heavy metals in size-segregated airborne particulate matter in Changsa. *Science of the total Environment*. 517, 215-221
- Lie, Y. Y., Liu, M., Wang, Y. J., 2011. Temporal variation characteristics of PGEs concentrations in road dust. *Chinese journal of environmental science* 32, 2676
- Lueng, A. O. W., Duzgoren-Aydin, N. S., Cheung, K. C., Wong, M. H.(2008). Heavy metal concentrations of surface dust from e-waste recycling and its human health implications in Southeast China. *Environmental Science and Technology*. 42, 2674-2680.
- Luo, X. S., Ding, J., Xu, B., Wang, J. Y., Li, H. B., Yu, S. (2012). Incorporating bioaccessibility into human health risk assessments of heavy metals in urban park soils. *Science of the Total Environment*. 424, 88-96.

- Mauderly, J. L., Toxicological and epidemiological evidence for health risks from inhaled engine emissions. *Environmental health perspectives* 102, 165-171
- Norouzi, S., Kahdemi, H., Ayoubi, S., Cano, A. F., Acosta, J. A., Seasonal and spatial variations in dust deposition rate and concentrations of dust-borne heavy metals, a case study from Isfahan, central Iran. *Atmospheric pollution research in press*
- Okorie, A., Entwistle, J., Dean, J. R., 2012. Estimation of daily intake of potentially toxic elements from urban street dust and the role of oral bioaccessibility testing. *Chemosphere* 86, 460-467
- Pant, P., Harrison, R. M., 2013. Estimation of the contribution of road traffic emissions to particulate matter concentrations from field measurements: A review. *Atmospheric environment* 77, 78-97
- Pelfrene, A., Cave, M. R., Wragg, J., Douay, F. 2017. In vitro investigations of human bioaccessibility from reference materials using simulated lung fluids. *Environmental research and public health* 14, 112-127
- Poggio, L., Vrscaj, B., Schulin, R., Hepperle, E., Marsan, F. A., 2009. Metals pollution and human bioaccessibility of topsoils in Grugliasco (Italy). *Environmental pollution* 157, 680-689
- Potgieter-Vermaak, S., Rotondo, G., Novakovic, V., Rollins, S., 2012. Component-specific toxic concerns of the inhalable fraction of urban road dust. *Environmental geochemistry and health* 34, 689-696
- Ram K, Sarin MM, Sudheer AK, Rengarajan R. 2012. Carbonaceous and secondary inorganic aerosols during wintertime fog and haze over urban sites in the Indo-Gangetic plain. *Aerosol and Air Quality Research*,12, 359–370
- Reis, A. T., Lopes, C. B., Davidson, C. M., Duarte, A. C., Periera, E. 2014. Extraction of mercury water-soluble fraction from soils – an optimisation study. *Geoderma* 21, 255-260
- Rexeis, M., Hausberger, S., 2009. Trend of vehicle emission levels until 2020 – Prognosis on current vehicle measurements and future emissions legislation. *Atmospheric environment* 43, 4689-4698
- Robertson, D. J., Taylor, K. G., Hoon, S. R., Geochemical and mineral magnetic characterisation of urban sediment particulates, Manchester, UK. *Applied geochemistry* 18, 269-282
- Rodrigues, s. M., Coehlo, C., Cruz, N., Monteiro, R. J. R., Henriques, B., Duarte, A. C., Romkens, P. F. A. M., Pereira, E., 2014. Oral bioaccessibility and human exposure to anthropogenic and geogenic mercury in urban, industrial and mining areas. *Science of the total environment* 496, 649-661
- Schaider, L. A., Senn, D. B., Brabander D. J., McCarthy, K. D., Shine, J. P., 2007. Characterization of Zinc, Lead, and Cadmium in Mine Waste: Implications for Transport, Exposure, and Bioavailability. *Environmental science and technology* 41, 4164-4171
- Schauer, J. J., Lough, G. C., Shafer, M. M., Christensen, W. F., Arndt, M. F., DeMinter, J. T., Park, J. S. (2006). Characterization of metals emitted from motor vehicles. *Health effects issues*. 133, 1-75
- Tang, Y., Han, G., 2017. Characteristics of major elements and heavy metals in atmospheric dust in Beijing, China. *Journal of geochemical exploration* 176, 114-119
- Tanner, P. A., Ma, H. L., Yu, P. K. N., 2008. Fingerprinting Metals in Urban Street Dust of Beijing, Shanghai, and Hong Kong. *Environmental science and technology* 42, 7111-7117
- Thorpe, A. J., Harrison, R. M., Boulter, P. G., McCrae, I. S. M., 2007. Estimation of particle resuspension source strength on a major London Road. *Atmospheric Environment* 41, 8007-8020
- Thrope, A., Harisson, R. M., 2008. Sources and properties of non-exhaust particulate matter from road traffic: A review. *Science of the total environment* 400, 270-282

- Twining, J., McGlenn, P., Loi, E., Smith, K., Giere, R., 2005. Risk Ranking of Bioaccessible Metals from Fly Ash Dissolved in Simulated Lung and Gut Fluids. *Environmental science and technology* 39, 7749-7756
- USEP. 1989. Risk assessment guidance for superfund, Vol.1:Human Health Evaluation Manual. EPA/540/1-89/002. Washington, D.C:Office of Solid Waste and Emergency Response
- USEPA. 1997. Exposure factors handbook. EPA/600/P-95/002F. Washington, DC: Environmental Protection Agency, Office of Research and Development
- USEPA. 2000. Soil screening guidance for radionuclides: Technical background document. <http://www.epa.gov/superfund/health/contaminants/radiation/pdfs/sstbd.pdf>
- USEPA. 2001. Risk Assessment Guidance for Superfund: Volume III – Part A, Process for Conducting Probabilistic Risk Assessment. US Environmental Protection Agency, Washington, D.C. EPA 540-R-02-002
- Wang, J., Li, S., Cui, X., Li, H., Qian, X., Wang, C., Sun, Y. 2016. Bioaccessibility, sources and health risk assessment of trace metals in urban park dust, Nanjing, China. *Ecotoxicology and environmental safety* 128, 161-170
- WHO., 2016. <http://www.who.int/mediacentre/factsheets/fs313/en/>
- Wragg, J., Klinck, B., 2007. The bioaccessibility of lead from Welsh mine waste using a respiratory uptake test. *Journal of environmental science and health. Part A, Toxic/hazardous substances & environmental engineering* 42, 1223-1231
- Xia, Q., Peng, C., Lamb, D., Mallavarapu, M., Naidu, R., Ng, J. C. 2016. Bioaccessibility of arsenic and cadmium assessed for in vitro bioaccessibility in spiked soils and their interaction during the Unified BARGE Method (UBM) extraction. *Chemosphere* 147, 444-450
- Zereni, F., Wiseman, C. L. S., Poprizki, J., Albers, P., Schneider, W., Leopold, K., 2017. Assessing the potential of inorganic anions ( $\text{Cl}^-$ ,  $\text{NO}_3^-$ ,  $\text{SO}_4^{2-}$  and  $\text{PO}_4^{3-}$ ) to increase the bioaccessibility of emitted palladium in the environment: Experimental studies with soils and a Pd model substance. *Environmental pollution* 220, 1050-1058
- Zereni, F., Wiseman, C. L., Puttmann, W., 2012. In Vitro Investigations of Platinum, Palladium, and Rhodium Mobility in Urban Airborne Particulate Matter (PM<sub>10</sub>, PM<sub>2.5</sub>, and PM<sub>1</sub>) Using Simulated Lung Fluids. *Environmental science and technology* 46, 10326-10333
- Zhao, H., Xia, B., Fan, C., Zhao, P., Shen, S. (2012). Human health risk from soil heavy metal contamination under different land uses near Dabaoshan mine, southern China. *Science of the Total Environment* 417-418, 45-54.
- Zissimos, A. M., Christoforou, I. C., Morriseau, E., Cohen, D. R., Rutherford, N. F. 2014. Distribution of water-soluble inorganic ions in the soils of Cyprus. *Journal of geochemical exploration* 146, 1-8

## Representation of PM<sub>10</sub> in the larger fraction of environmental particles

Andrew D. Brown<sup>a\*</sup>, Judith E. S. Barrett<sup>a</sup>, Michael Bennett<sup>a</sup>, Sanja Potgieter-Vermaak<sup>a,b</sup>

\*Corresponding author

<sup>a</sup> School of Science and the Environment, Manchester Metropolitan University, Manchester, U.K., M1 5GD

<sup>b</sup> Molecular Science Institute, University of the Witwatersrand, Johannesburg, South Africa

### Abstract

It is shown for the first time that the < 38 µm fraction of urban particles can be used as a proxy for PM<sub>10</sub>. This study probed similarities between the < 10 and <38 µm fractions of urban road dust to show that the larger of the two can be used for analysis for which larger sample masses are required. Road dust, initially segregated to size <38µm using sieves, was again size segregated to <10µm using water deposition. Both the original <38µm and the separated <10µm fractions were then subject to analysis by SEM-EDX and ICP-OES for its elemental composition. Dissolution tests in artificial lysosomal fluid were carried out on both samples to determine % bioaccessibility and thus investigate the differences in the form in which metals are present in either sample. The separation technique achieved 94.3% of particles <10µm (the original sample contained 90.4% as determined by SEM-EDX). Acid soluble metal concentrations results indicated differences between the samples. However, when manipulated to negate the input of Si, SEM-EDX data showed general similarities in metal concentrations. Dissolution testing results indicated similar behaviour between the two samples in a simulated biological fluid.

### Keywords

Road dust, PM<sub>10</sub>, representation, bioaccessibility

### Highlights

Urban road dust particles of <10µm are analytically comparable with <38µm fraction.

Use of single particle analysis illustrates particles report to the same clusters.

Both fractions have similar chemical structure according to single particle analysis.

Justification for the use of RD in *in vitro* studies

### Introduction

Urban air quality is of significant importance to the majority of us living or working in our cities worldwide. Short-term events such as the 1952 London smog episode have the ability to dominate headlines because of the 4000 deaths due to acute exposure to air pollution, 12000 when integrated over the whole of the winter (Whittaker et al, 2004). However, chronic exposure to air pollution, to which we are all subject, provides equally shocking statistics. The European Environment Agency estimates that poor air quality is responsible for 467,000 premature deaths per year amongst Europeans (EEA 2016). The World Health Organisation estimates that air pollution is responsible for 8% of lung cancer deaths, 5% of cardiopulmonary deaths and 3% of respiratory infection deaths (WHO 2009).

Such deleterious effects on the population are often attributed to particulate matter (PM). Emission sources of PM are numerous, and commonly include industrial and commercial output, vehicular emissions and wear, abrasion of road surfaces etc. (Wang et al. 2016). Another large source of PM is believed to be resuspended road dust (RD), which can account for as much as 74% of total suspended particles by mass (Hien et al. 1999;

Harrison et al. 1997) and has also been observed to be the largest and second largest contributor to PM<sub>10</sub> and PM<sub>2.5</sub> respectively (Landis et al. 2017). Emphasis on RD as possibly the most significant contributor to PM will continue to grow because it is currently unregulated, unlike vehicle exhaust emissions (Padoan et al. 2017)

Because of the range and nature of sources, PM should be considered unique for any given location. PM is a topic which has been studied extensively, although recent consensus amongst the scientific community indicates that the micro-chemical structure of PM is responsible for the degree of toxicity (Rohr et al. 2011).

Due to the nature of PM, and particularly respirable PM<sub>10</sub>, it can be difficult to analyse micro-chemical structure, without specialised techniques such as micro-Raman Spectroscopy (Worobiec et al. 2010) or surface enhanced Raman Spectroscopy (SERS) (Tian et al. 2014). There are further difficulties with obtaining a suitable sample mass with a view to carry out robust in-vitro studies, since common methods for modelling either the respiratory or the gastrointestinal route typically use upwards of 0.5g per sample, including replicates (Colombo et al. 2008; Wragg et al. 2011). Collection on filters using high volume samplers typically yields samples of less than 0.1g (Shahsavani et al. 2012; Behrooz et al. 2017).

The aim of this study is to see if <10µm fraction of RD is analogous to the <38µm fraction, and thus assess the possibility of using the larger, more abundant size fraction of RD as a proxy for PM<sub>10</sub>. This will be carried out using metal concentrations as a marker. A water deposition technique can be used to separate the RD fraction of <10µm from the original <38µm sample. The <38µm sample will also be soaked in deionised water to simulate the conditions to which the <10µm fraction was exposed, both samples will lose some water-soluble components in the process. Both fractions, the <10µm and the <38µm will then be acid digested to compare their elemental profiles and exposed to artificial lung fluid to compare mobility of metals within the body. RD used in the study was collected in 2014 from Oxford Road, Manchester. The collection technique and handling of RD has been described by Brown et al. (2015).

## Methods

### PM<sub>10</sub> Separation

PM<sub>10</sub> Separation was carried out using a sedimentation-in-water process based on the principles of Stokes' law, which gives the velocity of a sphere in a viscous fluid under the force of gravity. Equation 1 is Stokes' law, where  $V$  is velocity of a particle;  $g$  is acceleration due to gravity;  $a$  is the diameter of a particle (cm);  $d_1$  is the density of a particle;  $d_2$  is the density of water;  $\mu$  is the viscosity of water (Haynes 2016). Density of particles was measured to be 3.2 g/cm<sup>3</sup>, as determined by a water displacement technique similar to Blake and Hartage (1986).

Equation 6. Stokes' Law

$$V = \frac{2ga^2(d_1 - d_2)}{9\mu}$$

The separation technique is presented in figure 1. The process uses a bunged 100 cm<sup>3</sup> measuring cylinder. The distance between the 100 cm<sup>3</sup> mark on the cylinder and the 80 cm<sup>3</sup> mark was measured to be 3.1cm. The time taken for particles of 10µm to travel that distance is 259 s, as determined by equation 1.

A 2g sample of RD was accurately weighed into the measuring cylinder then made up to the 100 cm<sup>3</sup> mark with deionised water (18 MQ). The cylinder and contents were thoroughly agitated by hand and then placed on a bench, this is shown as step a. in figure 1. A stopwatch was then used to time 259 seconds, the amount of time taken for particles larger than 10µm to travel 3.1cm, shown as step b. in figure 1. A 20 cm<sup>3</sup> pipette was then inserted

into the cylinder to siphon off the top 20 cm<sup>3</sup> of water. This process removes suspended particles <10µm from the cylinder, shown as step c. in figure 1. The water in the pipette, containing the <10µm particles, is then aspirated into a clean centrifuge vial, step d. in figure 1. The centrifuge vial and contents were then centrifuged at 2000rpm for 15 minutes, the supernatant was then discarded, step e. in figure 1. The particles remaining in the centrifuge tube were transferred to a clean weighing boat and left to dry at room temperature in a clean brown paper bag. This process is repeated 20 times for each sample with another 20 cm<sup>3</sup> of deionised water added to the measuring cylinder before step a. to replace the 20 cm<sup>3</sup> removed at step c. on the previous iteration. The method described here is based on one described by Boisa et al. (2014).

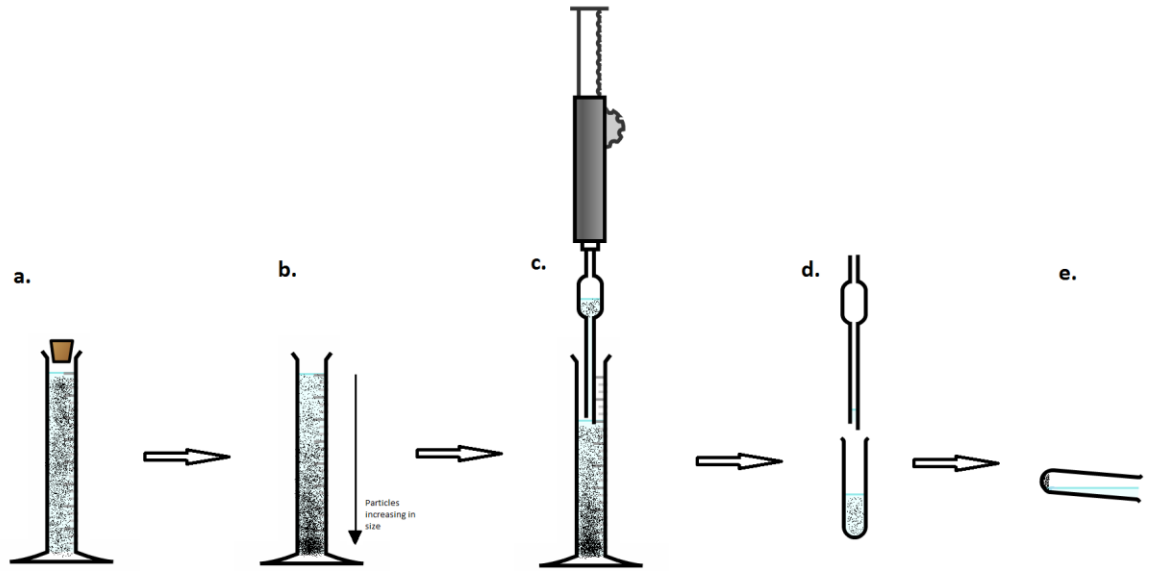


Figure 1. Separation schematic (Chemix.org)

### Particle size analysis

A Zeiss Supra 40VP field emission computer controlled scanning electron microscope with energy dispersive X-ray microanalysis (CC-SEM-EDX) was used to determine particle size distribution (PSD) of both samples once mounted by dispersion onto silver foil. A backscattered electron detector was used at 1000x magnification to acquire an image of the stub surface, the heavy elemental background from the silver foil enables a high contrast black and white image to be obtained. EDAX Genesis software is used to control the instrument, generating a series of images spiralling out from the centre of the stub, essentially mapping it. The program recognises particles based on their dark colour relative to the background, greyscale sensitivity is programmed by the operator beforehand. The program measures the x and y ferets of a particle based on number of pixels.

Particle size can be represented by average diameter, calculated from the two-dimensional projection of a given particle. Equation 2, as used by Potgieter-Vermaak et al. (2012), shows how average particle diameter is calculated for each particle. Where,  $D_p$  is average particle diameter,  $D_{max}$  is maximum feret diameter,  $D_{min}$  is minimum feret diameter.

Equation 2. Average particle diameter

$$D_p = \sqrt[3]{(D_{max} \times D_{min}^2)}$$

### Acid soluble metals determination

250mg  $\pm$ 10mg of each PM<sub>10</sub> sample was analysed for its acid soluble metal content by dissolution in *aqua regia* (7.5 cm<sup>3</sup> HCl, 2. cm<sup>3</sup> HNO<sub>3</sub>), three extractions were carried out per sample. This process was facilitated with a 1600W CEM Mars 5 Microwave equipped with Teflon digestion tubes. Analysis was carried out using a Varian Vista MPX ICP-OES with SeaSpray nebulizer. Initial system stability checks were carried out with a 5mg cm<sup>-3</sup> solution of Mn during the torch alignment whereby the upper values must be in excess of 300,000 counts per second, sample analysis exclusively used the axial position. A four-point linear calibration was achieved for each element, a calibration coefficient of >0.99 for all elements was determined. Five replicates were carried out per sample

### Metal dissolution determination

For the dissolution method, 150mg  $\pm$  10mg of PM<sub>10</sub> was measured into a PET centrifuge tube along with 15cm<sup>3</sup> of artificial lysosomal fluid (ALF). ALF (Colombo et al. 2008) was selected as an appropriate representation of the lung environment cells encounter following contact with the macrophage immune response (Wiseman and Zereni 2014). The mixture was then placed in an incubator shaker for 24 h. This was deemed an appropriate length of time to expose the samples to ALF, as residence time for particles in the lung is still somewhat disputed by the scientific community. Despite this, the aim of this paper is to investigate the use of larger particles as a proxy for PM<sub>10</sub> so extraction time should not be important. The analysis method for the ALF extracted samples was the same as for the acid extracted samples. Al, As, Cr, Cu, Fe, Mn, Ni, Pb, Sn and Zn were quantified in each sample. These particular metals were selected to give an insight into the effective change for metals deemed to be of both crustal and anthropogenic origin (Alomary and Belhadj 2007; Gunawardana et al. 2012)

### Single Particle Analysis

Single Particle Analysis (SPA) was carried out using the same instrumentation technique as described in section 2.1. Elemental data were then separated into clusters based on mole fractions per element, as described by Kandler et al. (2011). Clusters for these data are defined in Table 1, along with mole fraction criteria. AE refers to total mole fraction; in each case the contributions of C, O and Ag have been subtracted.

Table 5: SPA clusters and criteria

Cluster	Criteria
Silicates	Si/AE>0.2, Mg/Si<1.33, Al/Si<1.33, Fe/Si<0.5, Ti/Si<0.5, Na/Si<0.7
Calcites	Ca/AE >0.5, Mg/Ca <0.33, Si/Ca <0.5, S/Ca<0.25, P/Ca<0.15
Ti rich	Ti/AE >0.3, Mg/Ti <1, Al/Ti <1, Fe/Ti <1, Si/Ti <1, S/Ti <1, Na/Ti <1
Fe rich	Fe/AE >0.15, Si/Fe <1.05, Ti/Fe <1.3
Al rich – not aluminosilicates	Al/AE>0.15, Si/AE<0.2, Ti/Al<1.3
Trace containing	(Cu+Cr+Mn+Ni+Pb+Sn+V+Zn)/AE>0.05

## Results

### PM<sub>10</sub> separation

Particle size was determined using CC-SEM-EDX. 1500 particles were analysed for each of the two fractions. The smallest measurable diameter was 0.5µm, particles smaller than this are indistinguishable from imperfections in the silver foil surface. Figure 1 shows particle size distribution as determined by CC-SEM-EDX for the <10µm and <38µm fractions. The figure divides particles into bins based on particle size, starting with 0.5-1.5µm, then 1.5-2.5µm etc. presented along the x-axis as average particle diameter ( $D_p$ ). The primary y-axis shows the number of particles in each bin divided by the total number of particles ( $n_j/n_t$ ). Presenting particle size distribution data in this manner is common for particulate matter (Chen et al. 1997; Lin et al. 2005; Potgieter-Vermaak et al. 2012; Yue et al. 2013) and RD (McKenzie et al. 2008); these studies tend to log the number of particles in each bin. The authors felt that logging the number of particles in each bin failed to give a clearer visual representation of the particle size distribution. The secondary y-axis of figure 1 show a cumulative distribution of particles, by summing the number of particles in each preceding bin, as a percentage of the total number of particles ( $N(D_p)/n_t$ ). The cumulative distribution is included to give an indication of the type of distribution observed. Both the <38µm and the <10µm fraction showed somewhat of a lognormal distribution, however there are too many smaller particles to fit this distribution with statistical confidence. It is observed that the number of particles smaller than 1.5µm dropped off in the <38µm fraction, but carried on increasing in the <10µm fraction. It is possible that this was caused by the separation technique failing to remove some particles between 1.5-10µm from the <38µm, therefore under representing them in the <10µm fraction. This is unavoidable using a technique, which assumes uniform density of particles.

Geometric median and geometric standard deviation are calculated using equations given by Potgieter-Vermaak et al. (2012). The geometric median particle size in the <10µm fraction is 1.7µm (geometric standard deviation 2.3µm), 94.3% of particles were smaller than 10µm. In the <38 fraction, the geometric median particle size was 3.5µm (geometric standard deviation 2.3µm), 90.4% of particles were smaller than 10µm. These results show that a good separation efficiency was achieved with this technique, a significant portion of the particles larger than 10µm have been removed. The distribution of particles observed here in the <10µm fraction was similar to that reported by McKenzie et al. (2008). In both cases, particles were measured down to a size of 0.5µm, albeit using different instrumentation. Interestingly results from this study showed a greater exponential skew toward the smallest particles. This could possibly be due to differences in sites or the vacuum collection method used by McKenzie et al. (2008). The large number of small particles observed here in the <38µm fraction supports the concept that RD inherently contains a large number of small particles (Kong et al. 2012). This is a crucial observation with respect to the aim of this study; thoracic particles do make up a significant portion of RD.

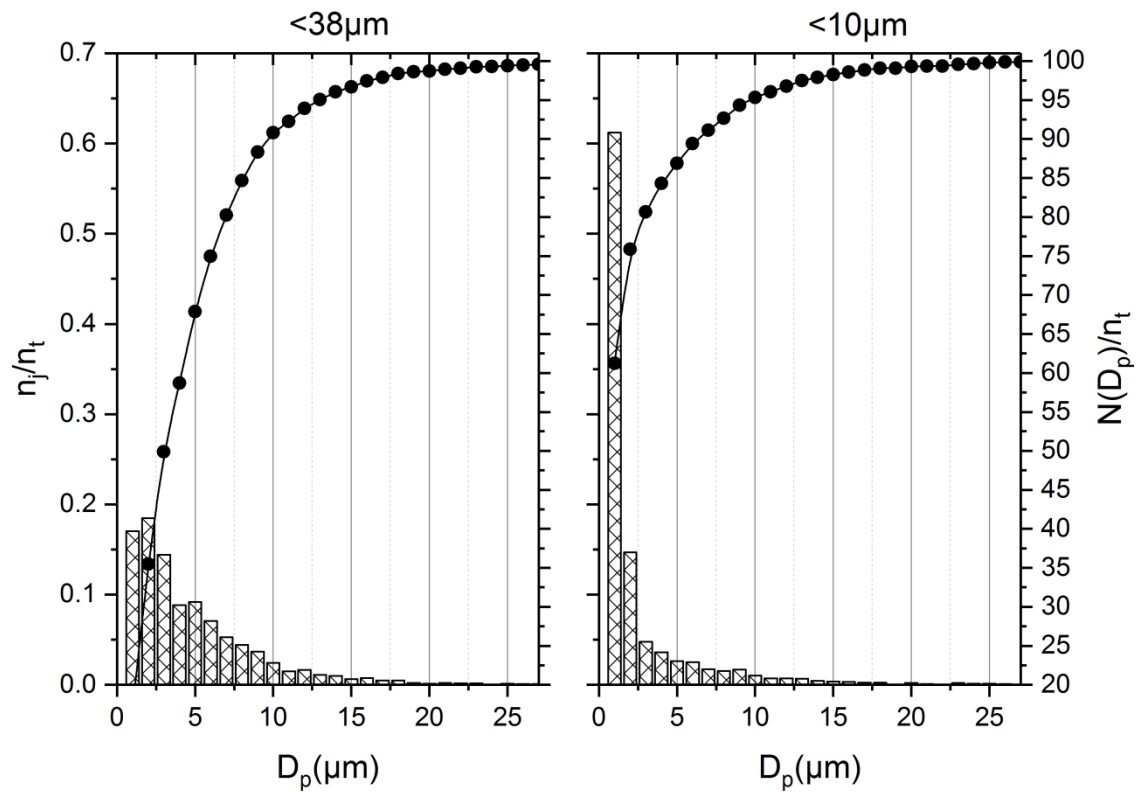


Figure 2. Particle size distributions from each fraction

### Bulk Elemental Concentration

Results from the acid digestion experiment indicated a significant difference in metal concentrations observed between the <38µm and <10µm fractions. Elemental concentrations were increased in the <10µm fraction for each element quantified. Table 2 represents the data from both fractions and includes the % increase from <38µm to <10µm.

Table 6: Acid soluble metal concentrations

	Al	As	Cr	Cu	Fe	Mn	Ni	Pb	Sn	Zn
<10µm (mg/kg)	21270	49.7	674.	7224	39700	6180	258.	3290	535.	1124
	0	±8.6	8	±0.9	0	±0.8	1	±0.8	5	0
	±7.9%	%	±5.1	%	±1.1%	%	±6.7	%	±1.4	±0.9
			%				%		%	%
<38µm (mg/kg)	14010	30.0	636.	4576	35540	5788	209.	2320	461.	7564
	0	±11	8	±1.6	0	±1.6	7	±0.4	3	±1.6
	±3.6%	%	±3%	%	±1.5%	%	±3.8	%	±1.6	%
							%		%	
Increase (%)	51.8	66.3	6.0	57.8	11.7	6.8	23.1	41.8	16.1	48.6

Elemental concentrations in the <10µm fractions showed the trend Fe>Al>Zn>Cu>Mn>Pb>Cr>Sn>Ni>As. The same pattern was observed in the <38µm fraction, with the exception of Mn, which was more abundant than copper. Albuquerque et

al. (2016) concluded a similar pattern of metal concentration of PM<sub>10</sub>, Zn>Cu>Pb>Mn>Cr>Ni>As, the notable difference being the increased Pb concentration relative to Mn. Other studies investigating metal concentrations of PM<sub>10</sub> also indicated a similar order, again with Pb being more abundant than Mn (Lim et al. 2010). It is worth noting that specific metal concentrations, in terms of absolute concentration and relative to other metals are very dependent on site. It is also worth acknowledging that literature quoting concentrations of metals within PM<sub>10</sub> will generally be reported in units of mass per volume (of air), as collection on filters is the most common method of quantification.

Such large differences in metal concentrations between the fractions may appear to conclusively disprove any possibility that the two samples may be comparable. However, it is documented that the largest constituent of RD is Si, and that the concentration of Si increases in larger grain fractions (Brown et al. 2015). It is feasible that the difference between the two samples may be the significantly larger concentration of Si in the <38µm fraction.

In an attempt to bypass this issue, we are able to refer back to the SEM-EDX work originally carried out as a means of ascertaining particle size distribution. Recalculating the percentage weight (%Wt) composition for each particle once C, O and Si have been removed, we can compare quantities of each remaining element present in each sample. A full suite of crustal and trace elements quantified by SEM-EDX were left in the %Wt equation to increase accuracy. Distribution for each element also quantified by ICP-OES was found to be skewed left (Al, As, Cr, Cu, Fe, Mn, Ni, Pb, Sn and Zn). Therefore the Mann-Whitney U test was used to compare each of them between the <10µm and <38µm fraction, the null hypothesis (H<sub>0</sub>) being that the samples are statistically not the same. With the exception of Fe, Zn and As, it was found that we can accept the alternative hypothesis for all other elements. In the case of As, the SEM-EDX data indicated too few As containing particles in either fraction to perform a Mann-Whitney U test. With regards to Fe and Zn, the Mann-Whitney U test indicated that these elements were more enriched in the <10µm fraction.

### ALF soluble metals results

Concentrations of ALF leachate were normalised to mg/kg, in the same way as the acid digested samples were. For simplicity, the data can then be represented as bioaccessibility (%) for each element using equation 3. Results for each metal are presented in table 3.

Equation 3. Bioaccessibility (%)

$$\text{Bioaccessibility (\%)} = \frac{[\text{ALF leachates}](\text{mg kg}^{-1})}{[\text{Acid digestion}](\text{mg kg}^{-1})}$$

Table 7: Bioaccessibility data

	Al	As	Cr	Cu	Fe	Mn	Ni	Pb	Sn	Zn
<10µm	1.74 ±0.08	10.79 ±0.1	5.14 ±0.08	8.39 ±0.03	3.11 ±0.08	7.61 ±0.06	9.93 ±0.07	7.56 ±0.05	5.03 ±0.1	10.08 ±0.05
<38µm	1.56 ±0.04	12.35 ±0.12	3.33 ±0.04	5.51 ±0.03	2.24 ±0.02	5.64 ±0.02	8.98 ±0.04	6.26 ±0.03	4.57 ±0.02	8.49 ±0.02

Table 3 shows the bioaccessibility data presented as %. Standard deviations for each metal are given as calculated by propagation of errors (Miller and Miller 2005). The results do

seem to indicate a strong similarity between the leaching behaviour of the two samples across the full range of metals: there is an average difference of just 1.35% between any given element with respect to fraction size. The largest absolute difference is 2.88mg kg<sup>-1</sup> for Cu; the smallest is 0.18mg kg<sup>-1</sup> for Al. This appears to support the elemental composition results obtained using SEM-EDX. The results here suggest that it is likely that the forms in which the metals are present in both samples, *i.e* mineralogically or otherwise are the same. Vastly different leaching behaviour between the two samples would suggest that different minerals or free metals are present in one sample but not the other. In comparison to other studies, the bioaccessibility in ALF results achieved here are significantly lower than those collected by Wiseman and Zereni (2014), who achieved bioaccessibility around an order of magnitude higher across the suite of metals analysed, generally between 60-80% bioaccessible. Pelfrene et al. (2017) carried out ALF dissolution tests on a range of certified reference materials. Results indicated large variability in dissolution of metals between each of the reference materials, % bioaccessibility of Mn was found to be 5.5% ( $\pm 0.1$ ), 44.3% ( $\pm 0.2$ ) and 46.8% ( $\pm 2.6$ ) amongst the three analysed reference materials

### Single Particle Analysis

To attempt to elucidate the somewhat conflicting results achieved between the acid digest data and the data from both the SEM-EDX and leachates, further analysis of RD was carried out using CC-SEM-EDX. In this section, all data referred to are from the original <38 $\mu$ m fraction sample, unexposed to water. Particles have been clustered in accordance with Table 1, with extra criteria added to group particles with a diameter of <10 $\mu$ m. Table 4 shows cluster data for the original <38 $\mu$ m fraction and for particles within this sample that have a diameter of <10 $\mu$ m, the portion within each cluster observed is presented as a percentage, in order to normalise the number of particles of a given observed size. A large number of particles were found to match the criteria for more than one cluster. These mixed clusters are also defined in Table 4.

Table 8: Cluster data

Cluster	Clusters present in <38 $\mu$ m fraction (%)	Clusters present in <10 $\mu$ m fraction (%)
Silicates	57.7	56.3
Silicates and Calcites mixed	0.3	0.4
Silicates and Trace mixed	6.9	7.3
Calcites	0.4	0.4
Calcites and Al rich mixed	4.2	4.3
Calcites, Al rich and Trace mixed	7.1	7.3
Ti rich	0.2	0.1
Fe rich	2.5	2.3
Fe rich and Trace mixed	0.3	0.3
Al rich	1.6	1.3
Al rich and Trace mixed	8.2	7.4
Trace	7.2	7.3
Undefined	3.4	5.2

Table 4 shows markedly similar clustering data between the two size fractions. The largest absolute difference between the two fractions was the silicates cluster, the <38µm fraction contained 1.4% more Silicates than the <10µm fraction. Calcites, Ti rich, Fe rich, Al rich and Trace clusters were all within 0.3% of each other with respect to the different size fractions. There was a slightly more noticeable difference between the mixed clusters, where the differences between the size fractions ranged up to 0.8%. This could suggest that in both samples particles are commonly present as aggregated collections of particles, in agreement with previous research on the topic (Thorpe et al. 2007)

The undefined row indicates that particles fit none of the clustering criteria. In most circumstances, this classification was attributed to highly carbonaceous particles, containing trace amounts of various other elements. It is observed that there is a significantly larger portion of undefined particles in the <10µm size fraction.

## Conclusions

The aim of this study was to assess the possibility of using larger size fractions of urban particles to act as a proxy for PM<sub>10</sub>, in terms of metal concentrations and their possible biological behaviour. While acid digestion results seem to indicate that this is not possible, assessing manipulated SEM-EDX data, leaching behaviour and SPA data suggested the opposite conclusion. Manipulating the SEM-EDX data and the leaching experimentation methods ignores the well-regarded, sizable input of Si. This is supported by the clustering data where it can be observed that silicate particles are slightly more abundant in the <38µm fraction than the <10µm fraction. Possibly the most likely explanation for the similarity in composition and behaviour of the two samples here is that the larger fraction is simply a precursor to the smaller, with the larger fraction having a significant presence of aggregates which ultimately disintegrate to form the smaller fraction. This conclusion is touched upon in the discussion section 3.4.

Referring back to the aim as outlined in the introduction section of this paper, it does appear that the <38µm fraction could be used as at least a first approximation of metal enrichment in PM<sub>10</sub> for the purpose of *in vitro* tests. It therefore enables researchers to easily use a larger sample size and thus provide more representative results. Further work on the topic using intra-molecular analytical techniques could broaden the conclusions drawn here and offer a firmer explanation of the role of Si within these particles.

## References

- Albuquerque, M., Coutinho, M., Rodrigues, J., Ginja, J., Borreo, C. 2016. Long-term monitoring of trace metals in PM<sub>10</sub> and total gaseous mercury in the atmosphere of Porto, Portugal. Atmospheric pollution research - in press
- Alomary, A. A., Belhadj, S. (2007). Determination of heavy metals (Cd, Cr, Cu, Fe, Ni, Pb, Zn) by ICP-OES and their speciation in Algerian Mediterranean Sea sediments after a five-stage sequential extraction procedure. Environmental Monitoring and Assessment, 135, 265-280.
- Behrooz, R., Esmaili-Sari, A., Bahramifar, N., Kaskaoutis, D. G., 2017. Analysis of the TSP, PM<sub>10</sub> concentrations and water-soluble ionic species in airborne samples over Sistan, Iran during the summer dusty period. Atmospheric pollution research 8, 403-417
- Blake, G. R., Hartage, K. H., 1986. Particle density. Methods of soil analysis part 1 – physical and mineralogical methods. American society of agronomy, Madison, WI
- Boisa, N., Entwistle, J., Dean, J. R., 2014. A new simple; low-cost approach for generation of the PM<sub>10</sub> fraction from soil and related materials: Application to human health risk assessment. Analytica Chimica Acta 852, 97-104
- Brown, A., Barrett, J. E. S., Robinson, H., Potgieter-Vermaak, S. 2015. Risk assessment to particulate output of a demolition site. Environmental geochemistry and health 37, 675-687

Chemix.org

Chen, Shui-Jen., Liao Shi-Hu., Jian, Wei-Jain., Lin, Chih-Chung, 1997. Particle size distribution of ambient aerosol carbons in ambient air. *Environment international* 23, 475-488

Colombo, C., Monhemius, A. J., & Plant, J. A., 2008. Platinum, palladium and rhodium release from vehicle exhaust catalysts and road dust exposed to simulated lung fluids. *Ecotoxicology and Environmental Safety* 71, 722-730

EEA, 2016. <http://www.eea.europa.eu/themes/air/air-emissions-data>

Gunawardana, C., Goonetilleke, A., Egodawatta, P., Dawes, L., Kokot, S., 2012. Source characterisation of road dust based on chemical and mineral composition. *Chemosphere*, 87, 163-170.

Haynes (Ed.) *CRC Handbook of Chemistry and Physics*, 97th edition CRC Press

Harrison, R. M., Smith, D. G. T., Pio, C. A., Castro L. M. (1997) Comparative receptor modelling study of airborne particulate pollutants in Birmingham, United Kingdom, Coimbra (Portugal) and Lahore (Pakistan). *Atmospheric Environment*, 31, 3309-3321

Hien, P. D., Binh, N. T., Truong, Y., Ngo, N. T.N. (1999). Temporal variations of source impacts at the receptor, as derived from particulate monitoring data in Ho Chi Minh City, Vietnam. *Atmospheric Environment*, 33, 3133-3142.

Kandler K, Leike K, Benker N, Emmel C, Kupper M, Muller-Ebert D, Scheuvsens D, Schladitz A, Schutz L., 2011. Electron microscopy of particles collected at Praia, Cape Verde, during the Saharan Mineral Dust Experiment: particle chemistry, shape, mixing state and complex refractive index. *Tellus* 63, 475-496

Kong, S., Lu, B., Ji, Y., Zhao, X., Bai, Z., Xu, Y., Liu, Y., Jiang, H. 2012. Risk assessment of heavy metals in road and soils dust within PM<sub>2.5</sub>, PM<sub>10</sub>, and PM<sub>100</sub> fraction in Dongying city, Shandong province, China. *Journal of environmental monitoring* 14, 791-803

Landis, M. S., Pancras, J. P., Graney, J. R., White, E. M., Edgerton, E. S., Legge, A., Percy, K. E. 2017. Source apportionment of ambient fine and coarse particulate matter at the Fort McKay community site, in the Athabasca Oil Sands Region, Alberta, Canada. *Science of the total environment* 584-585, 105-117

Lim, J. M., Lee, J. H., Moon, J. H., Chung, Y. S., Kim, K. H. 2010. Airborne PM<sub>10</sub> and metals from multifarious sources in an industrial complex area. *Atmospheric research* 96, 53-64

Lin, Chih-Chung., Chen, Shui-Jen., Huang, Kuo-li., 2005. *x*. *Environmental science and technology* 39, 8113-8122

McKenzie, E. R., Wong, C. M., Green, P. G., Kayhanian, M., Young, T. M. 2008. Size dependant elemental composition of road-associated particles. *Science of the total environment* 398 145-153

Padoan, E., Rome, C., Ajmone-Marsan, F. 2017. Bioaccessibility and size distribution of metals in road dust and road side soils along a peri-urban transect. *Science of the total environment* 601-602, 89-98

Pelfrene, A., Cave, M. R., Wragg, J., Douay, F. 2017. In vitro investigations of human bioaccessibility from reference materials using simulated lung fluids. *Environmental research and public health* 14, 112-127

Potgieter-Vermaak, S., Hoiremans, B., Anaf, W., Cardell, C., Van Grieken, R. 2012. Degradation potential of airborne particulate matter at the Alhambra monument: a Raman spectroscopic and electron probe X-ray microanalysis study. *Raman spectroscopy* 43, 1570-1577

Rohr, A. C., Kamal, A., Morishota, M., Mukherjee, B., Keeler, G. J., Harkema, J. R., Wagner, J. G., 2011. Altered heart rate variability in spontaneously hypertensive rats is associated

with specific particulate matter components in Detroit, Michigan. *Environmental Health Perspective* 119, 474-480

A. Shahsavani, K. Naddafi, N.J. Haghighifard, A. Mesdaghinia, M. Yunesian, R. Nabizadeh, M. Arhami, M. Yarahmadi, M.H. Sowlat, M. Ghani, A.J. Jafari, M. Alimohamadi, S.A. Motevalian, Z. Soleimani. 2012. Characterization of ionic composition of TSP and PM10 during the Middle Eastern dust (MED) storms in Ahvaz, Iran. *Environmental Monitoring and Assessment* 184, 6683-6692

Thorpe, A. J., Harrison, R. M., Boulter, P. G., McCrae, I. S. M., 2007. Estimation of particle resuspension source strength on a major London road. *Atmospheric Environment* 41, 8007-8020

Tian, F., Bonnier, F., Casey, A., Shanahan, A., Byrne, H., 2014. Surface enhanced Raman scattering with gold nanoparticles: effects of particular shape. *Analytical methods* 6, 9116-9123

Wang, J., Zhou, M., Liu, B., Wu, J., Peng, X., Zhang, Y., Han, S., Feng, Y., Zhu, T. 2016. Characterization and source appointment of size segregated atmospheric particulate matter collected at ground level and from the urban canopy in Tianjin. *Environmental pollution* 219, 982-992

Whittaker, A., Berube, K., Jones, T., Maynard, R., Richards, R. Killer smog of London, 50 years on: Particle properties and oxidative capacity. *Science of the Total Environment*, 2004: 435-445.

Wiseman, C., Zereni, F., 2014. Characterizing metal(loid) solubility in airborne PM10, PM2.5 and PM1 in Frankfurt, Germany using simulated lung fluids. *Atmospheric Environment* 89, 282-289

WHO., 2009. Global health risks, mortality and burden of disease attributable to selected major risks.

[http://www.who.int/healthinfo/global\\_burden\\_disease/GlobalHealthRisks\\_report\\_full.pdf](http://www.who.int/healthinfo/global_burden_disease/GlobalHealthRisks_report_full.pdf)

Worobiec, A., Potgieter-Vermaak, S., Brooker, A., Darchuck, L., Van Grieken, R., 2010. Interfaced SEM/EDX and micro-Raman Spectroscopy for characterisation of heterogeneous environmental particles – Fundamental and practical challenges. *Microchemical Journal* 94, 65-72

Wragg, J., Cave, M., Basta, N., Brandon, E., Casteel, S., Denys, S., Gron, C., Oomen, A., Reimer, K., Tack, K., Van de Wiele, T. An inter-laboratory trial of the unified BARGE bioaccessibility method for arsenic, cadmium and lead in soil. *Science of the total environment*, 40, 4016-4030

Yue, D. L., Hu, M., Wang, Z. B., Wen, M. T., Guo, S., Zhong, L. J., Weidensohler, A., Zhang, y. H. 2013. Comparison of particle number size distribution and new particle formation between the urban and rural sites in the PRD region, China. *Atmospheric environment* 76, 181-188.